

OROD RAEESI

Analysis and Mitigation of Channel Non-Reciprocity in TDD MIMO Systems

OROD RAEESI

Analysis and Mitigation of
Channel Non-Reciprocity
in TDD MIMO Systems

ACADEMIC DISSERTATION

To be presented, with the permission of
the Faculty of Information Technology and Communication Sciences
of Tampere University,
for public discussion in the auditorium S2
of the Sähköotalo building, Korkeakoulunkatu 10, Tampere,
on 11 October 2019, at 12 o'clock.

ACADEMIC DISSERTATION

Tampere University,

Faculty of Information Technology and Communication Sciences

Finland

<i>Responsible supervisor and Custos</i>	Professor Mikko Valkama Tampere University Finland	
<i>Co-supervisor</i>	D.Sc. Ahmet Gökceoglu Huawei Technologies Sweden	
<i>Pre-examiners</i>	Professor Robert Schober Friedrich-Alexander-Universität Germany	Professor Tommy Svensson Chalmers University of Technology Sweden
<i>Opponent</i>	Professor Jyri Hämmäläinen Aalto University Finland	

The originality of this thesis has been checked using the Turnitin OriginalityCheck service.

Copyright ©2019 author

Cover design: Roihu Inc.

ISBN 978-952-03-1253-4 (print)

ISBN 978-952-03-1254-1 (pdf)

ISSN 2489-9860 (print)

ISSN 2490-0028 (pdf)

<http://urn.fi/URN:ISBN:978-952-03-1254-1>

PunaMusta Oy – Yliopistopaino

Tampere 2019

ABSTRACT

The ever-growing demands for higher number of connected devices as well as higher data rates and more energy efficient wireless communications have necessitated the use of new technical solutions. One of the main enablers in this respect is Multiple-Input Multiple-Output (MIMO) systems in which transmitting and receiving sides are equipped with multiple antennas. Such systems need precise information of the MIMO radio channel available at the transmitter side to reach their full potential. Owing to the reciprocity of uplink and downlink channels in Time Division Duplexing (TDD) systems, Base Stations (BSs) may acquire the required channel state information for downlink transmission by processing the received uplink pilots. However, such reciprocity only applies to the physical propagation channels and does not take into consideration the so-called observable or effective uplink and downlink channels which also include the possible non-reciprocal behavior of the involved transceiver circuits and antenna systems.

This thesis focuses on the channel non-reciprocity problem in TDD MIMO systems due to mismatches in Frequency Response (FR) and mutual coupling of transmitting and receiving chains of transceivers and associated antenna systems. The emphasis in the work and developments is placed on multi-user MIMO precoded downlink transmission. In this respect, the harmful impacts of channel non-reciprocity on the performance of such downlink transmission are analyzed. Additionally, non-reciprocity mitigation methods are developed seeking to reclaim TDD reciprocity and thus to avoid the involved performance degradations.

Firstly, the focus is on the small-scale MIMO systems where BSs are equipped with relatively limited number of antennas, say in the order of 4 to 8. The provided analysis on Zero-Forcing (ZF) and eigen-based precoding schemes in single-cell scenario shows that both schemes experience considerable performance degradations in the presence of FR and mutual coupling mismatches. Whereas, in general, the system performance is more sensitive to i) non-reciprocity sources in the BS transceiver; and ii) mutual coupling mismatches. Then, assuming reasonably good antenna isolation, an Over-The-Air (OTA) pilot-based algorithm is proposed to efficiently mitigate the BS transceiver non-reciprocity. The numerical results indicate high accuracy in estimating the BS transceiver non-reciprocity parameters as well as considerable improvement in the performance of the system. In multi-cell scenario, both centralized and decentralized precoding approaches are covered while the focus is on the impacts of FR mismatches of UE transceivers. The results show that there is severe degradation in the performance of decentralized precoding while centralized precoding is immune to such channel non-reciprocity impacts.

Secondly, the so-called massive MIMO systems are considered in which the number of antennas in the BS side is increased with an order of magnitude or more. Based on the detailed developed signal models, closed-form analytical expressions are first provided for effective signal-to-interference-plus-noise ratios of both ZF and maximum ratio transmission precoding schemes. The analysis covers the joint impacts of channel non-reciprocity and imperfect uplink channel estimation and shows that while both precoding schemes suffer from channel non-reciprocity impacts, ZF is more sensitive to such non-idealities. Next, a concept and an algorithm are proposed, involving UE side measurements and processing, to be deployed in the UE side to efficiently estimate the level of BS transceiver non-reciprocity. This enables the UEs to inform the BS about the optimum time to perform channel non-reciprocity mitigation round and thus improves the spectral efficiency. Finally, in order to mitigate channel non-reciprocity in massive MIMO systems, an efficient iterative OTA pilot-based algorithm is proposed which estimates and mitigates transceiver non-reciprocity impacts in both BS and UE sides. Compared to the state-of-the-art methods, the simulation results indicate substantial improvements in system spectral efficiency when the proposed method is being used.

Overall, the analyses provided in this thesis can be used as valuable tools to better understand practical TDD MIMO systems which can be very helpful in designing such systems. Furthermore, the channel non-reciprocity mitigation methods proposed in this thesis can be deployed in practical TDD MIMO systems to restore channel reciprocity and thus significantly increase the spectral efficiency.

PREFACE

The research work for this thesis was carried out during the years 2014 – 2017 in the Laboratory of Electronics and Communications Engineering, Tampere University of Technology, Tampere, Finland. The research work was financially supported by the Tampere University of Technology Graduate School (during the years 2014 – 2017), Nokia Foundation, and Industrial Research Fund of Tampere University of Technology (Tuula and Yrjö Neuvo Fund). I would like to also acknowledge the funding received from Finnish Funding Agency for Technology and Innovation (Tekes; under the projects “Energy-Efficient Wireless Networks and Connectivity of Devices – Densification (EWINE-D)” and “5th Evolution Take of Wireless Communication Networks (TAKE-5)”), the Academy of Finland (under the projects 251138 “Digitally-Enhanced RF for Cognitive Radio Devices”, 138424 “Joint Analysis and DSP-Based Mitigation of Multiple RF Impairments in Future Radio Devices”, 284694 “Fundamentals of Ultra Dense 5G Networks with Application to Machine Type Communication”, and 288670 “Massive MIMO: Advanced Antennas, Systems and Signal Processing at mm-Waves”), and Broadcom Communications Finland and Huawei Finland under the project “Energy-Efficient Wireless Networks and Connectivity of Devices – Densification (EWINE-D)”.

First and foremost, I would like to express my gratitude to my supervisor Prof. Mikko Valkama for his guidance and support throughout the years. Learning from his deep knowledge and experience has been a great privilege for me. I wish to also thank D.Sc. Ahmet Gökçeoglu for his invaluable help and supervision throughout the second half of my doctoral research. I would like to also extend my thanks to D.Sc. Yaning Zou for sharing her knowledge and instructing me during the first half of my doctoral research. I am also grateful to my pre-examiners Prof. Robert Schober and Prof. Tommy Svensson for reviewing and providing their valuable comments for this thesis. Furthermore, I wish to thank Prof. Jyri Hämäläinen for agreeing to act as the opponent in the public examination of my dissertation.

I am thankful to my co-authors, Prof. Risto Wichman, Prof. Qimei Cui, Prof. Emil Björnson, Dr. Paschalis C. Sofotasios, and Prof. Markku Renfors, with whom I had the pleasure of working during these years. In this regard, I like to especially thank Antti Tölli for sharing his knowledge and the guidance. I want to extend my gratitude to D.Sc. Ali Hazmi, D.Sc. Toni Levanen, and D.Sc. Jukka Talvitie. It was a pleasure to share an office with you and thanks for the nice environment and valuable insights.

I would also like to express my warmest thanks to my friends, especially Afsaneh, Kamiar, Nader, Parinaz, Saeed, and Sajjad whose friendship helped me through all the ups and downs of life as a doctoral student.

Most importantly, I would like to sincerely thank my parents who have endlessly supported and encouraged me all the way and in every way, especially during my studies. Finally, I wish to thank Mona for her love and support over the years.

Espoo, September 2019

Orod Raeesi

Contents

Abstract	iii
Preface	v
Acronyms	ix
List of Publications	xi
1 Introduction	1
1.1 Background and Motivation	1
1.2 Objectives and Scope of the Thesis	2
1.3 Outline and Contributions of the Thesis	3
1.4 Author's Contribution to the Publications	4
1.5 Mathematical Notations and Definitions	4
2 TDD MIMO Systems and the Associated Channel Non-Reciprocity	5
2.1 MIMO	5
2.1.1 Principal System Model	8
2.1.2 Transmit Precoding	9
2.1.3 Receiver Processing	12
2.1.4 Rate Calculation	12
2.1.5 Massive MIMO	13
2.2 TDD	13
2.3 Channel Non-Reciprocity Problem	13
3 Analysis and Mitigation of Channel Non-Reciprocity in Small-Scale MIMO Systems	17
3.1 Background and Prior Art	17
3.2 General Assumptions	18
3.2.1 Receiver Processing	18
3.3 Single-Cell	19
3.3.1 Analysis	19
3.3.2 Mitigation	21
3.4 Multi-Cell	24
3.4.1 Multi-Cell System Model	24
3.4.2 Centralized Precoding	25
3.4.3 Decentralized Precoding	26
3.4.4 Analysis	28
3.5 Numerical Evaluations and Results	30

3.5.1	Single-Cell	30
3.5.2	Multi-Cell	34
4	Analysis and Mitigation of Channel Non-Reciprocity in Massive MIMO Systems	37
4.1	Background and Prior Art	37
4.2	General Assumptions	38
4.2.1	Channel Estimation	38
4.3	Analysis	39
4.3.1	ZF Precoding	41
4.3.2	MRT Precoding	42
4.3.3	Asymptotic Performance for Large N	42
4.3.4	SINR Degradation due to Channel Non-Reciprocity	43
4.4	Level Estimation	44
4.5	Mitigation	46
4.5.1	Estimating BS Transceiver Non-Reciprocity Matrix	48
4.5.2	Estimating UE-Side Transceivers Non-Reciprocity Matrix	49
4.6	Numerical Evaluations and Results	50
4.6.1	Performance Evaluation Under Channel Non-Reciprocity	51
4.6.2	BS Transceiver Non-Reciprocity Level Estimation	53
4.6.3	Channel Non-Reciprocity Mitigation	55
5	Summary	59
	Bibliography	63
	Publications	73

ACRONYMS

3GPP	3rd Generation Partnership Project
BS	Base Station
CoMP	Coordinated Multi-Point
CSI	Channel State Information
FDD	Frequency Division Duplexing
FFT	Fast Fourier Transform
FIR	Finite Impulse Response
FR	Frequency Response
GSM	Global System for Mobile Communications
HSPA	High Speed Packet Access
IAB	Integrated Access and Backhaul
IFFT	Inverse Fast Fourier Transform
IoT	Internet of Things
ISI	Inter-Stream Interference
IUI	Inter-User Interference
LMMSE	Linear Minimum Mean Squared Error
LS	Least Squares
LTE	Long-Term Evolution
LTE-A	LTE Advanced
MIMO	Multiple-Input Multiple-Output
MISO	Multiple-Input Single-Output

MMSE	Minimum Mean Squared Error
mmWave	Millimeter Wave
MRT	Maximum Ratio Transmission
MSE	Mean Squared Error
MTC	Machine-Type Communications
MU-MIMO	Multi-User MIMO
NOMA	Non-Orthogonal Multiple Access
NRC	Non-Reciprocal Channel
OFDM	Orthogonal Frequency Division Multiplexing
OTA	Over-The-Air
RZF	Regularized Zero-Forcing
SIMO	Single-Input Multiple-Output
SINR	Signal-to-Interference-plus-Noise Ratio
SISO	Single-Input Single-Output
SNR	Signal-to-Noise Ratio
SU-MIMO	Single-User MIMO
SVD	Singular Value Decomposition
TDD	Time Division Duplexing
TE	Test Equipment
UE	User Equipment
UMTS	Universal Mobile Telecommunications System
WSR	Weighted Sum-Rate
ZF	Zero-Forcing

LIST OF PUBLICATIONS

The following eight publications form the basis of this thesis.

- [P1] O. Raeesi, A. Gokceoglu and M. Valkama, “Estimation and mitigation of channel non-reciprocity in massive MIMO,” *IEEE Transactions on Signal Processing*, vol. 66, no. 10, pp. 2711–2723, May 2018.
- [P2] O. Raeesi, A. Gokceoglu, Y. Zou, E. Björnson and M. Valkama, “Performance analysis of multi-user massive MIMO downlink under channel non-reciprocity and imperfect CSI,” *IEEE Transactions on Communications*, vol. 66, no. 6, pp. 2456–2471, June 2018.
- [P3] O. Raeesi, Y. Zou, A. Tölili, and M. Valkama, “Closed-form analysis of channel non-reciprocity due to transceiver and antenna coupling mismatches in multi-user massive MIMO network,” in *2014 IEEE Globecom Workshops (GC Wkshps)*, Dec 2014, pp. 333–339.
- [P4] O. Raeesi, A. Gokceoglu, Y. Zou, Q. Cui, and M. Valkama, “Estimation of BS transceiver non-reciprocity in multi-user massive MIMO systems,” in *European Wireless 2016; 22th European Wireless Conference*, May 2016, pp. 1–8.
- [P5] O. Raeesi, A. Gokceoglu, P. C. Sofotasios, M. Renfors, and M. Valkama, “Modeling and estimation of massive MIMO channel non-reciprocity: Sparsity-aided approach,” in *2017 25th European Signal Processing Conference (EUSIPCO)*, Aug 2017, pp. 2596–2600.
- [P6] O. Raeesi, Y. Zou, A. Tölili, and M. Valkama, “On the effects of UE transceiver non-reciprocity in coordinated TDD multi-cell MIMO network,” in *2015 IEEE Global Communications Conference (GLOBECOM)*, Dec 2015, pp. 1–7.
- [P7] Y. Zou, O. Raeesi, R. Wichman, A. Tölili, and M. Valkama, “Analysis of channel non-reciprocity due to transceiver and antenna coupling mismatches in TDD precoded multi-user MIMO-OFDM downlink,” in *2014 IEEE 80th Vehicular Technology Conference (VTC2014-Fall)*, Sept 2014, pp. 1–7.
- [P8] Y. Zou, O. Raeesi, and M. Valkama, “Efficient estimation and compensation of transceiver non-reciprocity in precoded TDD multi-user MIMO-OFDM systems,” in *2014 IEEE 80th Vehicular Technology Conference (VTC2014-Fall)*, Sept 2014, pp. 1–7.

CHAPTER 1

INTRODUCTION

1.1 Background and Motivation

Wireless technologies have experienced rapid development and growth in the past twenty years or so, most notably in the form of mobile cellular radio evolution from Global System for Mobile Communications (GSM) [1] to Universal Mobile Telecommunications System (UMTS)/High Speed Packet Access (HSPA) [2] and thereon to Long-Term Evolution (LTE) and LTE Advanced (LTE-A) [3]. LTE/LTE-A which shaped the fourth generation of mobile broadband wireless technology, known as 4G, has been an outstanding technology satisfying many of our current needs, particularly in the mobile broadband domain. There are still improvements coming to 4G but at much lower pace compared to its early days. However, new services, applications, and use cases are continuing to ask for significantly higher data rates and substantially lower end-to-end latency compared to what LTE/LTE-Advanced networks can provide. Additionally, the number of connected devices including smartphones, tablets, laptops, sensors, vehicles, as well as Machine-Type Communications (MTC) [4–7] and Internet of Things (IoT) [8–12] devices is expected to increase exponentially. These demands are the driving forces for an evolution of the fifth generation (5G [13–15]) of cellular networks.

In order to fulfill all the mentioned requirements, numerous technical solutions/enablers, e.g., Non-Orthogonal Multiple Access (NOMA) [16–20], optimized waveforms [21–24], network slicing [25–28], dynamic Time Division Duplexing (TDD) [29–31], and Integrated Access and Backhaul (IAB) [32–35], are being studied and developed in 5G standardization context. One of the key elements is to be able to provide more bandwidth to the User Equipment (UE) side. To achieve this goal, the first solution is acquiring more spectrum for 5G transmission systems. In sub-6 GHz band, e.g., C-band [36], there are efforts and prospects to adopt spectrum of few hundreds of MHz, e.g., by operating in shared/unlicensed spectrum [37–39]. However, in this context, the main focus in the long-term development is on Millimeter Wave (mmWave) frequencies [40–43], i.e., 30 GHz–300 GHz, where the amount of potential spectrum is in the order of tens of GHz. Although mmWave frequencies can help in providing more bandwidth for the mobile networks, in practice, the amount of highly valuable spectral resources is always

limited in a certain network. Thus, more efficient spectrum utilization and higher spatial spectrum reuse is necessary to meet 5G requirements. In this respect, especially in highly populated areas, small cells and networks densification [44–46] help by adding more Base Stations (BSs) and shrinking cell sizes which result into reusing the spectrum more aggressively within a certain area. Multi-antenna communications in which transmitting and/or receiving sides are equipped with multiple antennas can help increasing the spectral efficiency by enabling the system to employ diversity and spatial multiplexing techniques [47–50]. In such systems, when the transmitter knows the communication channel, it can use this information to increase the quality of the received signal, e.g., by making the received streams orthogonal, and/or multiplex different UEs in spatial domain which can significantly increase the spectral efficiency and spatial spectrum reuse [48, 51].

However, having timely and accurate Channel State Information (CSI) at the transmitter side is challenging. In Frequency Division Duplexing (FDD) [52] systems, where uplink and downlink transmission are carried out on separate bands, acquiring CSI at the BS requires two rounds of signaling and considerable amount of overhead [53]. In the previous generation of cellular systems, FDD was the main duplexing scheme. However, TDD scheme, in which uplink and downlink transmissions share the channel and are being separated in time [52], is becoming more important in 5G, especially in higher frequencies, i.e., above 10 GHz [54]. The reasons behind that are i) simplicity in finding one TDD band compared to two joint FDD bands; ii) flexibility in dynamically assigning resources between downlink and uplink transmissions. However, TDD systems have their own drawbacks, e.g., 3 dB average power loss compared to FDD systems assuming power amplifier is active only half the times, and the need for precise timing synchronization. Additional advantage in using TDD systems is the reciprocity between physical uplink and downlink propagation channels. Using this reciprocity, BSs can estimate downlink channels based on the received uplink pilots and thus reduce the required overhead and increase the spectral efficiency significantly [55]. This is even more interesting in massive Multiple-Input Multiple-Output (MIMO) [14, 55–63] scenario where generally the BS is equipped with massive amount of antennas, as the overhead for feedback signaling in FDD systems is proportional to the number of antennas in the BS side [55]. Massive MIMO technology is one of the main enablers of 5G networks and essential in higher frequencies as it can compensate for greater path-loss experienced in such frequencies [41]. However, in practice, the effective uplink and downlink channels which include also the effect of transceiver circuitries are generally not reciprocal due to non-reciprocity sources between transmitting and receiving modes of a particular hardware. Thus, such channel non-reciprocity impacts need to be analyzed and mitigated and this problem forms the core of this thesis.

1.2 Objectives and Scope of the Thesis

Channel Reciprocity is an essential assumption in the capacity enhancement promises of TDD (massive) MIMO. One of the two main objectives of this thesis is to build a good scientific understanding of the potential loss over these promised capacity gains in the presence of non-reciprocal radio front-ends. In order to achieve that, the nature of effective channel non-reciprocity in TDD multi-antenna systems is studied and the corresponding system and signal models are developed. Based on those, the impact of channel non-reciprocity on the performance of multi-antenna systems is analyzed which provides valuable insights in dimensioning and designing practical systems. The second objective is to reclaim the significant percentage of the capacity loss and approach towards

the promises of fully reciprocal TDD (massive) MIMO. For that reason, efficient digital signal processing based channel non-reciprocity estimation and mitigation frameworks are proposed which effectively compensate for the considered non-idealities in practical multi-antenna systems. Finally, extensive computer simulations are carried out to evaluate the accuracy of the provided analysis and the performance of the proposed mitigation methods.

1.3 Outline and Contributions of the Thesis

The main contributions of this thesis are as follows.

- Considering a generic and realistic channel non-reciprocity model which takes into account both transceiver Frequency Response (FR) and antenna mutual coupling mismatches, detailed signal and system models are derived for different system scenarios and precoding schemes in [P2], [P3], [P6] and [P7].
- Stemming from the signal and system models, joint impacts of the considered channel non-reciprocity sources on performance of TDD Multi-User MIMO (MU-MIMO) Orthogonal Frequency Division Multiplexing (OFDM) downlink transmission are analyzed for i) small-scale MIMO systems with Zero-Forcing (ZF) and eigen-based precoding schemes [P7]; ii) massive MIMO systems with ZF and Maximum Ratio Transmission (MRT) precoding schemes with imperfect CSI [P2] and [P3]. These performance degradations are quantified in terms of Signal-to-Interference-plus-Noise Ratio (SINR) and achievable sum-rate [P2], [P3] and [P7].
- Efficient Over-The-Air (OTA)-based estimation and mitigation frameworks are proposed to increase the performance of TDD MU-MIMO OFDM downlink transmission by compensating transceiver non-reciprocity impacts at i) BS side in small-scale MIMO systems [P8]; ii) both BS and UE sides in massive MIMO systems [P1] and [P5].
- The impacts of FR mismatches in the UE side on the performance of both centralized and decentralized precoding schemes in coordinated TDD multi-cell MIMO network are analyzed [P6]. In this context, an algorithm is proposed to address the precoder convergence problem in presence of channel non-reciprocity.
- Efficient algorithms are proposed to estimate the level of BS transceiver non-reciprocity at the UE side in TDD multi-user massive MIMO OFDM networks [P4]. Employing such methods, the UEs are able to request for non-reciprocity calibration rounds only when needed to increase spectral efficiency.
- Numerical evaluations of the analytical expressions and of the achievable mitigation algorithm performance are carried out by the means of extensive computer simulations which confirm the findings [P1]–[P8].

The details of all the contributions can be found in [P1]–[P8], while this thesis summary tries to give an overview of the essential information and main results. In order to offer consistency throughout this thesis summary, the notation used here slightly differs from that of the publications.

The thesis is organized as follows. Chapter 2 provides the necessary background theory, describing the principles of MIMO transmission including the fundamental signal and

system models. In addition to that, it introduces the basics of TDD systems and the associated channel non-reciprocity problem. Chapters 3 and 4 focus on the contributions of the thesis. Specifically, based on the presented results in [P6]–[P8], Chapter 3 provides discussion about the effects of channel non-reciprocity on small-scale TDD MU-MIMO downlink transmission in both single-cell and multi-cell scenarios. A proposed OTA type pilot-based BS transceiver non-reciprocity mitigation framework is also covered in Chapter 3. Extending the studies to massive MIMO systems based on the works in [P1]–[P5], Chapter 4 first focuses on closed-form analysis of channel non-reciprocity impacts on TDD multi-user massive MIMO downlink transmission. Subsequently, it introduces proposed frameworks to i) estimate the level of BS transceiver non-reciprocity at the UE side; and ii) mitigate transceiver non-reciprocity impacts in both BS and UE sides. Finally, the conclusions are drawn in Chapter 5.

1.4 Author’s Contribution to the Publications

The research topic was proposed by Prof. Mikko Valkama. He has been a co-author and contributed to all of the publications by sharing his feedback and thoughts in both stages of conducting the research and writing the publications. This thesis is based on the results of the research which were reported in publications [P1]–[P8]. The author of the thesis is the main contributor for conducting the research, simulations and writing [P1]–[P6]. The main contributor in [P7] and [P8] was D.Sc. Yaning Zou while the author of the thesis was responsible mainly for simulations and partly for derivations and composition. D.Sc. Yaning Zou was the instructor for the first half of this thesis, i.e., small-scale MIMO study. Whereas, D.Sc. Ahmet Gökceoglu was the instructor for the massive MIMO research which forms the second half of this doctoral study.

1.5 Mathematical Notations and Definitions

Throughout the thesis, bold and lower-case letters are used to denote vectors (e.g., \mathbf{v}), while bold and upper-case ones represent matrices (e.g., \mathbf{V}). Transpose, complex-conjugate, Hermitian-transpose, Moore-Penrose pseudo inverse, and matrix inverse operations are indicated by superscripts $(\cdot)^T$, $(\cdot)^*$, $(\cdot)^H$, $(\cdot)^\dagger$, and $(\cdot)^{-1}$, respectively. Whereas, statistical expectation and trace operators are denoted by $\mathbb{E}[\cdot]$ and $\text{Tr}(\cdot)$, respectively. Variance and covariance operators are shown by $\text{Var}(\cdot)$ and $\text{Cov}(\cdot)$, respectively, while $\text{Sum}(\cdot)$ is used as element-wise sum of the argument matrix. All-zero and identity matrices are represented by $\mathbf{0}_n$ and \mathbf{I}_n , respectively. The i -th element in vector \mathbf{v} is shown by v_i , whereas the j -th column of matrix \mathbf{V} is shown by \mathbf{v}_j , and correspondingly, the element on the i -th row and the j -th column of matrix \mathbf{V} is represented by v_{ij} . The $\text{diag}(\cdot)$ operator extracts the main diagonal of the input matrix as a column vector, and vice versa, transforms a vector \mathbf{v} to a diagonal matrix with v_i being the i -th element on its main diagonal. Finally, $\mathcal{CN}(0, \sigma^2)$ denotes a complex-valued zero-mean circularly symmetric Gaussian distribution with variance σ^2 , while $\Re\{\cdot\}$ and $\Im\{\cdot\}$ are used to element-wise extract real and imaginary parts of a complex-valued argument, respectively.

CHAPTER 2

TDD MIMO SYSTEMS AND THE ASSOCIATED CHANNEL NON-RECIPROCITY

In this chapter, we shortly concentrate on the basic concepts used throughout this thesis. We first review the fundamentals of MIMO and the associated precoding schemes. We also present the massive MIMO idea which has attracted much attention during the last few years. Then, we focus on TDD duplexing scheme, and finally, we discuss the channel non-reciprocity problem in TDD MIMO systems.

2.1 MIMO

Almost all the new systems and solutions which are designed to satisfy current and the future needs for wireless communications are built on the multi-antenna principle as opposed to Single-Input Single-Output (SISO) transmission where both the transmitter and the receiver have only one antenna, as depicted in Figure 2.1(a). The main drawback in using SISO systems is the challenge to have a reliable communication as the quality of a transmission is highly dependent on its corresponding propagation channel properties, namely, fading due to multi-path propagation and shadowing due to large obstacles. Whereas, MIMO systems can enhance the link reliability by employing diversity techniques, i.e., transmitting the same data streams through two or more channels with different characteristics. In addition to that, in a well-designed MIMO system where there are more than one antenna in both transmitting and receiving ends, the spatial degrees of freedom allow to simultaneously send multiple streams on the same frequency, resulting in spatial multiplexing gain which significantly improves the spectral efficiency.

Depending on the number of antennas in the transmitter and the receiver sides, multi-antenna systems can be divided into three categories, namely, Multiple-Input Single-Output (MISO) where the transmitter is a multi-antenna device and the receiver has only one antenna (Figure 2.1(b)), Single-Input Multiple-Output (SIMO) where the transmitter is a single-antenna device and the receiver is a multi-antenna one (Figure 2.1(c)),

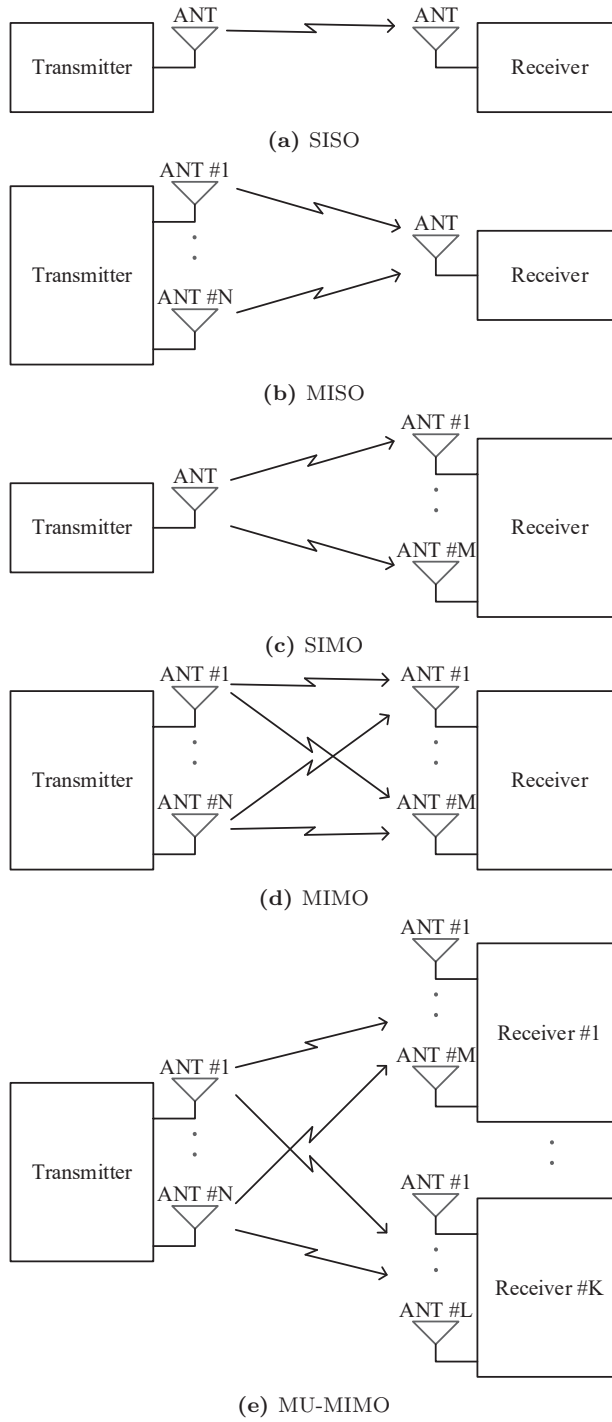


Figure 2.1: Different types of communication cases depending on the number of antennas and devices in the transmitter and the receiver sides.

and MIMO where both the transmitter and the receiver are multi-antenna devices (Figure 2.1(d)).

In the case that MIMO is used to communicate with several terminals at the same time, the term MU-MIMO is used (Figure 2.1(e)). MU-MIMO systems can cope with one of the main limitations in Single-User MIMO (SU-MIMO) scenario which is the propagation channel conditions, e.g., channel rank and antenna correlation, by the means of scheduler. As opposed to SU-MIMO which needs multi-antenna UEs to reap the benefits of MIMO, MU-MIMO/MISO can benefit from the spatial multiplexing gain even with single-antenna UEs, allowing to have small and cheap devices in MIMO systems. The drawback of MU-MIMO is the interference caused from the transmissions targeted to other UEs on the same time-frequency resources which may have significant impacts on the performance of the initial transmission. In order to fully exploit the spatial multiplexing capabilities of MU-MIMO and potentially mitigate Inter-Stream Interference (ISI) and Inter-User Interference (IUI), transmitters require to have accurate and timely CSIs. Note that, in this definition and throughout the thesis, ISI refers to the interference caused by other streams targeted to the same UE and IUI refers to the interference due to the transmissions targeted to other UEs.

In a basic MU-MIMO scenario, called single-cell MIMO system, a BS simultaneously serves several UEs over the same spectrum. For downlink transmission in a single-cell MIMO system, which is the general theme in [P1]–[P5], [P7] and [P8], the BS gathers all CSIs from all the associated UEs in order to perform the spatial multiplexing and eliminate both ISI and IUI without any form of information exchange with possible neighboring BSs that are generally present in a real network. Such systems can suffer from inter-cell interference from neighboring BSs. However, for single-cell analysis in this thesis, it is for simplicity assumed that there is no inter-cell interference present in the system. In more advanced network deployments, called multi-cell MIMO systems, there can be more than one BS or transmission point on the network side which are communicating to each other to improve the network performance by either i) jointly precoding and transmitting the data streams, called Coordinated Multi-Point (CoMP) transmission [44, 64]; or ii) seeking to reduce inter-cell interference and IUI through joint precoder (and receiver filter) optimization while still supporting each UE by only one BS. The considered scenario in this thesis is the latter which is discussed in details in [P6]. In general, such multi-cell MIMO systems are categorized into two classes as shown in Figure 2.2 and are listed below [65].

- *Centralized:* The optimal system performance in the considered multi-cell MIMO network can be achieved by adopting a central controller which collects all the CSIs between all the BSs and the UEs [65]. Network-level optimization is then carried out at the central controller to perform the optimal spatial multiplexing, i.e., jointly optimize the precoders of the involved BSs and possibly also the UE side receiver spatial filters. The knowledge about the calculated optimal multiplexing is then distributed among all the corresponding transmitting BSs. In order to have feasible delay between CSI acquisition and data transmission phases in this method, large number of low-latency links are required.
- *Decentralized:* In many scenarios, networks cannot afford enough low-latency backhaul resources and/or there is no central controller. Decentralized spatial multiplexing can then be deployed which is carried out at each BS as shown in [65]. In such systems, due to lack of a centralized spatial multiplexer which has all the

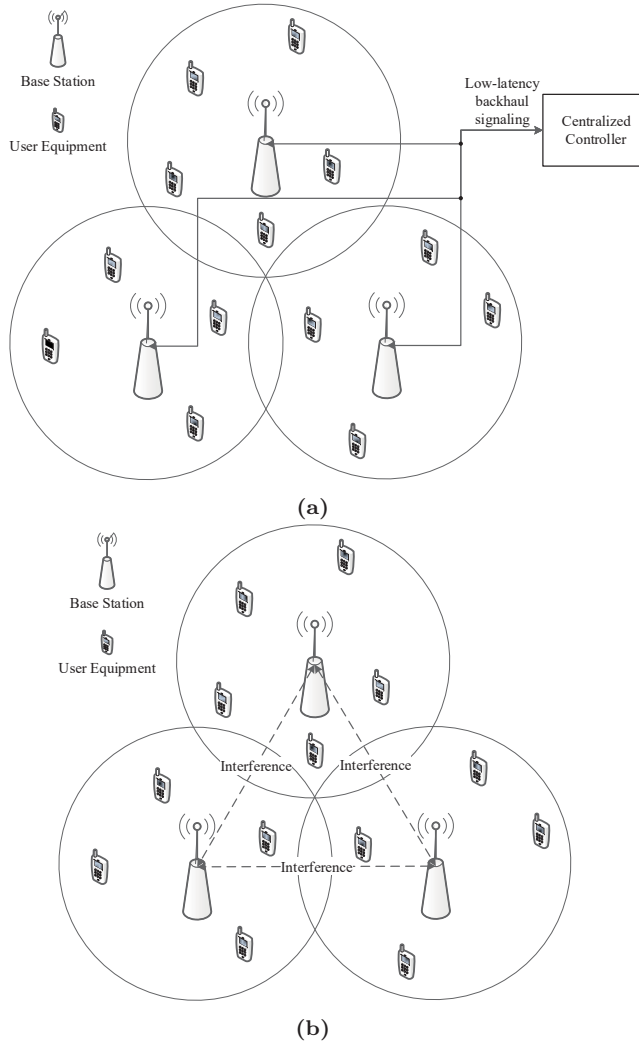


Figure 2.2: Multi-cell MU-MIMO systems (a) centralized; (b) decentralized.

CSIs between all the transmitters and receivers, BSs calculate their own set of precoders and then exchange limited information with their neighboring cells to avoid interference in the network.

In addition to the two main scenarios mentioned above, there can be other deployments based on the requirements of the system, e.g., semi-distributed, which are out of the scope of this thesis.

2.1.1 Principal System Model

For simplicity, let us consider downlink data transmission in a single-cell MU-MIMO system, while the multi-cell system model is presented in details later in Section 3.4. In the considered scenario, a BS serves K UEs on the same time-frequency resources. The BS is equipped with N antenna elements, while the number of antennas in the k -th UE is denoted

by M_k and $\sum_{i=1}^K M_k = M_{tot}$. Note that, all the following signal and system models are written for an arbitrary subcarrier of the underlying orthogonal frequency division multiplexing/multiple access (OFDM/OFDMA) waveform. For notational simplicity, the subcarrier index is not shown explicitly throughout the thesis. The fundamental multi-user downlink transmission signal model can be expressed as

$$\mathbf{r} = \sqrt{\rho_d} \mathbf{H} \mathbf{x} + \mathbf{n}, \quad (2.1)$$

where $\mathbf{H} \in \mathbb{C}^{M_{tot} \times N}$ is the effective downlink channel matrix and can be written as $\mathbf{H} = [\mathbf{H}_1^T, \dots, \mathbf{H}_K^T]^T$ with $\mathbf{H}_k \in \mathbb{C}^{M_k \times N}$ being the effective downlink channel matrix towards the k -th UE. In above, $\mathbf{r} \in \mathbb{C}^{M_{tot} \times 1}$ denotes the received multi-user downlink signal vector corresponding to all M_{tot} antennas in the UE side, $\mathbf{x} \in \mathbb{C}^{N \times 1}$ is the signal vector transmitted from the BS antennas, ρ_d is the transmitted Signal-to-Noise Ratio (SNR) of the downlink channel, and $\mathbf{n} \in \mathbb{C}^{M_{tot} \times 1}$ is the additive receiver noise vector at UE side with independent and identically distributed (i.i.d.) $\mathcal{CN}(0, 1)$ elements.

2.1.2 Transmit Precoding

Precoding is a processing technique responsible to perform spatial multiplexing, i.e., it splits the transmit signal into several spatial signals towards different receivers and tries to modify the input signal to optimally match the channel [51]. As mentioned earlier, in order to perform such processing, the transmitter requires to have CSI of all the involved radio links.

In (2.1), the precoded spatial transmit signal vector in the BS is denoted by $\mathbf{x} = [x_1, \dots, x_N]^T$, where x_n is the precoded sample transmitted from the n -th antenna in the BS. The precoded downlink transmit vector \mathbf{x} can be expressed as

$$\mathbf{x} = \beta \mathbf{U} \mathbf{s}, \quad (2.2)$$

where $\mathbf{U} = [\mathbf{U}_1, \dots, \mathbf{U}_K] \in \mathbb{C}^{N \times Q_{tot}}$ is the precoder matrix with $\mathbf{U}_k \in \mathbb{C}^{N \times Q_k}$ being precoder matrix corresponding to the data streams targeted to the k -th UE. Here, the total number of streams in the network is $Q_{tot} = \sum_{i=1}^K Q_k$, where Q_k is the number of downlink data streams towards the k -th UE before precoding. The precoder column vector corresponding to the q -th data stream towards the k -th UE can be shown as $\mathbf{u}_{k,q} \in \mathbb{C}^{N \times 1}$. The normalized UE data vector is denoted by $\mathbf{s} = [\mathbf{s}_1^T, \dots, \mathbf{s}_K^T]^T \in \mathbb{C}^{Q_{tot} \times 1}$, where $\mathbf{s}_k \in \mathbb{C}^{Q_k \times 1}$ is the data vector targeted to the k -th UE, $s_{k,q}$ denotes the q -th data stream in \mathbf{s}_k , and $\mathbb{E}[\mathbf{s} \mathbf{s}^H] = \mathbf{I}_{Q_{tot}}$. The transmit sum-power normalization is achieved through β which constrains the total BS transmit sum-power to 1, i.e., $\mathbb{E}[\mathbf{x}^H \mathbf{x}] = 1$. In order to satisfy this condition, β is chosen as [66]

$$\beta = \left(\sqrt{\mathbb{E}[\text{Tr}(\mathbf{U}^H \mathbf{U})]} \right)^{-1}. \quad (2.3)$$

The received downlink multi-user signal vector corresponding to all M_{tot} antennas in the UE side can be re-written by substituting (2.2) in (2.1) as

$$\mathbf{r} = \beta \sqrt{\rho_d} \mathbf{H} \mathbf{U} \mathbf{s} + \mathbf{n}. \quad (2.4)$$

Figure 2.3 illustrates downlink transmission chain in the presence of transmit precoding and receiver processing which is denoted by $\mathbf{W}_k = [\mathbf{w}_{k,1}, \dots, \mathbf{w}_{k,Q_k}] \in \mathbb{C}^{M_k \times Q_k}$ where

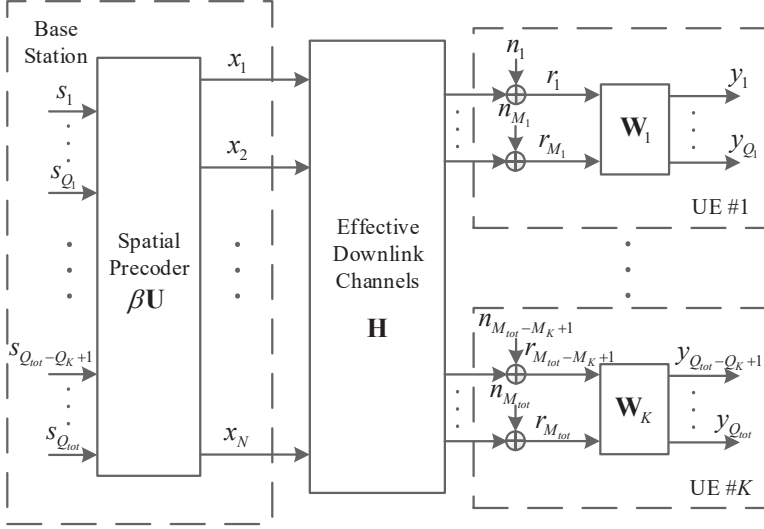


Figure 2.3: Principal illustration of downlink transmission, including transmit precoding and receiver processing.

$\mathbf{w}_{k,q} \in \mathbb{C}^{M_k \times 1}$. Note that the precoder matrix \mathbf{U} is constructed based on the estimated effective downlink channel matrix $\hat{\mathbf{H}} \in \mathbb{C}^{M_{tot} \times N}$, and its design varies depending on the available CSI and the performance criterion. In this thesis, we have covered three forms of precoders, namely, ZF, MRT, and eigen-decomposition based ones.

2.1.2.1 Zero-Forcing

For ZF precoding scheme, the precoder matrix tries to cancel out spatial multiplexing induced interference received at each UE and is constructed using the pseudo-inverse of the estimated effective downlink channel matrix as [62]

$$\mathbf{U}^{\text{ZF}} = \hat{\mathbf{H}}^H \left(\hat{\mathbf{H}} \hat{\mathbf{H}}^H \right)^{-1}. \quad (2.5)$$

The normalization scalar β^{ZF} in (2.3) can be shown to read [62]

$$\beta^{\text{ZF}} = \left(\sqrt{\mathbb{E} \left[\text{Tr} \left(\left(\hat{\mathbf{H}} \hat{\mathbf{H}}^H \right)^{-1} \right) \right]} \right)^{-1}. \quad (2.6)$$

Then, based on (2.4) and (2.5), the reception at the k -th UE is given in the following which shows that both ISI and IUI are suppressed when the BS has perfect CSI.

$$\mathbf{r}_k^{\text{ZF}} = \beta^{\text{ZF}} \sqrt{\rho_d} \mathbf{H}_k \mathbf{U} \mathbf{s} + \mathbf{n}_k = \beta^{\text{ZF}} \sqrt{\rho_d} \mathbf{s}_k + \mathbf{n}_k. \quad (2.7)$$

In order to keep the consistency of the signal model and for simplicity, throughout the thesis, it is assumed that $M_k = Q_k$, i.e., there is one data stream per UE antenna, for ZF precoding scheme.

2.1.2.2 Maximum Ratio Transmission

The goal in MRT precoding scheme is to maximize the received SNR. Having low implementation complexity is one of the reasons for popularity of this precoding scheme.

The MRT precoder matrix is constructed as [66]

$$\mathbf{U}^{\text{MRT}} = \hat{\mathbf{H}}^{\text{H}}, \quad (2.8)$$

which, based on (2.3), leads to the normalization scalar β^{MRT} being [66]

$$\beta^{\text{MRT}} = \left(\sqrt{\mathbb{E} \left[\text{Tr} \left(\hat{\mathbf{H}} \hat{\mathbf{H}}^{\text{H}} \right) \right]} \right)^{-1}. \quad (2.9)$$

Next, having perfect CSI, the signal at the receiver of the k -th UE can be shown as

$$\mathbf{r}_k^{\text{MRT}} = \beta^{\text{MRT}} \sqrt{\rho_d} \mathbf{H}_k \mathbf{U} \mathbf{s} + \mathbf{n}_k = \beta^{\text{MRT}} \sqrt{\rho_d} \mathbf{H}_k \hat{\mathbf{H}}^{\text{H}} \mathbf{s} + \mathbf{n}_k. \quad (2.10)$$

Similar to ZF precoding scheme, throughout the thesis, there is one data stream per UE antenna when MRT precoding is deployed.

2.1.2.3 Eigen-Based

Eigen-based precoding is based on Singular Value Decomposition (SVD) [67]. The SVD of the estimated effective downlink channel matrix from the BS to the k -th UE, $\hat{\mathbf{H}}_k \in \mathbb{C}^{M_k \times N}$, consists of three matrices and can be written as

$$\hat{\mathbf{H}}_k = \mathbf{\Lambda}_k \mathbf{\Xi}_k \mathbf{V}_k^{\text{H}}, \quad (2.11)$$

where $\mathbf{\Xi}_k \in \mathbb{C}^{M_k \times N}$ is a square/rectangular diagonal matrix of the non-negative singular values and $\mathbf{\Lambda}_k \in \mathbb{C}^{M_k \times M_k}$ and $\mathbf{V}_k \in \mathbb{C}^{N \times N}$ are complex unitary matrices.

In order to construct the precoder matrix, we first form $\mathbf{V} = [\bar{\mathbf{V}}_1, \dots, \bar{\mathbf{V}}_K] \in \mathbb{C}^{N \times M_{\text{tot}}}$ where $\bar{\mathbf{V}}_k \in \mathbb{C}^{N \times M_k}$ is achieved by collecting the first M_k columns of \mathbf{V}_k , i.e., first M_k right singular vectors of $\hat{\mathbf{H}}_k$. Next, $\mathbf{\Upsilon} \in \mathbb{C}^{N \times M_{\text{tot}}}$ is calculated as $\mathbf{\Upsilon} = \mathbf{V} (\mathbf{V}^{\text{H}} \mathbf{V})^{-1}$ which can be shown as $\mathbf{\Upsilon} = [\mathbf{\Upsilon}_1, \dots, \mathbf{\Upsilon}_K]$. In the next step, we form another reduced-size matrix called $\tilde{\mathbf{\Upsilon}}_k \in \mathbb{C}^{N \times Q_k}$ by taking the first Q_k columns of $\mathbf{\Upsilon}_k \in \mathbb{C}^{N \times M_k}$. Finally, we form the precoder matrix as

$$\mathbf{U}^{\text{EIG}} = [\tilde{\mathbf{\Upsilon}}_1, \dots, \tilde{\mathbf{\Upsilon}}_K], \quad (2.12)$$

and the normalization scalar β^{eig} reads

$$\beta^{\text{EIG}} = \left(\sqrt{\mathbb{E} \left[\text{Tr} \left(\mathbf{U}^{\text{EIG}} \mathbf{U}^{\text{EIG}}^{\text{H}} \right) \right]} \right)^{-1}. \quad (2.13)$$

Thus, for the perfect CSI scenario, the received signal at the k -th UE can be expressed as

$$\mathbf{r}_k^{\text{EIG}} = \beta^{\text{EIG}} \sqrt{\rho_d} \mathbf{H}_k \mathbf{U} \mathbf{s} + \mathbf{n}_k = \beta^{\text{EIG}} \sqrt{\rho_d} \bar{\mathbf{\Lambda}}_k \bar{\mathbf{\Xi}}_k \mathbf{s}_k + \mathbf{n}_k, \quad (2.14)$$

where $\bar{\mathbf{\Lambda}}_k \in \mathbb{C}^{M_k \times Q_k}$ contains the first Q_k columns (left singular vectors) of $\mathbf{\Lambda}_k$ and $\bar{\mathbf{\Xi}}_k \in \mathbb{C}^{Q_k \times Q_k}$ is a diagonal matrix with the Q_k largest singular values of $\hat{\mathbf{H}}_k$ as its diagonal entries.

2.1.3 Receiver Processing

As can be seen in (2.7), (2.10), and (2.14), even with perfect CSI at the BS side, the received signals are not necessarily the corresponding transmitted data streams and additional receiver processing stage may thus be adopted. For detection purposes, the receiver at the k -th UE, \mathbf{W}_k , then seeks to further separate the Q_k desired parallel data streams from the received signal \mathbf{r}_k , while also taking the noise into account, as follows

$$\mathbf{y}_k = \mathbf{W}_k^H \mathbf{r}_k = \sqrt{\rho_d} \mathbf{W}_k^H \mathbf{H} \mathbf{x} + \mathbf{W}_k^H \mathbf{n}. \quad (2.15)$$

There are various types of receiver processing approaches which can be employed based on their complexity and the assumed precoder and system scenario. Chapter 3 and Chapter 4 provide more details regarding the ones which are used in this thesis work.

2.1.4 Rate Calculation

Having the information about the received signal, incorporating also the impacts of the receiver spatial filters, if adopted, one can calculate SINR which is then used to determine transmission rate. In this thesis, depending on the type of information available at the receiver side, there are two different rate expressions which are based on either instantaneous SINR, denoted by γ , or effective SINR, denoted by SINR in the mathematical expressions.

In the case that the receiver has information regarding the current instance of the precoded downlink channel, SINR can be calculated for that particular channel realization and is called instantaneous SINR. Having instantaneous SINR corresponding to the q -th data stream in the k -th UE, $\gamma_{k,q}$, a lower bound on the capacity associated to this stream, can be expressed as [56, 66]

$$\zeta_{k,q} \geq R_{k,q} = \mathbb{E}[\log_2 (1 + \gamma_{k,q})], \quad (2.16)$$

where the expectation is with respect to channel and non-reciprocity parameters realizations. In (2.16), $\zeta_{k,q}$ is the capacity and $R_{k,q}$ is its lower bound which is called achievable rate. This achievable rate can be summed over all the available streams and UEs to obtain achievable sum-rate, R , as

$$\zeta \geq R = \sum_{k=1}^K \sum_{q=1}^{Q_k} \mathbb{E}[\log_2 (1 + \gamma_{k,q})]. \quad (2.17)$$

where ζ is the system capacity.

In case the channel is deterministic and there is no information regarding the current instance of the channel and thus statistical properties of the channel are employed to decode the received signal [56, 62], the term effective SINR is used, which is discussed in details in Chapter 4. Having effective SINR for the q -th data stream in the k -th UE, $\text{SINR}_{k,q}$, corresponding achievable rate and achievable sum-rate, can be given as [56, 62]

$$\begin{aligned} \zeta_{k,q} &\geq R_{k,q} = \log_2 (1 + \text{SINR}_{k,q}) \\ \zeta \geq R &= \sum_{k=1}^K \sum_{q=1}^{Q_k} \log_2 (1 + \text{SINR}_{k,q}). \end{aligned} \quad (2.18)$$

2.1.5 Massive MIMO

Small-scale wireless devices and systems using MU-MIMO are allowing for relatively limited number of antennas to be deployed at a particular device, i.e., at most 8. In contrast, massive MIMO is based on the challenging idea of increasing the number of antennas in the BS side with an order of magnitude or more, where $N \gg M_{tot}$, hence improving the performance of the system in all the metrics, including spectral and radiated energy efficiencies. Massive MIMO tries to benefit from all the advantages of small-scale MIMO on a much greater scale. Thus, it is envisioned to be one of the key enabling technologies for the next generation of cellular networks known as 5G [14, 15].

Utilizing more antennas in the BS side provides more degrees of freedom to massive MIMO systems which in turn increases the maximum number of UEs that can be supported in the same time-frequency resources. Although, conventional signal processing techniques (e.g., maximum likelihood detection) become prohibitively complex in massive MIMO systems, linear precoding techniques, e.g., ZF and MRT are shown to be asymptotically optimal with increasing N [62]. It is also shown that very high spectral efficiencies can already be achieved with N being in the order of several tens or hundreds [60–63]. A very interesting phenomenon which helps massive MIMO systems reach such high spectral efficiencies is called channel hardening. Channel hardening means having less fluctuations in the norms of the beamformed channel vectors and happens as the number of antennas in a device grows larger [68]. This phenomenon has lots of implications in massive MIMO systems. For example, due to channel hardening, a fading MIMO channel can be seen as a deterministic scalar channel after beamforming [69]. This characteristic of massive MIMO systems is later on used in Chapter 4.

2.2 TDD

In order to employ the mentioned precoding schemes, the BS is required to have accurate CSI. Generally, in FDD-based MIMO systems, this CSI is acquired by feedback received from the UE side. In such systems, UEs try to estimate downlink channels based on the received downlink pilots transmitted by the BS and signal the estimated downlink channel information back to the BS [53]. This dedicated feedback signaling, however, is not needed in TDD-based systems as they rely on the reciprocity of physical downlink and uplink channels within each coherence interval to acquire CSI at the transmitter [55]. In such systems, UEs transmit uplink pilots to BS to facilitate uplink channel estimation. The BS can then employ the information about the uplink channels, which in theory matches the one of the downlink channels, for precoding purposes.

Note that, in FDD-based networks, the number of pilots required for estimating the downlink channel is proportional to the number of antennas in the BS side which leads to huge overhead in massive MIMO systems. Thus, massive MIMO systems are typically assumed to employ TDD, where, especially with single-antenna UEs, the required amount of resources is only proportional to the number of served UEs which is typically much smaller than the number of BS antennas, i.e., $K \ll N$ [55, 60].

2.3 Channel Non-Reciprocity Problem

The channel reciprocity law in TDD systems applies to physical propagation channels. However, the effective downlink and the effective uplink channels, which incorporate also the impacts of the involved transceiver circuits and antenna systems in addition to the

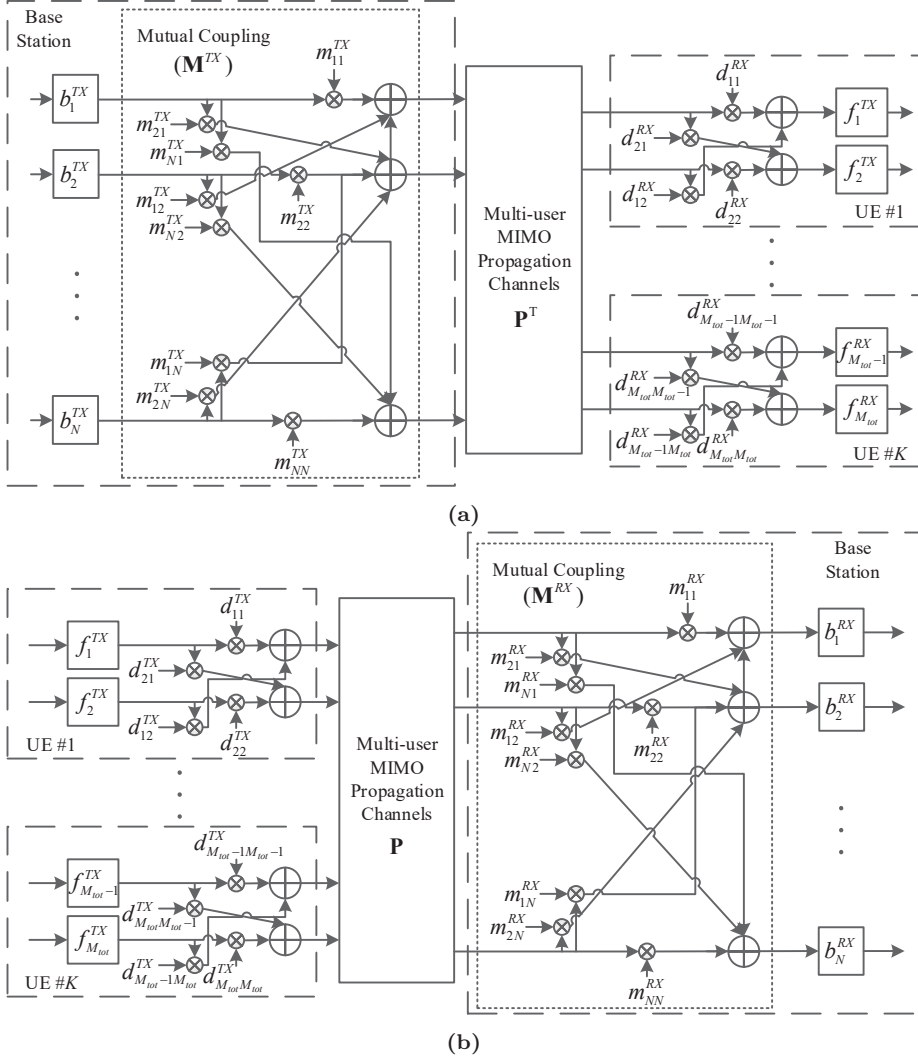


Figure 2.4: Principal illustration of effective (a) downlink and (b) uplink channels including propagation channels, transceivers FRs and antenna mutual coupling in the devices. Note that a specific example of dual antenna UEs is shown here.

propagation channels, are generally not reciprocal. This non-reciprocity is caused by the differences in transmitting and receiving mode behaviors of the transceivers and antenna systems, which depend on the hardware configuration and the operating conditions, e.g., temperature, [70–76]. In particular, such differences are caused by unavoidable mismatches between transmitter and receiver chains of any individual transceiver, namely, i) FR mismatches; ii) mismatches in mutual coupling effects between the antenna elements (in multi-antenna devices) [77, 78].

As illustrated in Figure 2.4, the effective downlink and uplink channels are generally cascades of transceiver FRs and antenna mutual coupling at the transmitting side, physical propagation channels, and transceiver FRs and antenna mutual coupling at the receiving side. Based on this, the effective downlink channel \mathbf{H} and the effective uplink channel

$\mathbf{G} \in \mathbb{C}^{N \times M_{tot}}$ can be shown to read [77]

$$\begin{aligned}\mathbf{H} &= \mathbf{F}^{RX} \mathbf{D}^{RX} \mathbf{P}^T \mathbf{M}^{TX} \mathbf{B}^{TX} \\ \mathbf{G} &= \mathbf{B}^{RX} \mathbf{M}^{RX} \mathbf{P} \mathbf{D}^{TX} \mathbf{F}^{TX},\end{aligned}\tag{2.19}$$

where $\mathbf{F} = \text{diag}(f_1, \dots, f_{M_{tot}}) \in \mathbb{C}^{M_{tot} \times M_{tot}}$ is the FR matrix of the UEs, block-diagonal matrix $\mathbf{D} \in \mathbb{C}^{M_{tot} \times M_{tot}}$ represents the antenna mutual coupling matrix at UE side, $\mathbf{B} = \text{diag}(b_1, \dots, b_N) \in \mathbb{C}^{N \times N}$ is the FR matrix of the BS, $\mathbf{M} \in \mathbb{C}^{N \times N}$ is the antenna mutual coupling matrix of the BS, and $\mathbf{P} \in \mathbb{C}^{N \times M_{tot}}$ is the reciprocal physical propagation channel. The superscripts TX and RX represent the transmitting and receiving modes, respectively.

Based on (2.19), the relation between the effective downlink and uplink channels can now be established as

$$\mathbf{H} = \mathbf{A} \mathbf{G}^T \mathbf{C},\tag{2.20}$$

where the matrices \mathbf{A} and \mathbf{C} read

$$\begin{aligned}\mathbf{A} &= \mathbf{F}^{RX} \mathbf{D}^{RX} (\mathbf{D}^{TX})^{-T} (\mathbf{F}^{TX})^{-1} \\ \mathbf{C} &= (\mathbf{B}^{RX})^{-1} (\mathbf{M}^{RX})^{-T} \mathbf{M}^{TX} \mathbf{B}^{TX}.\end{aligned}\tag{2.21}$$

In (2.20) and (2.21), the matrices $\mathbf{A} \in \mathbb{C}^{M_{tot} \times M_{tot}}$ and $\mathbf{C} \in \mathbb{C}^{N \times N}$ are denoting the transceivers' non-reciprocity at the UE and the BS sides, respectively. The UE side non-reciprocity matrix \mathbf{A} is block-diagonal and can be written as

$$\mathbf{A} = \begin{bmatrix} \mathbf{A}_1 & \mathbf{0} & \cdots & \mathbf{0} \\ \mathbf{0} & \mathbf{A}_2 & \ddots & \vdots \\ \vdots & \ddots & \ddots & \mathbf{0} \\ \mathbf{0} & \cdots & \mathbf{0} & \mathbf{A}_K \end{bmatrix}.\tag{2.22}$$

In above, $\mathbf{A}_k \in \mathbb{C}^{M_k \times M_k}$ represents the transceivers non-reciprocity matrix in the k -th UE. Matrices \mathbf{A} and $\mathbf{A}_k \in \mathbb{C}^{M_k \times M_k}$ can then be decomposed as $\mathbf{A} = \mathbf{I}_{M_{tot}} + \mathbf{A}'$ and $\mathbf{A}_k = \mathbf{I}_{M_k} + \mathbf{A}'_k$, respectively. Whereas, the overall BS transceiver non-reciprocity matrix \mathbf{C} which includes mutual coupling mismatch, is generally a full matrix and can be written as $\mathbf{C} = \mathbf{I}_N + \mathbf{C}'$. Based on (2.20), the effective downlink and uplink channels can be assumed to be reciprocal if and only if $\mathbf{A}' = \mathbf{0}_{M_{tot}}$ and $\mathbf{C}' = \mathbf{0}_N$. Throughout this thesis, we assume that the elements in \mathbf{A}' , and \mathbf{C}' are zero-mean.

Generally, the channel non-reciprocity characteristics in transceivers vary very slowly compared to the variations in the propagation channel and thus \mathbf{A} and \mathbf{C} can be assumed to remain constant over many channel coherence intervals [76].

CHAPTER 3

ANALYSIS AND MITIGATION OF CHANNEL NON-RECIPROCITY IN SMALL-SCALE MIMO SYSTEMS

This chapter is based on the work in [P6]–[P8] and focuses on channel non-reciprocity in small-scale TDD MU-MIMO downlink transmission. [P7] and [P8] address the non-reciprocity problem in TDD single-cell MU-MIMO systems, while [P6] focuses on the non-reciprocity issues in multi-cell MIMO scenario. In particular, in [P7], joint impacts of both channel non-reciprocity sources, namely transceiver FR mismatch and antenna mutual coupling mismatches, on precoded single-cell MU-MIMO are analyzed. Furthermore, based on the detailed derived signal and system models, the resulting performance degradation in terms of instantaneous SINR and the corresponding achievable downlink sum-rate are characterized in [P7]. Efficient OTA type pilot-based estimation framework for estimation and mitigation of FR mismatch in BS transceiver is proposed in [P8] for precoded single-cell MU-MIMO systems. The effects of transceiver FR mismatches at the UE side on the performance of coordinated TDD multi-cell MIMO is covered in [P6] where both centralized and decentralized precoding schemes are considered. In general, only the main steps and results are summarized in the following sections while all the detailed derivations are available in the thesis publications [P6]–[P8].

3.1 Background and Prior Art

This section briefly reviews the related work in the literature focusing on channel non-reciprocity problem in small-scale TDD MU-MIMO systems.

The impacts of transceivers FR mismatches on small-scale TDD single-cell ZF precoded MU-MIMO systems are studied in [71, 77, 79] and references therein. [71, 77] also acknowledge the channel non-reciprocity problem due to antenna mutual coupling mismatches, however do not analyze their impact on the signal and system characteristics. Also, eigen-based precoding, which is another important precoding technique, has not been analyzed in this context in the existing literature. In TDD multi-cell MIMO context, only

few works, e.g., [80], have focused on addressing the channel non-reciprocity problem. In such systems, more sophisticated processing is required to construct precoders compared to, e.g., ZF or eigen-based precoding schemes. More specifically, as described in [65], dedicated signaling exchange between the connected UEs and the BS is needed in decentralized precoding. It can be shown that, in this scenario, OTA signaling process can be potentially influenced by UE transceiver non-reciprocity. However, to the best of our knowledge, there is no previous work analyzing the impacts of such UE transceiver non-reciprocity problem on the performance of multi-cell MIMO networks.

In the literature, there are mainly two types of estimation-mitigation approaches to cope with transceiver non-reciprocity problem. The first one is direct offline hardware estimation-calibration which provides a standard independent solution by employing additional circuitries [77, 81, 82]. However, this approach substantially increases the implementation complexity and cost for each device. The other option is OTA type estimation-mitigation algorithms [71, 76, 77, 83–85]. In this approach, in order to estimate the non-reciprocity parameters, a test calibration and feedback link with external Test Equipment (TE) requires to be established. OTA estimation algorithms do not require extra hardware to be implemented in BS devices. However, the BS needs to communicate with the TE in dedicated calibration periods. Current OTA solutions in the literature [71, 76, 77, 83–85] assume that the BS always has the knowledge about the downlink channel matrix towards the TE, e.g., via accurate high-rate feedback signaling, and uses that to compare against the measured uplink channel matrix from the TE in order to extract the non-reciprocity parameters. In practice, however, the performance of such solutions is always limited by the finite rate of feedback signaling from the TE to the BS. In addition to that, the computational complexities of deployed matrix decompositions applied in [71, 76, 77, 83–85] are far from trivial.

3.2 General Assumptions

In TDD systems, when CSI at the BS is obtained by estimating the effective uplink channel, the estimated downlink channel reads

$$\hat{\mathbf{H}} = \hat{\mathbf{G}}^T, \quad (3.1)$$

where $\hat{\mathbf{G}} \in \mathbb{C}^{N \times M_{tot}}$ is the estimated effective uplink channel. Assuming perfect effective uplink channel estimation, the resulting downlink channel estimate reads

$$\hat{\mathbf{H}} = \mathbf{G}^T, \quad (3.2)$$

which will be used to construct precoders. However, based on (2.19), even without any additive noise or other interference sources in the estimation process, biased estimation due to mismatches in transceivers is unavoidable.

3.2.1 Receiver Processing

In this chapter, we focus on one of the most common forms of the receiver processing, namely, Linear Minimum Mean Squared Error (LMMSE)-based [86], which is known to maximize the received SINR when treating the interference as noise. It minimizes the Mean Squared Error (MSE) between the transmitted and estimated data symbol vectors as

$$\mathbf{W}_k = \arg \min_{\mathbf{W}_k} \mathbb{E} \left[\left\| \mathbf{W}_k^H \mathbf{r}_k - \mathbf{s}_k \right\|^2 \right], \quad (3.3)$$

and is given by [86]

$$\mathbf{W}_k = \beta \sqrt{\rho_d} \left(\beta^2 \rho_d \sum_{i=1}^K \mathbf{H}_k \mathbf{U}_i (\mathbf{H}_k \mathbf{U}_i)^H + \mathbf{I}_{M_k} \right)^{-1} \mathbf{H}_k \mathbf{U}_k. \quad (3.4)$$

Throughout this chapter, it is assumed that UEs have perfect estimation of precoded downlink channels when constructing such receivers.

3.3 Single-Cell

In this section, we focus on channel non-reciprocity in TDD single-cell MU-MIMO systems. First, the impacts of channel non-reciprocity in terms of received instantaneous SINR and achievable downlink sum-rate are analyzed. Next, an OTA type pilot-based estimation algorithm, proposed in [P8], is employed to efficiently identify BS transceiver FR mismatch parameters, which are then used in the BS to properly pre-compensate/precoding the multi-user data to mitigate the channel non-reciprocity problem.

3.3.1 Analysis

Here, the impacts of channel non-reciprocity on the performance of ZF and eigen-based precoded TDD MU-MIMO downlink transmission are evaluated.

3.3.1.1 ZF Precoding

Incorporating (3.2), (2.20), and (2.6), in the downlink system model in (2.4), the received signal at the k -th UE reads

$$\begin{aligned} \mathbf{r}_k^{\text{ZF}} &= \beta^{\text{ZF}} \sqrt{\rho_d} \mathbf{H}_k \mathbf{U}^{\text{ZF}} \mathbf{s} + \mathbf{n}_k = \beta^{\text{ZF}} \sqrt{\rho_d} \mathbf{A}_k \hat{\mathbf{H}}_k \mathbf{C} \mathbf{U}^{\text{ZF}} \mathbf{s} + \mathbf{n}_k \\ &= \beta^{\text{ZF}} \sqrt{\rho_d} \mathbf{A}_k \mathbf{s}_k + \beta^{\text{ZF}} \sqrt{\rho_d} \mathbf{A}_k \hat{\mathbf{H}}_k \mathbf{C}' \mathbf{U}^{\text{ZF}} \mathbf{s} + \mathbf{n}_k. \end{aligned} \quad (3.5)$$

In above, the first term in the last line consists of the desired streams while the term following that is mostly IUI.

One interesting observation, based on (3.5), is that despite having transceiver FR and antenna mutual coupling mismatches at the UE side, we can achieve IUI-free reception if the BS has ideal reciprocal transceiver. This can be observed in (3.5) by having $\mathbf{C}' = \mathbf{0}_N$ (i.e., perfect reciprocity at the BS side), which then reduces to

$$\mathbf{r}_k^{\text{ZF}} = \beta^{\text{ZF}} \sqrt{\rho_d} \mathbf{A}_k \mathbf{s}_k + \mathbf{n}_k. \quad (3.6)$$

Thus, based on the provided analysis, it can be claimed that the non-reciprocity characteristics of BSs transceivers are clearly more critical than those of the UE side.

In the general case, when the BS transceiver is not totally reciprocal, i.e., $\mathbf{C}' \neq \mathbf{0}_N$, then the second term in the last line of (3.5) becomes a non-zero matrix with entries depending on the values of the effective downlink channel matrix \mathbf{H}_k and the non-reciprocity parameters. In this general case, both ISI and IUI occur at the receiver of the k -th UE even if the implementation at the UE side is perfect.

After receiving the downlink signal in the k -th UE receiver, an LMMSE-based receiver spatial processing, $\mathbf{w}_{k,q}$, based on (3.4), tries to separate the q -th data stream in the k -th

UE from the received signal and possibly suppress the interference as

$$y_{k,q}^{\text{ZF}} = \mathbf{w}_{k,q}^{\text{H}} \mathbf{r}_k^{\text{ZF}} = \underbrace{\beta^{\text{ZF}} \sqrt{\rho_d} \mathbf{w}_{k,q}^{\text{H}} \left(\mathbf{a}_{k,q} + \mathbf{A}_k \hat{\mathbf{H}}_k \mathbf{C}' \mathbf{u}_{k,q}^{\text{ZF}} \right)}_{\text{useful signal}} s_{k,q} + \underbrace{z_{k,q}^{\text{ZF,ISI}} s_{k,i}}_{\text{ISI}} + \underbrace{z_{k,q}^{\text{ZF,IUI}} s_{j,l}}_{\text{IUI}} + \mathbf{w}_{k,q}^{\text{H}} \mathbf{n}_k, \quad (3.7)$$

where $\mathbf{a}_{k,q} \in \mathbb{C}^{M_k \times 1}$ is the q -th column of \mathbf{A}_k which corresponds to the q -th data stream. Next, $z_{k,q}^{\text{ZF,ISI}}$ and $z_{k,q}^{\text{ZF,IUI}}$ can be expressed respectively as

$$z_{k,q}^{\text{ZF,ISI}} = \sum_{\substack{i=1 \\ i \neq q}}^{Q_k} \beta^{\text{ZF}} \sqrt{\rho_d} \mathbf{w}_{k,q}^{\text{H}} \left(\mathbf{a}_{k,i} + \mathbf{A}_k \hat{\mathbf{H}}_k \mathbf{C}' \mathbf{u}_{k,i}^{\text{ZF}} \right) \quad (3.8)$$

$$z_{k,q}^{\text{ZF,IUI}} = \sum_{\substack{j=1 \\ j \neq k}}^K \sum_{l=1}^{Q_j} \beta^{\text{ZF}} \sqrt{\rho_d} \mathbf{w}_{k,q}^{\text{H}} \mathbf{A}_k \hat{\mathbf{H}}_k \mathbf{C}' \mathbf{u}_{j,l}^{\text{ZF}}.$$

Considering the useful terms, ISI, and IUI, in (3.7), the corresponding instantaneous SINR for the q -th data stream in the k -th UE is given by

$$\gamma_{k,q}^{\text{ZF}} = \frac{\left| \beta^{\text{ZF}} \sqrt{\rho_d} \mathbf{w}_{k,q}^{\text{H}} \left(\mathbf{a}_{k,q} + \mathbf{A}_k \hat{\mathbf{H}}_k \mathbf{C}' \mathbf{u}_{k,q}^{\text{ZF}} \right) \right|^2}{\left| z_{k,q}^{\text{ZF,ISI}} \right|^2 + \left| z_{k,q}^{\text{ZF,IUI}} \right|^2 + \left\| \mathbf{w}_{k,q}^{\text{H}} \right\|^2}. \quad (3.9)$$

Thus, based on (2.17), the achievable sum-rate can be expressed as

$$R^{\text{ZF}} = \sum_{k=1}^K \sum_{q=1}^{Q_k} \mathbb{E} \left[\log_2 (1 + \gamma_{k,q}^{\text{ZF}}) \right]. \quad (3.10)$$

3.3.1.2 Eigen-Based Precoding

Next, we carry out the similar type of analysis for TDD MU-MIMO downlink transmission system with eigen-based precoding. With channel non-reciprocity effect in downlink channel estimation, the eigen-based precoder is constructed by decomposing the UE level sub-matrices of $\hat{\mathbf{H}}$ in (3.2), following the procedure described in Section 2.1.2.3.

The precoded downlink data signal at the receiver of the k -th UE can be expressed as

$$\begin{aligned} \mathbf{r}_k^{\text{EIG}} &= \beta^{\text{EIG}} \sqrt{\rho_d} \mathbf{H}_k \mathbf{U}^{\text{EIG}} \mathbf{s} + \mathbf{n}_k = \beta^{\text{EIG}} \sqrt{\rho_d} \mathbf{A}_k \hat{\mathbf{H}}_k \mathbf{C} \mathbf{U}^{\text{EIG}} \mathbf{s} + \mathbf{n}_k \\ &= \beta^{\text{EIG}} \sqrt{\rho_d} \mathbf{A}_k \bar{\mathbf{\Lambda}}_k \bar{\mathbf{\Xi}}_k \mathbf{s}_k + \beta^{\text{EIG}} \sqrt{\rho_d} \mathbf{A}_k \hat{\mathbf{H}}_k \mathbf{C}' \mathbf{U}^{\text{EIG}} \mathbf{s} + \mathbf{n}_k. \end{aligned} \quad (3.11)$$

Based on (3.11), when $\mathbf{C}' = \mathbf{0}_N$ which corresponds to perfect transceiver reciprocity at the BS side, there is no IUI at the k -th UE reception as the second term in the last line of (3.11) becomes zero. In this case, only ISI cancellation at the UE side is required.

In the practical scenario of $\mathbf{C}' \neq \mathbf{0}_N$, the second term in the last line of (3.11) would be a non-zero matrix with elements depending on the effective downlink channel and the mismatch parameters. In this case, the received signal at the UE receiver contains both

ISI and IUI. Next, by applying LMMSE-based spatial processing on the received signal in (3.11), the reception of the q -th stream in the k -th UE can be expressed as

$$\begin{aligned}
 y_{k,q}^{\text{EIG}} &= \mathbf{w}_{k,q}^H \mathbf{r}_k^{\text{EIG}} \\
 &= \underbrace{\beta^{\text{EIG}} \sqrt{\rho_d} \mathbf{w}_{k,q}^H \left(\mathbf{A}_k \bar{\mathbf{\Lambda}}_k \bar{\boldsymbol{\xi}}_{k,q} + \mathbf{A}_k \hat{\mathbf{H}}_k \mathbf{C}' \mathbf{u}_{k,q}^{\text{EIG}} \right)}_{\text{useful signal}} s_{k,q} \\
 &\quad + \underbrace{z_{k,q}^{\text{EIG,ISI}}}_{\text{ISI}} s_{k,i} + \underbrace{z_{k,q}^{\text{EIG,IUI}}}_{\text{IUI}} s_{j,l} + \mathbf{w}_{k,q}^H \mathbf{n}_k,
 \end{aligned} \tag{3.12}$$

with $\bar{\boldsymbol{\xi}}_{k,q} \in \mathbb{C}^{Q_k \times 1}$ being the q -th column of $\bar{\boldsymbol{\Xi}}_k$. Here, $z_{k,q}^{\text{EIG,ISI}}$ and $z_{k,q}^{\text{EIG,IUI}}$ can be written as follows

$$\begin{aligned}
 z_{k,q}^{\text{EIG,ISI}} &= \sum_{\substack{i=1 \\ i \neq q}}^{Q_k} \beta^{\text{EIG}} \sqrt{\rho_d} \mathbf{w}_{k,q}^H \left(\mathbf{A}_k \bar{\mathbf{\Lambda}}_k \bar{\boldsymbol{\xi}}_{k,i} + \mathbf{A}_k \hat{\mathbf{H}}_k \mathbf{C}' \mathbf{u}_{k,i}^{\text{EIG}} \right) \\
 z_{k,q}^{\text{EIG,IUI}} &= \sum_{\substack{j=1 \\ j \neq k}}^K \sum_{l=1}^{Q_j} \beta^{\text{EIG}} \sqrt{\rho_d} \mathbf{w}_{k,q}^H \mathbf{A}_k \hat{\mathbf{H}}_k \mathbf{C}' \mathbf{u}_{j,l}^{\text{EIG}}.
 \end{aligned} \tag{3.13}$$

Considering the desired useful signal and interference and noise terms in (3.12), the corresponding instantaneous SINR for the q -th data stream in the k -th UE is given by

$$\gamma_{k,q}^{\text{EIG}} = \frac{\left| \beta^{\text{EIG}} \sqrt{\rho_d} \mathbf{w}_{k,q}^H \left(\mathbf{A}_k \bar{\mathbf{\Lambda}}_k \bar{\boldsymbol{\xi}}_{k,q} + \mathbf{A}_k \hat{\mathbf{H}}_k \mathbf{C}' \mathbf{u}_{k,q}^{\text{EIG}} \right) \right|^2}{\left| z_{k,q}^{\text{EIG,ISI}} \right|^2 + \left| z_{k,q}^{\text{EIG,IUI}} \right|^2 + \left\| \mathbf{w}_{k,q}^H \right\|^2}. \tag{3.14}$$

Finally, the achievable system sum-rate which includes all the streams and UEs can be obtained similarly as

$$R^{\text{EIG}} = \sum_{k=1}^K \sum_{q=1}^{Q_k} \mathbb{E} \left[\log_2 \left(1 + \gamma_{k,q}^{\text{EIG}} \right) \right]. \tag{3.15}$$

3.3.2 Mitigation

Assuming reasonably good antenna isolation in each device and thus no antenna mutual coupling mismatch, there are always unavoidable FR mismatches between a transmitter and a receiver causing the channel non-reciprocity effect which degrades the system performance. For such systems, in general case for an arbitrary precoder, the received signal at the k -th UE can be shown as

$$\mathbf{r}_k = \beta \sqrt{\rho_d} \mathbf{H}_k \mathbf{U} \mathbf{s} + \mathbf{n}_k = \beta \sqrt{\rho_d} \bar{\mathbf{F}}_k \hat{\mathbf{H}}_k \bar{\mathbf{B}} \mathbf{U} \mathbf{s} + \mathbf{n}_k, \tag{3.16}$$

where $\bar{\mathbf{F}}_k \in \mathbb{C}^{M_k \times M_k}$ and $\bar{\mathbf{B}}$ are diagonal non-reciprocity matrices, containing only the FR mismatch effects in the k -th UE and the BS, respectively, and can be expressed as

$$\begin{aligned}
 \bar{\mathbf{F}}_k &= \mathbf{F}_k^{RX} (\mathbf{F}_k^{TX})^{-1} \\
 \bar{\mathbf{B}} &= (\mathbf{B}^{RX})^{-1} \mathbf{B}^{TX}.
 \end{aligned} \tag{3.17}$$

As discussed earlier, ISI and IUI are inherent in such downlink transmission systems.

In order to mitigate such non-idealities, ideally, the BS requires to have the information about the non-reciprocity parameters of its own transceiver and transceivers of all the associated UEs. However, due to dynamic changes in the UEs accessing the channel as well as time-dependent behavior of FRs of the UE transceivers, considerable amount of overhead is required to follow the transceiver non-reciprocity behavior of the UE side in a timely manner. On the other hand, as discussed in Section 3.3.1, in order to mitigate IUI, it is enough to calibrate the non-reciprocity at the BS side, while the non-reciprocity at the UE side can be handled by proper receiver processing.

Based on the above reasoning and the received signal model in (3.16), in order to have IUI-free transmission under Non-Reciprocal Channel (NRC), the transformed precoder can be given as

$$\mathbf{U}_{\text{NRC}} = \hat{\mathbf{B}}^{-1} \mathbf{U}, \quad (3.18)$$

where $\hat{\mathbf{B}} \in \mathbb{C}^{N \times N}$ is the estimated BS transceiver non-reciprocity matrix. Thus, after perfect BS transceiver non-reciprocity mitigation, the received signal at the k -th UE receiver reads

$$\mathbf{r}_k = \beta \sqrt{\rho_d} \mathbf{H}_k \mathbf{U}_{\text{NRC}} \mathbf{s} + \mathbf{n}_k = \beta \sqrt{\rho_d} \bar{\mathbf{F}}_k \hat{\mathbf{H}}_k \mathbf{U} \mathbf{s} + \mathbf{n}_k, \quad (3.19)$$

which does not contain IUI.

In order to estimate the BS transceiver non-reciprocity matrix, a single antenna TE, which can be one of the UEs or a separate device is assumed to be connected to the BS to facilitate the estimation of non-reciprocity parameters in the BS transceiver. The FR mismatch parameter in the TE is denoted by

$$\bar{f}_e = f_e^{RX} (f_e^{TX})^{-1}. \quad (3.20)$$

The effective uplink channel vector from the TE to the BS is denoted by $\mathbf{g}_e = [g_{e,1}, \dots, g_{e,N}]^T \in \mathbb{C}^{N \times 1}$. Considering the TE transceiver non-reciprocity, the relation between the effective downlink channel and the effective uplink channel vectors can be established as

$$\mathbf{h}_e = \bar{f}_e \mathbf{g}_e^T \bar{\mathbf{B}} \in \mathbb{C}^{1 \times N}. \quad (3.21)$$

During the estimation period, both the effective uplink and the effective downlink channels are assumed to remain unchanged. In developing the estimator below, the additive noise is ignored for notational convenience, while its impact is naturally considered in all the simulations for evaluating the performance of the estimator.

In the first stage of estimating the BS transceiver non-reciprocity, the BS transmits one complex pilot OFDM symbol from each of its antennas at a time to the single-antenna TE, shown as $s_{p,1}^d, \dots, s_{p,N}^d$. Thus, having a diagonal matrix representation, the received pilot sequence of length N at the TE receiver can be expressed as

$$\mathbf{r}_p^{\text{DL}} = \mathbf{h}_e \mathbf{S}_p^{\text{DL}}, \quad (3.22)$$

where, $\mathbf{S}_p^{\text{DL}} = \text{diag}(s_{p,1}^d, \dots, s_{p,N}^d) \in \mathbb{C}^{N \times N}$.

Next, in order to estimate the effective downlink channel vector, \mathbf{h}_e , at the TE side, pure ZF processing is employed which results into the following estimation

$$\hat{\mathbf{h}}_e = \mathbf{r}_p^{\text{DL}} (\mathbf{S}_p^{\text{DL}})^{-1}. \quad (3.23)$$

In [71, 77, 83], the estimated effective downlink channel, $\hat{\mathbf{h}}_e \in \mathbb{C}^{1 \times N}$ is transmitted back from the TE to the BS in order for the BS to compare the effective downlink and the effective uplink channels and extract its own transceiver non-reciprocity parameters. This feedback is assumed to be performed via perfectly accurate (infinite) feedback signaling, while in practice the accuracy of such feedback signaling is always limited to the amount of resources allocated to this stage. In addition to that, as shown in [71, 77, 83], the computational complexity of extracting non-reciprocity parameters by comparing the effective downlink and uplink channels is far from trivial. In order to tackle such problems, [P8] proposed a method where in the first step the TE precodes an uplink pilot sequence, $\mathbf{s}_P^{\text{UL}} = [s_{p,1}^u, \dots, s_{p,N}^u]^T \in \mathbb{C}^{N \times 1}$, using the estimated effective downlink channel as

$$\mathbf{x}_P^{\text{UL}} = \text{diag}(\hat{\mathbf{h}}_e)^{-1} \mathbf{s}_P^{\text{UL}} = [s_{p,1}^u/\hat{h}_{e,1}, \dots, s_{p,N}^u/\hat{h}_{e,N}]^T. \quad (3.24)$$

Next, the precoded pilot sequence is transmitted to the BS using N OFDM symbols. Note that, this procedure is done similarly in all the subcarriers. Assuming perfect effective downlink channel estimation in the TE, i.e., $\hat{\mathbf{h}}_e = \mathbf{h}_e$, the received signal matrix over all BS antennas and N OFDM symbols reads

$$\mathbf{R}_P^{\text{UL}} = \mathbf{g}_e (\mathbf{x}_P^{\text{UL}})^T = \bar{f}_e^{-1} \bar{\mathbf{B}}^{-1} \begin{bmatrix} s_{p,1}^u & \dots & \frac{s_{p,N}^u h_{e,1}}{h_{e,N}} \\ \vdots & \ddots & \vdots \\ \frac{s_{p,1}^u h_{e,N}}{h_{e,1}} & \dots & s_{p,N}^u \end{bmatrix}, \quad (3.25)$$

where each column in the received signal matrix corresponds to the received signal vector at an individual OFDM symbol instant. As can be seen in (3.25), assuming the pilot sequence \mathbf{s}_P^{UL} is known at the BS side, a scaled version of non-reciprocity parameters of the BS transceiver, $\bar{\mathbf{B}}$, can be easily extracted from the diagonal entries of $\mathbf{R}_P^{\text{UL}} \in \mathbb{C}^{N \times N}$ as

$$\hat{\bar{\mathbf{B}}}^{-1} = \text{diag}(\mathbf{s}_P^{\text{UL}})^{-1} \text{diag}(\mathbf{r}_{P,\text{diag}}^{\text{UL}}) = \bar{f}_e^{-1} \bar{\mathbf{B}}^{-1}, \quad (3.26)$$

where $\mathbf{r}_{P,\text{diag}} \in \mathbb{C}^{N \times 1}$ is the vector containing the diagonal elements of \mathbf{R}_P^{UL} . Note that, based on (3.8) and (3.13), in order to have IUI-free transmission, the BS needs to mitigate its transceiver non-reciprocity up to a constant scaling. Thus, the term \bar{f}_e^{-1} in the estimated BS non-reciprocity matrix will not cause any IUI. Finally, after estimating the non-reciprocity parameters of the BS, the precoder can be updated as (3.18).

Practical Aspects

In practice, the non-idealities in (3.22) and (3.25), e.g., additive channel noise, impact the accuracy of the BS transceiver non-reciprocity estimation. However, in order to achieve close-to-ideal performance, the accuracy of non-reciprocity parameter estimates at the BS side should be fairly high [77]. Thus, in order to further increase the accuracy of the proposed BS non-reciprocity estimation method, the following strategies are proposed in [P8].

- *Averaging*: The accuracy of BS transceiver non-reciprocity estimation can be improved by averaging several estimates which are collected from one or several TEs over consecutive pilot signaling slots. The calibration time and overhead will also increase in this method.

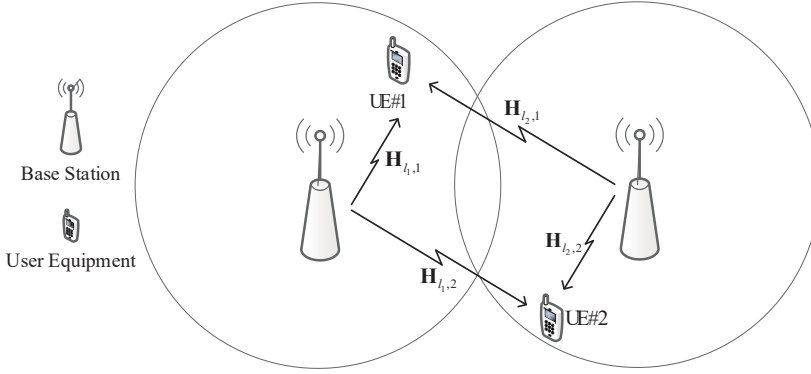


Figure 3.1: Illustration of simple multi-cell scenario example with two cells, each serving one UE, while having the corresponding precoder optimization coordination.

- *Nulling:* As mentioned earlier, in the basic scenario, the BS transceiver non-reciprocity estimation is performed over all the subcarriers while, in practice, the transceiver non-reciprocity parameters in \mathbf{B} are only mildly frequency-selective [80]. Thus, if each diagonal entry of the BS transceiver non-reciprocity matrix in time domain is modeled as an L_B -tap Finite Impulse Response (FIR) filter, the length of the filter would be much smaller than the size of the used Inverse Fast Fourier Transform (IFFT)/Fast Fourier Transform (FFT), i.e., $L_B \ll N$. Based on this, in order to filter down part of the estimation errors, the diagonal entries in $\hat{\mathbf{B}}$ are transformed to time domain using an N point IFFT and then the last N_{null} samples are nulled, where $N - N_{null} > L_B$. Similar approach can be performed in the effective downlink channel estimation stage in (3.23), given that the propagation channel from the BS to TE side has short delay spread.
- *Choice of TE:* It is preferred to have TE/s with good channel quality in order to achieve better accuracy in the estimation process.

More detailed discussion regarding the practical aspects of the proposed method can be found in [P8].

3.4 Multi-Cell

This section analyzes the impacts of UE side transceiver FR mismatches on the performance of coordinated TDD multi-cell MIMO with centralized and decentralized precoding schemes. In this part of the thesis work, we deliberately focus on UE side non-reciprocity to show and demonstrate that in multi-cell precoding systems, also that can be a clear performance limiting factor.

3.4.1 Multi-Cell System Model

We expand the system model described in Section 2.1 to cover multi-cell scenario. In this model, the network consists of L BSs where each BS is equipped with N antennas, while the total number of UEs, antennas in the UE side, and downlink data streams are kept as K , M_{tot} , and Q_{tot} , respectively. It is assumed that the k -th UE is associated to only one BS in the network, called l_k , and thus the effective downlink channel matrix between

the k -th UE and the BS serving the j -th UE can be written as $\mathbf{H}_{l_j,k} \in \mathbb{C}^{M_k \times N}$ as shown in the simple example of having 2 BSs having one associated UE each in Figure 3.1.

Here, all the downlink streams are first precoded in their respective BSs and then transmitted simultaneously to the UEs in the network. Thus, after applying an LMMSE-based receiver processing, $\mathbf{w}_{k,q}$, the q -th data stream in the k -th UE can be extracted as

$$y_{k,q} = \mathbf{w}_{k,q}^H \mathbf{H}_{l_k,k} \mathbf{u}_{k,q} s_{k,q} + \sum_{i=1}^K \sum_{\substack{j=1 \\ (i \neq k, j \neq q)}}^{Q_i} \mathbf{w}_{k,q}^H \mathbf{H}_{l_i,k} \mathbf{u}_{i,j} s_{i,j} + \mathbf{w}_{k,q}^H \mathbf{n}_k. \quad (3.27)$$

Note that, in the multi-cell scenario study, the transmit sum-power in each BS is not always equal to 1 and thus the notation of β is not going to be used. Instead the precoder matrices are designed such that the transmit sum-power in each BS is always less than a predefined value, \mathcal{P} . For notational simplicity, we do not use transmitted downlink SNR notation ρ_d in the multi-cell scenario while instead the power of the additive receiver noise vector \mathbf{n}_k is denoted by σ_n^2 which essentially defines the transmitted SNR.

The LMMSE receiver in (3.27) can be shown to read

$$\mathbf{w}_{k,q} = \mathbf{R}_k^{-1} \mathbf{H}_{l_k,k} \mathbf{u}_{k,q}, \quad (3.28)$$

where $\mathbf{R}_k \in \mathbb{C}^{M_k \times M_k}$ corresponds to the covariance matrix at the k -th UE reception and can be expressed as

$$\mathbf{R}_k = \sum_{i=1}^K \sum_{j=1}^{Q_i} \mathbf{H}_{l_i,k} \mathbf{u}_{i,j} \mathbf{u}_{i,j}^H \mathbf{H}_{l_i,k}^H + \sigma_n^2 \mathbf{I}_{M_k}. \quad (3.29)$$

Considering $\mathbf{w}_{k,q}^H \mathbf{H}_{l_k,k} \mathbf{u}_{k,q} s_{k,q}$ as the desired signal, instantaneous SINR for the q -th data stream in the k -th UE reads [87]

$$\gamma_{k,q} = \frac{\left| \mathbf{w}_{k,q}^H \mathbf{H}_{l_k,k} \mathbf{u}_{k,q} \right|^2}{\sum_{i=1}^K \sum_{\substack{j=1 \\ (i \neq k, j \neq q)}}^{Q_i} \left| \mathbf{w}_{k,q}^H \mathbf{H}_{l_i,k} \mathbf{u}_{i,j} \right|^2 + \left\| \mathbf{w}_{k,q}^H \right\|^2 \sigma_n^2}. \quad (3.30)$$

Having the optimum LMMSE receiver, the minimum MSE for receiving the q -th stream of the k -th UE, $\zeta_{k,q}$, and its relation to the instantaneous SINR for the same stream, $\gamma_{k,q}$, can be expressed as [88]

$$\zeta_{k,q} = 1 - \mathbf{w}_{k,q}^H \mathbf{H}_{l_k,k} \mathbf{u}_{k,q} = \frac{1}{1 + \gamma_{k,q}}. \quad (3.31)$$

3.4.2 Centralized Precoding

In the centralized scenario, a central controller collects all the CSI between the BSs and all the associated UEs, $\mathbf{H}_{l_i,k}$ for $i = 1, \dots, K$ and $k = 1, \dots, K$, to achieve the optimal network performance. For this reason, antenna specific pilots are first sent from the UE side to facilitate uplink channel estimation in the BSs and then this CSI is transmitted from the BSs to the central controller via low-latency backhaul links. Next, the central controller carries out network-level weighted sum-rate maximization and

obtains the optimal precoders and receivers $\mathbf{u}_{k,q}$ and $\mathbf{w}_{k,q}$ for all the data streams in the network. Based on (3.31), for rate calculation purposes, one can substitute $\log_2(1 + \gamma_{k,q})$ with $-\log_2(\zeta_{k,q})$. Thus, the Weighted Sum-Rate (WSR) maximization problem can be transformed to a log-MSE minimization one with a constraint on transmit sum-power in each BS, expressed as

$$\begin{aligned} \min_{\mathbf{u}_{k,q}, \mathbf{w}_{k,q}} \quad & \sum_{k=1}^K \sum_{q=1}^{Q_k} \mu_k \log_2(\zeta_{k,q}) \\ \text{s. t.} \quad & \sum_{\substack{k=1 \\ l_k=l}}^K \sum_{q=1}^{Q_k} \|\mathbf{u}_{k,q}\| \leq \mathcal{P} \quad \forall l, \end{aligned} \quad (3.32)$$

where μ_k is the scheduling priority weight for the k -th UE. As described in [65, 88–90], (3.32) is generally a non-convex problem which requires unfeasible amount of resources to be solved. Thus, in practice, suboptimal set of precoders and receivers are calculated via iterative processing [65, 88–90].

3.4.3 Decentralized Precoding

In many scenarios, the network cannot afford the required low-latency backhaul resources and/or there is no central controller. In such cases, in order to maximize the network performance, the network-level cost function in (3.32) is decomposed into smaller parts which correspond to the contribution of each BS to the overall cost function by neglecting all terms that do not involve any variables of that specific cell [65]. Using such method, in addition to having some form of UE-BS signaling, each BS can construct its own local cost function. Thus, based on [65] and references therein, with a given receiver filter, each BS can independently maximize WSR by optimizing its precoders as

$$\begin{aligned} \min_{\mathbf{u}_{k,q}} \quad & \zeta_l \\ \text{s. t.} \quad & \sum_{\substack{k=1 \\ l_k=l}}^K \sum_{q=1}^{Q_k} \|\mathbf{u}_{k,q}\| \leq \mathcal{P} \quad \forall l, \end{aligned} \quad (3.33)$$

where ζ_l is the cost function at the l -th BS. As shown in [65], such decentralized precoding approach can reach the performance of a centralized one.

Next, the two main strategies proposed in [65] to implement decentralized precoding are shortly described. Then, the impacts of transceiver non-reciprocity in the UE side on both approaches are analyzed.

3.4.3.1 Strategy A : Network-wide iterations with busy bursts

The contribution of the l -th BS to the network-level cost function can be shown to read [65]

$$\zeta_l^A = -2 \sum_{\substack{k=1 \\ l_k=l}}^K \sum_{q=1}^{Q_k} \Re(p_{k,q} \mathbf{w}_{k,q}^H \mathbf{H}_{l_k,k} \mathbf{u}_{k,q}) + \sum_{k=1}^K \sum_{q=1}^{Q_k} \sum_{\substack{k'=1 \\ l'_k=l}}^K \sum_{q'=1}^{Q'_k} p_{k,q} |\mathbf{w}_{k,q}^H \mathbf{H}_{l,k} \mathbf{u}_{k',q'}|^2, \quad (3.34)$$

where $p_{k,q}$ is the weight value corresponding to the q -th stream of the k -th UE and is calculated as $p_{k,q} = \zeta_{k,q}^{-1}$. The second term in the right hand side of (3.34) comprises all the signal and interference powers generated by the l -th BS.

The l -th BS requires to have the knowledge about downlink channels towards all the UEs as well as their LMMSE receivers to evaluate (3.34). As proposed in [65], with given precoders, UEs precode their uplink pilots with the calculated LMMSE receivers and transmit these so-called busy bursts to BSs. Thus, after estimation, the l -th BS knows the equivalent channels $\mathbf{w}_{k,q}^H \mathbf{H}_{l,k}$ for $k = 1, \dots, K$ and $q = 1, \dots, Q_k$. If $l_k \neq l$, the information about the stream weight value, $p_{k,q}$, is sent from the BS l_k to the BS l via backhaul [65]. This procedure is repeated until all the BSs reach their desired convergence and find their suboptimal precoder sets.

Due to having LMMSE receive feedback rounds for each precoder update step in each BS, strategy A has slow convergence. In order to improve the convergence speed, another method can be employed in which each BS has local iteration rounds over precoders and receiver filters. This method is called strategy B and is discussed in the following.

3.4.3.2 Strategy B: Cell-specific iterations with separate busy bursts and channel sounding

As discussed in [65], in this strategy, UEs do not precode uplink pilots with their LMMSE receiver filters. Instead, the k -th UE uses the so-called whitening filter, $\Theta_k \in \mathbb{C}^{M_k \times M_k}$, as the precoder for its uplink pilots which tries to whiten the inter-cell interference and noise at its receivers as

$$\Theta_k^H \Theta_k = \bar{\mathbf{R}}_k^{-1}, \quad (3.35)$$

where $\bar{\mathbf{R}}_k \in \mathbb{C}^{M_k \times M_k}$ corresponds to the covariance matrix of inter-cell interference and noise at the k -th UE reception and can be written as

$$\bar{\mathbf{R}}_k = \sum_{\substack{i=1 \\ l_i \neq l_k}}^K \sum_{j=1}^{Q_i} \mathbf{H}_{l_i,k} \mathbf{u}_{i,j} \mathbf{u}_{i,j}^H \mathbf{H}_{l_i,k}^H + \sigma_n^2 \mathbf{I}_{M_k}, \quad (3.36)$$

with given precoders. Thus, following the reception of precoded uplink pilots, the l -th BS, which serves UE k , can obtain the following information

$$\mathbf{H}'_{l_k,k} = \Theta_k \mathbf{H}_{l_k,k}. \quad (3.37)$$

Based on this information and with given precoders, BS l_k can calculate an LMMSE receiver for receiving the q -th stream of the k -th UE, $\bar{\mathbf{w}}_{k,q} \in \mathbb{C}^{M_k \times 1}$, such that

$$\bar{\mathbf{w}}_{k,q}^H \mathbf{H}'_{l_k,k} = \mathbf{w}_{k,q}^H \mathbf{H}_{l_k,k}. \quad (3.38)$$

In the next step, at the l -th BS, the local cost function for WSR maximization can be written as [65]

$$\zeta_l^B = \sum_{\substack{k=1 \\ l_k=l}}^K \left(\bar{p}_k - \sum_{q=1}^{Q_k} p_{k,q} \mathbf{u}_{k,q}^H \mathbf{H}_{l_k,k}^H \vec{\mathbf{R}}_k^{-H} \mathbf{H}_{l_k,k} \mathbf{u}_{k,q} \right) + \mathcal{I}_l^{inter}, \quad (3.39)$$

where $\bar{p}_k = \text{Tr}(\mathbf{P}_k - \log(\det(\mathbf{P}_k)))$ and $\mathbf{P}_k = \text{diag}(p_{k,1}, \dots, p_{k,Q_k}) \in \mathbb{C}^{Q_k \times Q_k}$, while

$$\begin{aligned} \vec{\mathbf{R}}_k &= \sum_{\substack{i=1 \\ l_i=l_k}}^K \sum_{j=1}^{Q_i} \mathbf{H}_{l_k,i} \mathbf{u}_{i,j} \mathbf{u}_{i,j}^H \mathbf{H}_{l_k,i}^H + \bar{\mathbf{R}}_k \\ \mathcal{I}_l^{inter} &= \sum_{\substack{i'=1 \\ l'_i \neq l}}^K \sum_{j'=1}^{Q'_i} \sum_{\substack{i=1 \\ l_i=l}}^K \sum_{j=1}^{Q_i} p_{i',j'} |\mathbf{w}_{i',j'}^H \mathbf{H}_{l,i'} \mathbf{u}_{i,j}|^2. \end{aligned} \quad (3.40)$$

The term \mathbf{I}_l^{inter} corresponds to the inter-cell interference seen by the l -th BS, which requires information from other cells to be calculated. To facilitate that, the k -th UE broadcasts $\zeta_{k,q}^{-1/2} \mathbf{w}_{k,q}$ to be used by the interfering BSs, where $\zeta_{k,q} = p_{k,q}^{-1}$. Next, the l -th BS can construct its suboptimal set of precoders based on the cost function in (3.39) using both local and OTA iteration processes, as described in more details in [65].

3.4.4 Analysis

In this section, assuming perfect reciprocity in BS side transceivers, the impacts of transceiver non-reciprocity in the UE side on the considered coordinated multi-cell MIMO network is analyzed. Similar to 3.3.2, UEs are assumed to have reasonably good antenna isolation and thus UE transceiver FR mismatch is the only source of channel non-reciprocity. Therefore, the relation between the effective downlink channel, $\mathbf{H}_{l,k}$, and the effective uplink channel, $\mathbf{G}_{l,k}$, between the l -th BS and the k -th UE can be expressed as

$$\mathbf{H}_{l,k} = \mathbf{F}_k^{RX} (\mathbf{F}_k^{TX})^{-1} \mathbf{G}_{l,k}^T = \bar{\mathbf{F}}_k \mathbf{G}_{l,k}^T, \quad (3.41)$$

where $\bar{\mathbf{F}}_k = \mathbf{I}_{M_k} + \bar{\mathbf{F}}'_k$ and $\bar{\mathbf{F}}'_k \in \mathbb{C}^{M_k \times M_k}$ represents the non-reciprocal part of the k -th UE's transceiver. Similar to the single-cell scenario, having perfect uplink channel estimation, the estimated downlink channel from the l -th BS to the k -th UE can be acquired as $\hat{\mathbf{H}}_{l,k} = \mathbf{G}_{l,k}^T \in \mathbb{C}^{M_k \times N}$.

3.4.4.1 Centralized Precoding

In centralized precoding, the centralized controller acquires downlink channel matrices between all the BSs and all the serving UEs and calculates the MSE for all the streams based on that information. Thus, under non-reciprocal UE transceivers, the MSE corresponding to the q -th data stream of the k -th UE can be shown to read

$$\hat{\zeta}_{k,q} = 1 - \mathbf{u}_{k,q}^H \mathbf{H}_{l_k,k}^H (\mathbf{R}_k + \Omega(\bar{\mathbf{F}}'_k))^{-H} \mathbf{H}_{l_k,k} \mathbf{u}_{k,q}, \quad (3.42)$$

where

$$\Omega(\bar{\mathbf{F}}'_k) = \sigma_n^2 \bar{\mathbf{F}}'_k \bar{\mathbf{F}}_k'^H - 2\sigma_n^2 \Re(\bar{\mathbf{F}}'_k). \quad (3.43)$$

With fixed precoders and the same weights, the difference between MSEs in the ideal reciprocal scenario and the non-reciprocal case can be expressed as

$$\hat{\zeta}_{k,q} - \zeta_{k,q} = \mathbf{u}_{k,q}^H \mathbf{H}_{l_k,k}^H \left((\mathbf{R}_k + \Omega(\bar{\mathbf{F}}'_k))^{-H} - \mathbf{R}_k^{-H} \right) \mathbf{H}_{l_k,k} \mathbf{u}_{k,q}. \quad (3.44)$$

Based on (3.44), it can be shown that transceiver non-reciprocity in the UE side does not have essential impact on the performance of centralized precoding, unless both levels of UE side transceiver non-reciprocity and additive noise are very high.

3.4.4.2 Decentralized Precoding

In decentralized precoding scenario, as a result of transceiver non-reciprocity in the UE side, the obtained weight based on $\hat{p}_{k,q} = \hat{\zeta}_{k,q}^{-1}$ is deviated from the correct weight calculation using true MSE information. Thus, in this section, we assume that $\hat{p}_{k,q}$ is fixed and focus on the impacts of UE transceiver non-reciprocity on the local cost functions of both decentralized precoding strategies.

Strategy A : Network-wide iterations with busy bursts

With transceiver non-reciprocity in the UE side, instead of having $\mathbf{w}_{k,q}^H \mathbf{H}_{l,k}$ in the l -th BS, the received busy bursts can be shown to read $\mathbf{w}_{k,q}^H \bar{\mathbf{F}}_k^{-1} \mathbf{H}_{l,k}$. Thus, at the l -th BS, with given precoders and weights, the difference between the reciprocal cost function and the one with non-reciprocal UE transceivers can be expressed as

$$\begin{aligned} \hat{\zeta}_l^A - \zeta_l^A &= \sum_{i=1}^K \sum_{j=1}^{Q_i} \sum_{\substack{i'=1 \\ l'_i=l}}^K \sum_{j'=1}^{Q'_i} \hat{p}_{i,j} \left| \mathbf{w}_{i,j}^H \bar{\mathbf{F}}_i'' \mathbf{H}_{l,i} \mathbf{u}_{i',j'} \right|^2 \\ &\quad + 2\Re \left(\sum_{i=1}^K \sum_{j=1}^{Q_i} \sum_{\substack{i'=1 \\ l'_i=l}}^K \sum_{j'=1}^{Q'_i} \hat{p}_{i,j} \mathbf{w}_{i,j}^H \bar{\mathbf{F}}_i'' \mathbf{H}_{l,i} \mathbf{u}_{i',j'} (\mathbf{w}_{i,j}^H \mathbf{H}_{l,i} \mathbf{u}_{i',j'})^H \right. \\ &\quad \left. - \sum_{\substack{i=1 \\ l'_i=l}}^K \sum_{j=1}^{Q_i} \hat{p}_{i,j} \mathbf{w}_{i,j}^H \bar{\mathbf{F}}_i'' \mathbf{H}_{l,i} \mathbf{u}_{i,j} \right), \end{aligned} \quad (3.45)$$

where $\bar{\mathbf{F}}_i'' = \bar{\mathbf{F}}_i^{-1} - \mathbf{I}_{M_i} \in \mathbb{C}^{M_i \times M_i}$.

Based on (3.45), transceiver non-reciprocity in each and every UE causes divergence between the two cost functions. Therefore, severe performance degradation is expected when combined with the mentioned inaccuracies in weight calculation for $\hat{p}_{k,q}$.

Strategy B: Cell-specific iterations with separate busy bursts and channel sounding

With transceiver non-reciprocity in the UE side, the received signaling at the l -th BS reads $\hat{\mathbf{H}}_{l,i}' = \Theta_i \bar{\mathbf{F}}_i^{-1} \mathbf{H}_{l,i} \in \mathbb{C}^{M_i \times N}$ for $l_i = l$ and $\mathbf{w}_{j,q}^H \bar{\mathbf{F}}_j^{-1} \mathbf{H}_{l,j}$ for $l_j \neq l$. Thus, at the l -th BS, with given precoders and weights, the difference between the reciprocal cost function and the one with non-reciprocal UE transceivers can be written as

$$\begin{aligned} \hat{\zeta}_l^B - \zeta_l^B &= \sum_{i=1}^K \sum_{j=1}^{Q_i} \hat{p}_{i,j} \mathbf{u}_{i,j}^H \mathbf{H}_{l,i} \left(\vec{\mathbf{R}}_i^{-H} - \vec{\mathbf{R}}_i'^{-H} \right) \mathbf{H}_{l,i} \mathbf{u}_{i,j} \\ &\quad + \sum_{\substack{i'=1 \\ l'_i \neq l}}^K \sum_{j'=1}^{Q'_i} \sum_{i=1}^K \sum_{\substack{j=1 \\ l_i=l}}^{Q_i} p_{i',j'} \left(\left| \mathbf{w}_{i',j'}^H \bar{\mathbf{F}}_{i'}'' \mathbf{H}_{l,i'} \mathbf{u}_{i,j} \right|^2 + 2\Re \left(\mathbf{w}_{i',j'}^H \bar{\mathbf{F}}_{i'}'' \mathbf{H}_{l,i'} \mathbf{u}_{i,j} (\mathbf{w}_{i',j'}^H \mathbf{H}_{l,i'} \mathbf{u}_{i,j})^H \right) \right), \end{aligned} \quad (3.46)$$

where

$$\vec{\mathbf{R}}_i^{-1} - \vec{\mathbf{R}}_i'^{-1} = \vec{\mathbf{R}}_i^{-1} (\bar{\mathbf{F}}_i' \bar{\mathbf{R}}_i \bar{\mathbf{F}}_i'^H + 2\Re(\bar{\mathbf{F}}_i' \bar{\mathbf{R}}_i)) (\bar{\mathbf{F}}_i' \bar{\mathbf{R}}_i \bar{\mathbf{F}}_i'^H + 2\Re(\bar{\mathbf{F}}_i' \bar{\mathbf{R}}_i) + \vec{\mathbf{R}}_i)^{-1}. \quad (3.47)$$

Based on (3.46) and (3.47), and following the detailed discussion in [P6], under limiting assumptions of operating in high SNR region and good enough cell-separation, i.e., little inter-cell interference, the impact of transceiver non-reciprocity at the UE side is not severe. It can be further shown that without any inter-cell interference, the impacts of UE transceiver non-reciprocity on the performance would be as small as the one in a single-cell networks.

Discussion

- *Performance degradation:* As shown in (3.45) and (3.46), there is clear deviation between the cost functions in the ideal reciprocal transceivers scenario and the one with non-reciprocal UE transceivers. Due to iterative nature of the problem, it is quite challenging to carry out closed-form analysis for mapping such differences to the resulting performance degradation. However, computer simulations provided in the next section confirm that even with practically small UE side transceiver non-reciprocity levels, the resulting performance degradation can be severe. Thus, in the design and deployment of decentralized precoding scenarios, the transceiver non-reciprocity in the UE side can be considered as a limiting factor which requires to be mitigated.
- *Convergence:* As shown in [P6], in strategy B, under UE transceiver non-reciprocity, the system sum-rate decreases after certain number of iterations. The reason is the deviation between the cost functions in the ideal reciprocal scenario and the non-reciprocal case. Thus, by detecting such sum-rate declining point and stopping the iterative optimization at that particular iteration, system performance can be improved. Based on this idea, a convergence-aware processing algorithm is proposed in [P6] where the BS side can stop the WSR maximization process after two consecutive drops in the calculated sum-rate. The details of this algorithm can be found in [P6]. Computer simulation results, provided in the next section, show that the mentioned convergence-aware algorithm can effectively eliminate the performance degradation caused by the convergence problem.

More detailed discussion can be found in [P6].

3.5 Numerical Evaluations and Results

In this section, we first focus on the single-cell scenario where we evaluate the derived analysis results as well as the performance of the proposed channel non-reciprocity estimation and mitigation method. Next, for multi-cell scenario, the impacts of transceiver non-reciprocity in the UE side on the performance of different precoding schemes are evaluated. All the simulation results are averaged over enough channel and non-reciprocity parameters realizations in order to achieve reliable performance results.

3.5.1 Single-Cell

In order to evaluate the impacts of channel non-reciprocity on the performance of single-cell MU-MIMO OFDM scenario, we consider a practical case where a BS with a linear antenna array of size 4 simultaneously serves two UEs over the same subcarriers. The carrier frequency is assumed to be 2 GHz where 600 out of 1024 used subcarriers are active. The subcarrier spacing is chosen to be 15 kHz to be aligned with the basic 3rd Generation Partnership Project (3GPP) LTE specification [91]. For downlink data transmission, the propagation channel is modeled as a Rayleigh fading multi-path channel with extended Vehicular A channel power delay profile [92].

In order to better distinguish the impacts of FR and antenna mutual coupling mismatches, (2.21) can be approximated by the following

$$\begin{aligned}\mathbf{A} &\approx (\mathbf{F}^{TX})^{-1} \mathbf{F}^{RX} \mathbf{D}^{RX} (\mathbf{D}^{TX})^{-T} \\ \mathbf{C} &\approx (\mathbf{M}^{RX})^{-T} \mathbf{M}^{TX} \mathbf{B}^{TX} (\mathbf{B}^{RX})^{-1},\end{aligned}\tag{3.48}$$

where compared to (2.21) FR mismatch matrices \mathbf{F}^{TX} and \mathbf{B}^{RX} have moved to the other side of their corresponding expressions. The approximations can be justified by the fact that with practical levels of antenna mutual coupling mismatches, the only non-diagonal matrices, i.e., $\mathbf{D}^{RX} (\mathbf{D}^{TX})^{-T}$ and $(\mathbf{M}^{RX})^{-T} \mathbf{M}^{TX}$, are close to identity (diagonal) matrices.

Then, to characterize FR mismatches over 10 MHz waveform bandwidth at each transceiver at both the BS and the UE sides, 9 tap FIR filters are used which have randomly selected coefficients in time-domain. The level of these mismatches is controlled such that the variances of diagonal elements of the mismatch matrices $(\mathbf{F}_k^{TX})^{-1} \mathbf{F}_k^{RX}$ and $\mathbf{B}^{TX} (\mathbf{B}^{RX})^{-1}$, denoted with σ_F^2 and σ_B^2 , respectively, can be set to specific values. In case of having mutual coupling mismatches in transceivers, the mutual coupling mismatch matrices are chosen such that only the neighboring antenna elements interfere with each other, i.e., having $\bar{\mathbf{D}}_k = \mathbf{D}_k^{RX} (\mathbf{D}_k^{TX})^{-1} \in \mathbb{C}^{M_k \times M_k}$ and $\bar{\mathbf{M}} = (\mathbf{M}^{RX})^{-1} \mathbf{M}^{TX} \in \mathbb{C}^{N \times N}$, $\bar{d}_{k,ij} = \bar{m}_{ij} = 0$ for $|i - j| > 1$. The mutual coupling mismatches between neighboring antenna elements in the UE and the BS sides, i.e., $\bar{d}_{k,ij}$ and \bar{m}_{ij} for $|i - j| = 1$, are modeled by i.i.d. $\mathcal{CN}(0, \sigma_D^2)$ and $\mathcal{CN}(0, \sigma_M^2)$, respectively. It can be shown that even with high levels of non-reciprocity parameters, e.g., $\sigma_F^2 = \sigma_D^2 = \sigma_B^2 = \sigma_M^2 = -20$ dB (the highest non-reciprocity levels used in numerical evaluation part), in an example scenario consisting of a quad-antenna BS and a dual-antenna UE, the approximation in (3.48) leads to less than 2 percent relative error in downlink channel calculation which justifies its use.

3.5.1.1 Performance Evaluation Under Channel Non-Reciprocity

Here, we evaluate achievable system sum-rates under transceiver FR and mutual coupling mismatches at BS and UE sides. For this scenario, two parallel data streams are targeted to UE #1 while a single data stream is targeted to UE #2. In the ZF precoding scenario, UE #1 is equipped with two antennas while UE #2 is assumed to be a single-antenna device. Whereas, in the eigen-based precoding scenario, both UEs are assumed to have two antennas which allows UE #2 to take advantage of receiver diversity. As shown in Figure 3.2 (ZF precoding) and Figure 3.3 (eigen-based precoding), while UE side non-reciprocity has negligible impact on the system performance, the transceiver non-reciprocity in the BS can cause severe performance degradation, especially in high SNR region. These observations are well inline with the findings established already in Section 3.3.1.

3.5.1.2 Channel Non-Reciprocity Mitigation

Next, the performance of the proposed transceiver non-reciprocity mitigation method is evaluated. In this setup, all the transceivers are assumed to have good antenna isolation ($\sigma_M^2 = \sigma_D^2 = 0$) and thus FR mismatches are the only source of non-reciprocity in the channel. The level of FR mismatches in the BS and the UEs are set to $\sigma_B^2 = \sigma_F^2 = -20$ dB. The propagation environment between the BS and each TE, in the non-reciprocity

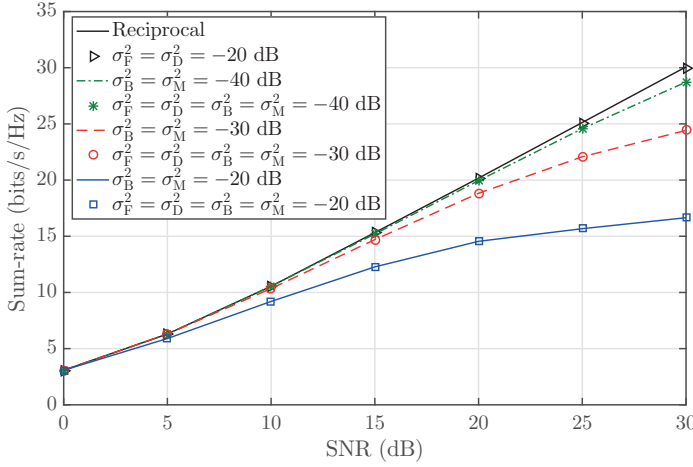


Figure 3.2: Achievable system sum-rate vs. downlink SNR (ρ_d) for a ZF precoding system with two UEs. Two parallel data streams are targeted to UE #1 while a single data stream is targeted to UE #2. The BS has 4 antennas while UE #1 is equipped with two antennas and UE #2 is assumed to be a single-antenna device.

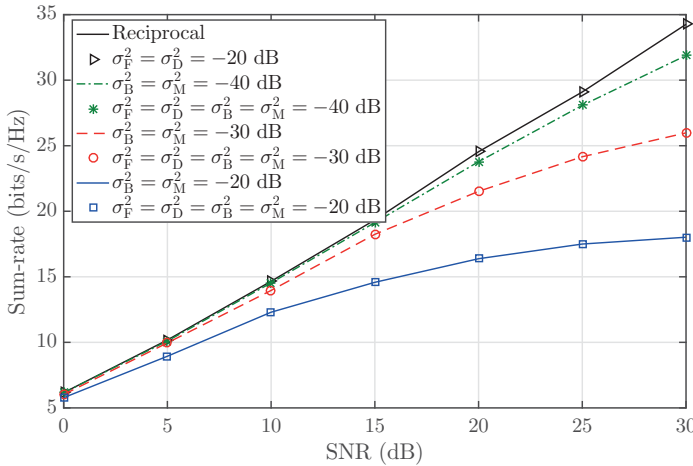


Figure 3.3: Achievable system sum-rate vs. downlink SNR (ρ_d) for an eigen-based precoding system with two UEs. Two parallel data streams are targeted to UE #1 while a single data stream is targeted to UE #2. The BS is equipped with 4 antennas while both UEs are assumed to have two antennas which allows UE #2 to take advantage of receiver diversity.

estimation phase, is modeled as a Rayleigh fading multi-path channel with pedestrian A channel power delay profile with delay spread of 410 ns [91]. The details of reference signals used in this stage can be found in [P8]. The considered simulation scenario evaluates the system performance in both single TE and dual TEs cases. The impacts of the mentioned nulling technique is also evaluated where it is employed in both downlink channel estimation in (3.23) with $N_{null} = 30$ and non-reciprocity parameters estimation in (3.26) with $N_{null} = 20$.

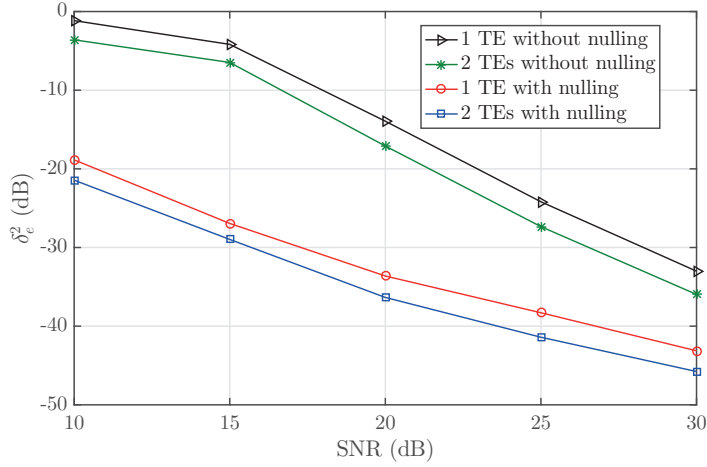


Figure 3.4: BS transceiver non-reciprocity estimation MSE vs. SNR in the estimation phase. The BS is equipped with 4 antennas while TEs are assumed to be single-antenna devices.

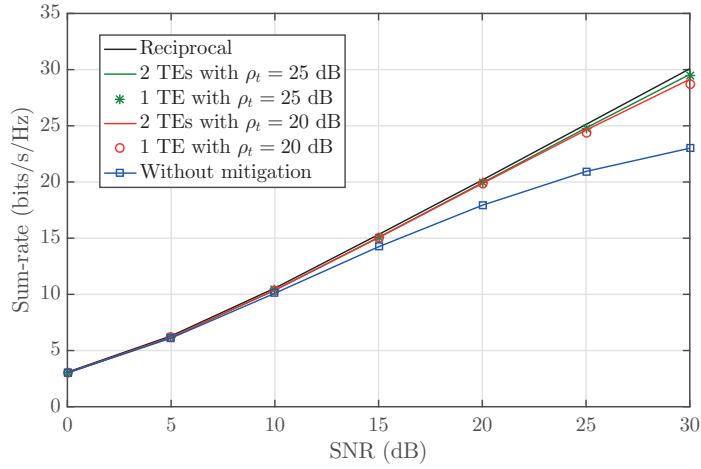


Figure 3.5: Achievable system sum-rate vs. downlink SNR (ρ_d) for a ZF precoding system with two UEs after BS transceiver mitigation. Two parallel data streams are targeted to UE #1 while a single data stream is targeted to UE #2. The BS has 4 antennas while UE #1 is equipped with two antennas and UE #2 is assumed to be a single-antenna device.

Figure 3.4 shows the effect of number of TEs, nulling technique, and SNR, on BS transceiver non-reciprocity estimation MSE. As can be seen, increasing the number of TEs, from one to two, helps the BS to have more accurate non-reciprocity estimation through averaging and improves the system performance by around 3 dB. Whereas, there is up to 10 dB gain in BS transceiver non-reciprocity estimation by employing the proposed nulling technique. As shown, MSE of the proposed BS transceiver non-reciprocity estimation method can be as low as -35 dB and -40 dB for downlink SNR values of 20 dB and 25 dB, respectively.

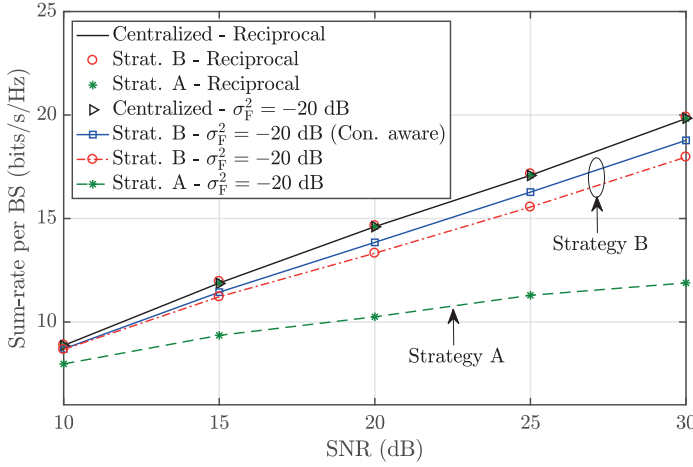


Figure 3.6: Per BS achievable sum-rate vs. downlink SNR. There are two BSs, each one is equipped with 4 antennas and serves 3 dual-antenna UEs.

The performance of the system after BS transceiver non-reciprocity mitigation is evaluated in Figure 3.5. The setup is the same as Figure 3.2 where the UEs employ LMMSE receivers while the BS utilizes ZF precoding in order to send two data streams to a dual-antenna UE and one data stream to a single-antenna UE. For simplicity, the rate loss due to adding a non-reciprocity estimation phase is not taken into account as the signaling overhead is very small. As can be seen in Figure 3.5, without mitigation, the resulting link and system performance degradation is substantial. However, when two TEs with high SNR are deployed for non-reciprocity estimation purposes, the performance of the calibrated system is very close to the reciprocal ZF precoded MU-MIMO system.

3.5.2 Multi-Cell

In this part, the impacts of UE transceiver FR mismatch on the performance of multi-cell MIMO networks are evaluated for both centralized and decentralized precoding schemes while $\sigma_B^2 = \sigma_M^2 = \sigma_D^2 = 0$. As an example, we consider a scenario where there are two quad-antenna BSs each supporting 3 dual-antenna UEs which leads to having 6 UEs in total in the network. Frequency flat Rayleigh fading channel is chosen as the propagation environment between each BS and UE pair. The average path-loss between a BS and its associated UEs is assumed to be 0 dB, while the same parameter is chosen to be 3 dB for the non-associated UEs which are supported by other BSs. The considered scenario represents a case in which all the UEs are close to cell edges. The number of iterations for in-cell optimization in strategy B for the faster convergence is chosen to be 15.

Figure 3.6 demonstrates the impacts of UE transceiver FR mismatch on the average achievable sum-rate for each BS where the number of iterations is assumed to be 30. As shown, with UE transceiver FR mismatch being $\sigma_F^2 = -20$ dB, there is essentially no performance degradation in the centralized precoding scheme. Whereas, there is substantial loss in sum-rate when decentralized precoding is used. In general, strategy A is found to be more sensitive to UE transceiver non-reciprocity compared to strategy B. It can be partially justified by the fact that impact of transceiver non-reciprocity in the UE side is related to inter-cell interference in strategy B, while, in strategy A, the

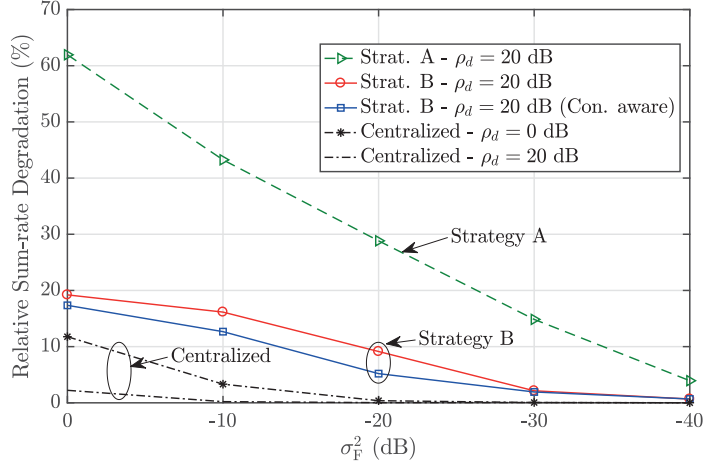


Figure 3.7: Relative per BS achievable sum-rate degradation vs. level of FR mismatch in the UE side. There are two BSs, each one is equipped with 4 antennas and serves 3 dual-antenna UEs.

impacts of UE transceiver non-reciprocity depends on all the interference sources and even the useful signal.

Finally, we evaluate the impacts of transceiver FR mismatch in the UE side on relative achievable sum-rate degradations in Figure 3.7. As illustrated, with high downlink SNR, even with extremely high values of UE transceiver FR mismatch ($\sigma_F^2 = 0$ dB), the centralized precoding scheme has negligible performance degradation. Whereas, with lower downlink SNR values, there is clear performance degradation with relatively high levels of UE transceiver FR mismatch, i.e., $\sigma_F^2 > -10$ dB. On the other hand, the performance of decentralized precoding schemes is certainly impacted even by small levels of UE transceiver FR mismatch and high SNR values. In this example scenario, in order to achieve performance close to the one in ideal reciprocal case the maximum level of transceiver FR mismatch at the UE side should be around -40 dB with strategy A, and around -30 dB with strategy B. Such low levels of FR mismatches are in general very hard to maintain in practical transceivers without efficient calibration procedures.

CHAPTER 4

ANALYSIS AND MITIGATION OF CHANNEL NON-RECIPROCITY IN MASSIVE MIMO SYSTEMS

In this chapter we extend the channel non-reciprocity analysis and mitigation studies to massive MIMO systems based on the publications [P1]–[P5]. The impacts of FR and mutual coupling mismatches on the performance of precoded TDD single-cell scenario is first analyzed based on the work in [P2] and [P3] where closed-form analytical expressions are derived for effective SINRs and the corresponding achievable sum-rates. In particular, [P2] investigates the channel non-reciprocity problem with multi-antenna UEs under imperfect CSI, i.e., without assuming perfect effective uplink channel estimation. Then, based on the analysis and depending on the availability of downlink pilots, [P4] proposes two different algorithms to efficiently estimate the level of BS transceiver non-reciprocity at the UE side which allows the network to schedule BS transceiver non-reciprocity calibration rounds more efficiently. An algorithm is then proposed in [P5] to estimate BS transceiver non-reciprocity parameters. Finally, considering the more generic case of having imperfect uplink CSI, [P1] proposes a framework in which transceiver non-reciprocity impacts in both BS and UE sides are estimated and mitigated. In this framework, owing to the proposed pilot signaling scheme, BS and UE sides' transceiver non-reciprocity matrices are first estimated and then used in the proposed channel non-reciprocity aware precoder to achieve performance close to that of ideal reciprocal channels.

4.1 Background and Prior Art

Due to the large potential of massive MIMO systems, there have been numerous studies focusing on such networks and their performances during the past few years, e.g., [58, 62, 72–75, 93–95] and references therein. Most of the massive MIMO studies in the literature, including [58, 62, 72–75, 93–95], have assumed UEs to be single-antenna devices as BSs can employ the available extra degrees of freedom offered by massive MIMO systems to reduce the required complexity of UEs [95]. However, in practice, most of the current

generation UEs are equipped with more than one antenna. This would allow the network to have higher per UE data rate. Another common assumption in many massive MIMO studies, e.g., [58, 62, 75, 93, 94], is the use of statistical properties of precoded downlink channels to acquire downlink CSIs required for detection purposes at the UE side. This is in contrast to the small-scale MIMO system scenario where UEs rely on pilot symbols sent from the BS side for estimating the effective precoded downlink channel for data decoding [66].

The impacts of channel non-reciprocity on the performance of TDD massive MIMO systems are discussed in [72–75]. In particular, [73] considers BS transceiver FR mismatch as the only source of channel non-reciprocity while [74, 75] take also FR mismatch at the UE side into account. The effects of mutual coupling mismatch in the BS side are then discussed in [72] where UEs are assumed to have ideal reciprocal transceivers. [72, 74] have focused on evaluating the impacts of channel non-reciprocity on ZF precoded TDD massive MIMO systems, whereas [73, 75] also considered MRT precoding scheme. All the mentioned works, i.e., [72–75], have considered perfect uplink channel estimation and thus do not provide any insight on the joint impacts of channel non-reciprocity and imperfect CSI in TDD networks.

The channel non-reciprocity mitigation works mentioned in Chapter 3, e.g., [71, 76, 77, 77, 81–85] are mainly developed to be applied in small-scale MIMO systems where the number of antennas in a given BS is relatively small. In general, such methods cannot be directly applied on massive MIMO systems as their implementations and computational complexities grow with the number of antennas in the BS side. In this respect, [96–99] have focused on designing channel non-reciprocity compensation methods which are feasible for massive MIMO system use. In [96–99], each BS performs self-calibration where pilots signals are sent from a chosen reference antenna in the BS and received from all other antennas in the same BS. Such methods do not require additional circuitry to be developed in the BS side. On the other hand, they only focus on mitigating FR mismatches in the BS side while neglecting mutual coupling mismatches and also transceiver non-reciprocity in the UE side.

4.2 General Assumptions

As mentioned in Chapter 2, each data stream is assumed to be allocated to one antenna in the UE side in case of having ZF or MRT precoding schemes. Since the only considered precoding schemes in this chapter are ZF and MRT, $\{m, M_k, M_{total}\}$ are used interchangeably with $\{q, Q_k, Q_{total}\}$, for notational simplicity. In this chapter, the signal models are written for a given antenna in the UE side, e.g., the m -th antenna in the UE side, as opposed to a given stream in a given UE, e.g., the q -th stream in the k -th UE. Furthermore, since each antenna has its own data stream, there is no special receiver processing as the ones in common multi-antenna receivers. A common massive MIMO assumption is also used throughout this chapter where the effective uplink channel matrix, \mathbf{G} , has i.i.d. $\mathcal{CN}(0, 1)$ elements [58, 61, 62, 66]. As shown in [100], with increasing number of antennas, such assumption very accurately models the behavior of practical massive MIMO measurements.

4.2.1 Channel Estimation

As mentioned in Chapter 2, the BS requires to estimate effective downlink channel matrix, $\hat{\mathbf{H}}$, in order to construct precoders. While in Chapter 3, perfect effective uplink channel

estimation was assumed for this purpose, the more realistic scenario of having imperfect uplink CSI at the BS side is considered here.

In order to carry out channel estimation at the BS side, mutually orthogonal uplink pilot sequences are simultaneously transmitted from UEs to the BS which can be illustrated as [58, 61, 62, 66]

$$\mathbf{Y}^p = \sqrt{\tau_u \rho_u} \mathbf{G} \mathbf{X}^p + \mathbf{N}^p, \quad (4.1)$$

where ρ_u is the transmitted SNR of the uplink channel and τ_u is the number of uplink pilots sent from each antenna in the UE side which satisfies $\tau_u \geq M_{tot}$ in order to fulfill the orthogonality condition. The uplink pilot matrix containing all the transmitted pilots from all the UEs is denoted by $\mathbf{X}^p = [\mathbf{x}_1^p, \dots, \mathbf{x}_{M_{tot}}^p]^T \in \mathbb{C}^{M_{tot} \times \tau_u}$ where $\mathbf{x}_m^p \in \mathbb{C}^{\tau_u \times 1}$ represents the uplink pilot vector transmitted from the m -th antenna in the UE side and $\mathbf{X}^p (\mathbf{X}^p)^H = \mathbf{I}_{M_{tot}}$. The received pilot matrix over all N antennas in the BS side and the additive receiver noise matrix at the BS are denoted by $\mathbf{Y}^p \in \mathbb{C}^{N \times \tau_u}$ and $\mathbf{N}^p \in \mathbb{C}^{N \times \tau_u}$, respectively, where \mathbf{N}^p has i.i.d. $\mathcal{CN}(0, 1)$ elements.

In general, after performing channel estimation, the estimated effective uplink channel can be given as

$$\hat{\mathbf{G}} = \alpha_{est} \mathbf{G} + \hat{\mathbf{G}}_e, \quad (4.2)$$

where α_{est} is a scaling factor and $\hat{\mathbf{G}}_e \in \mathbb{C}^{N \times M_{tot}}$ is the corresponding channel estimation error.

In common massive MIMO example scenario of having Minimum Mean Squared Error (MMSE) channel estimator and i.i.d. $\mathcal{CN}(0, 1)$ elements for \mathbf{G} , (4.2) can be shown to read [58, 61, 62, 66, 101]

$$\hat{\mathbf{G}} = \frac{\tau_u \rho_u}{\tau_u \rho_u + 1} \mathbf{G} + \frac{\sqrt{\tau_u \rho_u}}{\tau_u \rho_u + 1} \mathbf{Q}, \quad (4.3)$$

where $\mathbf{Q} \in \mathbb{C}^{N \times M_{tot}}$ represents the estimation error with i.i.d. $\mathcal{CN}(0, 1)$ elements. Then, based on (3.1), (4.3), and MMSE estimation orthogonality properties [101], the effective uplink channel matrix can be expressed as

$$\mathbf{G} = \hat{\mathbf{G}} + \mathcal{E}^T = \hat{\mathbf{H}}^T + \mathcal{E}^T, \quad (4.4)$$

where the estimated effective downlink channel, $\hat{\mathbf{H}}$, and the uplink channel estimation error matrix, $\mathcal{E} = [\mathcal{E}_1, \dots, \mathcal{E}_{M_{tot}}]^T \in \mathbb{C}^{M_{tot} \times N}$, are independent from each other and have i.i.d. $\mathcal{CN}\left(0, \frac{\tau_u \rho_u}{\tau_u \rho_u + 1}\right)$ and i.i.d. $\mathcal{CN}\left(0, \frac{1}{\tau_u \rho_u + 1}\right)$ elements, respectively.

Incorporating (4.4) into (2.20), the relation between the effective downlink channel and its estimation can then be established as

$$\mathbf{H} = \mathbf{A} \mathbf{G}^T \mathbf{C} = \mathbf{A} (\hat{\mathbf{H}} + \mathcal{E}) \mathbf{C}, \quad (4.5)$$

which includes the impacts of both imperfect CSI and channel non-reciprocity on the effective downlink channel estimation.

4.3 Analysis

In this section, the impacts of channel non-reciprocity on the performance of precoded TDD massive MIMO single-cell systems are analyzed. For this purpose, generic and realistic

system and channel non-reciprocity models are considered. In particular, the system model takes into account multi-antenna UEs and imperfect uplink channel estimation for CSI acquisition at the BS side, while the channel non-reciprocity model incorporates the impacts of both FR and mutual coupling mismatches at both BS and UE sides. In addition to that, the considered channel non-reciprocity model and the analysis are valid for any statistical distributions or mutual correlation of transceivers non-reciprocity matrices and variables, which enables them to also model any residual non-reciprocity after performing a given channel non-reciprocity mitigation method.

In order to have such generic channel non-reciprocity model, the following assumptions and definitions are used throughout the analysis. The elements in matrices \mathbf{A}' and \mathbf{C}' are assumed to have zero mean while the power of a'_{mi} is shown by $\sigma_{a'_{mi}}^2 = \mathbb{E}[|a'_{mi}|^2]$.

Next, matrix \mathbf{A}'_k can be represented as $\mathbf{A}'_k = [\mathbf{a}'_1^k, \dots, \mathbf{a}'_{M_k}^k]^T$. By stacking all \mathbf{a}' vectors over all the antennas in the UE side, the UE index can be dropped and thus \mathbf{a}'_m can be used for the m -th antenna in the UE side where m ranges from 1 to M_{tot} . The covariance matrix of \mathbf{a}'_m can then be denoted by $\mathbf{R}_{\mathbf{a}'_m} = \text{Cov}(\mathbf{a}'_m)$. Similarly, in the BS side, the covariance matrices $\mathbf{R}_{\mathbf{c}'_d} = \text{Cov}(\mathbf{c}'_d)$ and $\mathbf{R}_{\mathbf{c}'_{od}} = \text{Cov}(\mathbf{c}'_{od})$ can be defined based on $\mathbf{c}'_d = [c'_{11}, c'_{22}, \dots, c'_{NN}]$ and $\mathbf{c}'_{od} = [c'_{12}, c'_{13}, \dots, c'_{NN-1}]$ which are constructed by stacking all the diagonal and non-diagonal elements of \mathbf{C}' , respectively. As shown in [P2], from analysis perspective, only these defined covariances are required and the results do not depend on the exact distribution of channel non-reciprocity variables.

Based on (2.4) and (4.5), the received downlink signal at the m -th antenna in the UE side, which is assumed to be deployed in the k -th UE, can be written as

$$\begin{aligned} r_m &= \sqrt{\rho_d}\beta \mathbf{h}_m^T \mathbf{u}_m s_m + \sqrt{\rho_d}\beta \sum_{\substack{i=1 \\ i \neq m}}^{M_{tot}} \mathbf{h}_m^T \mathbf{u}_i s_i + n_m \\ &= \sqrt{\rho_d}\beta \sum_{l \in \text{UE}_k} a_{ml} \left(\hat{\mathbf{h}}_l^T + \boldsymbol{\varepsilon}_l^T \right) \mathbf{C} \mathbf{u}_m s_m + \sqrt{\rho_d}\beta \sum_{\substack{i=1 \\ i \neq m}}^{M_{tot}} \sum_{l \in \text{UE}_k} a_{ml} \left(\hat{\mathbf{h}}_l^T + \boldsymbol{\varepsilon}_l^T \right) \mathbf{C} \mathbf{u}_i s_i + n_m, \end{aligned} \quad (4.6)$$

where $\mathbf{h}_m^T \in \mathbb{C}^{1 \times N}$ in $\mathbf{H} = [\mathbf{h}_1, \dots, \mathbf{h}_{M_{tot}}]^T$ denotes the effective downlink channel towards the m -th antenna in the UE side. In above, \mathbf{u}_m and s_m are the precoding column vector and the data stream corresponding to the m -th antenna in the UE side, respectively. Whereas, UE_k refers to the set of antennas belonging to the k -th UE.

Then, following the common massive MIMO assumption discussed earlier in this chapter, UEs employ statistical properties of precoded downlink channels for detection purposes, i.e., the k -th UE uses only $\mathbb{E}[\beta \mathbf{h}_m^T \mathbf{u}_m]$ to detect s_m . Thus, the received signal at the m -th antenna in the UE side can be re-written as

$$r_m = \underbrace{\sqrt{\rho_d}\beta \mathbb{E}[\mathbf{h}_m^T \mathbf{u}_m]}_{\text{useful signal}} s_m + \underbrace{z_m^{\text{SI}} s_m}_{\text{self-interference}} + \underbrace{z_m^{\text{ISUI}} s_i}_{\text{ISI and IUI}} + n_m, \quad (4.7)$$

where

$$\begin{aligned} z_m^{\text{SI}} &= \sqrt{\rho_d} \beta \sum_{l \in \text{UE}_k} a_{ml} \left(\hat{\mathbf{h}}_l^T + \boldsymbol{\varepsilon}_l^T \right) \mathbf{C} \mathbf{u}_m - \sqrt{\rho_d} \beta \mathbb{E} \left[\mathbf{h}_m^T \mathbf{u}_m \right] \\ z_m^{\text{ISUI}} &= \sqrt{\rho_d} \beta \sum_{\substack{i=1 \\ i \neq m}}^{M_{\text{tot}}} \sum_{l \in \text{UE}_k} a_{ml} \left(\hat{\mathbf{h}}_l^T + \boldsymbol{\varepsilon}_l^T \right) \mathbf{C} \mathbf{u}_i. \end{aligned} \quad (4.8)$$

Based on (4.7), the effective SINR of the downlink data stream targeted to the m -th antenna in the UE side can be shown to read

$$\text{SINR}_m = \frac{|\sqrt{\rho_d} \beta \mathbb{E} [\mathbf{h}_m^T \mathbf{u}_m]|^2}{\mathbb{E} [z_m^{\text{SI}}]^2 + \mathbb{E} [z_m^{\text{ISUI}}]^2 + 1}, \quad (4.9)$$

which can be used, based on (2.18), to calculate the achievable sum-rate as follows

$$R = \sum_{m=1}^{M_{\text{tot}}} \log_2 (1 + \text{SINR}_m). \quad (4.10)$$

Next, analytical SINR expressions are written for ZF and MRT precoding schemes. Building on that, performances of the two precoding schemes under non-reciprocal channels and imperfect CSI are compared against each other.

4.3.1 ZF Precoding

For ZF precoding scheme, the normalization factor β^{ZF} can be expressed as [62]

$$\beta^{\text{ZF}} = \left(\mathbb{E} \left[\text{Tr} \left(\left(\hat{\mathbf{H}} \hat{\mathbf{H}}^H \right)^{-1} \right) \right] \right)^{-1} = \sqrt{\frac{(N - M_{\text{tot}}) \tau_u \rho_u}{M_{\text{tot}} (\tau_u \rho_u + 1)}}, \quad (4.11)$$

while the useful signal in (4.7) reads

$$\sqrt{\rho_d} \beta^{\text{ZF}} \mathbb{E} [\mathbf{h}_m^T \mathbf{u}_m^{\text{ZF}}] s_m = \sqrt{\rho_d} \beta^{\text{ZF}} s_m. \quad (4.12)$$

Having (4.11) and (4.12), the effective SINR at the m -th antenna in the UE side shown in (4.9) can be expressed as

$$\text{SINR}_m^{\text{ZF}} = \frac{N - M_{\text{tot}}}{M_{\text{tot}}} \times \frac{\tau_u \rho_u \rho_d}{I_{\text{RC}}^{\text{ZF}} + I_{\text{NRC},m}^{\text{ZF}}}, \quad (4.13)$$

where

$$I_{\text{RC}}^{\text{ZF}} = \rho_d + \tau_u \rho_u + 1, \quad (4.14)$$

is the interference plus noise power in ideal reciprocal scenario, whereas the additional interference power term due to non-reciprocity in the channel can be given as

$$\begin{aligned} I_{\text{NRC},m}^{\text{ZF}} &\approx \rho_d \left[\left(1 + \frac{N - M_{\text{tot}}}{M_{\text{tot}}} \tau_u \rho_u \right) \text{Tr} (\mathbf{R}_{\mathbf{a}'_m}) + \frac{\tau_u \rho_u}{M_{\text{tot}}} \left(\text{Tr} (\mathbf{R}_{\mathbf{a}'_m}) - \sigma_{a'_{mm}}^2 \right) \right. \\ &\quad + \frac{\tau_u \rho_u}{N M_{\text{tot}}} (1 + \text{Tr} (\mathbf{R}_{\mathbf{a}'_m})) \text{Sum} (\mathbf{R}_{\mathbf{c}'_d}) \\ &\quad \left. + \left[\frac{\tau_u \rho_u + 1}{N} (1 + \text{Tr} (\mathbf{R}_{\mathbf{a}'_m})) - \frac{\tau_u \rho_u}{N M_{\text{tot}}} \left(\text{Tr} (\mathbf{R}_{\mathbf{a}'_m}) - \sigma_{a'_{mm}}^2 \right) \right] \left(\text{Tr} (\mathbf{R}_{\mathbf{c}'_d}) + \text{Tr} (\mathbf{R}_{\mathbf{c}'_{od}}) \right) \right]. \end{aligned} \quad (4.15)$$

4.3.2 MRT Precoding

For MRT precoding, the normalization factor β^{MRT} can be expressed as [66]

$$\beta^{\text{MRT}} = \left(\sqrt{\mathbb{E}[\text{Tr}(\hat{\mathbf{H}}\hat{\mathbf{H}}^H)]} \right)^{-1} = \sqrt{\frac{\tau_u \rho_u + 1}{NM_{\text{tot}} \tau_u \rho_u}}, \quad (4.16)$$

while the useful signal in (4.7) is given as

$$\sqrt{\rho_d} \beta^{\text{MRT}} \mathbb{E}[\mathbf{h}_m^T \mathbf{u}_m^{\text{MRT}}] s_m = \sqrt{\rho_d} \beta^{\text{MRT}} \frac{N \tau_u \rho_u}{\tau_u \rho_u + 1} s_m. \quad (4.17)$$

Next, based on (4.16) and (4.17), the effective SINR at the m -th antenna in the UE side can be shown as

$$\text{SINR}_m^{\text{MRT}} = \frac{N}{M_{\text{tot}}} \times \frac{\tau_u \rho_u \rho_d}{I_{\text{RC}}^{\text{MRT}} + I_{\text{NRC},m}^{\text{MRT}}}. \quad (4.18)$$

Similar to ZF precoding scenario, $I_{\text{RC}}^{\text{MRT}}$ and $I_{\text{NRC},m}^{\text{MRT}}$ denote the power of interference plus noise in ideal reciprocal channel and interference power due to channel non-reciprocity, respectively, and can be given as

$$I_{\text{RC}}^{\text{MRT}} = (\rho_d + 1)(\tau_u \rho_u + 1), \quad (4.19)$$

and

$$\begin{aligned} I_{\text{NRC},m}^{\text{MRT}} = & \rho_d \left[\left(1 + \frac{N + M_{\text{tot}}}{M_{\text{tot}}} \tau_u \rho_u \right) \text{Tr}(\mathbf{R}_{\mathbf{a}'_m}) - \frac{\tau_u \rho_u}{M_{\text{tot}}} \left(\text{Tr}(\mathbf{R}_{\mathbf{a}'_m}) - \sigma_{a'_{mm}}^2 \right) \right. \\ & + \frac{\tau_u \rho_u}{NM_{\text{tot}}} (1 + \text{Tr}(\mathbf{R}_{\mathbf{a}'_m})) \text{Sum}(\mathbf{R}_{\mathbf{c}'_d}) \\ & \left. + \left[\frac{\tau_u \rho_u + 1}{N} (1 + \text{Tr}(\mathbf{R}_{\mathbf{a}'_m})) - \frac{\tau_u \rho_u}{NM_{\text{tot}}} \left(\text{Tr}(\mathbf{R}_{\mathbf{a}'_m}) - \sigma_{a'_{mm}}^2 \right) \right] \left(\text{Tr}(\mathbf{R}_{\mathbf{c}'_d}) + \text{Tr}(\mathbf{R}_{\mathbf{c}'_{od}}) \right) \right]. \end{aligned} \quad (4.20)$$

As can be seen in (4.15) and (4.20), the performance of the system under channel non-reciprocity does not necessarily depend on all the characteristics of the involved non-reciprocity parameters, e.g., it depends on the sum of variances of diagonal elements in \mathbf{C}' while it is independent of the cross-correlations of off-diagonal elements in the same matrix. In order to better distinguish such characteristics, Table 4.1 summarizes only those statistical properties of non-reciprocity parameters which impact the power of interference due to channel non-reciprocity and consequently the performance of the system.

4.3.3 Asymptotic Performance for Large N

For large values of N and in the presence of channel non-reciprocity, the derived SINR expressions for ZF and MRT precoded systems are asymptotically identical. They both saturate to the same value which can be given as

$$\lim_{N \rightarrow \infty} \text{SINR}_m^{\text{ZF}} = \lim_{N \rightarrow \infty} \text{SINR}_m^{\text{MRT}} = \frac{1}{\text{Tr}(\mathbf{R}_{\mathbf{a}'_m}) + t_{c'_d}^m \delta_{c'_d}^2 + t_{c'_{od}}^m \sigma_{c'_{od}}^2}, \quad (4.21)$$

Table 4.1: Essential Second-Order Statistics of Channel Non-Reciprocity Variables

Variable	Definition
$\sigma_{a'_{mm}}^2$	Variance of the m -th diagonal element of UE side non-reciprocity matrix \mathbf{A}'
$\sigma_{a'_{od}}^2$	Average of variances of off-diagonal elements of UE side non-reciprocity matrix \mathbf{A}'
$\sigma_{c'_d}^2$	Average of variances of diagonal elements of BS transceiver non-reciprocity matrix \mathbf{C}'
$\delta_{c'_d}^2$	Average of cross-correlations of diagonal elements of BS transceiver non-reciprocity matrix \mathbf{C}'
$\sigma_{c'_{od}}^2$	Average of variances of off-diagonal elements of BS transceiver non-reciprocity matrix \mathbf{C}'

where

$$t_{c'_d}^m = 1 + \text{Tr}(\mathbf{R}_{\mathbf{a}'_m}),$$

$$t_{c'_{od}}^m = M_{tot} \frac{\tau_u \rho_u + 1}{\tau_u \rho_u} (1 + \text{Tr}(\mathbf{R}_{\mathbf{a}'_m})) - \text{Tr}(\mathbf{R}_{\mathbf{a}'_m}) + \sigma_{a'_{mm}}^2. \quad (4.22)$$

Note that increasing N leads to having higher number of mismatched transceiver chains and antenna units and thus results into having higher interference power due to channel non-reciprocity. This additional interference reduces the advantage of ZF over MRT in terms of IUI suppression to the point that there is no difference in SINRs of ZF and MRT precoded systems for very large values of N .

Next, the achievable sum-rates of ZF and MRT precoded systems are calculated by substituting (4.13) and (4.18) into (4.10) and are shown as R^{ZF} and R^{MRT} , respectively. Based on those, the asymptotic behavior of the relative performance of ZF and MRT precoding schemes is given for large number of BS antennas as

$$\lim_{N \rightarrow \infty} \frac{R^{\text{ZF}}}{R^{\text{MRT}}} = \lim_{N \rightarrow \infty} \frac{\sum_{m=1}^{M_{tot}} \log_2(1 + \text{SINR}_m^{\text{ZF}})}{\sum_{m=1}^{M_{tot}} \log_2(1 + \text{SINR}_m^{\text{MRT}})} = 1. \quad (4.23)$$

Although the asymptotic behavior of relative performance expression in (4.23) is similar to the one of ideal reciprocal scenario presented in [62], the implications are largely different. Combining (4.21) and (4.23), it can be concluded that, in the presence of channel non-reciprocity, achievable sum-rate for both ZF and MRT precoded systems saturates to an identical finite value. Whereas, for an ideal reciprocal scenario, the achievable sum-rate grows without bound for both precoding schemes. Thus, the impacts of channel non-reciprocity and uplink channel estimation errors are fundamentally different.

4.3.4 SINR Degradation due to Channel Non-Reciprocity

By setting the ideal reciprocal channel as the reference, the relative SINR degradation due to non-reciprocity in the channel can be defined as

$$\alpha = \frac{\text{SINR}_{\text{RC}} - \text{SINR}_{\text{NRC}}}{\text{SINR}_{\text{RC}}}, \quad (4.24)$$

where SINR_{RC} and SINR_{NRC} denote calculated SINRs under ideal reciprocal and non-reciprocal channels, respectively. While, in general, (4.13) and (4.18) provide closed-form expressions for SINR under non-reciprocal channels, they can also be used to calculate SINR in ideal reciprocal scenario by setting $I_{\text{NRC},m}$ to 0.

In order to compare the impacts of channel non-reciprocity on the performance of ZF and MRT precoding schemes, another metric is defined as $\alpha^{\text{ZF/MRT}} = \frac{\alpha^{\text{ZF}}}{\alpha^{\text{MRT}}}$ which shows the ratio of the relative SINR degradations in ZF and MRT precoded systems. For the cases where $\rho_d \gg 1$, i.e., high SNR region, $\alpha^{\text{ZF/MRT}}$ for the m -th antenna in the UE side can be given as

$$\lim_{\rho_d \rightarrow \infty} \frac{\alpha_m^{\text{ZF}}}{\alpha_m^{\text{MRT}}} \triangleq \alpha_{\infty,m}^{\text{ZF/MRT}} = \frac{I_0 + \tau_u \rho_u I_{\text{NRC},m}^{\text{ZF}} / \rho_d}{I_0 + 2\tau_u \rho_u \left(\text{Tr}(\mathbf{R}_{\mathbf{a}'_m}) - \left(\text{Tr}(\mathbf{R}_{\mathbf{a}'_m}) - \sigma_{a'_{mm}}^2 \right) / M_{\text{tot}} \right)}, \quad (4.25)$$

where

$$I_0 = \left(2\tau_u \rho_u \left(\text{Tr}(\mathbf{R}_{\mathbf{a}'_m}) - \left(\text{Tr}(\mathbf{R}_{\mathbf{a}'_m}) - \sigma_{a'_{mm}}^2 \right) / M_{\text{tot}} \right) + I_{\text{NRC},m}^{\text{ZF}} / \rho_d + 1 \right) I_{\text{NRC},m}^{\text{ZF}} / \rho_d. \quad (4.26)$$

Based on (4.25) and the detailed explanation and derivation in [P2], at high SNR region, ZF precoding is more sensitive to non-reciprocity sources in the channel compared to MRT, i.e., $\alpha_{\infty,m}^{\text{ZF/MRT}} > 1$, when

$$\rho_u > \frac{1}{N}, \quad (4.27)$$

which, in general, holds for all practical values of ρ_u . This can be justified by the fact that ZF precoding scheme requires accurate CSI in order to suppress the interference.

4.4 Level Estimation

As shown in the previous section, channel non-reciprocity can degrade the performance of precoded TDD massive MIMO systems which certainly calls for non-reciprocity mitigation methods to be developed at involved transceivers. However, selecting the right times to perform such non-reciprocity mitigation rounds, e.g., [P1] and [96–99], is very important due to i) the associated system overhead; ii) non-reciprocity characteristics deviation rate which depends on the hardware configuration and the operating conditions [76]. Thus, in this section, UEs try to measure the level of BS transceiver non-reciprocity to inform the BS regarding the need for a possible non-reciprocity mitigation round.

Considering a TDD massive MIMO system with single-antenna UEs and assuming perfect uplink channel estimation, for simplicity, the received downlink signal at the k -th UE can be re-written based on (4.6) as

$$r_k = \sqrt{\rho_d} \beta a_{kk} \hat{\mathbf{h}}_k^T \mathbf{C} \mathbf{u}_k s_k + \sqrt{\rho_d} \beta \sum_{\substack{i=1 \\ i \neq k}}^K a_{kk} \hat{\mathbf{h}}_k^T \mathbf{C} \mathbf{u}_i s_i + n_k. \quad (4.28)$$

By defining the precoded downlink channel towards the k -th UE as

$$h_k^p = \sqrt{\rho_d} \beta a_{kk} \hat{\mathbf{h}}_k^T \mathbf{C} \mathbf{u}_k, \quad (4.29)$$

and following the same format as in (4.7), (4.28) can be illustrated as

$$r_k = \underbrace{\hat{h}_k^p s_k}_{\text{useful signal}} + \underbrace{z_k^{\text{SI}} s_k}_{\text{self-interference}} + \underbrace{z_k^{\text{IUI}} s_i}_{\text{IUI}} + n_k, \quad (4.30)$$

where \hat{h}_k^p is the estimated version of h_k^p used in the k -th UE for detection purposes and

$$\begin{aligned} z_k^{\text{SI}} &= h_k^p - \hat{h}_k^p \\ z_k^{\text{IUI}} &= \sqrt{\rho_d} \beta \sum_{\substack{i=1 \\ i \neq k}}^K a_{kk} \hat{\mathbf{h}}_k^T \mathbf{C} \mathbf{u}_i. \end{aligned} \quad (4.31)$$

Note that, there is no ISI as the UEs are assumed to be single-antenna devices.

Assuming reasonably good antenna isolation in BS transceiver, the non-reciprocity matrix in the BS side can also be given as $\mathbf{C} = \bar{\mathbf{B}}$ where $\bar{\mathbf{B}}$ is the FR mismatch matrix of BS transceiver as in (3.17) and thus $\mathbf{c}'_{\text{od}} = \mathbf{0}_{N(N-1) \times 1}$. Next, focusing on ZF precoded systems scenario, based on the detailed derivation in [P4], the power of IUI in (4.30) for one realization of channel non-reciprocity parameters can be shown to read

$$\mathbb{E} \left[|z_k^{\text{IUI}}|^2 \right] = \mathbb{E} \left[\left| \sqrt{\rho_d} \beta \sum_{\substack{i=1 \\ i \neq k}}^K a_{kk} \hat{\mathbf{h}}_k^T \mathbf{C} \mathbf{u}_i \right|^2 \right] \approx \sqrt{\rho_d} \frac{K-1}{K} \sigma_{c'_d}^2, \quad (4.32)$$

where, as mentioned in Table 4.1, $\sigma_{c'_d}^2$ denotes the average of variances of diagonal elements in the BS transceiver non-reciprocity matrix, \mathbf{C}' . The approximations used in (4.32) are justified by the law of large numbers and the fact that for practical values of UE transceiver non-reciprocity parameters $1 + |a'_{kk}|^2 \approx 1$.

The power of the self-interference at the k -th UE depends on the type of downlink CSI acquisition method used in the UE side for detection purposes, which can be based on either i) received downlink pilots sent from the BS as proposed in [66]; or ii) statistical properties of precoded downlink channels as discussed earlier. In the former method, the BS sends downlink pilots, proportional to the number of associated UEs, to UEs to facilitate the estimation of precoded downlink channel at the UE side where MMSE estimation is assumed to be deployed [66]. The estimated precoded downlink channel can then be given as

$$\hat{h}_k^{p, \text{pilot}} = h_k^p + e_k^{\text{pilot}}, \quad (4.33)$$

where e_k^{pilot} is the corresponding estimation error whose power, denoted as $\sigma_{e^{\text{pilot}}}^2$, is assumed to be known to UEs [66]. Having the power of self-interference and IUI as in (4.32), the total interference power for the case that downlink pilots are employed for downlink CSI acquisition can be shown to read

$$\sigma_{z_k^{\text{pilot}}}^2 = \sqrt{\rho_d} \sigma_{e^{\text{pilot}}}^2 + \mathbb{E} \left[|z_k^{\text{IUI}}|^2 \right] \approx \sqrt{\rho_d} \left(\sigma_{e^{\text{pilot}}}^2 + \frac{K-1}{K} \sigma_{c'_d}^2 \right). \quad (4.34)$$

In the case where the precoded downlink channel is estimated statistically, although the accuracy of the estimation, $\mathbb{E}[h_k^p]$, is enough for detection purposes, it needs to be improved for estimating the level of BS transceiver non-reciprocity. In order to achieve that, the BS adds a new downlink CSI acquisition round based on the already detected downlink data symbols as

$$\hat{h}_k^{p, \text{stat}} = \frac{1}{T_{\text{coh}}} \sum_{t=1}^{T_{\text{coh}}} \frac{r_k[t]}{s_k[t]} = h_k^p + \underbrace{\frac{1}{T_{\text{coh}}} \sum_{t=1}^{T_{\text{coh}}} \frac{z_k^{\text{IUI}} s_i[t] + n_k[t]}{s_k[t]}}_{e_k^{\text{stat}}}, \quad (4.35)$$

where T_{coh} is the duration of each coherence interval in data symbols. The average level of estimation error can then be written as

$$\sigma_{e^{stat}}^2 = \mathbb{E}\left[|e_k^{stat}|^2\right] \approx 0, \quad (4.36)$$

since in practice $z_k^{\text{IUI}} s_i + n_k \ll s_k$ and $\mathbb{E}[z_k^{\text{IUI}} s_i + n_k] = 0$. The estimation accuracy can be improved with higher SNR and longer coherence interval duration. Based on (4.36), after having additional round of precoded downlink channel estimation on top of the statistical one, the total interference power reads

$$\sigma_{z_k^{stat}}^2 = \sigma_{e^{stat}}^2 + \mathbb{E}\left[|z_k^{\text{IUI}}|^2\right] \approx \mathbb{E}\left[|z_k^{\text{IUI}}|^2\right] \approx \sqrt{\rho_d} \frac{K-1}{K} \sigma_{c_d'}^2. \quad (4.37)$$

Having (4.34) and (4.37), the level of BS transceiver non-reciprocity can be estimated based on the total interference power. In order to do that, after extracting interference and noise from the received signal based on (4.30) and given \hat{h}_k^p in (4.33) and (4.35) depending on the employed downlink CSI acquisition method, the k -th UE estimates the power of total interference using a sample variance estimator as

$$\sigma_{z_k}^2 = \frac{1}{N_{coh} T_{coh}} \sum_{i=1}^{N_{coh} T_{coh}} \left| r_k[i] - \hat{h}_k^p[i] s_k[i] \right|^2 - 1, \quad (4.38)$$

where N_{coh} is the number of coherence intervals used in estimating the level of BS transceiver non-reciprocity.

Next, for the pilot-based downlink CSI acquisition scenario, based on (4.34) and assuming that the k -th UE has information about SNR, i.e., its own receiver noise level, as well as the downlink CSI estimation error, $\sigma_{e^{pilot}}^2$, the level of BS transceiver non-reciprocity can be estimated as

$$\hat{\sigma}_{c_d'|pilot}^2 = \frac{K (\sigma_{z_k}^2 / \sqrt{\rho_d} - \sigma_{e^{pilot}}^2)}{K - 1}. \quad (4.39)$$

Similarly, for statistical downlink channel estimation scenario, based on (4.37), the k -th UE estimates the BS transceiver non-reciprocity level as

$$\hat{\sigma}_{c_d'|stat}^2 = \frac{K \sigma_{z_k}^2}{\sqrt{\rho_d} (K - 1)}. \quad (4.40)$$

4.5 Mitigation

In order to tackle the channel non-reciprocity problem, the BS requires to have knowledge regarding the non-reciprocity behavior of all the transceivers in the network. As shown in Section 3.3.2, assuming that the BS only has an estimation of its own transceiver non-reciprocity matrix, $\hat{\mathbf{C}}$, the precoder can be transformed as $\mathbf{U}_{\text{NRC}} = \hat{\mathbf{C}}^{-1} \mathbf{U}$ to take the non-reciprocity into account. In more general case where the BS has estimates of both BS and UE sides' non-reciprocity matrices, i.e., $\hat{\mathbf{C}}$ and $\hat{\mathbf{A}}$, respectively, the precoder can be transformed as

$$\mathbf{U}_{\text{NRC}} = \hat{\mathbf{C}}^{-1} \mathbf{U} \hat{\mathbf{A}}^{-1}, \quad (4.41)$$

to mitigate the channel non-reciprocity problem. As shown in [P1], assuming perfect estimates of uplink channel and non-reciprocity matrices, the performance of the precoder in (4.41) reaches the one of an ideal reciprocal channel in ZF and MRT scenarios.

In order to estimate channel non-reciprocity matrices, an iterative OTA estimation framework was proposed in [P1]. In this method, in order to gather enough information at the BS to start the actual non-reciprocity estimation processing, the BS transmits a unitary pilot matrix, called $\mathbf{X}_{\text{NRC}} \in \mathbb{C}^{N \times N}$, and UEs send the conjugated version of the received samples back to the BS without decoding them. Assuming single-antenna UEs, the signal model for this pilot signaling phase can be written as

$$\begin{aligned} \mathbf{R}_{\text{NRC}} &= \sqrt{\tilde{\rho}_d} \mathbf{H} \mathbf{X}_{\text{NRC}} + \tilde{\mathbf{Z}}_d \\ \mathbf{Y}_{\text{NRC}} &= \sqrt{\tilde{\rho}_u} \mathbf{G} \mathbf{R}_{\text{NRC}}^* + \tilde{\mathbf{Z}}_u = \sqrt{\tilde{\rho}_u} \sqrt{\tilde{\rho}_d} \mathbf{G} \mathbf{H}^* \mathbf{X}_{\text{NRC}}^* + \tilde{\mathbf{Z}}_{\text{tot}}, \end{aligned} \quad (4.42)$$

where $\mathbf{R}_{\text{NRC}} \in \mathbb{C}^{K \times N}$ and $\mathbf{Y}_{\text{NRC}} \in \mathbb{C}^{N \times N}$ denote the received downlink and uplink matrices, respectively. In (4.42), $\tilde{\rho}_d$ denotes the downlink SNR, $\tilde{\rho}_u$ is the uplink SNR, $\tilde{\mathbf{Z}}_d \in \mathbb{C}^{K \times N}$ and $\tilde{\mathbf{Z}}_u \in \mathbb{C}^{N \times N}$ have i.i.d. $\mathcal{CN}(0, 1)$ elements and are corresponding to receiver noise matrices at the BS and the UE side, respectively, while $\tilde{\mathbf{Z}}_{\text{tot}} = \sqrt{\tilde{\rho}_u} \mathbf{G} \tilde{\mathbf{Z}}_d^* + \tilde{\mathbf{Z}}_u \in \mathbb{C}^{N \times N}$ is the effective noise received at the BS. The tilde sign is used in (4.42) to differentiate the parameters used in pilot transmission stage from the ones used in the actual downlink data transmission phase.

The duration of such pilot signaling method is $2N$ symbols. In practice, the duration of a coherence interval is in the range of several hundreds of symbols, while the exact value depends on the carrier frequency as well as the mobility of the UEs. Here, the coherence interval is assumed to be at least $2N + K$ to take the uplink channel estimation phase into account as well. As mentioned earlier, since realizations of channel non-reciprocity parameters vary much slower than channel realizations, they can be assumed to remain unchanged during both the channel non-reciprocity estimation, including OTA signaling, and the actual data transmission phases.

After the pilot signaling stage and assuming that the BS has already estimated the effective uplink channel, it tries to estimate \mathbf{A} and \mathbf{C} . In the first stage, using the unitary property of \mathbf{X}_{NRC} , the BS processes the received signal \mathbf{Y}_{NRC} as follows

$$\mathbf{Q} = \mathbf{Y}_{\text{NRC}}^* \mathbf{X}_{\text{NRC}}^H = \sqrt{\tilde{\rho}_u} \sqrt{\tilde{\rho}_d} \mathbf{G}^* \mathbf{A} \mathbf{G}^T \mathbf{C} + \mathbf{V}, \quad (4.43)$$

where $\mathbf{Q} \in \mathbb{C}^{N \times N}$ and $\mathbf{V} = \tilde{\mathbf{Z}}_{\text{tot}}^* \mathbf{X}_{\text{NRC}}^H \in \mathbb{C}^{N \times N}$ are the processed signal and noise matrices, respectively.

In the next stage, the BS employs an iterative framework to estimate transceiver non-reciprocity matrices at the BS and UE sides, where $\hat{\mathbf{A}}[t]$ and $\hat{\mathbf{C}}[t]$ denote the estimates at the t -th iteration. The iterative steps can be summarized as follows.

1. Initialize $\hat{\mathbf{A}}[0] = \mathbf{I}_K$.
2. Substitute $\hat{\mathbf{A}}[0]$ for \mathbf{A} in (4.43) and obtain $\hat{\mathbf{C}}[1]$.
3. Substitute $\hat{\mathbf{C}}[1]$ for \mathbf{C} in (4.43) and obtain $\hat{\mathbf{A}}[1]$.
4. Improve the estimates $\hat{\mathbf{A}}$ and $\hat{\mathbf{C}}$ by iteratively going through steps 2 and 3 while increasing the iteration number.

In an OFDM/OFDMA system, the expression in (4.43) is valid per subcarrier. Subsequently, the described estimation framework can be performed per subcarrier. While \mathbf{G} varies based on the frequency selectivity of the propagation channel, as mentioned in

Section 3.3.2, non-reciprocity parameters are only mildly frequency-selective, thus can be assumed to remain unchanged over small set of adjacent subcarriers called C_{sc} where it is conservatively assumed that $C_{sc} \leq 10$. Therefore, the estimation framework can be carried out over C_{sc} adjacent subcarriers and the resulting $\hat{\mathbf{A}}$ and $\hat{\mathbf{C}}$ can be averaged to improve the estimation accuracy as

$$\begin{aligned}\hat{\mathbf{A}} &= \frac{1}{C_{sc}} \sum_{l=1}^{C_{sc}} \hat{\mathbf{A}}_l \\ \hat{\mathbf{C}} &= \frac{1}{C_{sc}} \sum_{l=1}^{C_{sc}} \hat{\mathbf{C}}_l.\end{aligned}\tag{4.44}$$

In the continuation, the actual algorithms to estimate \mathbf{C} and \mathbf{A} are discussed while dropping the relative subcarrier index, l , for notational simplicity.

4.5.1 Estimating BS Transceiver Non-Reciprocity Matrix

Having the uplink channel estimate $\hat{\mathbf{G}}$ and using $\hat{\mathbf{A}}$ from the previous iteration to fix \mathbf{A} in (4.43), the estimator tries to solve (4.43) and find an estimate for \mathbf{C} by minimizing the Frobenius norm criterion as

$$\hat{\mathbf{C}}(m+1) = \underset{\mathbf{C}}{\operatorname{argmin}} \left\| \mathbf{Q} - \sqrt{\tilde{\rho}_u} \sqrt{\tilde{\rho}_d} \hat{\mathbf{G}}^* \hat{\mathbf{A}}(m) \hat{\mathbf{G}}^T \mathbf{C} \right\|_F^2, \tag{4.45}$$

where the Frobenius norm is denoted by the subscript F .

By defining $\mathbf{T}(m) = \sqrt{\tilde{\rho}_u} \sqrt{\tilde{\rho}_d} \hat{\mathbf{G}}^* \hat{\mathbf{A}}(m) \hat{\mathbf{G}}^T \in \mathbb{C}^{N \times N}$, the expression on the right hand side of (4.45) can be written as

$$\| \mathbf{Q} - \mathbf{T}(m) \mathbf{C} \|_F^2 = \sum_{j=1}^K \| \mathbf{q}_j - \mathbf{T}(m) \mathbf{c}_j \|^2, \tag{4.46}$$

where the $\mathbf{q}_j \in \mathbb{C}^{N \times 1}$ and $\mathbf{c}_j \in \mathbb{C}^{N \times 1}$ are the j -th column of matrices \mathbf{Q} and \mathbf{C} , respectively. Since, there is one-to-one mapping between the terms in the sum and the columns in \mathbf{C} , estimating \mathbf{C} can be simplified to separately estimating each of its columns.

In practice, the physical distance between two antenna elements controls the mutual coupling power between those, which in turn impacts the corresponding off-diagonal element in \mathbf{C} . Thus, if the i -th and the j -th antenna elements in BS are far enough, c_{ij} can be assumed to be zero. To characterize such behavior, a parameter called sparsity threshold, D , is defined which is the maximum distance between two antenna elements for which the corresponding off-diagonal element in \mathbf{C} is non-zero. Any off-diagonal element corresponding to two antennas with a distance larger than D is assumed to be zero for estimation purposes which leads to having sparse structure for \mathbf{C} and consequently $\hat{\mathbf{C}}$. Figure 4.1 illustrates this concept in an example scenario of a 10×10 square BS antenna grid with $\lambda/2$ antenna spacing where the sparsity threshold, D , is defined in multiples of $\lambda/2$. As can be seen in Figure 4.1, there is another parameter called $L(D)$ which defines the maximum number of coupled neighboring antenna elements as a function of D . For example, for the case where $D = 1$, the number of coupled antennas in the bottom right corner of the antenna grid is only 2 while the maximum number of coupled antennas for this sparsity threshold value can be found in the center of the antenna grid and thus $L(1) = 4$.

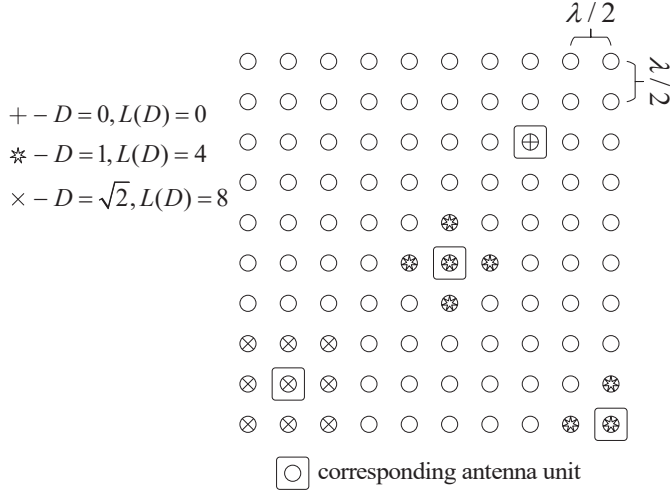


Figure 4.1: Principal illustration of sparsity threshold, D , on a 10×10 square BS antenna grid with $\lambda/2$ antenna spacing.

Having the information regarding the geometry and the architecture of the antenna system, the BS can determine the sparse structure of its transceiver non-reciprocity matrix, \mathbf{C} . The number of non-zero entries in the j -th column of \mathbf{C} is denoted by R_j which always satisfies $R_j \leq L(D) + 1$. Based on the sparse structure of \mathbf{C} , the BS knows the index of all R_j non-zero entries of \mathbf{c}_j and thus forms a reduced vector, called $\mathbf{c}_j^{red} \in \mathbb{C}^{R_j \times 1}$, which contains all the non-zero elements of \mathbf{c}_j . Next, the BS constructs a reduced version of $\mathbf{T}(m)$, called $\mathbf{T}_j^{red}(m) \in \mathbb{C}^{N \times R_j}$, which is formed by keeping the columns in $\mathbf{T}(m)$ whose column numbers are the same as the indexes of non-zero entries in \mathbf{c}_j . In other words, if the i -th row is kept in forming \mathbf{c}_j^{red} , then the i -th column will be kept in forming $\mathbf{T}_j^{red}(m)$.

In the next step, the BS estimates a reduced version of the j -th column of its transceiver non-reciprocity matrix based on \mathbf{c}_j^{red} and $\mathbf{T}_j^{red}(m)$ as

$$\hat{\mathbf{c}}_j^{red}(m+1) = \underset{\mathbf{c}_j^{red}}{\operatorname{argmin}} \left\| \mathbf{q}_j - \mathbf{T}_j^{red}(m) \mathbf{c}_j^{red} \right\|^2, \quad (4.47)$$

for which the solution can be written as

$$\hat{\mathbf{c}}_j^{red}(m+1) = (\mathbf{T}_j^{red}(m))^\dagger \mathbf{q}_j. \quad (4.48)$$

The full vector corresponding to the j -th column of $\hat{\mathbf{C}}(m+1)$, $\hat{\mathbf{c}}_j(m+1)$, can then be formed based on $\hat{\mathbf{c}}_j^{red}(m+1)$ by appending zeros to the proper entries.

4.5.2 Estimating UE-Side Transceivers Non-Reciprocity Matrix

Having an estimate for BS transceiver non-reciprocity matrix, i.e., $\hat{\mathbf{C}}(m)$, the BS can refine its UE-side transceivers non-reciprocity matrix estimation by minimizing the Frobenius norm criterion as

$$\hat{\mathbf{A}}(m) = \underset{\mathbf{A}}{\operatorname{argmin}} \left\| \mathbf{Q} - \sqrt{\tilde{\rho}_u} \sqrt{\tilde{\rho}_d} \hat{\mathbf{G}}^* \mathbf{A} \hat{\mathbf{G}}^T \hat{\mathbf{C}}(m) \right\|_F^2. \quad (4.49)$$

Since \mathbf{A} is assumed to be diagonal, based on the single-antenna UEs assumption, (4.49) can be solved as

$$\hat{\mathbf{A}}(m) = \text{diag}(\hat{\boldsymbol{\xi}}), \quad (4.50)$$

where $\hat{\boldsymbol{\xi}} = [\mathbf{I}_K, i\mathbf{I}_K] \hat{\boldsymbol{\psi}} \in \mathbb{C}^{K \times 1}$ while $\hat{\boldsymbol{\psi}} \in \mathbb{C}^{2K \times 1}$ is given as

$$\hat{\boldsymbol{\psi}} = \left(\sum_{j=1}^N \bar{\mathbf{W}}_j^T \bar{\mathbf{W}}_j \right)^{-1} \sum_{j=1}^N \bar{\mathbf{W}}_j^T \bar{\mathbf{q}}_j. \quad (4.51)$$

In (4.51), $\bar{\mathbf{q}}_j = [\Re\{\mathbf{q}_j^T\}, \Im\{\mathbf{q}_j^T\}]^T \in \mathbb{C}^{2N \times 1}$ and the matrix $\bar{\mathbf{W}}_j \in \mathbb{C}^{2N \times 2K}$ is constructed as

$$\bar{\mathbf{W}}_j = \begin{bmatrix} \Re\{\mathbf{W}_j\}, & -\Im\{\mathbf{W}_j\} \\ \Im\{\mathbf{W}_j\}, & \Re\{\mathbf{W}_j\} \end{bmatrix}, \quad (4.52)$$

where $\mathbf{W}_j = \sqrt{\rho_u} \sqrt{\rho_d} \hat{\mathbf{G}}^* \text{diag} \left(\left[\hat{\mathbf{G}}^T \hat{\mathbf{C}}(m) \right]_j \right)$, with $\left[\hat{\mathbf{G}}^T \hat{\mathbf{C}}(m) \right]_j$ being the j -th column of $\hat{\mathbf{G}}^T \hat{\mathbf{C}}(m)$.

4.6 Numerical Evaluations and Results

In this section, extensive computer simulations are used to evaluate and illustrate the performance of i) the derived closed-form analytical SINR expressions for precoded multi-user massive MIMO systems under channel non-reciprocity and imperfect CSI; ii) BS transceiver non-reciprocity level estimation algorithm; iii) channel non-reciprocity estimation and mitigation method. To achieve reliable outputs, the simulation results are averaged over large enough number of channel and non-reciprocity parameters realizations.

The performance of the system is also studied from spectral efficiency point of view which is defined as [66]

$$\eta_s = \left(1 - \frac{\tau_u + \tau_d}{T_{coh}} \right) R, \quad (4.53)$$

where τ_d is the number of downlink pilots sent from the BS to UEs to facilitate downlink CSI acquisition. In the cases where the statistical average of the precoded downlink channel is used for detection purposes, the BS does not send any downlink pilots and thus $\tau_d = 0$, while the achievable sum-rate, R , is calculated using (2.18). If downlink pilots are used, then $\tau_d \geq M_{tot}$ and (2.17) is used to calculate R [66]. As mentioned earlier, τ_u is the number of uplink pilots sent from each antenna in the UE side, whereas T_{coh} is the duration of each coherence interval in data symbols.

The baseline simulation scenario consists of a BS which is equipped with $N = 100$ antennas, simultaneously serving K single-antenna UEs, thus $K = M_{tot}$. The uplink channel matrix between the UEs and the BS, \mathbf{G} , is assumed to have i.i.d. $\mathcal{CN}(0, 1)$ elements. The downlink SNR in data transmission phase is chosen high enough to ensure possibility of detecting some data even without channel non-reciprocity estimation, $\rho_d = 20$ dB. The uplink SNR of pilot transmission for channel estimation is chosen to be $\rho_u = 0$ dB while the number of such uplink pilots are assumed to be $\tau_u = M_{tot}$. Finally, in case of using downlink pilots for detection purposes, the BS sends $\tau_d = M_{tot}$ pilot signals with the same SNR as of downlink data, i.e., ρ_d . These are baseline simulation parameters and may vary in some simulation scenarios.

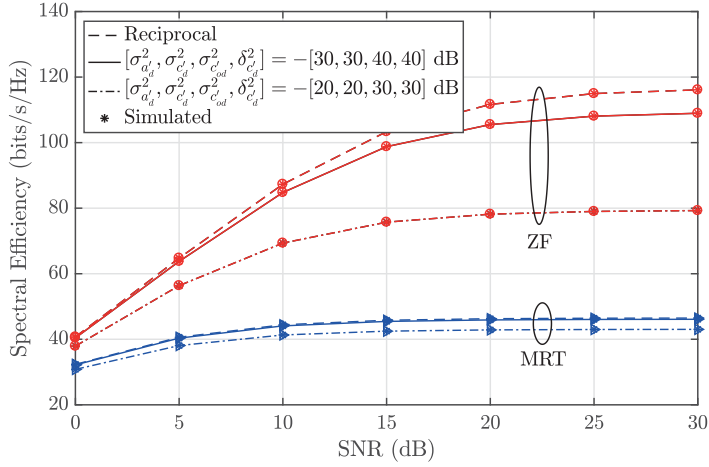


Figure 4.2: System spectral efficiency vs. downlink SNR (ρ_d) for $N = 100$, $M_{tot} = K = 20$, $\tau_u = M_{tot}$, $\rho_u = 0$ dB, $T_{coh} = 250$.

4.6.1 Performance Evaluation Under Channel Non-Reciprocity

The simulation scenario considered for evaluating the performance of ZF and MRT precoded multi-user massive MIMO downlink transmission consists of $K = 20$ UEs while $T_{coh} = 250$. The non-reciprocity matrices \mathbf{A} and \mathbf{C} are constructed based on their essential statistical properties in Table 4.1. Since the UEs are assumed to be single-antenna devices, off-diagonal entries of \mathbf{A} are zero and thus $\sigma_{a'_{od}}^2 = 0$. The variance of the m -th diagonal element in \mathbf{A}' , $\sigma_{a'_{mm}}^2$, is assumed to be equal for all the values of m and is set to $\sigma_{a'_d}^2$. Next, for each channel non-reciprocity realization, the diagonal elements of \mathbf{A}' and off-diagonal elements of \mathbf{C}' are assumed to be i.i.d. $\mathcal{CN}(0, \sigma_{a'_d}^2)$ and $\mathcal{CN}(0, \sigma_{c'_{od}}^2)$, respectively. The diagonal elements of \mathbf{C}' are assumed to have Gaussian distribution with zero mean, variance set to $\sigma_{c'_d}^2$ and cross-correlation equal to $\delta_{c'_d}^2$.

The spectral efficiency and relative SINR degradation of the example scenario are plotted against downlink SNR in Figure 4.2 and Figure 4.3, respectively, where the lines are representing the results based on the closed-form analysis and star markers, *, are the corresponding simulation results. The perfect alignment between analytical and simulation results proves the accuracy of the closed-form analysis and the used approximations. As can be seen in Figure 4.2 and Figure 4.3, the impact of non-reciprocity in the channel is much more severe in high SNR region as the performance in low SNR region is mainly limited by noise and not the channel non-reciprocity. While both precoding schemes, namely ZF and MRT, are suffering from channel non-reciprocity mainly in high SNR region, it is clear that ZF precoding scheme is much more sensitive to such non-idealities, as expected based on the analysis in Section 4.3.4.

The impacts of increasing the number of BS antennas on the spectral efficiency are evaluated in Figure 4.4. As can be seen, the results are perfectly inline with the implications made by analytical asymptotic performance study in Section 4.3.3 where it was concluded that under non-reciprocal channels i) both ZF and MRT precoded systems have a finite achievable sum-rate saturation level; ii) the saturation level is identical for both precoding schemes. The results clearly confirm that the spectral efficiency of both ZF and MRT

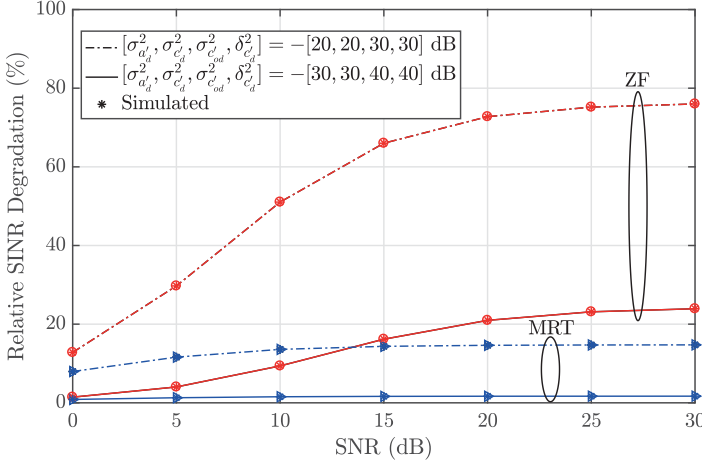


Figure 4.3: Relative SINR degradation vs. downlink SNR (ρ_d) for $N = 100$, $M_{tot} = K = 20$, $\tau_u = M_{tot}$, $\rho_u = 0$ dB.

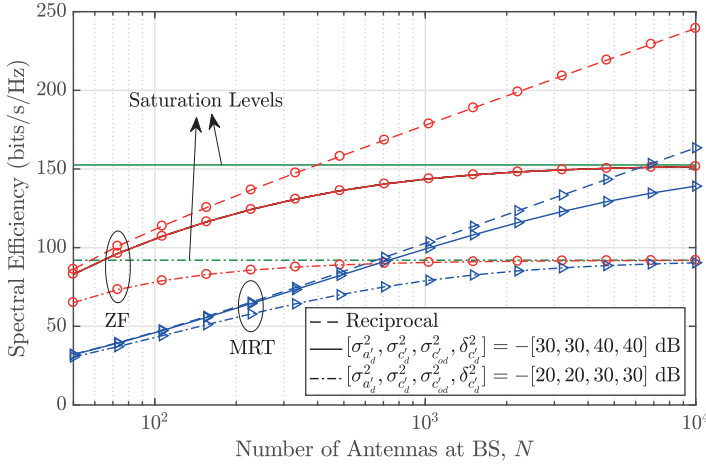


Figure 4.4: System spectral efficiency vs. the number of antennas at BS (N) for $M_{tot} = K = 20$, $\rho_d = 20$, $\tau_u = M_{tot}$, $\rho_u = 0$ dB, $T_{coh} = 250$. Saturation levels based on (4.21) are plotted in green horizontal lines for the two indicated channel non-reciprocity parameter settings.

precoded systems saturate towards the value derived in Section 4.3.3. As discussed earlier, increasing the number of antennas in the BS side, which increases the number of non-reciprocal transceiver chains and antenna units, causes reduction in advantage of ZF over MRT to the point that the performance of both systems saturates to the same value. Note that as opposed to, e.g., pilot contamination [94] problem where the performance saturation happens with having around 10^5 BS antennas [102], the number of BS antennas that causes performance saturation due to channel non-reciprocity is around 10^3 or even lower which shows the practical relevance of the results.

In Figure 4.5, the optimal number of simultaneously scheduled single-antenna UEs is calculated as a function of channel non-reciprocity for two example values of downlink

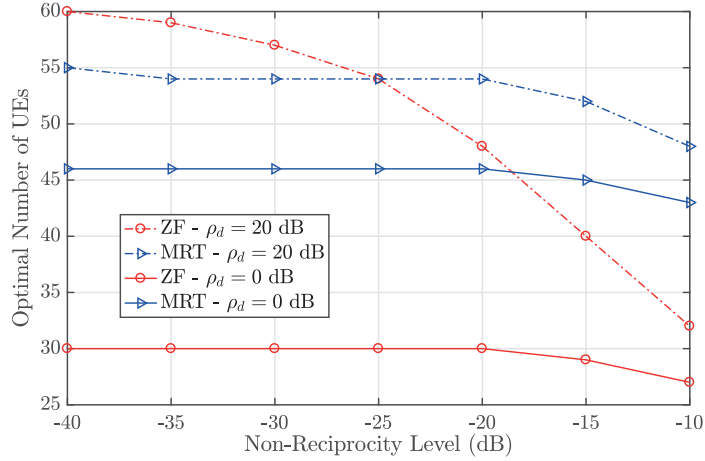


Figure 4.5: Optimal number of single-antenna UEs to maximize system spectral efficiency vs. non-reciprocity level ($\sigma_{a'_d}^2 = \sigma_{c'_d}^2 =$ channel non-reciprocity level, while $\sigma_{c'_{od}}^2 = \delta_{c'_d}^2 =$ channel non-reciprocity level -10 dB) for $N = 100$, $M_{tot} = K = 20$, $\rho_d = 20$, $\tau_u = M_{tot}$, $\rho_u = 0$ dB, $T_{coh} = 250$.

SNR, namely, $\rho_d = 20$ dB, 0 dB. This optimal number of simultaneously scheduled single-antenna UEs, K_{opt} , refers to the K which maximizes the spectral efficiency and is derived by evaluating (4.10) for all the values of $N \geq K \geq 1$. Based on the obtained results, K_{opt} drops for both precoding schemes as the channel non-reciprocity level, and subsequently interference in the UE side, increases. Such drops are more visible in high SNR region, i.e., $\rho_d = 20$ dB, while in low SNR region, i.e., $\rho_d = 0$ dB, the performance is limited mainly by the receiver thermal noise. Comparing ZF and MRT precoded systems, such drops can be experienced in the case of MRT precoding scheme in fairly severe non-reciprocity levels, e.g., $\sigma_{a'_d}^2 > -15$ dB, whereas ZF precoded systems suffer from a significant drop already with moderate channel non-reciprocity levels, e.g., -30 dB $< \sigma_{a'_d}^2 < -20$ dB. It is interesting to note that as opposed to ideal reciprocal scenario, the optimal number of simultaneously scheduled single-antenna for MRT is higher than that of ZF for high SNR values under moderate channel non-reciprocity levels.

Figure 4.6 illustrates the maximum tolerable channel non-reciprocity level as function of downlink SINR at the UE side based on the derived SINR expressions in (4.13) and (4.18). The considered example scenario covers two downlink SNR values, namely, $\rho_d = 20$ dB, 0 dB. As an example point in the obtained results, in order to guarantee 15 dB for downlink SINR at the UE side in ZF precoded system with $\rho_d = 20$ dB, channel non-reciprocity level cannot be higher than around -20 dB. Such analysis can be used in practical system design and deployments, e.g., to calculate the required channel non-reciprocity calibration levels for a given target downlink transmission performance, which proves the applicability of the provided analytical results in practical systems.

4.6.2 BS Transceiver Non-Reciprocity Level Estimation

Assuming good antenna isolation in BS transceiver, the accuracy of the BS transceiver non-reciprocity level estimation method is evaluated with regards to the relative estimation

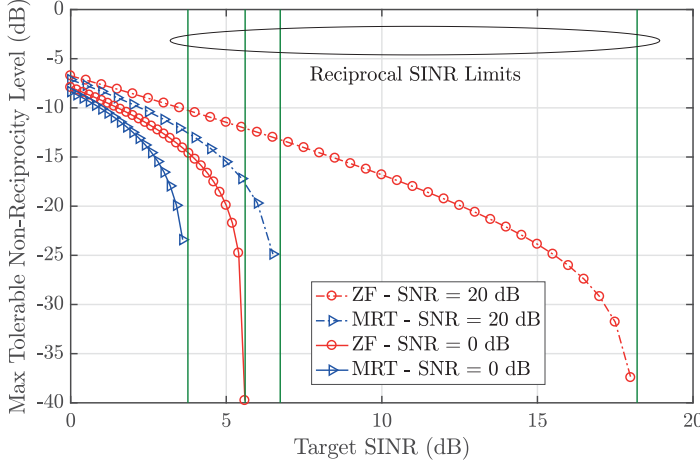


Figure 4.6: Maximum tolerable non-reciprocity level vs. target SINR ($\sigma_{a'_d}^2 = \sigma_{c'_d}^2 =$ channel non-reciprocity level, while $\sigma_{c_{od}}^2 = \delta_{c'_d}^2 =$ channel non-reciprocity level -10 dB) for $N = 100$, $M_{tot} = K = 20$, $\tau_u = M_{tot}$, $\rho_u = 0$ dB.

error which is defined as

$$\delta_{c'_d} = \frac{|\sigma_{c'_d}^2 - \hat{\sigma}_{c'_d}^2|}{\sigma_{c'_d}^2}, \quad (4.54)$$

where $\hat{\sigma}_{c'_d}^2$ can be calculated based on (4.39) or (4.40), depending on the use of downlink pilots. In the basic scenario, this estimation error is calculated directly based on the estimated values of BS transceiver non-reciprocity level in the UE side. In order to improve the estimation accuracy, the UEs can report their estimations to the BS where they are averaged. In such scenarios, the averaged value is used as $\hat{\sigma}_{c'_d}^2$ in (4.54).

Since it is not required to have BS transceiver non-reciprocity level estimation in every single UE, only subset of UEs which have better channel conditions can be selected for this purpose. Thus, in this simulation example, the number of UEs which are simultaneously supported by ZF precoding is set to $K = 10$ while the duration of each coherence interval is assumed to be $T_{coh} = 500$ symbols. The number of coherence intervals used for estimation is chosen to be $N_{coh} = 50$. The only channel non-reciprocity statistics assumed in this example are $\sigma_{a'_d}^2 = \sigma_{c'_d}^2 = -20$ dB while other channel non-reciprocity characteristics are assumed to be ideal. In case of having downlink pilots, the variance of downlink channel estimation error in the UE side is set to $\sigma_{e_{pilot}}^2 = -20$ dB.

The estimation accuracy is plotted with respect to the number of antennas in the BS, N , in Figure 4.7. As illustrated, the accuracy of the estimation increases with the number of BS antennas mainly since the approximation used in (4.32), based on the law of large numbers, gets more accurate with higher values of N . While the estimation errors are always less than 1 dB, it can be observed that estimation of BS transceiver non-reciprocity level gets more accurate with averaging in the BS side and employing downlink pilots.

Figure 4.8 illustrates the accuracy of BS transceiver non-reciprocity level estimation as a function of downlink SNR. As can be seen, when downlink pilots are used, downlink SNR has negligible impact on the accuracy of the estimation. Whereas, as expected based

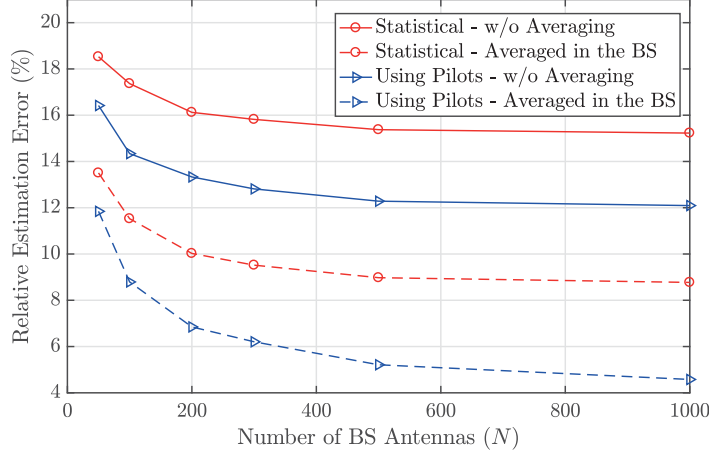


Figure 4.7: Relative estimation error vs. number of BS antennas (N) for $M_{tot} = K = 10$, $\tau_u = M_{tot}$, $\rho_u = 0$ dB, $\rho_d = 20$ dB, $\sigma_{a'_d}^2 = \sigma_{c'_d}^2 = -20$ dB, $\sigma_{epilot}^2 = -20$ dB, $T_{coh} = 500$.

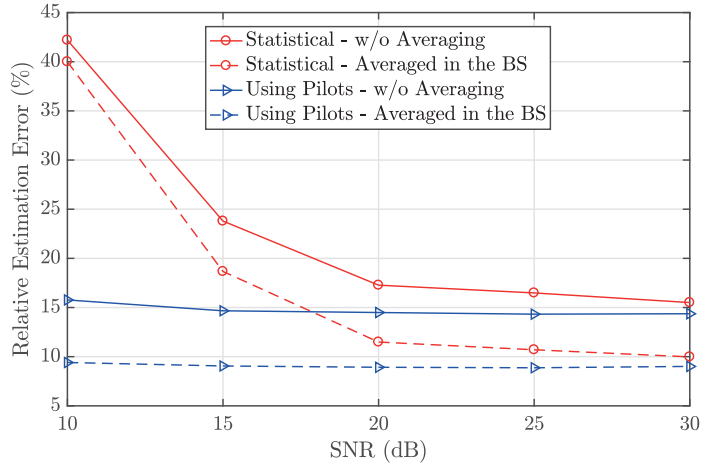


Figure 4.8: Relative estimation error vs. downlink SNR (ρ_d) for $N = 100$, $M_{tot} = K = 10$, $\tau_u = M_{tot}$, $\rho_u = 0$ dB, $\sigma_{a'_d}^2 = \sigma_{c'_d}^2 = -20$ dB, $\sigma_{epilot}^2 = -20$ dB, $T_{coh} = 500$.

on (4.35), estimation accuracy is very sensitive to downlink SNR in case of statistical downlink channel estimation. Note that, while even in low SNR regime the estimation accuracy is less than 3 dB, in practice, UEs with higher SNRs and better channel qualities can be selected for BS transceiver non-reciprocity level estimation.

4.6.3 Channel Non-Reciprocity Mitigation

Here, the performance of channel non-reciprocity estimation and mitigation framework is evaluated and compared to two other existing schemes in the literature, namely the direct-path based Least Squares (LS) known as “Argos” [97] and the generalized neighbor LS [96]. Both LS-based methods rely on downlink pilots to compensate the transceiver

non-reciprocity in the UE side while employing mutual coupling between the BS antennas to estimate and mitigate BS transceiver non-reciprocity. It should be noted that the conventional method of sending downlink pilots in which the number of sent pilots is equal to the number of antennas in the BS side is not feasible in massive MIMO context. Thus, here we take advantage of the method proposed in [66] for massive MIMO systems, in which the number of downlink pilots can be $\tau_d \geq M_{tot}$. As mentioned earlier, exact number of such pilots used in the simulations is $\tau_d = M_{tot}$.

In order to quantify the accuracy of BS and UE sides' transceiver non-reciprocity estimation, the normalized MSE metric is employed which is defined as

$$\delta_e^2 = \begin{cases} \frac{\|\mathbf{C} - \hat{\mathbf{C}}\|_F^2}{\|\mathbf{C}\|_F^2}, & \text{for BS side} \\ \frac{\|\text{diag}(\mathbf{A}) - \text{diag}(\hat{\mathbf{A}})\|_F^2}{\|\text{diag}(\mathbf{A})\|_F^2}, & \text{for UE side.} \end{cases} \quad (4.55)$$

The example simulation scenario consists of 20 single-antenna UEs where the BS is assumed to estimate channel non-reciprocity in 4 iterations over $C_{sc} = 10$ neighboring subcarriers. The convergence aspects of the channel non-reciprocity estimation method, which resulted into having 4 as the number of iterations of choice, is covered in details in [P1]. In pilot signaling stage, uplink and downlink SNRs are assumed to be $\tilde{\rho}_u = 0$ dB and $\tilde{\rho}_d = 10$ dB, respectively, while for the two LS-based methods, the coupling SNR between two neighboring antennas is 80 dB [96]. The entries of channel non-reciprocity matrices are drawn based on the channel non-reciprocity model introduced in [77]. Based on such modeling, in this example, variances of diagonal elements in \mathbf{F}^{RX} , \mathbf{F}^{TX} , \mathbf{B}^{RX} , and \mathbf{B}^{TX} , shown in (2.21), are set to -20 dB while the power of elements in \mathbf{M}^{RX} and \mathbf{M}^{TX} is controlled by input reflection coefficients which have the variance σ_{rc}^2 [77]. The antenna layout follows the one in Figure 4.1 and the carrier frequency is assumed to be $f_c = 3.5$ GHz.

The impacts of sparsity threshold on the channel non-reciprocity estimation normalized MSE and the system spectral efficiency is evaluated and visualized in Figure 4.9. Here, the baseline system settings are followed while the x-axis represents varying σ_{rc}^2 . In this respect, Figure 4.9a shows the normalized MSE of BS and UE sides' transceiver non-reciprocity estimation. Based on the results, highest accuracy in UE transceiver non-reciprocity estimation is achieved when $D = 0$, i.e., only the diagonal elements of \mathbf{C} are estimated. Note that, while the choice of D has direct impact only on estimating \mathbf{C} , it will in turn influence the estimation accuracy of \mathbf{A} as \mathbf{A} and \mathbf{C} are estimated iteratively. On the other hand, the lowest BS transceiver non-reciprocity estimation error is obtained for $D = 0$ only when $\sigma_{rc}^2 \leq -21$ dB, while for higher values of σ_{rc}^2 , i.e., $\sigma_{rc}^2 > -21$ dB, $D = 1$ is the optimum choice. Figure 4.9b illustrates combined impacts of sparsity threshold on both BS and UE transceiver channel non-reciprocity estimation through evaluating spectral efficiency. Here, the choice of $D = 0$ results into having highest spectral efficiency when $\sigma_{rc}^2 \leq -22$ dB while for $\sigma_{rc}^2 > -22$ dB, $D = 1$ is the best choice.

Figure 4.10 illustrates the spectral efficiency as a function of number of scheduled UEs for $\sigma_{rc}^2 = -20$ where based on Figure 4.9 the sparsity threshold is set to $D = 1$. As can clearly be observed, the proposed method outperforms both LS-based algorithms in both ZF and MRT precoded scenarios. The difference in spectral efficiency of the

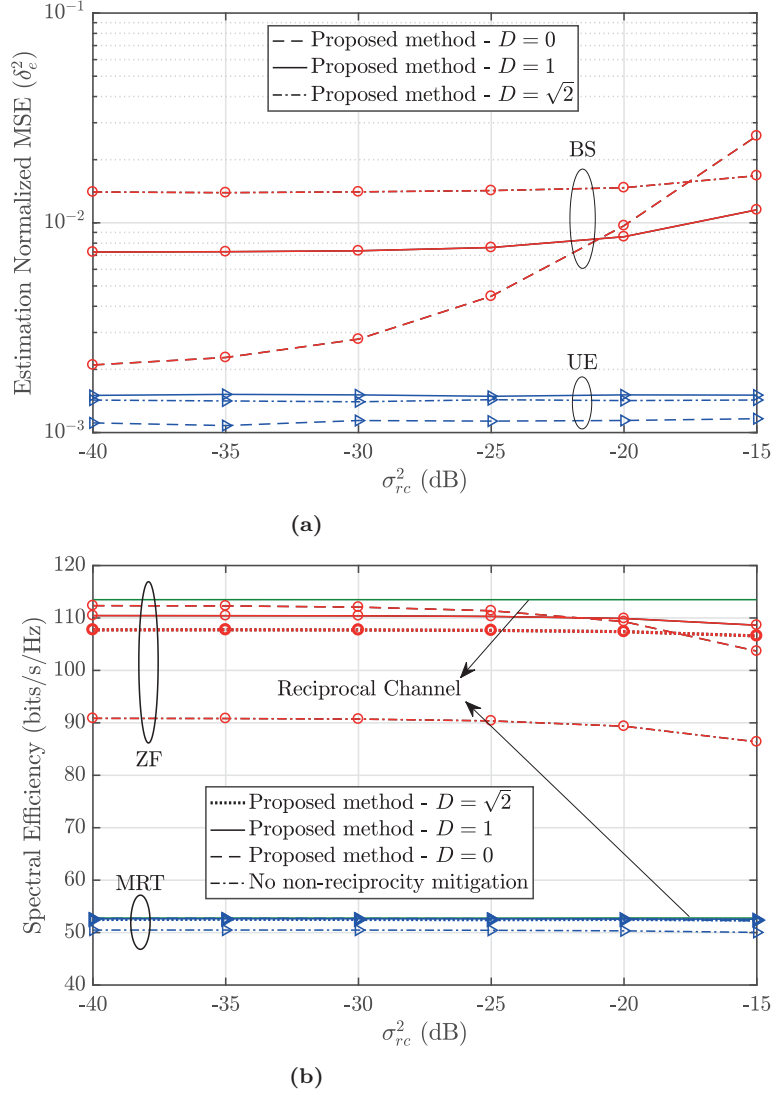


Figure 4.9: (a) Non-reciprocity estimation normalized MSE and (b) system spectral efficiency vs. input reflection coefficients variance (σ_{rc}^2) for different values of sparsity threshold D with $N = 100$, $M_{tot} = K = 20$, $\tau_u = \tau_d = M_{tot}$, $\rho_u = 0$ dB, $\rho_d = 20$ dB, $T_{coh} = 250$.

proposed method and the other two methods gets larger as the number of UEs increases. Additionally, using the proposed method, the BS can simultaneously schedule more UEs without sacrificing the overall spectral efficiency as the number of scheduled UEs which maximizes the spectral efficiency is higher in the proposed method compared to the other two methods.

Finally, the impact of the variance of input reflection coefficients, which controls the power of non-diagonal elements in \mathbf{C} , on spectral efficiency is evaluated in Figure 4.11. As can be seen, mainly for ZF precoding which is more sensitive to channel non-reciprocity, the performance of both LS-based methods degrades as σ_{rc}^2 increases while the impact of

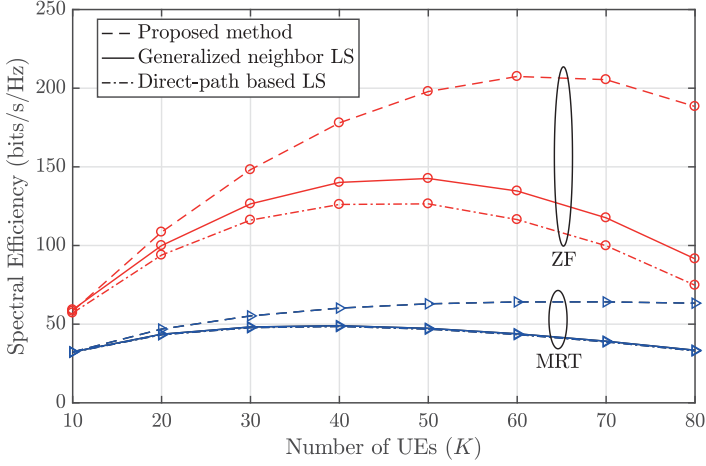


Figure 4.10: System spectral efficiency vs. the number of scheduled UEs (K) for $N = 100$, $M_{tot} = K$, $D = 1$, $\tau_u = \tau_d = M_{tot}$, $\rho_u = 0$ dB, $\rho_d = 20$ dB, $\sigma_{rc}^2 = -20$ dB, $T_{coh} = 250$.

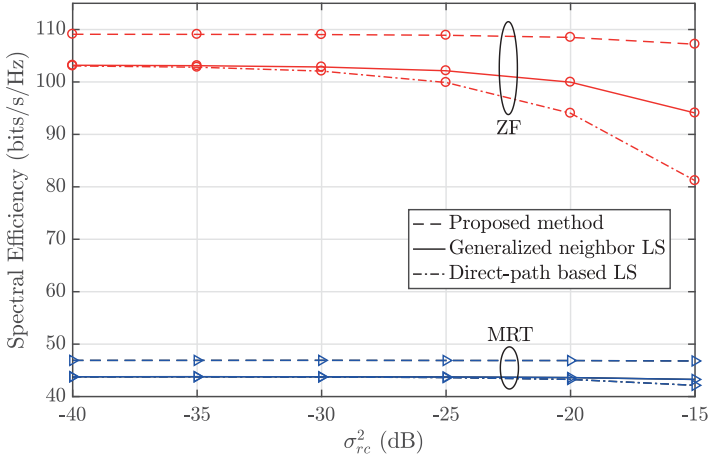


Figure 4.11: System spectral efficiency vs. input reflection coefficients variance (σ_{rc}^2) for $N = 100$, $M_{tot} = K = 20$, $D = 1$, $\tau_u = \tau_d = M_{tot}$, $\rho_u = 0$ dB, $\rho_d = 20$ dB, $T_{coh} = 250$.

σ_{rc}^2 on the performance of the proposed method is negligible. This is due to the fact that the proposed method is the only method that estimates the non-diagonal entries in the BS transceiver matrix while the other two methods only focus on the diagonal elements.

CHAPTER 5

SUMMARY

It is evident that MIMO technology is going to be one of the key elements in upcoming wireless communication systems, especially 5G. In this respect, this thesis addressed the problems associated with channel non-reciprocity in TDD MIMO systems due to mismatches in transmitter and receiver chains of a certain transceiver circuit and antenna system. Such channel non-reciprocity problem in TDD networks complicates having timely and accurate information of the channel at the transmitter side which is essential in MIMO systems. The overall contribution of the thesis is two folds, namely analysis of the performance degradation affect of various non-reciprocity parameters and mitigation of these harmful affects via appropriate pilot signaling and digital signal processing.

Chapter 3 and [P6]–[P8] focused on channel non-reciprocity problem in small-scale MIMO TDD systems. In single-cell scenario, for ZF and eigen-based precoded downlink transmission, performance degradations due to channel non-reciprocity caused by both FR and mutual coupling mismatches were analyzed. It was observed that, compared to FR mismatch, mutual coupling mismatch has more destructive impacts on the system performance. In addition to that, the system performance is more sensitive to BS transceiver non-reciprocity which causes both ISI and IUI, while non-reciprocity at the UE side only causes ISI. Based on these findings and assuming reasonably good antenna isolation, in order to have IUI-free transmission, a pilot-based OTA BS transceiver estimation and mitigation method was proposed. The proposed method was shown to be capable of efficiently estimating BS transceiver non-reciprocity parameters with high accuracy and thus improve the system performance significantly. In multi-cell scenario, the performance impacts of FR mismatch at the UE side were analyzed in both centralized and decentralized precoding scenarios. The results implied that while centralized precoding is resistant to such non-reciprocity in the channel, there is severe performance degradation in the performance of decentralized precoding. Overall, the observation that UE side FR mismatch can severely limit the performance is one clear difference between single-cell and multi-cell precoded systems.

In Chapter 4 and [P1]–[P5], the focus was turned to massive MIMO systems. In this respect, closed-form analytical expressions were derived for the effective SINRs of ZF and MRT precoded downlink transmission systems under channel non-reciprocity and

imperfect uplink channel estimation. The provided analysis showed significant performance loss under non-reciprocal channels in ZF precoded system, i.e., 42% with practical channel non-reciprocity levels, while MRT precoded system proved to be less sensitive to such non-idealities, i.e., 13% for the same example scenario. Due to such difference in the behaviors of ZF and MRT precoded systems, the performance gap between ZF and MRT precoded systems was shown to decrease significantly with the presence of channel non-reciprocity. The study also presented very interesting findings and implications for TDD massive MIMO systems under channel non-reciprocity which are different than those of the ideal reciprocal one, namely, i) the asymptotic performance for large number of BS antennas saturates to an identical finite level for both ZF and MRT precoded systems, whereas in ideal reciprocal scenario the achievable sum-rate grows without bound; ii) as opposed to ideal reciprocal scenario where the optimal number of simultaneously scheduled single-antenna UEs is always higher in ZF precoded systems compared to MRT precoded ones, under non-reciprocal channels and in high SNR regime, MRT can optimally serve more UEs simultaneously. In order to efficiently choose optimum time to perform channel non-reciprocity mitigation rounds at the BS and thus avoid wasting channel resources, an efficient BS transceiver non-reciprocity level estimation method was proposed to be deployed in the UE side. This enables UEs to report the need for a BS transceiver calibration round using simple one-bit feedback without any additional overhead. Additionally, in order to mitigate channel non-reciprocity in massive MIMO TDD systems, an efficient iterative pilot-based OTA channel non-reciprocity estimation and mitigation framework was proposed. As opposed to the existing state-of-the-art channel non-reciprocity estimation methods used in massive MIMO systems which only estimate the non-reciprocity in BS transceiver, the proposed method also estimates UE side non-reciprocity matrix. The proposed method does not require having demodulation downlink pilots to compensate for UE side non-reciprocity and can work in common massive MIMO systems where UEs rely on statistical properties of the precoded channel for detection purposes. The practical examples and computer simulations showed clear advantage in using the proposed method over the existing state-of-the-art methods in terms of the system spectral efficiency.

Overall, having timely and accurate CSI at the transmitter side is very crucial for MIMO systems to reach their full potential. In TDD systems, channel non-reciprocity due to FR and mutual coupling mismatches causes inaccuracies in CSI, and consequently significant performance loss, and thus needs to be properly taken into account. The analyses presented in this thesis provide valuable tools in understanding, dimensioning, and designing practical TDD MIMO systems with given performance targets. In addition to that, the proposed channel non-reciprocity mitigation methods can be deployed in practical TDD MIMO systems to significantly enhance the system performance and help bringing out all the benefits of MIMO systems.

Lastly, the contributions of this thesis provide a good and comprehensive starting point for future research regarding, e.g., generalizing the performance analysis and evaluations to cases where i) other precoding schemes such as Regularized Zero-Forcing (RZF) precoding scheme [58] are considered; ii) receiver filters for joint processing of UE antennas and/or pilot contamination are also considered for massive MIMO scenarios; iii) more complex well-known estimation methods, such as maximum likelihood, are employed for non-reciprocity estimation purposes to establish performance upper bound for computationally-feasible approaches; iv) path-losses and shadowing are taken into account to reflect different locations of the scheduled UEs in the network, which does not add additional complexity when it comes to channel non-reciprocity analysis; v) and generalizing analysis and

performance evaluations to “cell-free” massive MIMO cases with distributed beamforming [103, 104].

BIBLIOGRAPHY

- [1] *Digital cellular telecommunications system (Phase 2+) (GSM); GSM/EDGE Physical layer on the radio path; General description.* The 3rd Generation Partnership Project (3GPP), TS 45.001, version 14.2.0, release 14, August 2017.
- [2] *Universal Mobile Telecommunications System (UMTS); Physical layer - general description.* The 3rd Generation Partnership Project (3GPP), TS 25.201, version 14.0.0, release 14, April 2017.
- [3] *LTE; Evolved Universal Terrestrial Radio Access (E-UTRA); LTE physical layer; General description.* The 3rd Generation Partnership Project (3GPP), TS 36.201, version 14.1.0, release 14, April 2017.
- [4] C. Bockelmann, N. Pratas, H. Nikopour, K. Au, T. Svensson, C. Stefanovic, P. Popovski, and A. Dekorsy, “Massive machine-type communications in 5G: physical and MAC-layer solutions,” *IEEE Communications Magazine*, vol. 54, no. 9, pp. 59–65, Sep. 2016.
- [5] T. Taleb and A. Kunz, “Machine type communications in 3GPP networks: potential, challenges, and solutions,” *IEEE Communications Magazine*, vol. 50, no. 3, pp. 178–184, March 2012.
- [6] R. Ratasuk, A. Prasad, Z. Li, A. Ghosh, and M. A. Uusitalo, “Recent advancements in M2M communications in 4G networks and evolution towards 5G,” in *2015 18th International Conference on Intelligence in Next Generation Networks*, Feb 2015, pp. 52–57.
- [7] M. Condoluci, M. Dohler, G. Araniti, A. Molinaro, and K. Zheng, “Toward 5G densenets: architectural advances for effective machine-type communications over femtocells,” *IEEE Communications Magazine*, vol. 53, no. 1, pp. 134–141, January 2015.
- [8] International Telecommunications Union - Telecommunications Standardization Sector (ITU-T), *Recommendation ITU-T Y.2060 - Overview of the Internet of Things*, June 2012, last accessed 23.01.2018. [Online]. Available: <https://www.itu.int/rec/T-REC-Y.2060-201206-I/en>

- [9] A. Al-Fuqaha, M. Guizani, M. Mohammadi, M. Aledhari, and M. Ayyash, "Internet of things: A survey on enabling technologies, protocols, and applications," *IEEE Communications Surveys Tutorials*, vol. 17, no. 4, pp. 2347–2376, Fourthquarter 2015.
- [10] A. Zanella, N. Bui, A. Castellani, L. Vangelista, and M. Zorzi, "Internet of things for smart cities," *IEEE Internet of Things Journal*, vol. 1, no. 1, pp. 22–32, Feb 2014.
- [11] L. D. Xu, W. He, and S. Li, "Internet of things in industries: A survey," *IEEE Transactions on Industrial Informatics*, vol. 10, no. 4, pp. 2233–2243, Nov 2014.
- [12] J. A. Stankovic, "Research directions for the internet of things," *IEEE Internet of Things Journal*, vol. 1, no. 1, pp. 3–9, Feb 2014.
- [13] *5G; NR; Physical layer; General description*. The 3rd Generation Partnership Project (3GPP), TS 38.201, version 15.0.0, release 15, September 2018.
- [14] F. Boccardi, R. Heath, A. Lozano, T. L. Marzetta, and P. Popovski, "Five disruptive technology directions for 5G," *IEEE Communications Magazine*, vol. 52, no. 2, pp. 74–80, February 2014.
- [15] J. G. Andrews, S. Buzzi, W. Choi, S. V. Hanly, A. Lozano, A. C. K. Soong, and J. C. Zhang, "What will 5G be?" *IEEE Journal on Selected Areas in Communications*, vol. 32, no. 6, pp. 1065–1082, June 2014.
- [16] Z. Ding, R. Schober, and H. V. Poor, "A general MIMO framework for NOMA downlink and uplink transmission based on signal alignment," *IEEE Transactions on Wireless Communications*, vol. 15, no. 6, pp. 4438–4454, June 2016.
- [17] Z. Ding, X. Lei, G. K. Karagiannidis, R. Schober, J. Yuan, and V. K. Bhargava, "A survey on non-orthogonal multiple access for 5G networks: Research challenges and future trends," *IEEE Journal on Selected Areas in Communications*, vol. 35, no. 10, pp. 2181–2195, Oct 2017.
- [18] Y. Sun, D. W. K. Ng, Z. Ding, and R. Schober, "Optimal joint power and subcarrier allocation for full-duplex multicarrier non-orthogonal multiple access systems," *IEEE Transactions on Communications*, vol. 65, no. 3, pp. 1077–1091, March 2017.
- [19] Y. Saito, Y. Kishiyama, A. Benjebbour, T. Nakamura, A. Li, and K. Higuchi, "Non-orthogonal multiple access (NOMA) for cellular future radio access," in *2013 IEEE 77th Vehicular Technology Conference (VTC Spring)*, June 2013, pp. 1–5.
- [20] L. Dai, B. Wang, Y. Yuan, S. Han, C. I, and Z. Wang, "Non-orthogonal multiple access for 5G: solutions, challenges, opportunities, and future research trends," *IEEE Communications Magazine*, vol. 53, no. 9, pp. 74–81, Sep. 2015.
- [21] A. A. Zaidi, J. Luo, R. Gerzaguet, A. Wolfgang, R. J. Weiler, J. Vihriala, T. Svensson, Y. Qi, H. Halbauer, Z. Zhao, P. Zetterberg, and H. Miao, "A preliminary study on waveform candidates for 5G mobile radio communications above 6 GHz," in *2016 IEEE 83rd Vehicular Technology Conference (VTC Spring)*, May 2016, pp. 1–6.

- [22] G. Wunder, P. Jung, M. Kasparick, T. Wild, F. Schaich, Y. Chen, S. T. Brink, I. Gaspar, N. Michailow, A. Festag, L. Mendes, N. Cassiau, D. Ktenas, M. Dryjanski, S. Pietrzyk, B. Eged, P. Vago, and F. Wiedmann, "5GNOW: non-orthogonal, asynchronous waveforms for future mobile applications," *IEEE Communications Magazine*, vol. 52, no. 2, pp. 97–105, February 2014.
- [23] J. Yli-Kaakinen, T. Levanen, S. Valkonen, K. Pajukoski, J. Pirskanen, M. Renfors, and M. Valkama, "Efficient fast-convolution-based waveform processing for 5G physical layer," *IEEE Journal on Selected Areas in Communications*, vol. 35, no. 6, pp. 1309–1326, June 2017.
- [24] P. Banelli, S. Buzzi, G. Colavolpe, A. Modenini, F. Rusek, and A. Ugolini, "Modulation formats and waveforms for 5G networks: Who will be the heir of OFDM?: An overview of alternative modulation schemes for improved spectral efficiency," *IEEE Signal Processing Magazine*, vol. 31, no. 6, pp. 80–93, Nov 2014.
- [25] J. Ordóñez-Lucena, P. Ameigeiras, D. Lopez, J. J. Ramos-Munoz, J. Lorca, and J. Folgueira, "Network slicing for 5G with SDN/NFV: Concepts, architectures, and challenges," *IEEE Communications Magazine*, vol. 55, no. 5, pp. 80–87, May 2017.
- [26] H. Zhang, N. Liu, X. Chu, K. Long, A. Aghvami, and V. C. M. Leung, "Network slicing based 5G and future mobile networks: Mobility, resource management, and challenges," *IEEE Communications Magazine*, vol. 55, no. 8, pp. 138–145, Aug 2017.
- [27] X. Foukas, G. Patounas, A. Elmokashfi, and M. K. Marina, "Network slicing in 5G: Survey and challenges," *IEEE Communications Magazine*, vol. 55, no. 5, pp. 94–100, May 2017.
- [28] P. Rost, C. Mannweiler, D. S. Michalopoulos, C. Sartori, V. Sciancalepore, N. Sastry, O. Holland, S. Tayade, B. Han, D. Bega, D. Aziz, and H. Bakker, "Network slicing to enable scalability and flexibility in 5G mobile networks," *IEEE Communications Magazine*, vol. 55, no. 5, pp. 72–79, May 2017.
- [29] Z. Shen, A. Khoryaev, E. Eriksson, and X. Pan, "Dynamic uplink-downlink configuration and interference management in TD-LTE," *IEEE Communications Magazine*, vol. 50, no. 11, pp. 51–59, November 2012.
- [30] J. Li, S. Farahvash, M. Kavehrad, and R. Valenzuela, "Dynamic TDD and fixed cellular networks," *IEEE Communications Letters*, vol. 4, no. 7, pp. 218–220, July 2000.
- [31] B. Yu, L. Yang, H. Ishii, and S. Mukherjee, "Dynamic TDD support in macrocell-assisted small cell architecture," *IEEE Journal on Selected Areas in Communications*, vol. 33, no. 6, pp. 1201–1213, June 2015.
- [32] C. Dehos, J. L. González, A. D. Domenico, D. Kténas, and L. Dussopt, "Millimeter-wave access and backhauling: the solution to the exponential data traffic increase in 5G mobile communications systems?" *IEEE Communications Magazine*, vol. 52, no. 9, pp. 88–95, Sep. 2014.
- [33] O. Tipmongkolsilp, S. Zaghloul, and A. Jukan, "The evolution of cellular backhaul technologies: Current issues and future trends," *IEEE Communications Surveys & Tutorials*, vol. 13, no. 1, pp. 97–113, First 2011.

- [34] M. Coldrey, J. Berg, L. Manholm, C. Larsson, and J. Hansryd, "Non-line-of-sight small cell backhauling using microwave technology," *IEEE Communications Magazine*, vol. 51, no. 9, pp. 78–84, Sep. 2013.
- [35] H. S. Dhillon and G. Caire, "Wireless backhaul networks: Capacity bound, scalability analysis and design guidelines," *IEEE Transactions on Wireless Communications*, vol. 14, no. 11, pp. 6043–6056, Nov 2015.
- [36] Huawei Technologies Co. Ltd., *5G Spectrum, Public Policy Position*, 2017, last accessed 23.01.2018. [Online]. Available: http://www-file.huawei.com/-/media/CORPORATE/PDF/public-policy/public_policy_position_5g_spectrum.pdf
- [37] R. Ratasuk, N. Mangalvedhe, and A. Ghosh, "LTE in unlicensed spectrum using licensed-assisted access," in *2014 IEEE Globecom Workshops (GC Wkshps)*, Dec 2014, pp. 746–751.
- [38] A. Mukherjee, J. Cheng, S. Falahati, H. Koorapaty, D. H. Kang, R. Karaki, L. Falconetti, and D. Larsson, "Licensed-assisted access LTE: coexistence with IEEE 802.11 and the evolution toward 5G," *IEEE Communications Magazine*, vol. 54, no. 6, pp. 50–57, June 2016.
- [39] N. Rupasinghe and . Güvenç, "Licensed-assisted access for WiFi-LTE coexistence in the unlicensed spectrum," in *2014 IEEE Globecom Workshops (GC Wkshps)*, Dec 2014, pp. 894–899.
- [40] T. S. Rappaport, G. R. MacCartney, M. K. Samimi, and S. Sun, "Wideband millimeter-wave propagation measurements and channel models for future wireless communication system design," *IEEE Transactions on Communications*, vol. 63, no. 9, pp. 3029–3056, Sep. 2015.
- [41] R. W. Heath, N. González-Prelcic, S. Rangan, W. Roh, and A. M. Sayeed, "An overview of signal processing techniques for millimeter wave MIMO systems," *IEEE Journal of Selected Topics in Signal Processing*, vol. 10, no. 3, pp. 436–453, April 2016.
- [42] A. Ghosh, T. A. Thomas, M. C. Cudak, R. Ratasuk, P. Moorut, F. W. Vook, T. S. Rappaport, G. R. MacCartney, S. Sun, and S. Nie, "Millimeter-wave enhanced local area systems: A high-data-rate approach for future wireless networks," *IEEE Journal on Selected Areas in Communications*, vol. 32, no. 6, pp. 1152–1163, June 2014.
- [43] W. Roh, J. Seol, J. Park, B. Lee, J. Lee, Y. Kim, J. Cho, K. Cheun, and F. Aryanfar, "Millimeter-wave beamforming as an enabling technology for 5G cellular communications: theoretical feasibility and prototype results," *IEEE Communications Magazine*, vol. 52, no. 2, pp. 106–113, February 2014.
- [44] V. Jungnickel, K. Manolakis, W. Zirwas, B. Panzner, V. Braun, M. Lossow, M. Sternad, R. Apelfrojd, and T. Svensson, "The role of small cells, coordinated multipoint, and massive MIMO in 5G," *IEEE Communications Magazine*, vol. 52, no. 5, pp. 44–51, May 2014.
- [45] N. Bhushan, J. Li, D. Malladi, R. Gilmore, D. Brenner, A. Damnjanovic, R. T. Sukhvasi, C. Patel, and S. Geirhofer, "Network densification: the dominant theme for wireless evolution into 5G," *IEEE Communications Magazine*, vol. 52, no. 2, pp. 82–89, February 2014.

- [46] M. Kamel, W. Hamouda, and A. Youssef, "Ultra-dense networks: A survey," *IEEE Communications Surveys & Tutorials*, vol. 18, no. 4, pp. 2522–2545, Fourthquarter 2016.
- [47] J. Mietzner, R. Schober, L. Lampe, W. H. Gerstacker, and P. A. Hoeher, "Multiple-antenna techniques for wireless communications - a comprehensive literature survey," *IEEE Communications Surveys Tutorials*, vol. 11, no. 2, pp. 87–105, Second 2009.
- [48] A. F. Molisch, *Wireless Communications*, 2nd ed. John Wiley & Sons, Ltd, 2011.
- [49] L. Zheng and D. N. C. Tse, "Diversity and multiplexing: a fundamental tradeoff in multiple-antenna channels," *IEEE Transactions on Information Theory*, vol. 49, no. 5, pp. 1073–1096, May 2003.
- [50] H. Bolcskei, D. Gesbert, and A. J. Paulraj, "On the capacity of OFDM-based spatial multiplexing systems," *IEEE Transactions on Communications*, vol. 50, no. 2, pp. 225–234, Feb 2002.
- [51] M. Vu and A. Paulraj, "MIMO wireless linear precoding," *IEEE Signal Processing Magazine*, vol. 24, no. 5, pp. 86–105, Sept 2007.
- [52] P. W. C. Chan, E. S. Lo, R. R. Wang, E. K. S. Au, V. K. N. Lau, R. S. Cheng, W. H. Mow, R. D. Murch, and K. B. Letaief, "The evolution path of 4G networks: FDD or TDD?" *IEEE Communications Magazine*, vol. 44, no. 12, pp. 42–50, Dec 2006.
- [53] M. Kobayashi, N. Jindal, and G. Caire, "Training and feedback optimization for multiuser MIMO downlink," *IEEE Transactions on Communications*, vol. 59, no. 8, pp. 2228–2240, August 2011.
- [54] Ericsson, "5g radio access," White paper, April 2016. [Online]. Available: <https://www.ericsson.com/assets/local/publications/white-papers/wp-5g.pdf>
- [55] E. G. Larsson, O. Edfors, F. Tufvesson, and T. L. Marzetta, "Massive MIMO for next generation wireless systems," *IEEE Communications Magazine*, vol. 52, no. 2, pp. 186–195, February 2014.
- [56] T. L. Marzetta, E. G. Larsson, H. Yang, and H. Q. Ngo, *Fundamentals of Massive MIMO*. Cambridge University Press, 2016.
- [57] E. Björnson, J. Hoydis, and L. Sanguinetti, "Massive MIMO networks: Spectral, energy, and hardware efficiency," *Foundations and Trends® in Signal Processing*, vol. 11, no. 3-4, pp. 154–655, 2017.
- [58] J. Hoydis, S. ten Brink, and M. Debbah, "Massive MIMO in the UL/DL of cellular networks: how many antennas do we need?" *IEEE Journal on Selected Areas in Communications*, vol. 31, no. 2, pp. 160–171, February 2013.
- [59] L. Lu, G. Y. Li, A. L. Swindlehurst, A. Ashikhmin, and R. Zhang, "An overview of massive MIMO: benefits and challenges," *IEEE Journal of Selected Topics in Signal Processing*, vol. 8, no. 5, pp. 742–758, Oct 2014.
- [60] T. L. Marzetta, "Noncooperative cellular wireless with unlimited numbers of base station antennas," *IEEE Transactions on Wireless Communications*, vol. 9, no. 11, pp. 3590–3600, November 2010.

- [61] H. Q. Ngo, E. G. Larsson, and T. L. Marzetta, "Energy and spectral efficiency of very large multiuser MIMO systems," *IEEE Transactions on Communications*, vol. 61, no. 4, pp. 1436–1449, April 2013.
- [62] H. Yang and T. L. Marzetta, "Performance of conjugate and zero-forcing beamforming in large-scale antenna systems," *IEEE Journal on Selected Areas in Communications*, vol. 31, no. 2, pp. 172–179, February 2013.
- [63] X. Gao, O. Edfors, F. Rusek, and F. Tufvesson, "Linear pre-coding performance in measured very-large MIMO channels," in *Vehicular Technology Conference (VTC Fall)*, 2011 IEEE, Sept 2011, pp. 1–5.
- [64] R. Irmer, H. Droste, P. Marsch, M. Grieger, G. Fettweis, S. Brueck, H. Mayer, L. Thiele, and V. Jungnickel, "Coordinated multipoint: Concepts, performance, and field trial results," *IEEE Communications Magazine*, vol. 49, no. 2, pp. 102–111, February 2011.
- [65] P. Komulainen, A. Tölli, and M. Juntti, "Effective CSI signaling and decentralized beam coordination in TDD multi-cell MIMO systems," *IEEE Transactions on Signal Processing*, vol. 61, no. 9, pp. 2204–2218, May 2013.
- [66] H. Q. Ngo, E. G. Larsson, and T. L. Marzetta, "Massive MU-MIMO downlink TDD systems with linear precoding and downlink pilots," in *51st Annual Allerton Conference on Communication, Control, and Computing (Allerton)*, Oct 2013, pp. 293–298.
- [67] G. Lebrun, J. Gao, and M. Faulkner, "Mimo transmission over a time-varying channel using SVD," *IEEE Transactions on Wireless Communications*, vol. 4, no. 2, pp. 757–764, March 2005.
- [68] H. Q. Ngo and E. G. Larsson, "No downlink pilots are needed in TDD massive MIMO," *IEEE Transactions on Wireless Communications*, vol. 16, no. 5, pp. 2921–2935, May 2017.
- [69] Z. Chen and E. Björnson, "Channel hardening and favorable propagation in cell-free massive MIMO with stochastic geometry," *IEEE Transactions on Communications*, vol. 66, no. 11, pp. 5205–5219, Nov 2018.
- [70] J. Liu, A. Bourdoux, J. Craninckx, P. Wambacq, B. Come, S. Donnay, and A. Barel, "OFDM-MIMO WLAN AP front-end gain and phase mismatch calibration," in *Radio and Wireless Conference, 2004 IEEE*, Sept 2004, pp. 151–154.
- [71] B. Kouassi, I. Ghauri, and L. Deneire, "Estimation of time-domain calibration parameters to restore MIMO-TDD channel reciprocity," in *7th International ICST Conference on Cognitive Radio Oriented Wireless Networks and Communications (CROWNCOM)*, June 2012, pp. 254–258.
- [72] H. Wei, D. Wang, and X. You, "Reciprocity of mutual coupling for TDD massive MIMO systems," in *Wireless Communications Signal Processing (WCSP), 2015 International Conference on*, Oct 2015, pp. 1–5.
- [73] F. Athley, G. Durisi, and U. Gustavsson, "Analysis of massive MIMO with hardware impairments and different channel models," in *2015 9th European Conference on Antennas and Propagation (EuCAP)*, May 2015, pp. 1–5.

- [74] H. Wei, D. Wang, J. Wang, and X. You, "Impact of RF mismatches on the performance of massive MIMO systems with ZF precoding," *Science China Information Sciences*, vol. 59, no. 2, pp. 1–14, 2016. [Online]. Available: <http://dx.doi.org/10.1007/s11432-015-5509-1>.
- [75] W. Zhang, H. Ren, C. Pan, M. Chen, R. de Lamare, B. Du, and J. Dai, "Large-scale antenna systems with UL/DL hardware mismatch: achievable rates analysis and calibration," *IEEE Transactions on Communications*, vol. 63, no. 4, pp. 1216–1229, April 2015.
- [76] M. Guillaud, D. T. M. Slock, and R. Knopp, "A practical method for wireless channel reciprocity exploitation through relative calibration," in *Proceedings of the Eighth International Symposium on Signal Processing and Its Applications, 2005.*, vol. 1, August 2005, pp. 403–406.
- [77] M. Petermann, M. Stefer, F. Ludwig, D. Wubben, M. Schneider, S. Paul, and K.-D. Kammeyer, "Multi-user pre-processing in multi-antenna OFDM TDD systems with non-reciprocal transceivers," *IEEE Transactions on Communications*, vol. 61, no. 9, pp. 3781–3793, September 2013.
- [78] S. Durrani and M. E. Bialkowski, "Effect of mutual coupling on the interference rejection capabilities of linear and circular arrays in CDMA systems," *IEEE Transactions on Antennas and Propagation*, vol. 52, no. 4, pp. 1130–1134, April 2004.
- [79] J. Liu, A. Bourdoux, J. Craninckx, P. Wambacq, B. Come, S. Donnay, and A. Barel, "OFDM-MIMO WLAN AP front-end gain and phase mismatch calibration," in *Proceedings. 2004 IEEE Radio and Wireless Conference (IEEE Cat. No.04TH8746)*, Sept 2004, pp. 151–154.
- [80] R. Rogalin, O. Y. Bursalioglu, H. Papadopoulos, G. Caire, A. F. Molisch, A. Michaloliakos, V. Balan, and K. Psounis, "Scalable synchronization and reciprocity calibration for distributed multiuser MIMO," *IEEE Transactions on Wireless Communications*, vol. 13, no. 4, pp. 1815–1831, April 2014.
- [81] J. Liu, G. Vandersteen, J. Craninckx, M. Libois, M. Wouters, F. Petre, and A. Barel, "A novel and low-cost analog front-end mismatch calibration scheme for MIMO-OFDM WLANs," in *2006 IEEE Radio and Wireless Symposium*, Jan 2006, pp. 219–222.
- [82] A. Bourdoux, B. Come, and N. Khaled, "Non-reciprocal transceivers in OFDM/SDMA systems: impact and mitigation," in *Radio and Wireless Conference, 2003. RAWCON '03. Proceedings*, Aug 2003, pp. 183–186.
- [83] P. Zetterberg, "Experimental investigation of TDD reciprocity-based zero-forcing transmit precoding," *EURASIP Journal on Advances in Signal Processing*, vol. 2011, no. 1, p. 137541, Dec 2010.
- [84] M. Guillaud and F. Kaltenberger, "Towards practical channel reciprocity exploitation: Relative calibration in the presence of frequency offset," in *2013 IEEE Wireless Communications and Networking Conference (WCNC)*, April 2013, pp. 2525–2530.
- [85] F. Kaltenberger, H. Jiang, M. Guillaud, and R. Knopp, "Relative channel reciprocity calibration in MIMO/TDD systems," in *2010 Future Network Mobile Summit*, June 2010, pp. 1–10.

- [86] J. Ketonen, M. Juntti, and J. R. Cavallaro, "Performance—complexity comparison of receivers for a LTE MIMO–OFDM system," *IEEE Transactions on Signal Processing*, vol. 58, no. 6, pp. 3360–3372, June 2010.
- [87] A. Tolli, M. Codreanu, and M. Juntti, "Cooperative MIMO-OFDM cellular system with soft handover between distributed base station antennas," *IEEE Transactions on Wireless Communications*, vol. 7, no. 4, pp. 1428–1440, April 2008.
- [88] Q. Shi, M. Razaviyayn, Z.-Q. Luo, and C. He, "An iteratively weighted MMSE approach to distributed sum-utility maximization for a MIMO interfering broadcast channel," *IEEE Transactions on Signal Processing*, vol. 59, no. 9, pp. 4331–4340, Sept 2011.
- [89] S. Kaviani and W. Krzymien, "Sum rate maximization of MIMO broadcast channels with coordination of base stations," in *IEEE Wireless Communications and Networking Conference*, March 2008, pp. 1079–1084.
- [90] J. Kaleva, A. Tölili, and M. Juntti, "Weighted sum rate maximization for interfering broadcast channel via successive convex approximation," in *IEEE Global Communications Conference (GLOBECOM)*, Dec 2012, pp. 3838–3843.
- [91] H. Holma and A. Toskala, *LTE for UMTS: evolution to LTE-Advanced*, 2nd ed. John Wiley & Sons, Ltd, 2011.
- [92] T. B. Sorensen, P. E. Mogensen, and F. Frederiksen, "Extension of the ITU channel models for wideband (OFDM) systems," in *VTC-2005-Fall. 2005 IEEE 62nd Vehicular Technology Conference, 2005.*, vol. 1, Sept 2005, pp. 392–396.
- [93] J. Jose, A. Ashikhmin, P. Whiting, and S. Vishwanath, "Channel estimation and linear precoding in multiuser multiple-antenna TDD systems," *IEEE Transactions on Vehicular Technology*, vol. 60, no. 5, pp. 2102–2116, Jun 2011.
- [94] J. Jose, A. Ashikhmin, T. L. Marzetta, and S. Vishwanath, "Pilot contamination and precoding in multi-cell TDD systems," *IEEE Transactions on Wireless Communications*, vol. 10, no. 8, pp. 2640–2651, August 2011.
- [95] L. Lu, G. Y. Li, A. L. Swindlehurst, A. Ashikhmin, and R. Zhang, "An overview of massive MIMO: benefits and challenges," *IEEE Journal of Selected Topics in Signal Processing*, vol. 8, no. 5, pp. 742–758, Oct 2014.
- [96] J. Vieira, F. Rusek, and F. Tufvesson, "Reciprocity calibration methods for massive MIMO based on antenna coupling," in *2014 IEEE Global Communications Conference*, Dec 2014, pp. 3708–3712.
- [97] C. Shepard, H. Yu, N. Anand, E. Li, T. Marzetta, R. Yang, and L. Zhong, "Argos: Practical many-antenna base stations," in *Proceedings of the 18th Annual International Conference on Mobile Computing and Networking*, ser. Mobicom '12. New York, NY, USA: ACM, 2012, pp. 53–64.
- [98] H. Wei, D. Wang, H. Zhu, J. Wang, S. Sun, and X. You, "Mutual coupling calibration for multiuser massive MIMO systems," *IEEE Transactions on Wireless Communications*, vol. 15, no. 1, pp. 606–619, Jan 2016.

- [99] H. Wei, D. Wang, J. Wang, and X. You, “TDD reciprocity calibration for multi-user massive MIMO systems with iterative coordinate descent,” *Science China Information Sciences*, vol. 59, no. 10, p. 102306, 2015.
- [100] F. Rusek, D. Persson, B. K. Lau, E. Larsson, T. L. Marzetta, O. Edfors, and F. Tufvesson, “Scaling up MIMO: opportunities and challenges with very large arrays,” *IEEE Signal Processing Magazine*, vol. 30, no. 1, pp. 40–60, Jan 2013.
- [101] S. M. Kay, *Fundamentals of Statistical Signal Processing: Estimation Theory*. Prentice Hall, Inc., 1993.
- [102] E. Björnson, E. G. Larsson, and M. Debbah, “Massive MIMO for maximal spectral efficiency: how many users and pilots should be allocated?” *IEEE Transactions on Wireless Communications*, vol. 15, no. 2, pp. 1293–1308, Feb 2016.
- [103] H. Q. Ngo, A. Ashikhmin, H. Yang, E. G. Larsson, and T. L. Marzetta, “Cell-free massive mimo versus small cells,” *IEEE Transactions on Wireless Communications*, vol. 16, no. 3, pp. 1834–1850, March 2017.
- [104] E. Nayeri, A. Ashikhmin, T. L. Marzetta, and H. Yang, “Cell-free massive mimo systems,” in *2015 49th Asilomar Conference on Signals, Systems and Computers*, Nov 2015, pp. 695–699.

Publications

PUBLICATION I

O. Raeesi, A. Gokceoglu and M. Valkama, “Estimation and mitigation of channel non-reciprocity in massive MIMO,” *IEEE Transactions on Signal Processing*, vol. 66, no. 10, pp. 2711–2723, May 2018.

© 2018 IEEE. Reprinted, with permission, from O. Raeesi, A. Gokceoglu and M. Valkama, “Estimation and mitigation of channel non-reciprocity in massive MIMO,” *IEEE Transactions on Signal Processing*, May 2018.

In reference to IEEE copyrighted material which is used with permission in this thesis, the IEEE does not endorse any of Tampere University’s products or services. Internal or personal use of this material is permitted. If interested in reprinting/republishing IEEE copyrighted material for advertising or promotional purposes or for creating new collective works for resale or redistribution, please go to http://www.ieee.org/publications_standards/publications/rights/rights_link.html to learn how to obtain a License from RightsLink.

Estimation and Mitigation of Channel Non-Reciprocity in Massive MIMO

Orod Raeesi, *Student Member, IEEE*, Ahmet Gokceoglu, *Member, IEEE*,
and Mikko Valkama, *Senior Member, IEEE*

Abstract—Time-division duplex (TDD) based massive MIMO systems rely on the reciprocity of the wireless propagation channels when calculating the downlink precoders based on uplink pilots. However, the effective uplink and downlink channels incorporating the analog radio front-ends of the base station (BS) and user equipments (UEs) exhibit non-reciprocity due to non-identical behavior of the individual transmit and receive chains. When the downlink precoder is not aware of such channel non-reciprocity (NRC), system performance can be significantly degraded due to the NRC induced interference terms. In this work, we consider a general TDD-based massive MIMO system where frequency-response mismatches at both the BS and UEs, as well as the mutual coupling mismatches at the BS large-antenna system all coexist and induce channel NRC. Based on the NRC-impaired signal models, we first propose a novel iterative estimation method for acquiring both the BS and UE side NRC matrices and then also propose an efficient NRC-aware downlink precoder design which utilizes the obtained estimates. Furthermore, an efficient pilot signaling scheme between the BS and UEs is introduced in order to facilitate executing the proposed estimation method and the NRC-aware precoding technique in practical systems. Comprehensive numerical results indicate substantially improved spectral efficiency performance when the proposed NRC estimation and NRC-aware precoding methods are adopted, compared to the existing state-of-the-art methods.

Index Terms—Beamforming, channel non-reciprocity, channel state information, frequency-response mismatch, linear precoding, massive MIMO, mutual coupling, time division duplexing (TDD).

I. INTRODUCTION

MASSIVE MIMO is one of the key potential technologies for upcoming 5G systems [1] where base stations (BSs) deploy very large antenna arrays, e.g., several tens or hundreds of antenna units per array, to facilitate high beamforming and spatial multiplexing gains. In such systems, it is not feasible to transmit downlink pilots from each BS antenna in order to estimate the corresponding spatial channels at user equipments (UEs) and feedback the channel state information (CSI) to BS, as the amount of overhead in such approach is proportional to the number of antennas in the BS side [2]. Massive MIMO systems are thus envisioned to primarily deploy time-division duplex (TDD) based radio access and rely on the reciprocity

of the physical uplink and downlink channels when obtaining CSI at the BS. This, in turn, requires substantially smaller pilot or reference signal overhead being only proportional to the number of UEs [3].

While it is a common assumption in TDD systems that the physical propagation channels are reciprocal within a coherence interval [2], [3], the impacts of the BS and UE side transceiver analog front-ends on the *effective downlink and uplink channels* are not reciprocal. This hardware induced phenomenon is often referred to as the channel non-reciprocity (NRC) problem [4], [5]. Typically, the mismatches in the frequency-responses (FRs) of both the BS and UE side radio front-ends between the transmit and receive modes are seen as the main cause of NRC. Another important source of NRC considered in literature is the differences in mutual coupling (MC) of BS antenna units and the associated RF transceivers under transmit and receive modes [6], [7].

The impacts of the NRC on the achievable system performance have been studied in various works in the recent literature. To this end, [5] provides downlink sum-rate analysis for a general multi-user MIMO system with zero-forcing (ZF) and eigen-beamforming types of precoding under NRC due to FR mismatch. Then, specifically focusing on massive MIMO systems, [8], [9] study achievable downlink sum-rates for maximum-ratio transmission (MRT) and ZF precoding schemes, demonstrating significant performance degradation under practical values of the NRC parameters.

There is also a large amount of work reported in the literature addressing the estimation and mitigation of NRC in TDD based MIMO systems [2], [4], [6], [10]–[17]. These studies can be divided into three main categories as follows:

- i) The BS carries out “self-calibration” using a reference antenna with the help of additional circuitry [4], [6]. This method is capable of estimating the BS side NRC only.
- ii) The BS carries out “self-calibration” without additional circuitry. Coupling between the BS antennas is utilized when exchanging pilot signals with the reference antenna [2], [10]–[13]. Similar to i), also this method estimates only the BS side NRC and commonly focuses only on the FR mismatch estimation, thus neglecting the mutual coupling mismatch.
- iii) The BS transmits specific pilot signals to UEs and UEs send back the received signals in certain properly precoded forms to facilitate the BS side NRC parameter estimation, which is often referred to as over-the-air (OTA) approach [6], [14]–[17].

O. Raeesi, A. Gokceoglu, and M. Valkama are with the Department of Electronics and Communications Engineering, Tampere University of Technology, Tampere 33720, Finland (e-mail: orod.raeesi@tut.fi; ahmet.gokceoglu@tut.fi; mikko.e.valkama@tut.fi).

This work was supported by the Finnish Funding Agency for Technology and Innovation (Tekes) under the project “5th Evolution Take of Wireless Communication Networks (TAKE-5)”, by the Academy of Finland under the projects 284694 and 288670 and TUT Graduate School.

In this work, we focus on OTA-based estimation and mitigation of NRC in a multi-user massive MIMO system context deploying MRT or ZF precoding. The novelty and contributions of this paper can be summarized as follows:

- 1) We consider generalized NRC induced by coexisting FR mismatches of all associated radio transceivers at UE and BS sides as well as the mutual coupling mismatches in the BS side large-array antenna system, unlike many of the earlier works, such as [2], [4], [10]–[17], that neglect BS mutual coupling mismatch. In this respect, only [6] reports similar modeling, however, the proposed estimation and mitigation scheme in [6] is suitable mainly for small scale MIMO systems, e.g., 2-4 BS antennas due to the excessive computational complexity as well as unaffordable overhead in signaling back the required downlink channel estimates from the UEs to the BS when large antenna arrays are considered.
- 2) We address estimation and mitigation of the NRC sources of both the UE and the BS sides, unlike many other works that address only BS side NRC, e.g., [2], [4], [10]–[13], [15]. As shown in [18], with the popular assumption of not having downlink demodulation pilots, UE side NRC can be a major cause of performance degradation in multi-user massive MIMO systems, thus strongly motivating to incorporate such effects in the NRC estimation and mitigation processes.
- 3) Unlike other massive MIMO NRC mitigation works [2], [10]–[13] which all assume the availability of downlink demodulation pilots, we consider the appealing massive MIMO scenario in which there are no downlink demodulation pilots and thus UEs rely on the statistical properties of the beamformed channels to decode the received downlink signals [8], [19]–[22]. This further motivates to include both the BS and UE side NRC sources in the estimator and mitigation developments.
- 4) We demonstrate and evaluate the performance of our proposed scheme under imperfect uplink CSI, unlike other works which commonly rely on the perfect uplink CSI assumption [4], [11]–[13], [15].

The organization of the paper is as follows. Fundamental signal models of the considered massive MIMO system with MRT and ZF-based precoding schemes under NRC are first presented in Section II. Then, the NRC-aware downlink precoding approach is formulated for given NRC estimates. In Section III, a novel pilot signaling method between the BS and UEs is introduced which is followed by the proposed novel iterative estimation of the BS and UE side NRC matrices. Also the corresponding complexity analysis is provided. The results of empirical performance evaluations in terms of the NRC estimation mean-squared error (MSE) and the achievable system spectral efficiency are presented in Section IV, incorporating the proposed estimation-mitigation scheme together with existing state-of-the-art NRC estimation/mitigation methods for reference. Finally, conclusions are drawn in Section V.

Notations: Throughout the paper, vectors and matrices are denoted with lower and upper case bold letters, respectively, e.g., vector \mathbf{x} , matrix \mathbf{Y} . The superscripts $(\cdot)^*$, $(\cdot)^T$, $(\cdot)^H$, and

$(\cdot)^\dagger$ indicate complex-conjugation, transposition, Hermitian transpose, and Moore-Penrose pseudo inverse operations, respectively. The expectation operator is shown by $\mathbb{E}[\cdot]$, while $\text{Tr}(\cdot)$ represents the trace operator. The $\text{diag}(\cdot)$ operator transforms a vector \mathbf{v} to a diagonal matrix with the elements of \mathbf{v} at its diagonal, and vice versa, reads the diagonal elements of the input matrix into a column vector. $\Re\{\cdot\}$ and $\Im\{\cdot\}$ work element-wise and return real and imaginary parts of complex-valued arguments, respectively. The element in the i 'th row and j 'th column of matrix \mathbf{V} is represented by v_{ij} , whereas the i 'th element on the main diagonal of a diagonal matrix \mathbf{C} is shown by c_i . The complex-valued zero-mean circularly symmetric Gaussian distribution with variance σ^2 is denoted as $\mathcal{CN}(0, \sigma^2)$. Finally, \mathbf{I}_n and $\mathbf{0}_n$ denote the $n \times n$ identity and all-zero matrices, respectively.

II. SYSTEM MODEL AND PROBLEM FORMULATION

We consider a TDD based single-cell multi-user downlink transmission scenario where the BS with a large number of antenna units, denoted by N , transmits to K single-antenna UEs simultaneously in the same time-frequency resource, where $N \gg K$. All signal and system models are written for an arbitrary subcarrier of the underlying orthogonal frequency division multiplexing/multiple access (OFDM/OFDMA) waveform, that is, before IFFT and after FFT on the TX and RX sides, respectively.

In an ideal TDD massive MIMO system, the effective uplink and downlink channels consist of only the reciprocal physical channels. Building on that, the downlink transmission is done by beamforming the multi-user downlink data based on the estimated channels from uplink pilot sequences of length τ_u symbols [2], [3]. A fundamental assumption is that the uplink training and downlink transmission both take place clearly within one channel coherence interval, meaning that the channels are essentially static. In this work, we assume the same procedure for the uplink training and downlink transmission, however, we consider more generalized uplink and downlink effective channel models which are *non-reciprocal* due to the radio front-end mismatches and non-idealities. In this respect, the uplink model for channel estimation phase [19] and the corresponding downlink received signal model in beamformed data transmission phase under the non-reciprocal effective channels can be expressed as

$$\begin{aligned} \text{Uplink Training :} \quad & \mathbf{Y} = \sqrt{\rho_u \tau_u} \mathbf{G} + \mathbf{Z}_u \\ \text{Downlink Transmission :} \quad & \mathbf{r} = \sqrt{\rho_d} \mathbf{H} \mathbf{x} + \mathbf{z}_d, \end{aligned} \quad (1)$$

where $\mathbf{x} \in \mathbb{C}^{N \times 1}$ denotes the precoded multi-user data, whereas $\mathbf{G} \in \mathbb{C}^{N \times K}$ and $\mathbf{H} \in \mathbb{C}^{K \times N}$ are the effective non-reciprocal uplink and downlink multi-user MIMO channels, respectively, which will be elaborated in detail later in Section II-A. $\mathbf{Z}_u \in \mathbb{C}^{N \times K}$ is the processed noise matrix at the BS, while $\mathbf{z}_d \in \mathbb{C}^{K \times 1}$ denotes the UE side multi-user thermal noise vector, both assumed to consist of i.i.d. $\mathcal{CN}(0, 1)$ elements. The average signal to noise ratios (SNRs) in the uplink and downlink are denoted as ρ_u and ρ_d , respectively. This basic system framework is largely based on and following the seminal work by Marzetta in [19], [23] where reciprocal channels were assumed.

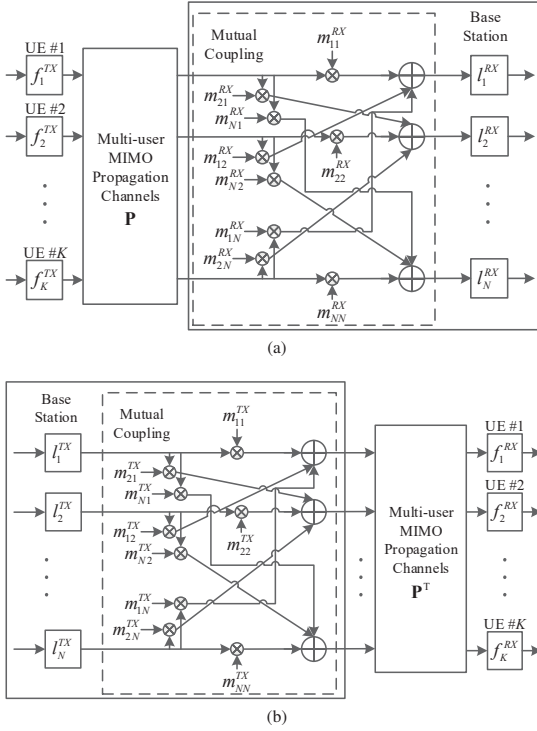


Fig. 1. Basic system models for (a) uplink and (b) downlink transmission and reception including physical propagation channels, transceiver frequency responses and antenna mutual coupling in the devices.

A. Effective and Relative Uplink and Downlink Channels

As illustrated in Fig. 1, the complete description of the uplink and downlink effective channels appearing in (1) can be expressed as

$$\left. \begin{aligned} \mathbf{G} &= \mathbf{E}_r \mathbf{P} \mathbf{F}_t \\ \mathbf{H} &= \mathbf{F}_r \mathbf{P}^T \mathbf{E}_t \end{aligned} \right\} \Rightarrow \mathbf{H} \neq \mathbf{G}^T, \quad (2)$$

with $\mathbf{E}_r = \mathbf{L}_r \mathbf{M}_r$ and $\mathbf{E}_t = \mathbf{M}_t \mathbf{L}_t$. In above, $\mathbf{F} \in \mathbb{C}^{K \times K}$ is the joint frequency-response matrix of the UEs, $\mathbf{L} \in \mathbb{C}^{N \times N}$ is the frequency-response matrix of the BS, $\mathbf{M} \in \mathbb{C}^{N \times N}$ is the mutual coupling matrix of the BS, $\mathbf{P} \in \mathbb{C}^{N \times K}$ is the reciprocal physical channel, while the subscripts t and r denote the transmitting and receiving modes, respectively. Note that the frequency-response matrices, \mathbf{F} and \mathbf{L} , are diagonal, while the mutual coupling matrix \mathbf{M} in general has both non-zero diagonal and off-diagonal entries.

In general, the effective channels with above assumptions and modeling are clearly non-reciprocal, i.e., $\mathbf{H} \neq \mathbf{G}^T$, due to differences in the TX and RX modes of the radio front-end and array responses, i.e., $\mathbf{F}_t \neq \mathbf{F}_r$, $\mathbf{L}_t \neq \mathbf{L}_r$ and $\mathbf{M}_t \neq \mathbf{M}_r^T$. Hence, the effective uplink and downlink channels can be described relative to each other as

$$\mathbf{H} = \mathbf{A} \mathbf{G}^T \mathbf{B}, \quad (3)$$

where, $\mathbf{A} = \mathbf{F}_r \mathbf{F}_t^{-1}$ and $\mathbf{B} = \mathbf{L}_r^{-1} (\mathbf{M}_r^T)^{-1} \mathbf{M}_t \mathbf{L}_t$.

In general, $\mathbf{A} \in \mathbb{C}^{K \times K}$ is a diagonal matrix and the k 'th diagonal entry, denoted as a_k , corresponds to the frequency-response ratio of k 'th UE at TX and RX modes. In the following, similar to [5], [6], [8], we will use the decomposition of the form $\mathbf{A} = \mathbf{I}_K + \mathbf{A}'$, where the diagonal matrix $\mathbf{A}' \in \mathbb{C}^{K \times K}$ measures the deviation from the ideal unity frequency-response ratio. The k 'th diagonal entry of \mathbf{A}' is denoted as a'_k , such that $a_k = 1 + a'_k$.

In (3), $\mathbf{B} \in \mathbb{C}^{N \times N}$ is a full matrix that incorporates both the frequency-responses and mutual coupling at the BS side in TX and RX modes. In the following, for notational convenience, we will use the decomposition $\mathbf{B} = \mathbf{I}_N + \mathbf{B}'$, where $\mathbf{B}' \in \mathbb{C}^{N \times N}$ accounts for the deviation of diagonal and off-diagonal entries from the ideal reciprocal response.

The detailed modeling of the entries of the above matrices is based on the practical physical circuits driven NRC modeling introduced in [6], in which σ_F^2 is denoting the variance of the diagonal elements in \mathbf{F}_t and \mathbf{F}_r , while the corresponding variance of the diagonal elements in \mathbf{L}_t and \mathbf{L}_r is denoted by σ_L^2 . In this model [6], \mathbf{M}_t and \mathbf{M}_r are generated as

$$\begin{aligned} \mathbf{M}_t &= (\mathbf{I}_N - \mathbf{\Gamma}_t \mathbf{\Phi})^{-1} \\ \mathbf{M}_r &= (\mathbf{I}_N - \mathbf{\Gamma}_r \mathbf{\Phi})^{-1}, \end{aligned} \quad (4)$$

where $\mathbf{\Gamma}_t \in \mathbb{C}^{N \times N}$ and $\mathbf{\Gamma}_r \in \mathbb{C}^{N \times N}$ are diagonal matrices representing input reflection coefficients at transmitting and receiving modes, respectively, while $\mathbf{\Phi} \in \mathbb{C}^{N \times N}$ is the scattering matrix of the BS antenna system, defined as

$$\mathbf{\Phi} = \left(\frac{\mathbf{Z}}{Z_0} + \mathbf{I}_N \right)^{-1} \left(\frac{\mathbf{Z}}{Z_0} - \mathbf{I}_N \right). \quad (5)$$

In above, Z_0 denotes the reference impedance of the antenna ports and $\mathbf{Z} \in \mathbb{C}^{N \times N}$ is the BS impedance matrix whose elements depend on the antenna spacing and layout [24]. As illustrated in (4), for a chosen antenna spacing and layout which result into a certain BS antenna system scattering matrix $\mathbf{\Phi}$, the powers of the elements in \mathbf{M}_t and \mathbf{M}_r are controlled by the corresponding input reflection coefficient matrices $\mathbf{\Gamma}_t$ and $\mathbf{\Gamma}_r$, respectively. The variance of the diagonal elements in the input reflection coefficient matrices is denoted by σ_{rc}^2 .

The characterization as given in (2) and/or (3) is generally referred to in the literature as channel non-reciprocity [5], [6]. The ideal reciprocal channel model is a special case where $\mathbf{A} = \mathbf{B} = \mathbf{I}$, i.e., $\mathbf{A}' = \mathbf{B}' = \mathbf{0}$.

B. Channel Estimation and Beamforming under NRC

First, we shortly address the influence of NRC when the downlink transmission is carried out without any processing against the NRC, i.e., NRC-blind precoding is adopted. In this respect, the required downlink channel estimate in the BS is obtained from the orthogonal uplink training signals, with the observation model given already on the first line of (1), complemented, e.g., with LMMSE channel estimator as described in [19], [23]. This yields formally

$$\hat{\mathbf{H}} = \hat{\mathbf{G}}^T, \quad (6)$$

where $\hat{\mathbf{H}} \in \mathbb{C}^{K \times N}$ and $\hat{\mathbf{G}} \in \mathbb{C}^{N \times K}$ are the estimated downlink and uplink effective channels, respectively.

Using the estimated downlink effective channel in (6), the user data vector $\mathbf{s} = [s_1, \dots, s_K]^T \in \mathbb{C}^{K \times 1}$ which is assumed to have element-wise power normalization of the form $\mathbb{E}[|s_k|^2] = 1$, is precoded as

$$\mathbf{x} = \beta \mathbf{U} \mathbf{s}, \quad (7)$$

where the NRC-blind linear precoding matrix $\mathbf{U} \in \mathbb{C}^{N \times K}$ reads [23]

$$\mathbf{U} = \begin{cases} \hat{\mathbf{H}}^H, & \text{for MRT} \\ \hat{\mathbf{H}}^H (\hat{\mathbf{H}} \hat{\mathbf{H}}^H)^{-1}, & \text{for ZF.} \end{cases} \quad (8)$$

In above, without loss of generality, the scalar β can be chosen to satisfy unit average transmit power constraint as [19]

$$\beta = \left(\sqrt{\mathbb{E}[\text{Tr}(\mathbf{U}^H \mathbf{U})]} \right)^{-1}. \quad (9)$$

C. Received Signal at UE under NRC

The multi-user received downlink signal vector is given by the second line of (1). Plugging the precoded symbol vector expression in (7) into (1), the received signal for k 'th user corresponding to the k 'th element of \mathbf{r} can be written as

$$r_k = \sqrt{\rho_d} \beta \mathbf{h}_k^T \mathbf{u}_k s_k + \sqrt{\rho_d} \beta \sum_{i=1, i \neq k}^K \mathbf{h}_k^T \mathbf{u}_i s_i + z_{d,k}, \quad (10)$$

where \mathbf{u}_k and \mathbf{h}_k^T denote the k 'th column and row vectors of the precoder and the effective downlink channel matrices, respectively. Notice that by denoting the k 'th column of the uplink effective channel matrix as \mathbf{g}_k , the effective downlink channel towards the k 'th user can be expressed as

$$\mathbf{h}_k^T = a_k \mathbf{g}_k^T \mathbf{B}. \quad (11)$$

In general, conventional MIMO systems employ downlink pilots to acquire downlink CSI for detection purposes. However, in massive MIMO systems, as shown in [8], [19]–[22], it is commonly assumed that UEs employ only the statistical properties of the beamformed channel, namely $\mathbb{E}[\beta \mathbf{h}_k^T \mathbf{u}_k]$, as the downlink CSI to decode the received signal. This assumption is justified by the law of large numbers which implies that $\mathbf{h}_k^T \mathbf{u}_k \rightarrow \mathbb{E}[\mathbf{h}_k^T \mathbf{u}_k]$ when BS array size N increases, commonly known as the channel hardening concept [23], [25]. Utilizing such approach in acquiring downlink CSI in UEs eliminates the need for sending downlink demodulation pilots which directly reduces downlink overhead. Alternatively, blind downlink channel estimation [26] can also be pursued. Building on this and plugging (11) into (10), the received signal under NRC can be re-written in a general form as

$$r_k = \sqrt{\rho_d} \mathbb{E}[\beta \mathbf{h}_k^T \mathbf{u}_k] s_k + z_{\text{SI},k} + z_{\text{IUI},k} + z_{d,k}, \quad (12)$$

where the self-interference (SI), $z_{\text{SI},k}$, and the inter-user-interference (IUI), $z_{\text{IUI},k}$, are given by

$$\begin{aligned} z_{\text{SI},k} &= \sqrt{\rho_d} \beta (a_k \mathbf{g}_k^T \mathbf{B} \mathbf{u}_k - \mathbb{E}[\mathbf{h}_k^T \mathbf{u}_k]) s_k \\ z_{\text{IUI},k} &= \sqrt{\rho_d} \beta \sum_{i=1, i \neq k}^K a_k \mathbf{g}_k^T \mathbf{B} \mathbf{u}_i s_i. \end{aligned} \quad (13)$$

Note that the basic received signal model in (12) and (13) holds independently of the channel hardening phenomenon. However, the channel hardening assumption is in practice needed in order to obtain good decoding performance with statistical beamformed channel based downlink CSI. In general, the statistical beamformed downlink CSI, $\mathbb{E}[\mathbf{h}_k^T \mathbf{u}_k]$, can be interpreted either for given NRC realizations or averaged also over the NRC variable statistics. In this manuscript, we will take the latter approach as that is independent of the NRC realizations, and thus facilitates efficient UE data decoding without any downlink demodulation pilots. This is also well motivated by the main topic of the article which is the joint estimation and mitigation of the BS and UE side NRC at the BS. Finally, we note that static channels within uplink training and downlink transmission are assumed, and thus practical aspects such as channel aging within one uplink training and downlink transmission cycle are not considered.

Based on (13), it can be clearly observed that the NRC-blind precoder \mathbf{u} which is constructed based on the estimated uplink effective channel $\hat{\mathbf{G}}$, through $\hat{\mathbf{H}} = \hat{\mathbf{G}}^T$, cannot take into account the NRC effects from a_k and \mathbf{B} , which results into increased interference levels and thus reduced downlink spectral efficiency. This is illustrated through an elementary system spectral efficiency evaluation in Fig. 2, with the detailed evaluation assumptions being described in Section IV. It can be noticed that in particular in the ZF precoder case, NRC-blind precoding results into substantial performance degradation, hence strongly motivating to develop efficient NRC estimation and mitigation techniques.

D. NRC-Aware Downlink Precoding Principle

As shown in Section II-C above, if MRT and/or ZF precoders are applied naively without accounting for NRC, there are additional SI and IUI terms that can substantially degrade the quality of the received signal at the UE side. Here, we introduce an efficient NRC mitigation approach, called NRC-aware precoding, which seeks to cancel out the effects of NRC by properly modifying the precoder.

Assuming that the BS has already estimates of the NRC matrices \mathbf{A} and \mathbf{B} , denoted by $\hat{\mathbf{A}}$ and $\hat{\mathbf{B}}$, the NRC-aware precoding approach transforms the basic linear precoders given in (8) as

$$\mathbf{U}_{\text{nrc}} = \hat{\mathbf{B}}^{-1} \mathbf{U} \hat{\mathbf{A}}^{-1}. \quad (14)$$

With ideal estimates of \mathbf{A} and \mathbf{B} and ideal uplink channel estimation, the above transformed precoder can be easily shown to diagonalize the beamformed multi-user channel matrix $\mathbf{H} \mathbf{U}_{\text{nrc}}$. This applies in an exact form with ZF precoding while is a very good approximation with MRT precoding when the BS array size N is large. Note that, in the special case where the NRC estimation method is capable of estimating the BS side NRC only, (14) reduces to $\mathbf{U}_{\text{nrc}} = \hat{\mathbf{B}}^{-1} \mathbf{U}$.

The system spectral efficiency performance with the NRC-aware precoder, assuming ideal NRC estimates, is shown in Fig. 2. As can be observed, the NRC-aware precoder achieves the ideal system performance, i.e., the performance with fully reciprocal channels. The evaluation setup and details of spectral efficiency calculations will be described in Section IV.

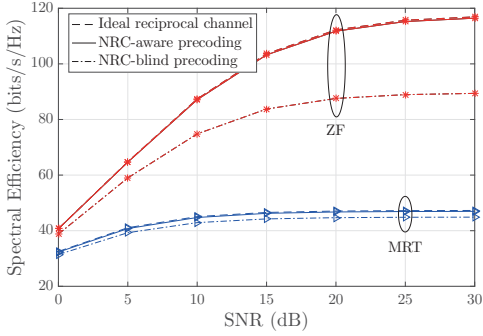


Fig. 2. Spectral efficiency vs. downlink SNR (ρ_d) for $N = 100$, $K = 20$, $\tau_u = K$, $\rho_u = 0$ dB, $T = 250$.

It is also noted that an alternative approach to construct NRC-aware downlink precoder is to first correct the effective downlink channel estimates based on the estimated NRC matrices $\hat{\mathbf{A}}$ and $\hat{\mathbf{B}}$ as $\hat{\mathbf{H}}_{cor} = \hat{\mathbf{A}}\hat{\mathbf{H}}\hat{\mathbf{B}}$, and then calculate the precoder matrix based on this corrected downlink channel estimate. However, in this work, we focus on the NRC mitigation approach described in (14) which is shown in Fig. 2 to practically reach the performance of the ideal reciprocal channel as long as accurate estimates of \mathbf{A} and \mathbf{B} are available.

III. PROPOSED ESTIMATION OF NRC MATRICES

The NRC mitigation method, i.e., the NRC-aware precoder described in Section II-D requires the knowledge of the matrices \mathbf{A} and \mathbf{B} at the BS. The information about these matrices is not readily available, hence calling for efficient estimation approaches. Thus, in this section, we will propose a novel iterative OTA estimation framework for acquiring accurate estimates of \mathbf{A} and \mathbf{B} , based on a novel pilot signaling concept between the BS and UEs. Furthermore, computational complexity analysis of the proposed estimation method is pursued.

In general, the NRC variances σ_F^2 , σ_L^2 , σ_{rc}^2 , and the corresponding realizations of the elements of \mathbf{A} and \mathbf{B} depend on hardware characteristics and operating conditions, e.g., temperature, which vary slowly in time. Thus, the NRC characteristics and the corresponding realizations of \mathbf{A} and \mathbf{B} can be assumed to stay constant over many propagation channel coherence intervals [14]. Therefore, it is sufficient to perform the NRC estimation relatively infrequently, e.g., once in every 10 minutes or even more irregularly [2], [10], which makes the estimation pilot overhead negligible, when compared to other signaling and pilot overheads that commonly rise from channel estimation procedures.

A. Proposed Pilot Signaling

In order to estimate the matrices \mathbf{A} and \mathbf{B} , we propose the following round-trip pilot signaling approach:

- 1) BS transmits an $N \times N$ orthonormal pilot matrix \mathbf{X}_{nrc} .

- 2) Upon reception, without decoding, UEs send back the conjugated versions of the received samples.

Based on the above scheme, the received multi-user pilot signal matrix at UE side can be written as

$$\mathbf{R}_{nrc} = \sqrt{\tilde{\rho}_d} \mathbf{H} \mathbf{X}_{nrc} + \tilde{\mathbf{Z}}_d, \quad (15)$$

where $\tilde{\rho}_d$ is the downlink SNR and $\tilde{\mathbf{Z}}_d$ is the $K \times N$ multi-user receiver noise matrix with i.i.d. $\mathcal{CN}(0, 1)$ entries. The tilde sign is used in above and what follows to distinguish these variables between the actual data transmission and pilot signaling phases. Then, the corresponding received signal at the BS with the UEs sending back the conjugated version of (15) reads

$$\begin{aligned} \mathbf{Y}_{nrc} &= \sqrt{\tilde{\rho}_u} \mathbf{G} \mathbf{R}_{nrc}^* + \tilde{\mathbf{Z}}_u \\ &= \sqrt{\tilde{\rho}_u} \sqrt{\tilde{\rho}_d} \mathbf{G} \mathbf{H}^* \mathbf{X}_{nrc}^* + \tilde{\mathbf{Z}}_{tot}, \end{aligned} \quad (16)$$

where $\tilde{\rho}_u$ is the uplink pilot SNR and $\tilde{\mathbf{Z}}_u$ is the $N \times N$ BS receiver noise matrix with i.i.d. $\mathcal{CN}(0, 1)$ entries. The total effective noise matrix seen at the BS is denoted as $\tilde{\mathbf{Z}}_{tot} = \sqrt{\tilde{\rho}_u} \mathbf{G} \tilde{\mathbf{Z}}_d^* + \tilde{\mathbf{Z}}_u$. Note that, for notational simplicity, we have assumed all the UEs to have the same uplink pilot SNR value $\tilde{\rho}_u$, while in practice, $\tilde{\rho}_u$ is likely to be different for different UEs.

In above, the duration of the described overall NRC-related pilot signaling is $2N$ symbols where the uplink and downlink channels are assumed to be fixed. The coherence time of the physical channels is typically in the order of several hundred symbol intervals, determined mostly by the mobility of the UEs and the system center-frequency. Hence, we assume a scenario where the coherence time is at least $2N + K$ symbols, taking into account both NRC-related pilot signaling and uplink channel estimation. As mentioned in the previous section, matrices \mathbf{A} and \mathbf{B} are expected to change very slowly compared to channel coherence time and hence it is assumed that their values are fixed during the above pilot signaling. Fig. 3 illustrates the overall assumed radio frame or sub-frame structure of the considered massive MIMO TDD system including the proposed NRC estimation phase.

B. Overall Estimation Framework

As the initial step in estimating \mathbf{A} and \mathbf{B} , the BS processes the received signal \mathbf{Y}_{nrc} in (16) as $\mathbf{Q} = \mathbf{Y}_{nrc}^* \mathbf{X}_{nrc}^H$. Since the pilot matrix \mathbf{X}_{nrc} has the property $\mathbf{X}_{nrc}^H \mathbf{X}_{nrc} = \mathbf{I}_N$, the processed signal can be expressed as

$$\mathbf{Q} = \sqrt{\tilde{\rho}_u} \sqrt{\tilde{\rho}_d} \mathbf{G}^* \mathbf{A} \mathbf{G}^T \mathbf{B} + \mathbf{V}, \quad (17)$$

where the processed noise matrix is given by $\mathbf{V} = \tilde{\mathbf{Z}}_{tot}^* \mathbf{X}_{nrc}^H$.

Now the target is to estimate \mathbf{A} and \mathbf{B} from (17) assuming that the BS has the uplink channel estimate $\hat{\mathbf{G}}$. In this respect, denoting the estimates at m 'th iteration as $\hat{\mathbf{A}}(m)$ and $\hat{\mathbf{B}}(m)$, we propose the following iterative estimation framework:

- 1) Initialize, $\hat{\mathbf{A}}(0) = \mathbf{I}_K$, obtain the estimate $\hat{\mathbf{B}}(1)$.
- 2) Substitute $\hat{\mathbf{B}}(1)$ for \mathbf{B} in (17) and obtain estimate $\hat{\mathbf{A}}(1)$.
- 3) Successively refine the estimates $\hat{\mathbf{A}}$ and $\hat{\mathbf{B}}$ by fixing the current value of one and solving for the other from (17).

In above, \mathbf{I}_K is used for initialization since the deviation matrix \mathbf{A}' in $\mathbf{A} = \mathbf{I}_K + \mathbf{A}'$ is in practice small. Notice that

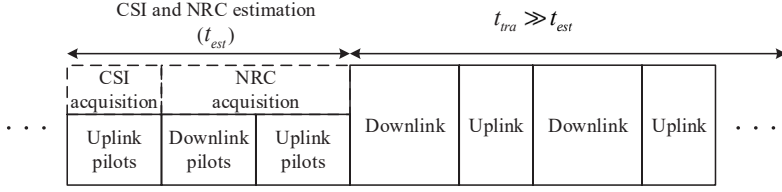


Fig. 3. Assumed radio frame or sub-frame structure incorporating CSI and NRC estimation as well as actual data transmission phases.

the processed received signal in (17) and the corresponding uplink channel estimate are available at multiple parallel subcarriers in an OFDM/OFDMA based radio system. Hence, the above iterative estimation scheme can be carried out in a per subcarrier manner as well. Furthermore, as mentioned in [6], transceivers' baseband-to-baseband behavior can be modeled by allpass-like transfer functions, therefore it is reasonable to assume that the NRC matrices \mathbf{A} and \mathbf{B} are largely similar over a set of adjacent subcarriers C_{sc} where we conservatively assume $C_{sc} \leq 10$, whereas \mathbf{G} is subject to variations depending on the frequency selectivity of the propagation channels. Based on these assumptions, the estimates $\hat{\mathbf{A}}$ and $\hat{\mathbf{B}}$ can be obtained by averaging the per subcarrier estimates over C_{sc} neighboring subcarriers, i.e.,

$$\begin{aligned}\hat{\mathbf{A}} &= \frac{1}{C_{sc}} \sum_{l=1}^{C_{sc}} \hat{\mathbf{A}}_l \\ \hat{\mathbf{B}} &= \frac{1}{C_{sc}} \sum_{l=1}^{C_{sc}} \hat{\mathbf{B}}_l,\end{aligned}\quad (18)$$

where l denotes the relative subcarrier index. Next we will present the actual proposed methods to obtain the estimates for \mathbf{A} and \mathbf{B} . To simplify the notation, we will drop the relative subcarrier index l . Note that the above averaging helps reducing the NRC estimation errors, mainly caused by additive receiver noise, regardless of how small the particular NRC values are, unless being below the machine precision and thus swallowed by finite word-length effects.

C. Proposed Estimation of \mathbf{B}

As described earlier, $\hat{\mathbf{B}}$ is iteratively refined using the current estimate of \mathbf{A} . The proposed estimator builds on solving the matrix equation in (17) based on minimizing the Frobenius norm criterion. With this setting, the refined estimate of \mathbf{B} can be formulated as

$$\hat{\mathbf{B}}(m+1) = \underset{\mathbf{B}}{\operatorname{argmin}} \left\| \mathbf{Q} - \sqrt{\hat{\rho}_u} \sqrt{\hat{\rho}_d} \hat{\mathbf{G}}^* \hat{\mathbf{A}}(m) \hat{\mathbf{G}}^T \mathbf{B} \right\|_F^2, \quad (19)$$

where the subscript F denotes the Frobenius norm.

Next, by denoting $\mathbf{T}(m) = \sqrt{\hat{\rho}_u} \sqrt{\hat{\rho}_d} \hat{\mathbf{G}}^* \hat{\mathbf{A}}(m) \hat{\mathbf{G}}^T \in \mathbb{C}^{N \times N}$, we have the following identity

$$\|\mathbf{Q} - \mathbf{T}(m)\mathbf{B}\|_F^2 = \sum_{j=1}^K \|\mathbf{q}_j - \mathbf{T}(m)\mathbf{b}_j\|^2, \quad (20)$$

where $\mathbf{q}_j \in \mathbb{C}^{N \times 1}$ and $\mathbf{b}_j \in \mathbb{C}^{N \times 1}$ denote the j 'th columns of \mathbf{Q} and \mathbf{B} , respectively. Since the j 'th term in the sum

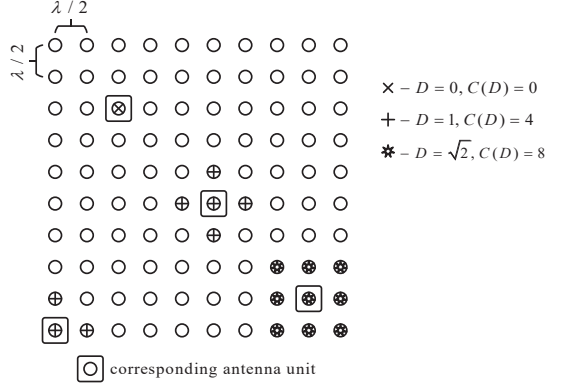


Fig. 4. Illustration of sparsity threshold D on 10×10 rectangular BS antenna grid with $\lambda/2$ antenna spacing.

depends only on \mathbf{b}_j , minimizing the total sum is equivalent to separately minimizing each term $\|\mathbf{q}_j - \mathbf{T}(m)\mathbf{b}_j\|^2$. Thus, the estimation of matrix \mathbf{B} is eventually simplified to estimation of each column of \mathbf{B} , independently.

As mentioned earlier, the BS NRC matrix incorporates both the frequency-responses and the mutual coupling effects at the BS side. The power of mutual coupling between two different antenna units is related to their physical distance, thus the off-diagonal elements in \mathbf{B} become smaller as the distance between the two corresponding antenna units increases. Here, in estimating the BS NRC matrix \mathbf{B} , we treat those off-diagonal entries which are corresponding to two antennas with a distance larger than a pre-defined threshold, called sparsity threshold D , as zeros, yielding a sparse matrix structure for $\hat{\mathbf{B}}$. We also define the maximum number of coupled neighboring antenna elements as $C(D)$. In Fig. 4 an example 10×10 rectangular antenna layout with $\lambda/2$ antenna spacing between the neighboring elements is shown with 3 different values of D , namely $D = 0, 1$ and $\sqrt{2}$, measured as multiples of $\lambda/2$. When $D = 0$, it is assumed that there is no mutual coupling and $C(D) = 0$, whereas for $D = 1$ and $D = \sqrt{2}$, the central antenna elements are coupled with at most $C(D) = 4$ and $C(D) = 8$ closest neighboring antenna elements. Note that, the antenna elements close to the edges of the grid are coupled with lower number of antenna units. This is illustrated in Fig. 4 where for $D = 1$, the bottom left antenna element is assumed to be coupled with only $2 \leq C(1) = 4$ antennas.

The following column-wise estimator will build on the

assumption that \mathbf{B} has a sparse structure and the number of non-zero row entries in any column j , denoted as R_j , satisfies

$$R_j \leq R(D), \quad (21)$$

where $R(D) = C(D) + 1$. It is further assumed that the index of non-zero entries of \mathbf{b}_j are known, which is directly determined by the antenna system architecture and geometry, and the assumed pre-defined coupling threshold discussed above. With these assumptions, we define a reduced vector of dimension $R_j \times 1$, $\mathbf{b}_j^{\text{red}}$, that contains the non-zero entries of \mathbf{b}_j . The indexes of non-zero entries of \mathbf{b}_j are then mapped to the column numbers which we keep when constructing $\mathbf{T}_j^{\text{red}}(m) \in \mathbb{C}^{N \times R_j}$. If the j 'th row is kept when constructing $\mathbf{b}_j^{\text{red}}$, then similarly, the j 'th column is kept to construct $\mathbf{T}_j^{\text{red}}(m)$. Based on these, we can formulate the estimation of columns of $\hat{\mathbf{B}}(m+1)$ through a reduced system of equations as

$$\hat{\mathbf{b}}_j^{\text{red}}(m+1) = \underset{\mathbf{b}_j^{\text{red}}}{\operatorname{argmin}} \|\mathbf{q}_j - \mathbf{T}_j^{\text{red}}(m)\mathbf{b}_j^{\text{red}}\|^2. \quad (22)$$

The solution to (22) is then given by

$$\hat{\mathbf{b}}_j^{\text{red}}(m+1) = (\mathbf{T}_j^{\text{red}}(m))^\dagger \mathbf{q}_j. \quad (23)$$

Once the vector $\hat{\mathbf{b}}_j^{\text{red}}(m+1)$ is solved from (23), then $\hat{\mathbf{b}}_j(m+1)$ can be obtained straightforwardly by appending zeros to the appropriate rows.

Note that, when $\mathbf{A} \approx \mathbf{I}_K$, we also have $\mathbf{G}^* \mathbf{A} \mathbf{G}^T \approx \mathbf{G}^* \mathbf{G}^T$, where the matrix $\mathbf{G}^* \mathbf{G}^T = (\mathbf{G} \mathbf{G}^H)^*$ is positive semi-definite matrix and of rank K if \mathbf{G} is of rank K . The obtained $\hat{\mathbf{b}}_j^{\text{red}}$ and the corresponding minimum expression from (22) depend on the corresponding values of K and D . The column space of $\mathbf{T}_j^{\text{red}}(m)$ has higher dimensionality for larger K . Thus, when D is fixed, for larger K one can solve for $\hat{\mathbf{b}}_j^{\text{red}}$ from (23) which yields smaller values of $\|\mathbf{q}_j - \mathbf{T}_j^{\text{red}}(m)\mathbf{b}_j^{\text{red}}\|^2$.

D. Proposed Estimation of \mathbf{A}

Next, given $\hat{\mathbf{B}}(m)$ from (19), the (refined) estimate of \mathbf{A} can be formulated based on minimizing the Frobenius norm criterion as

$$\hat{\mathbf{A}}(m) = \underset{\mathbf{A}}{\operatorname{argmin}} \left\| \mathbf{Q} - \sqrt{\hat{\rho}_u} \sqrt{\hat{\rho}_d} \hat{\mathbf{G}}^* \mathbf{A} \hat{\mathbf{G}}^T \hat{\mathbf{B}}(m) \right\|_F^2. \quad (24)$$

For diagonal \mathbf{A} , the solution to (24) can be obtained as

$$\hat{\mathbf{A}}(m) = \operatorname{diag}(\hat{\boldsymbol{\xi}}). \quad (25)$$

where $\hat{\boldsymbol{\xi}} = [\mathbf{I}_K, i\mathbf{I}_K] \hat{\boldsymbol{\psi}}$ and the vector $\hat{\boldsymbol{\psi}} \in \mathbb{C}^{2K \times 1}$ is given as

$$\hat{\boldsymbol{\psi}} = \left(\sum_{j=1}^N \bar{\mathbf{W}}_j^T \bar{\mathbf{W}}_j \right)^{-1} \sum_{j=1}^N \bar{\mathbf{W}}_j^T \bar{\mathbf{q}}_j. \quad (26)$$

In above, $\bar{\mathbf{q}}_j = [\Re\{\mathbf{q}_j^T\}, \Im\{\mathbf{q}_j^T\}]^T \in \mathbb{C}^{2N \times 1}$, and defining the $N \times K$ matrix $\mathbf{W}_j = \sqrt{\hat{\rho}_u} \sqrt{\hat{\rho}_d} \hat{\mathbf{G}}^* \operatorname{diag}(\hat{\mathbf{G}}^T \hat{\mathbf{B}}(m))_j$, with $[\hat{\mathbf{G}}^T \hat{\mathbf{B}}(m)]_j$ being the j 'th column of $\hat{\mathbf{G}}^T \hat{\mathbf{B}}(m)$, $\bar{\mathbf{W}}_j \in \mathbb{C}^{2N \times 2K}$ is given as

$$\bar{\mathbf{W}}_j = \begin{bmatrix} \Re\{\mathbf{W}_j\}, & -\Im\{\mathbf{W}_j\} \\ \Im\{\mathbf{W}_j\}, & \Re\{\mathbf{W}_j\} \end{bmatrix}. \quad (27)$$

Proof: See Appendix.

E. Computational Complexity Analysis

The computational complexity of the proposed NRC estimation method includes the complexity of both the BS side NRC estimation and the UE side NRC estimation phases, with all estimation processing carried out at the BS side. The order of the computing complexity is here analyzed, strictly-speaking per iteration round. However, since the numerical results of Section IV show that only 2–4 iterations are needed in practice, the below analysis reflects correctly the overall order of the estimation complexity.

For BS side, (23) should be performed to estimate j 'th column of \mathbf{B} . The first step here is to invert $\mathbf{T}_j^{\text{red}}(m)$. The size of $\mathbf{T}_j^{\text{red}}(m)$ is $N \times R_j$, thus the complexity is $\mathcal{O}(NR_j^2)$. In the next step, there is a matrix-vector multiplication as $(\mathbf{T}_j^{\text{red}}(m))^\dagger \mathbf{q}_j$ where the size of $(\mathbf{T}_j^{\text{red}}(m))^\dagger$ is $R_j \times N$ and the size of \mathbf{q}_j is $N \times 1$. Thus the complexity is $\mathcal{O}(NR_j)$. As mentioned, these two steps are required to be performed to construct each of the K columns of $\hat{\mathbf{B}}$. Therefore, the total complexity for BS NRC estimation is of the form

$$\mathcal{O} \left(\sum_{j=1}^K NR_j^2 \left(1 + \frac{1}{R_j} \right) \right) \approx \mathcal{O}(KNR(D)^2). \quad (28)$$

For UE side NRC estimation, the first step is to calculate $\sum_{j=1}^N \bar{\mathbf{W}}_j^T \bar{\mathbf{W}}_j$ where the size of $\bar{\mathbf{W}}_j$ is $2N \times 2K$. Thus the complexity of each matrix multiplication is $\mathcal{O}(NK^2)$ and total complexity is $\mathcal{O}(N^2K^2)$. Next, the obtained $2K \times 2K$ matrix is inverted and the complexity is $\mathcal{O}(K^3)$. Then, in order to calculate $\sum_{j=1}^N \bar{\mathbf{W}}_j^T \bar{\mathbf{q}}_j$, a $2K \times 2N$ by $2N \times 1$ matrix multiplication is required to be performed N times. Thus, the complexity is $\mathcal{O}(N^2K)$. Finally, a matrix-vector multiplication, $\left(\sum_{j=1}^N \bar{\mathbf{W}}_j^T \bar{\mathbf{W}}_j \right)^{-1} \sum_{j=1}^N \bar{\mathbf{W}}_j^T \bar{\mathbf{q}}_j$, is needed where the sizes of the matrix and the vector are $2K \times 2K$ and $2K \times 1$, respectively. Thus, the complexity is $\mathcal{O}(K^2)$. Therefore, the total complexity for UE NRC estimation is of the form

$$\mathcal{O} \left((N^2K^2 + K^3) \left(1 + \frac{1}{K} \right) \right) \approx \mathcal{O}(N^2K^2 + K^3). \quad (29)$$

Based on the derived complexity orders in (28) and (29), we can express the total complexity for our proposed NRC estimation method as

$$\text{Total complexity} \approx \mathcal{O}(KNR(D)^2 + N^2K^2 + K^3). \quad (30)$$

For reference, the computing complexity of the method proposed in [6] is shown in [27] to be of the order $\mathcal{O}((N^2 + K^2)^2)$. Thus, the method proposed in this manuscript is of substantially lower complexity, especially when the BS array size N is large.

IV. NUMERICAL EVALUATIONS AND ANALYSIS

A. Basic Evaluation Settings and Performance Measures

In this section, by using extensive computer simulations, we evaluate the performance of the proposed NRC estimation

and mitigation scheme. We also compare its performance to the performance of two other existing schemes in literature, namely the direct-path based least squares (LS) known as “Argos” [2] and the generalized neighbor LS [11]. The latter is the optimized version of the generalized LS method presented in [10] and is shown in [11] to have the best performance amongst several existing NRC estimation methods. Both LS based methods estimate the BS NRC by the means of mutual coupling between the BS antennas, while they depend on the downlink demodulation pilots to compensate the NRC in the UE side.

At communication system level, we consider the downlink spectral efficiency as the key performance metric. For the proposed method and the corresponding system which does not utilize downlink demodulation pilots, this is defined as

$$\eta_{s,1} = K \left(1 - \frac{\tau_u}{T}\right) \log_2(1 + \text{SINR}_{\text{eff}}). \quad (31)$$

In above, T refers to the total number of symbols in a channel coherence interval, while SINR_{eff} in (31) is the effective signal to interference and noise ratio (SINR) [19], [21], which can be written, based on (10)–(13), as

$$\text{SINR}_{\text{eff}} = \frac{|\sqrt{\rho_d} \hat{\alpha}_k|^2}{I_{\text{SI}} + I_{\text{UI}} + 1}, \quad (32)$$

where $\hat{\alpha}_k = \mathbb{E}[\beta \mathbf{h}_k^T \mathbf{u}_k]$ is the assumed statistical complex beamforming gain of the useful signal term available at the receiver of the k 'th UE. Note that the expression in (31) is strictly-speaking a lower-bound, reflecting a worst-case scenario with uncorrelated Gaussian interference [19], [21]. In (32), the powers of the SI and UI terms are given by

$$\begin{aligned} I_{\text{SI}} &= \rho_d \mathbb{E} \left[|\beta \mathbf{h}_k^T \mathbf{u}_k - \hat{\alpha}_k|^2 \right] \\ I_{\text{UI}} &= \rho_d \beta^2 \sum_{i=1, i \neq k}^K \mathbb{E} \left[|\mathbf{h}_k^T \mathbf{u}_i|^2 \right], \end{aligned} \quad (33)$$

where the expectations are over different NRC variable and propagation channel realizations. Finally, we note that the expectations in (33) are evaluated numerically.

On the contrary, the other two NRC estimation methods utilize $\tau_d \geq K$ downlink pilots for downlink CSI acquisition as described in [23]. Thus, we redefine the lower-bound on spectral efficiency as [23]

$$\eta_{s,2} = K \left(1 - \frac{\tau_u + \tau_d}{T}\right) \mathbb{E} [\log_2(1 + \text{SINR}_{\text{inst}})]. \quad (34)$$

Furthermore, the instantaneous SINR, $\text{SINR}_{\text{inst}}$, is defined as [23]

$$\text{SINR}_{\text{inst}} = \frac{|\sqrt{\rho_d} \hat{\alpha}_{k,\text{MMSE}}|^2}{\sum_{i=1}^K \mathbb{E} [|\sqrt{\rho_d} \epsilon_i|^2] + \sum_{i=1, i \neq k}^K |\sqrt{\rho_d} \hat{\alpha}_{i,\text{MMSE}}|^2 + 1}, \quad (35)$$

where $\hat{\alpha}_{i,\text{MMSE}}$ is the MMSE estimate of $\beta \mathbf{h}_k^T \mathbf{u}_i$, while $\epsilon_i = \beta \mathbf{h}_k^T \mathbf{u}_i - \hat{\alpha}_{i,\text{MMSE}}$ is the MMSE channel estimation error and is uncorrelated to $\hat{\alpha}_{i,\text{MMSE}}$ [23]. Finally, the expectations in (34)–(35) are evaluated numerically.

The other highly relevant performance metric is the normalized mean squared error (MSE) for NRC estimation which is defined as

$$\delta_e^2 = \begin{cases} \frac{\|\mathbf{B} - \hat{\mathbf{B}}\|_F^2}{\|\mathbf{B}\|_F^2}, & \text{for BS side} \\ \frac{\|\text{diag}(\mathbf{A}) - \text{diag}(\hat{\mathbf{A}})\|_F^2}{\|\text{diag}(\mathbf{A})\|_F^2}, & \text{for UE side.} \end{cases} \quad (36)$$

As a baseline simulation scenario, we consider a BS which is equipped with $N = 100$ infinitely thin $\lambda/2$ dipole antennas in a 10×10 square layout with $\lambda/2$ spacing as illustrated in Fig. 4. The impedance matrix \mathbf{Z} in (5) is computed based on [24] for the assumed carrier-frequency of $f_c = 3.5$ GHz while $Z_0 = 50 \Omega$ [6]. The impedances are assumed to be frequency-independent, as the modulated signal RF bandwidth is much smaller than the carrier frequency. The uplink channel matrix \mathbf{G} is assumed to have i.i.d. $\mathcal{CN}(0, 1)$ elements. The BS serves $K = 20$ single-antenna UEs simultaneously on the same time-frequency resource through either ZF or MRT precoding. We assume a block-fading scenario where each coherence interval contains $T = 250$ OFDM symbols. The number of uplink pilots sent by each UE in each coherence interval is equal to the number of scheduled UEs, $\tau_u = K$, and the uplink SNR in this phase is assumed to be $\rho_u = 0$ dB. As already stated in Section II-C, we assume that the statistical beamformed downlink CSI, $\mathbb{E}[\beta \mathbf{h}_k^T \mathbf{u}_k]$, used by the UEs for data detection when no downlink CSI pilots are available, is computed through averaging over both channel and NRC variables. For the specific assumed example case of \mathbf{G} having i.i.d. $\mathcal{CN}(0, 1)$ elements, this can be shown to yield [23]

$$\mathbb{E}[\beta \mathbf{h}_k^T \mathbf{u}_k] = \begin{cases} \sqrt{\frac{(N-K)\tau_u \rho_u}{K(\tau_u \rho_u + 1)}}, & \text{for ZF} \\ \sqrt{\frac{N\tau_u \rho_u}{K(\tau_u \rho_u + 1)}}, & \text{for MRT.} \end{cases} \quad (37)$$

Whereas, for the cases where UEs rely on downlink pilots for decoding purposes, i.e., direct-path based LS and generalized neighbor LS methods, the number of downlink pilots in each coherence interval is set to be $\tau_d = K$ [23], and their SNR is equal to the downlink SNR in data transmission phase which is assumed to be $\rho_d = 20$ dB. The SNR of the coupling channel between two neighboring antennas is set to be 80 dB for the two mentioned NRC mitigation reference methods [11]. The uplink and downlink SNRs for the pilot signaling in the proposed NRC estimation framework are set to be $\bar{\rho}_u = 0$ dB and $\bar{\rho}_d = 10$ dB, respectively. Note that while different UEs are likely to have different $\bar{\rho}_u$ values in practice, in order to have fair comparison between the proposed and the two mentioned state-of-the-art NRC estimation methods, we have deliberately assumed a worst case scenario in which all the UEs have very low uplink SNR value of $\bar{\rho}_u = 0$ dB. In the proposed method, the estimated NRC matrices are averaged over 10 neighboring subcarriers, $C_{sc} = 10$, over which the NRC realizations are assumed to be constant. Finally, the variances of transceivers frequency-responses in both the BS and the UE side are assumed to be -20 dB, i.e., $\sigma_L^2 = \sigma_F^2 =$

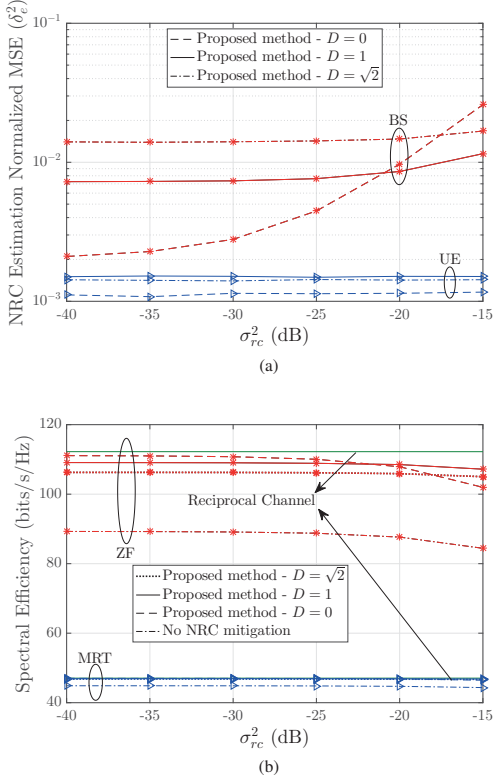


Fig. 5. (a) NRC estimation normalized MSE and (b) system spectral efficiency vs. input reflection coefficients variance (σ_{rc}^2) for different values of the sparsity threshold D with $N = 100$, $K = 20$, $\tau_u = K$, $\rho_u = 0$ dB, $T = 250$.

-20 dB. For simulation simplicity, the distributions of the NRC variables are assumed to be Gaussians. These are the baseline simulation settings, while some of the parameter values are also varied in the evaluations.

B. Numerical Results

1) *Effect of the Sparsity Distance Threshold D* : Here, we will study the effect of D on the normalized MSE and the system spectral efficiency. In this respect, Fig. 5a illustrates the normalized MSE of the UE and BS NRC estimation under the baseline system settings, with the value of σ_{rc}^2 being varied. It can be seen that the choice of $D = 0$, i.e., estimating only the diagonal elements of \mathbf{B} , yields the lowest MSE for UE NRC estimation. Note that, in the proposed NRC estimation method, the choice of D influences the UE side estimation as well since \mathbf{A} and \mathbf{B} are estimated iteratively as described in Section III-B. On the other hand, the highest BS NRC estimation accuracy is achieved for $D = 0$ only when $\sigma_{rc}^2 \leq -21$ dB, whereas higher estimation accuracy is obtained for $D = 1$ when $\sigma_{rc}^2 > -21$ dB. Following that, the spectral efficiencies plotted in Fig. 5b illustrate the combined effect of UE and BS NRC estimation. As can be seen, the highest spectral efficiency is achieved for

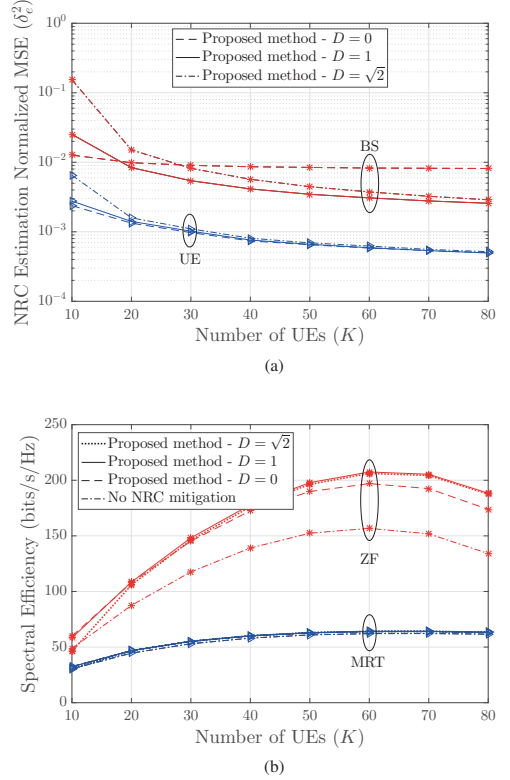


Fig. 6. (a) NRC estimation normalized MSE and (b) system spectral efficiency vs. number of UEs (K) for $N = 100$, $\tau_u = K$, $\rho_u = 0$ dB, $T = 250$.

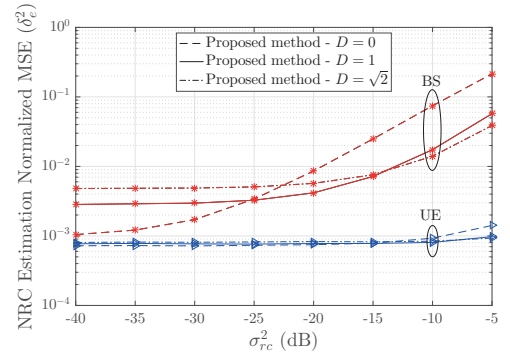


Fig. 7. NRC estimation normalized MSE vs. input reflection coefficients variance (σ_{rc}^2) for different values of the sparsity threshold D with $N = 100$, $K = 40$, $\tau_u = K$, $\rho_u = 0$ dB, $T = 250$.

$D = 0$ when $\sigma_{rc}^2 \leq -22$ dB and for $D = 1$ when $\sigma_{rc}^2 > -22$ dB.

For fixed NRC characteristics of $\sigma_L^2 = \sigma_F^2 = \sigma_{rc}^2 = -20$ dB, Fig. 6 evaluates the normalized estimation MSE and the system spectral efficiency for different values of D and against the number of scheduled UEs K . Fig. 6a shows that higher

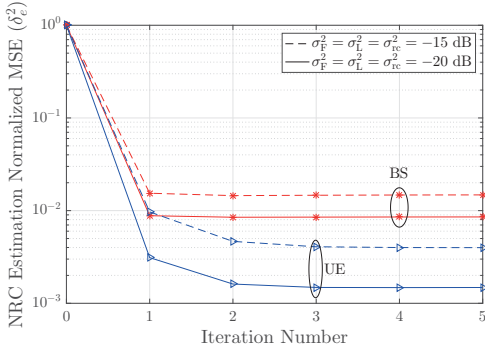


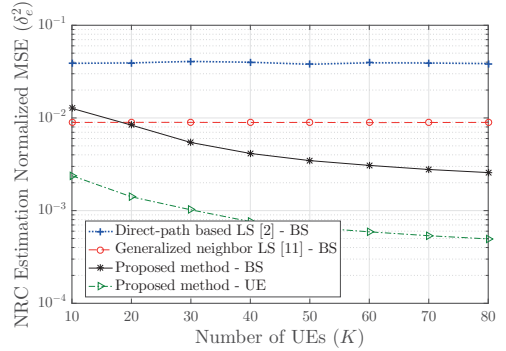
Fig. 8. NRC estimation normalized MSE vs. NRC estimation iteration number for $N = 100$, $K = 20$, $\tau_u = K$, $\rho_u = 0$ dB, $T = 250$.

UE and BS NRC estimation accuracy is achieved for $D = 0$ when $K < 20$, whereas when the number of scheduled users exceeds $K \geq 20$ the choice of $D = 1$ yields the highest BS NRC estimation accuracy. For $K \geq 20$, UE NRC estimation performances are largely similar for all three choices of D . Following these, Fig. 6b illustrates that from spectral efficiency perspective, the optimum sparsity distance threshold is $D = 0$ for $K < 20$ and $D = 1$ for $K \geq 20$. Thus, except in Fig. 7 which similarly evaluates the impacts of D on the NRC estimation performance, in the continuation $D = 0$ and $D = 1$ will be used under the settings of $K < 20$ and $K \geq 20$, respectively. As discussed in the previous section, when $\mathbf{A} \approx \mathbf{I}_K$, $\mathbf{G}^* \mathbf{A} \mathbf{G}^T$ which is used in the estimation process is of rank K . Therefore, having higher number of K increases the accuracy of the BS NRC estimation in the proposed method which facilitates the estimation of more non-diagonal elements in \mathbf{B} , i.e., higher values for D . In order to better illustrate this point, Fig. 7 provides additional results for higher σ_{rc}^2 values with $K = 40$, while keeping other simulation setup and parameter settings the same as in Fig. 5a. As expected, for the considered higher value of K (i.e., $K = 40$), $D = \sqrt{2}$ outperforms $D = 1$ at higher σ_{rc}^2 values.

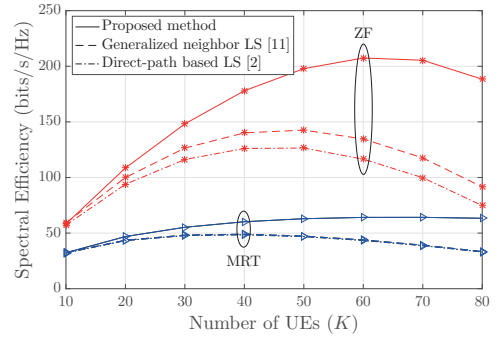
It should be noted that for all the cases in Fig. 5, Fig. 6, and Fig. 7, the proposed iterative NRC estimator is executed over a sufficient amount of iterations such that convergence is obtained. This is commonly in the order of 4 iterations, as illustrated more specifically next.

2) *Effect of the Number of Iterations:* Fig. 8 illustrates the reduction in NRC estimation normalized MSE over NRC estimation iteration steps. It is shown in Fig. 8 that, even with high NRC levels of $\sigma_L^2 = \sigma_F^2 = \sigma_{rc}^2 = -15$ dB, having 4 iteration rounds is sufficiently good for the proposed NRC estimator to converge. Therefore, in the continuation, we set the number of iteration rounds to 4.

3) *Effect of the Number of Scheduled Users K :* In Fig. 9, the NRC estimation normalized MSE and the system spectral efficiency are plotted against the number of scheduled UEs K for $\sigma_{rc}^2 = -20$ dB. Fig. 9a shows that while the direct-path based LS has the worst performance, the proposed method is the best option for estimating BS NRC for $K \geq 20$ with a



(a)



(b)

Fig. 9. (a) NRC estimation normalized MSE and (b) system spectral efficiency vs. number of UEs (K) for $N = 100$, $\tau_u = K$, $\rho_u = 0$ dB, $T = 250$.

high accuracy where MSE is in the order of 10^{-3} . For the direct-path based LS [2] and the generalized neighbor LS [11], the normalized MSE for UE side NRC is not shown. It is mentioned in [2] and [11] that additional downlink pilot signaling per coherence interval can be used together with UE side estimation for UE side NRC acquisition. However, no detailed description is provided on the actual pilot signal structure or the actual estimation method.

The corresponding system spectral efficiency performances are evaluated and shown in Fig. 9b. The proposed NRC estimation and mitigation scheme clearly outperforms the direct-path based LS and the generalized neighbor LS methods. The difference between the performance of the proposed method and the other two methods increases as K grows. Remarkably, for $K = 70$, the difference between the proposed method and the other two methods is already in the order of 100 bits/s/Hz. Another advantage in utilizing the proposed NRC estimation scheme is that the optimum number of UEs K_{opt} , which is defined as the number of scheduled UEs which maximizes the spectral efficiency, is higher compared to the other two NRC estimation methods. For instance under ZF precoding K_{opt} is around 60 for the proposed method whereas for the LS based methods K_{opt} is between 40 and 50.

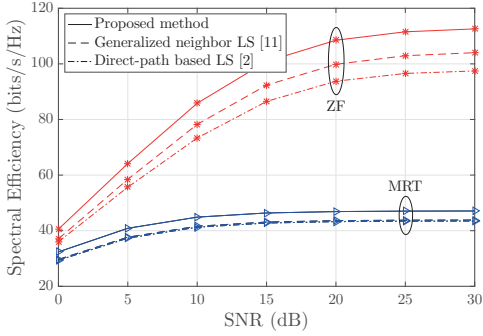


Fig. 10. Spectral efficiency vs. downlink SNR (ρ_d) for $N = 100$, $K = 20$, $\tau_u = K$, $\rho_u = 0$ dB, $T = 250$.

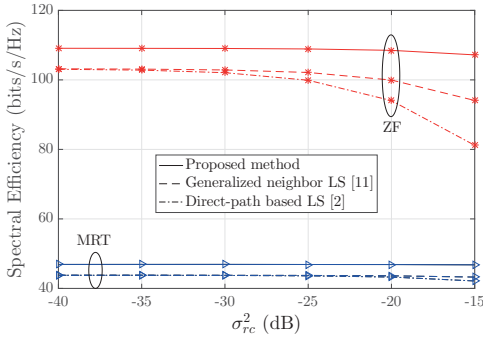


Fig. 11. Spectral efficiency vs. input reflection coefficients variance (σ_{rc}^2) for $N = 100$, $K = 20$, $\tau_u = K$, $\rho_u = 0$ dB, $T = 250$.

4) *Effect of Downlink SNR:* In Fig. 10, the system spectral efficiency is plotted against the downlink SNR when $\sigma_{rc}^2 = -20$ dB. The results show clear advantage in employing the proposed method in estimating NRC for all SNR values. The proposed estimation and mitigation method outperforms the LS based methods for both low and high SNR regions. Especially, the performance difference is most visible for high SNR region under ZF precoding.

5) *Effect of the Input Reflection Coefficient:* Fig. 11 shows the impact of the variance of the input reflection coefficients on the achievable spectral efficiency. The proposed estimation and mitigation method again outperforms the other two LS based methods. The difference between the proposed method and the other two methods increases as σ_{rc}^2 grows, which is due to the ability of the proposed method to estimate the non-diagonal elements in the BS NRC matrix. It should be noted that $D = 1$ is used for obtaining the results in Fig. 11, and there is still room for improving the performance of the proposed method by adaptively selecting the optimum D according to the level of σ_{rc}^2 as shown already in Fig. 5b and Fig. 7.

6) *Summary of the Obtained Results:* Overall, as observed through the extensive numerical evaluations in various scenarios, the proposed NRC estimation method outperforms the

other two state-of-the-art methods. Selected technical aspects can be summarized as follows:

- Employing the proposed NRC estimation method eliminates the need to send downlink demodulation pilots since the proposed OTA framework facilitates estimating both the BS side and UE side NRC characteristics in the base station. Therefore, more time-frequency resources can be allocated in each coherence interval for actual downlink data transmission purposes which improves the spectral efficiency.
- The proposed NRC estimation method is more and more superior over the two reference methods when the number of scheduled UEs K grows. One reason for this is that increasing K is forcing the other two NRC estimation methods to spend more time for downlink pilot transmission in each coherence interval, while a larger number of scheduled users improves the accuracy of the proposed NRC estimation method.
- Due to the ability to estimate also non-diagonal elements of the BS NRC matrix, the difference between the performance of the proposed NRC estimation method and the other two methods increases as the power of BS antenna mutual coupling mismatch grows.

V. CONCLUSION

In this work, we proposed an efficient NRC estimation and mitigation framework for multi-user massive MIMO TDD networks to compensate the jointly coexisting BS and UE side NRC. In general, even relatively modest NRC levels can cause significant performance loss in the achievable spectral efficiency when only standard NRC-blind MRT or ZF downlink precoding is employed. A novel OTA-based approach incorporating a dedicated round-trip pilot signaling with feasible pilot overhead together with sparsity-aided efficient iterative estimation techniques were proposed for the acquisition of the NRC matrices at the BS. Unlike the existing state-of-the-art methods, the proposed NRC estimation method acquires both the UE transceiver NRC as well as the BS transceiver and antenna system NRC, and does not rely on downlink demodulation pilots during the actual data transmission phase to compensate the NRC in the UE side. Therefore, it can be efficiently employed in massive MIMO systems that rely only on the statistical knowledge of the beamformed downlink channels at terminals for data decoding with very low system pilot overhead. The extensive computer simulations showed that for practical values of the NRC levels, SNRs and the number of spatially multiplexed users, the proposed estimation and mitigation method clearly outperforms the existing state-of-the-art methods in terms of the system spectral efficiency.

APPENDIX PROOF FOR ESTIMATION OF \mathbf{A}

Let

$$\mathcal{L} \triangleq \left\| \mathbf{Q} - \sqrt{\rho_u} \sqrt{\rho_d} \hat{\mathbf{G}}^* \mathbf{A} \hat{\mathbf{G}}^T \hat{\mathbf{B}}(m) \right\|_F^2. \quad (38)$$

Then,

$$\begin{aligned}\mathcal{L} &= \sum_{j=1}^N \left\| \mathbf{q}_j - \sqrt{\rho_u} \sqrt{\rho_d} \hat{\mathbf{G}}^* \mathbf{A} \left[\hat{\mathbf{G}}^T \hat{\mathbf{B}}(m) \right]_j \right\|^2 \\ &= \sum_{j=1}^N \left\| \mathbf{q}_j - \sqrt{\rho_u} \sqrt{\rho_d} \hat{\mathbf{G}}^* \text{diag} \left(\left[\hat{\mathbf{G}}^T \hat{\mathbf{B}}(m) \right]_j \right) \right\|^2,\end{aligned}\quad (39)$$

where $\boldsymbol{\xi} \triangleq [a_1, a_2, \dots, a_K]^T$.

By using $\mathbf{W}_j = \sqrt{\rho_u} \sqrt{\rho_d} \hat{\mathbf{G}}^* \text{diag} \left(\left[\hat{\mathbf{G}}^T \hat{\mathbf{B}}(m) \right]_j \right)$, (39) can be re-written as

$$\begin{aligned}\mathcal{L} &= \sum_{j=1}^N \|\mathbf{q}_j - \mathbf{W}_j \boldsymbol{\xi}\|^2 \\ &= \sum_{j=1}^N \|\bar{\mathbf{q}}_j - \bar{\mathbf{W}}_j \boldsymbol{\psi}\|^2 \triangleq \bar{\mathcal{L}}(\boldsymbol{\psi}),\end{aligned}\quad (40)$$

where $\boldsymbol{\psi} \triangleq [\Re\{\boldsymbol{\xi}^T\}, \Im\{\boldsymbol{\xi}^T\}]^T$. Therefore, the solution $\hat{\mathbf{A}}(m)$ can be obtained by

$$\hat{\mathbf{A}}(m) = \text{diag} \left([\mathbf{I}_K, i\mathbf{I}_K] \hat{\boldsymbol{\psi}} \right), \quad (41)$$

where

$$\hat{\boldsymbol{\psi}} = \underset{\boldsymbol{\psi} \in \mathbb{R}^K}{\text{argmin}} \bar{\mathcal{L}}(\boldsymbol{\psi}). \quad (42)$$

Since $\bar{\mathcal{L}}(\boldsymbol{\psi})$ is convex, (42) can be solved from the partial derivative equation $\frac{\partial \bar{\mathcal{L}}(\boldsymbol{\psi})}{\partial \boldsymbol{\psi}} = 0$, which finally yields the solution given by (26).

ACKNOWLEDGMENT

The estimation of \mathbf{A} is building on the work presented in [28]. The proof in Appendix A is a result of discussion with the authors of [28], H. Q. Ngo and E. G. Larsson, whose technical guidance is greatly acknowledged.

REFERENCES

- [1] F. Boccardi, R. W. Heath, A. Lozano, T. L. Marzetta, and P. Popovski, "Five disruptive technology directions for 5G," *IEEE Communications Magazine*, vol. 52, no. 2, pp. 74–80, February 2014.
- [2] C. Shepard, H. Yu, N. Anand, E. Li, T. Marzetta, R. Yang, and L. Zhong, "Argos: Practical many-antenna base stations," in *Proceedings of the 18th Annual International Conference on Mobile Computing and Networking*, ser. Mobicom '12. New York, NY, USA: ACM, 2012, pp. 53–64.
- [3] E. G. Larsson, O. Edfors, F. Tufvesson, and T. L. Marzetta, "Massive MIMO for next generation wireless systems," *IEEE Communications Magazine*, vol. 52, no. 2, pp. 186–195, February 2014.
- [4] A. Bourdoux, B. Come, and N. Khaled, "Non-reciprocal transceivers in OFDM/SDMA systems: Impact and mitigation," in *Radio and Wireless Conference, 2003. RAWCON '03. Proceedings*, Aug 2003, pp. 183–186.
- [5] Y. Zou, O. Raeesi, R. Wichman, A. Tolli, and M. Valkama, "Analysis of channel non-reciprocity due to transceiver and antenna coupling mismatches in TDD precoded multi-user MIMO-OFDM downlink," in *2014 IEEE 80th Vehicular Technology Conference (VTC2014-Fall)*, Sept 2014, pp. 1–7.
- [6] M. Petermann, M. Stefer, F. Ludwig, D. Wubben, M. Schneider, S. Paul, and K. D. Kammeyer, "Multi-user pre-processing in multi-antenna OFDM TDD systems with non-reciprocal transceivers," *IEEE Transactions on Communications*, vol. 61, no. 9, pp. 3781–3793, September 2013.
- [7] H. Wei, D. Wang, and X. You, "Reciprocity of mutual coupling for TDD massive MIMO systems," in *Wireless Communications Signal Processing (WCSP), 2015 International Conference on*, Oct 2015, pp. 1–5.
- [8] W. Zhang, H. Ren, C. Pan, M. Chen, R. C. de Lamare, B. Du, and J. Dai, "Large-scale antenna systems with UL/DL hardware mismatch: Achievable rates analysis and calibration," *IEEE Transactions on Communications*, vol. 63, no. 4, pp. 1216–1229, April 2015.
- [9] F. Athley, G. Durisi, and U. Gustavsson, "Analysis of massive MIMO with hardware impairments and different channel models," in *2015 9th European Conference on Antennas and Propagation (EuCAP)*, May 2015, pp. 1–5.
- [10] R. Rogalin, O. Y. Bursalioglu, H. Papadopoulos, G. Caire, A. F. Molisch, A. Michaloliakos, V. Balan, and K. Psounis, "Scalable synchronization and reciprocity calibration for distributed multiuser MIMO," *IEEE Transactions on Wireless Communications*, vol. 13, no. 4, pp. 1815–1831, April 2014.
- [11] J. Vieira, F. Rusek, and F. Tufvesson, "Reciprocity calibration methods for massive MIMO based on antenna coupling," in *2014 IEEE Global Communications Conference*, Dec 2014, pp. 3708–3712.
- [12] H. Wei, D. Wang, H. Zhu, J. Wang, S. Sun, and X. You, "Mutual coupling calibration for multiuser massive MIMO systems," *IEEE Transactions on Wireless Communications*, vol. 15, no. 1, pp. 606–619, Jan 2016.
- [13] H. Wei, D. Wang, J. Wang, and X. You, "TDD reciprocity calibration for multi-user massive MIMO systems with iterative coordinate descent," *Science China Information Sciences*, vol. 59, no. 10, p. 102306, 2015.
- [14] M. Guillaud, D. T. M. Slock, and R. Knopp, "A practical method for wireless channel reciprocity exploitation through relative calibration," in *Proceedings of the Eighth International Symposium on Signal Processing and Its Applications*, 2005., vol. 1, August 2005, pp. 403–406.
- [15] Y. Zou, O. Raeesi, and M. Valkama, "Efficient estimation and compensation of transceiver non-reciprocity in precoded TDD multi-user MIMO-OFDM systems," in *2014 IEEE 80th Vehicular Technology Conference (VTC2014-Fall)*, Sept 2014, pp. 1–7.
- [16] M. Guillaud and F. Kaltenberger, "Towards practical channel reciprocity exploitation: Relative calibration in the presence of frequency offset," in *2013 IEEE Wireless Communications and Networking Conference (WCNC)*, April 2013, pp. 2525–2530.
- [17] F. Kaltenberger, H. Jiang, M. Guillaud, and R. Knopp, "Relative channel reciprocity calibration in MIMO/TDD systems," in *2010 Future Network Mobile Summit*, June 2010, pp. 1–10.
- [18] O. Raeesi, A. Gokceoglu, Y. Zou, E. Bjrnson, and M. Valkama, "Performance analysis of multi-user massive MIMO downlink under channel non-reciprocity and imperfect CSI," *IEEE Transactions on Communications*, vol. PP, no. 99, pp. 1–1, 2018.
- [19] H. Yang and T. L. Marzetta, "Performance of conjugate and zero-forcing beamforming in large-scale antenna systems," *IEEE Journal on Selected Areas in Communications*, vol. 31, no. 2, pp. 172–179, February 2013.
- [20] J. Jose, A. Ashikhmin, P. Whiting, and S. Vishwanath, "Channel estimation and linear precoding in multiuser multiple-antenna TDD systems," *IEEE Transactions on Vehicular Technology*, vol. 60, no. 5, pp. 2102–2116, Jun 2011.
- [21] J. Jose, A. Ashikhmin, T. L. Marzetta, and S. Vishwanath, "Pilot contamination and precoding in multi-cell TDD systems," *IEEE Transactions on Wireless Communications*, vol. 10, no. 8, pp. 2640–2651, August 2011.
- [22] E. G. Larsson and H. V. Poor, "Joint beamforming and broadcasting in massive MIMO," *IEEE Transactions on Wireless Communications*, vol. 15, no. 4, pp. 3058–3070, April 2016.
- [23] H. Q. Ngo, E. G. Larsson, and T. L. Marzetta, "Massive MU-MIMO downlink TDD systems with linear precoding and downlink pilots," in *Communication, Control, and Computing (Allerton), 2013 51st Annual Allerton Conference on*, Oct 2013, pp. 293–298.
- [24] S. A. Schelkunoff and H. T. Friis, *Antennas Theory and Practice*. New York: John Wiley & Sons, 1952.
- [25] B. M. Hochwald, T. L. Marzetta, and V. Tarokh, "Multiple-antenna channel hardening and its implications for rate feedback and scheduling," *IEEE Transactions on Information Theory*, vol. 50, no. 9, pp. 1893–1909, Sept 2004.
- [26] H. Q. Ngo and E. G. Larsson, "No downlink pilots are needed in TDD massive MIMO," *IEEE Transactions on Wireless Communications*, vol. 16, no. 5, pp. 2921–2935, May 2017.
- [27] M. Petermann, M. Stefer, D. Wbenn, M. Schneider, and K. D. Kammeyer, "Low-complexity calibration of mutually coupled non-reciprocal multi-antenna OFDM transceivers," in *2010 7th International Symposium on Wireless Communication Systems*, Sept 2010, pp. 285–289.
- [28] H. Q. Ngo and E. G. Larsson, "EVD-based channel estimation in multicell multiuser MIMO systems with very large antenna arrays," in *2012 IEEE International Conference on Acoustics, Speech and Signal Processing (ICASSP)*, March 2012, pp. 3249–3252.



Orod Raeesi received his M.Sc. degree (with distinction) from Tampere University of Technology (TUT), Tampere, Finland, in 2011, and is currently pursuing the Ph.D. degree at TUT. Currently, he is working as a communications system specialist with Nokia Mobile Networks, Espoo, Finland. His research interests include IEEE 802.11 MAC and PHY layer challenges, massive MIMO systems, TDD channel non-reciprocity, ultra-reliable low latency communications, system-level simulations, and 5G mobile radio networks.



Ahmet Gokceoglu received M.Sc. (2010) and Ph.D. Degrees (2014) from the Department of Electronics and Communications Engineering, Tampere University of Technology, Finland, where he also held a postdoctoral researcher position (2014-2016) together with a visiting researcher position at Linköping university (2015). His research interests are information theory, modeling and performance analysis of MIMO-OFDM systems, advanced transmitter and receiver signal processing techniques and algorithm design for MAC and physical layer. He is currently working

as an algorithm specialist with Huawei, Stockholm, Sweden.



Mikko Valkama (S'00–M'01–SM'15) was born in Pirkkala, Finland, on November 27, 1975. He received the M.Sc. and Ph.D. Degrees (both with honors) in electrical engineering (EE) from Tampere University of Technology (TUT), Finland, in 2000 and 2001, respectively. In 2002, he received the Best Ph.D. Thesis -award by the Finnish Academy of Science and Letters for his dissertation entitled “Advanced I/Q signal processing for wideband receivers: Models and algorithms”. In 2003, he was working as a visiting post-doc research fellow with the

Communications Systems and Signal Processing Institute at SDSU, San Diego, CA. Currently, he is a Full Professor and Laboratory Head at the Laboratory of Electronics and Communications Engineering at TUT, Finland. His general research interests include radio communications, communications signal processing, estimation and detection techniques, signal processing algorithms for flexible radios, cognitive radio, full-duplex radio, radio localization, and 5G mobile radio networks.

PUBLICATION II

O. Raeesi, A. Gokceoglu, Y. Zou, E. Björnson and M. Valkama, “Performance analysis of multi-user massive MIMO downlink under channel non-reciprocity and imperfect CSI,” *IEEE Transactions on Communications*, vol. 66, no. 6, pp. 2456–2471, June 2018.

© 2018 IEEE. Reprinted, with permission, from O. Raeesi, A. Gokceoglu, Y. Zou, E. Björnson and M. Valkama, “Performance analysis of multi-user massive MIMO downlink under channel non-reciprocity and imperfect CSI,” *IEEE Transactions on Communications*, June 2018.

In reference to IEEE copyrighted material which is used with permission in this thesis, the IEEE does not endorse any of Tampere University’s products or services. Internal or personal use of this material is permitted. If interested in reprinting/republishing IEEE copyrighted material for advertising or promotional purposes or for creating new collective works for resale or redistribution, please go to http://www.ieee.org/publications_standards/publications/rights/rights_link.html to learn how to obtain a License from RightsLink.

Performance Analysis of Multi-User Massive MIMO Downlink under Channel Non-Reciprocity and Imperfect CSI

Orod Raeesi, *Student Member, IEEE*, Ahmet Gokceoglu, *Member, IEEE*, Yaning Zou, *Member, IEEE*, Emil Björnson, *Senior Member, IEEE*, and Mikko Valkama, *Senior Member, IEEE*

Abstract—This paper analyzes the performance of linearly precoded time division duplex based multi-user massive MIMO downlink system under joint impacts of channel non-reciprocity (NRC) and imperfect channel state information (CSI). We consider a generic and realistic NRC model that accounts for transceiver frequency-response as well as mutual coupling mismatches at both user equipment (UE) and base station (BS) sides. The analysis covers two most prominent forms of linear precoding schemes, namely, zero-forcing (ZF) and maximum-ratio transmission (MRT), and assumes that only the statistical properties of the beamformed channel are used at the UE side to decode the received signal. Under the approximation of i.i.d. Gaussian channels, closed-form analytical expressions are derived for the effective signal to interference and noise ratios (SINRs) and the corresponding capacity lower bounds. The expressions show that, in moderate to high SNR, the additional interference caused by imperfect NRC calibration can degrade the performance of both precoders significantly. Moreover, ZF is shown to be more sensitive to NRC than MRT. Numerical evaluations with practical NRC levels indicate that this performance loss in the spectral efficiency can be as high as 42% for ZF, whereas it is typically less than 13% for MRT. It is also shown that due to the NRC, the asymptotic large-antenna performance of both precoders saturate to an identical finite level. The derived analytical expressions provide useful tools and valuable technical insight, e.g., into calculating the NRC calibration requirements in BSs and UEs for any given specific performance targets in terms of effective SINR or the system capacity bound.

Index Terms—Capacity, channel reciprocity, frequency-response mismatch, inter-user interference, linear precoding, multi-user massive MIMO, mutual coupling, SINR.

I. INTRODUCTION

MASSIVE multiple-input multiple-output (MIMO) systems are envisioned to be one key enabling technology for the next generation cellular networks, known as 5G [1], [2]. In massive MIMO systems, a base station (BS) uses an array

with a large number of antennas N to serve K user equipments (UEs) simultaneously on the same time-frequency resource, where typically $N \gg K$ [2]–[5]. Large-scale system analysis shows that linear precoding techniques, e.g., zero-forcing (ZF) and maximum ratio transmission (MRT) are asymptotically optimal with increasing N , while very high spectral-efficiencies can already be achieved with N being in the order of several tens or hundreds [5]–[8].

The key requirement for employing the above precoding schemes is to have accurate channel state information (CSI) at the BS for efficient multi-user spatial precoding. In conventional frequency-division duplex (FDD) based MIMO systems, where the number of BS antennas is relatively low, UEs commonly estimate downlink (DL) channels based on the received DL training signals transmitted by the BS, and feed the estimated DL channels back to the BS [9]. The number of DL pilots required for estimating the channels is proportional to the number of antennas in the BS which complicates the adoption of such DL channel estimation and reporting methods in massive MIMO systems. As an alternative approach, massive MIMO systems are typically assumed to employ time-division duplex (TDD), and thus estimate the DL channel based on uplink (UL) pilots, relying on the reciprocity of the physical DL and UL channels within channel coherence interval [10]. Thereby, the required amount of resources in such a TDD based approach is only proportional to the number of served UEs which is typically much smaller than the number of BS antennas, i.e., $K \ll N$ [5], [10].

The channel reciprocity in TDD systems holds only for the physical propagation channels. However, when the effective baseband-to-baseband transmission channels between the BS and UEs are considered, incorporating also the impacts of the involved transceiver circuits and antenna systems, the reciprocity does not hold anymore due to the mismatches in transmit and receive mode characteristics of the transceivers and antenna systems [11]–[14]. More specifically, such mismatch characteristics include the unavoidable differences between the frequency-responses (FRs) of transmitter and receiver chains of any individual transceiver, as well as the mutual coupling effects between the antenna elements in multi-antenna devices [15]–[17]. The impacts of such transceiver hardware and antenna system induced non-reciprocity, also commonly referred to as channel non-reciprocity (NRC), have been studied for massive MIMO systems to a certain extent in [18]–[22]. To this end, [18]–[22] study the system performance degradation in terms

O. Raeesi, A. Gokceoglu, and M. Valkama are with the Department of Electronics and Communications Engineering, Tampere University of Technology, Tampere 33720, Finland (e-mail: orod.raeesi@tut.fi; ahmet.gokceoglu@tut.fi; mikko.e.valkama@tut.fi).

Y. Zou is with Technische Universität Dresden, Vodafone Chair Mobile Communications Systems, Dresden, Germany (e-mail: yaning.zou@ifn.et.tu-dresden.de).

E. Björnson is with the Department of Electrical Engineering (ISY), Linköping University, SE-581 83 Linköping, Sweden (e-mail: emil.bjornson@liu.se).

This work was supported by the Finnish Funding Agency for Technology and Innovation (Tekes) under the project “5th Evolution Take of Wireless Communication Networks (TAKE-5)”, by the Academy of Finland under the projects 284694 and 288670 and TUT Graduate School.

of signal to interference and noise ratios (SINRs) and the corresponding achievable rates due to NRC, while assuming otherwise ideal system with perfect CSI. Furthermore, the system models in [20]–[22] consider only FR mismatch and thus ignore the NRC induced by possible mutual coupling mismatches, reported, e.g., in [15]–[17], [19] to be one important practical source of non-reciprocity. Furthermore, only the BS side NRC is considered in [19], [20].

In this paper, we analyze the SINR and achievable sum-rate of linearly precoded TDD multi-user massive MIMO DL transmission systems under the joint impacts of imperfect CSI and NRC. We consider a generic and realistic NRC model which takes into account both the FR and mutual coupling mismatches at the UEs and the BS. The analysis is carried out for the two most widely-adopted forms of linear precoding, namely, ZF and MRT. As in [7], [22]–[24], we also assume that UEs rely only on statistical DL CSI to decode the received signals, and thus more sophisticated precoding schemes, e.g., block diagonalization-based precoding, requiring instantaneous demodulation CSI at UE receivers are excluded. Based on the developed signal and system models, closed-form expressions are derived for the effective SINRs and the corresponding capacity lower bounds. To highlight the substantial differences between this work and the existing literature on performance analysis of NRC impaired massive MIMO systems, we summarize the novel contributions of this manuscript as follows:

- 1) In contrast to the simplified NRC models in [20]–[22] which consider only FR mismatches, a more practical and generic NRC model is considered in this work which incorporates both FR and mutual coupling mismatches in both BS and UE sides.
- 2) In contrast to the existing literature, the analysis in this work does not impose any restrictions on the structure of NRC matrices and the involved NRC variables, in terms of their statistical distributions or mutual correlation. Therefore, in addition to covering the systems without explicit NRC calibration, the provided analytical results can also be used in connection with residual non-reciprocity after any given NRC calibration method, e.g., [25]–[27].
- 3) In contrast to [19], [21], a performance comparison between ZF and MRT precoding schemes is also carried out which shows the relative sensitivity of these precoders to different NRC levels, with and without UL channel estimation errors, in both non-asymptotic and asymptotic cases.
- 4) In contrast to [18]–[22] which consider NRC alone, in this work we consider the joint impacts of co-existing NRC and UL channel estimation errors (called imperfect CSI).
- 5) In contrast to [18]–[22], the derived analytical expressions decompose the total received interference into two parts, namely, interference power due to imperfect CSI, without NRC, and the interference term due to NRC (see expression (20) for ZF, and (25) for MRT). With this decomposition, it is straightforward to quantify

the specific performance degradation due to NRC with respect to the ideal reciprocal case, and also to draw technical insight and establish design criteria for both UL pilot signaling and reciprocity calibration.

In general, given the specific performance targets, such as effective SINRs and/or capacity lower bound, the derived analytical expressions reported in this manuscript can be directly used in designing and dimensioning the system, e.g., choosing the appropriate precoder based on the performance-complexity trade-off, deciding on the number of active antenna elements, and/or extracting the needed accuracy of NRC calibration schemes, as well as understanding the trade-offs between UL pilot based channel estimation accuracy, NRC calibration accuracy and the achievable system performance.

The rest of the paper is organized as follows. Section II describes the fundamental multi-user massive MIMO system model under transceiver and antenna system non-reciprocity and imperfect CSI. Then, in Section III, analytical expressions are derived for the effective DL SINR and capacity lower bound under ZF and MRT precoding schemes. In Section IV, the asymptotic SINR and achievable rate expressions are derived for ZF and MRT precoding schemes, and also an analytic performance comparison is pursued in both asymptotic and non-asymptotic cases. In Section V, extensive numerical results are provided to evaluate and verify the derived analytical expressions and illustrate the impact of various non-reciprocity sources and parameters on the system performance. Finally, conclusions are drawn in Section VI. Selected details regarding the derivations of the reported analytic expressions are provided in an Appendix.

Notations: Throughout this paper, matrices (vectors) are denoted with upper-case (lower-case) bold characters, e.g., \mathbf{V} (\mathbf{v}). The superscripts $(\cdot)^T$, $(\cdot)^*$, and $(\cdot)^H$ stand for transpose, conjugate, and conjugate-transpose, respectively. Expectation operator is shown by $\mathbb{E}[\cdot]$, $\text{Tr}(\cdot)$ represents the trace operator, $\text{Sum}(\cdot)$ yields the element-wise sum of the argument matrix, while $\text{Var}(\cdot)$ and $\text{Cov}(\cdot)$ refer to the variance and covariance operators, respectively. \mathbf{I}_n and $\mathbf{0}_n$ denote $n \times n$ identity and all-zero matrices, respectively. The element in i -th row and j -th column of matrix \mathbf{V} is represented by v_{ij} . A diagonal matrix with elements (v_1, \dots, v_n) is shown by $\text{diag}(v_1, \dots, v_n)$, corresponding block-diagonal matrix is denoted by $\text{blkdiag}(\mathbf{A}_1, \dots, \mathbf{A}_k)$, and $\mathcal{CN}(0, \sigma^2)$ represents a circularly symmetric zero-mean complex Gaussian distribution with variance σ^2 .

II. SYSTEM MODEL

We consider precoded downlink data transmission in a TDD based multi-user massive MIMO system, where a BS with N antennas serves K UEs simultaneously on the same time-frequency resource. The number of antennas in k -th UE is denoted by M_k and $\sum_{k=1}^K M_k = M_{\text{tot}}$, where $N \gg M_{\text{tot}}$. For notational convenience, we assume that the total set of M_{tot} antennas at the UE side is logically indexed such that the first M_1 antennas belong to UE 1, the next M_2 antennas belong to UE 2, and so forth. We also assume that all antenna elements in the considered system are omni-directional, for simplicity.

We further assume that the spatial transmit signal vector is generated using linear precoding techniques, e.g., ZF or MRT. All system models are written for an arbitrary subcarrier of the underlying orthogonal frequency division multiplexing/multiple access (OFDM/OFDMA) waveform, that is, before IFFT and after FFT on the TX and RX sides, respectively, without explicitly showing the subcarrier index. It is further assumed that the cyclic prefix (CP) length is larger than the channel delay spread.

A. Uplink Training, Downlink Transmission and Effective Channels

The DL linear precoder is designed based on the CSI acquired from UL pilots. The fundamental multi-user signal models for the UL pilot and DL data transmission phases can be expressed as [6], [28]

$$\begin{aligned} \text{UL: } \mathbf{Y}^p &= \sqrt{\tau_u \rho_u} \mathbf{G} \mathbf{X}^p + \mathbf{N}^p \\ \text{DL: } \mathbf{r} &= \sqrt{\rho_d} \mathbf{H} \mathbf{x} + \mathbf{n}, \end{aligned} \quad (1)$$

where $\mathbf{G} \in \mathbb{C}^{N \times M_{\text{tot}}}$ and $\mathbf{H} \in \mathbb{C}^{M_{\text{tot}} \times N}$ are the effective UL and DL channel matrices, respectively, that are explicitly defined in the next paragraph. Regarding the UL pilot signal model, ρ_u is the transmitted signal to noise ratio (SNR) of the UL pilots, $\mathbf{Y}^p = [\mathbf{y}_1^p, \dots, \mathbf{y}_N^p]^T$ is the received signal matrix at the BS receiver, stacking the received UL pilots over τ_u symbol durations, where $\mathbf{y}_n^p \in \mathbb{C}^{\tau_u \times 1}$ contains the received UL pilots at n -th BS antenna, and $\mathbf{N}^p = [\mathbf{n}_1^p, \dots, \mathbf{n}_N^p]^T$ is the additive receiver noise matrix at the BS with i.i.d. $\mathcal{CN}(0, 1)$ elements, where $\mathbf{n}_n^p \in \mathbb{C}^{\tau_u \times 1}$ is the additive receiver noise sequence at n -th BS antenna. The matrix stacking all the transmitted UL pilots at all the antennas in the UE side is shown by $\mathbf{X}^p = [\mathbf{x}_1^p, \dots, \mathbf{x}_{M_{\text{tot}}}^p]^T$, where $\mathbf{x}_m^p \in \mathbb{C}^{\tau_u \times 1}$ is the UL temporal pilot vector transmitted from m -th antenna in the UE side. Then, for the DL, $\mathbf{r} \in \mathbb{C}^{M_{\text{tot}} \times 1}$ denotes the received multi-user DL signal vector corresponding to all M_{tot} antennas at the UE side, ρ_d is the transmitted SNR of DL channel, and $\mathbf{n} \in \mathbb{C}^{M_{\text{tot}} \times 1}$ is the normalized additive receiver noise vector at UE side with i.i.d. $\mathcal{CN}(0, 1)$ elements. The precoded spatial transmit signal vector in the BS is shown by $\mathbf{x} = [x_1, \dots, x_N]^T$, where x_n is the precoded sample transmitted from n -th antenna in the BS.

As illustrated in Fig. 1, the effective DL and UL channels are generally cascades of transceiver frequency-responses and antenna mutual coupling at BS side, physical propagation channels, and transceiver frequency-responses and antenna mutual coupling at UE side. Thus, the effective DL channel \mathbf{H} and the effective UL channel \mathbf{G} can be written explicitly as [15], [16]

$$\begin{aligned} \mathbf{H} &= \mathbf{F}^{RX} \mathbf{D}^{RX} \mathbf{P}^T \mathbf{M}^{TX} \mathbf{B}^{TX} \\ \mathbf{G} &= \mathbf{B}^{RX} \mathbf{M}^{RX} \mathbf{P} \mathbf{D}^{TX} \mathbf{F}^{TX}, \end{aligned} \quad (2)$$

where $\mathbf{F} = \text{diag}(f_1, \dots, f_{M_{\text{tot}}})$ is the total FR matrix of the UEs, $\mathbf{D} = \text{blkdiag}(\mathbf{D}_1, \dots, \mathbf{D}_K) \in \mathbb{C}^{M_{\text{tot}} \times M_{\text{tot}}}$ is a block-diagonal matrix representing the antenna mutual coupling matrix at UE side, $\mathbf{B} = \text{diag}(b_1, \dots, b_N)$ is the FR matrix of the BS, $\mathbf{M} \in \mathbb{C}^{N \times N}$ is the antenna mutual coupling matrix of the BS, and $\mathbf{P} \in \mathbb{C}^{N \times M_{\text{tot}}}$ is the reciprocal physical channel,

while the superscripts TX and RX specify the transmit and receive modes, respectively. Notice that while the overall UE side antenna mutual coupling matrices, \mathbf{D}^{TX} and \mathbf{D}^{RX} , are assumed to be block-diagonal, because of clear physical separation of the different UE devices, the element matrices \mathbf{D}_k^{TX} and \mathbf{D}_k^{RX} are generally full matrices of size $M_k \times M_k$.

B. Channel Non-Reciprocity Problem

As outlined above, in TDD networks the BS obtains DL CSI based on the estimated UL channel, since DL and UL channels share the same spectrum and are assumed to be reciprocal within each channel coherence interval. The reciprocal nature applies, however, only to the physical propagation channels shown in Fig. 1. In addition to the physical channels, the effective channels also include the responses of electronics components used in the transmitting and receiving devices which results into the effective DL and UL channels expressed in (2).

Based on (2), the relation between the effective DL and UL channels can now be expressed as

$$\mathbf{H} = \mathbf{A} \mathbf{G}^T \mathbf{C}, \quad (3)$$

where the matrices \mathbf{A} and \mathbf{C} are

$$\begin{aligned} \mathbf{A} &= \mathbf{F}^{RX} \mathbf{D}^{RX} (\mathbf{D}^{TX})^{-T} (\mathbf{F}^{TX})^{-1} \\ \mathbf{C} &= (\mathbf{B}^{RX})^{-1} (\mathbf{M}^{RX})^{-T} \mathbf{M}^{TX} \mathbf{B}^{TX}. \end{aligned} \quad (4)$$

In (3) and (4), the matrices $\mathbf{A} \in \mathbb{C}^{M_{\text{tot}} \times M_{\text{tot}}}$ and $\mathbf{C} \in \mathbb{C}^{N \times N}$ are incorporating the effects of transceivers and antenna systems on the non-reciprocity in UEs and BS, respectively. The matrix \mathbf{A} is block-diagonal and can in general be written as $\mathbf{A} = \mathbf{I}_{M_{\text{tot}}} + \mathbf{A}'$ where \mathbf{A}' can be expressed as $\mathbf{A}' = \text{blkdiag}(\mathbf{A}'_1, \dots, \mathbf{A}'_K)$, while the full matrix $\mathbf{A}'_k \in \mathbb{C}^{M_k \times M_k}$ represents the NRC in the k -th UE. On the other hand, \mathbf{C} which represents the overall BS transceiver and antenna system non-reciprocity, including mutual coupling mismatch, is generally an $N \times N$ full matrix and can be decomposed as $\mathbf{C} = \mathbf{I}_N + \mathbf{C}'$.

In general, the channel non-reciprocity values vary very slowly in time with respect to the variations in the propagation channel [26] and hence \mathbf{A} and \mathbf{C} can be assumed to remain constant over many channel coherence intervals. Furthermore, it can easily be deduced that the effective DL and UL channels are reciprocal if and only if the mismatch matrices satisfy $\mathbf{A}' = \mathbf{0}_{M_{\text{tot}}}$ and $\mathbf{C}' = \mathbf{0}_N$.

For the purpose of the upcoming analysis, we next define and assume the following. First, we write \mathbf{A}'_k as $\mathbf{A}'_k = [\mathbf{a}'_1^k, \dots, \mathbf{a}'_{M_k}^k]^T$ and by dropping the UE index k for notational simplicity, we define $\mathbf{R}_{\mathbf{a}'_m} = \text{Cov}(\mathbf{a}'_m)$ for the m -th antenna at the UE side ranging from 1 to M_{tot} . In matrix \mathbf{A}' , the elements are assumed to be zero-mean and the power of \mathbf{a}'_{mi} is denoted by $\sigma_{\mathbf{a}'_{mi}}^2 = \mathbb{E}[|\mathbf{a}'_{mi}|^2]$. Similarly at the BS side, \mathbf{C}' is also assumed to have zero-mean elements. Then, we stack all the diagonal and non-diagonal elements of \mathbf{C}' in $\mathbf{c}'_d = [c'_{11}, c'_{22}, \dots, c'_{NN}]$ and $\mathbf{c}'_{\text{od}} = [c'_{12}, c'_{13}, \dots, c'_{NN-1}]$, respectively, and define $\mathbf{R}_{\mathbf{c}'_d} = \text{Cov}(\mathbf{c}'_d)$ and $\mathbf{R}_{\mathbf{c}'_{\text{od}}} = \text{Cov}(\mathbf{c}'_{\text{od}})$. Then, as explicitly shown in the appendix, the final closed-form analysis results depend only on these NRC covariances

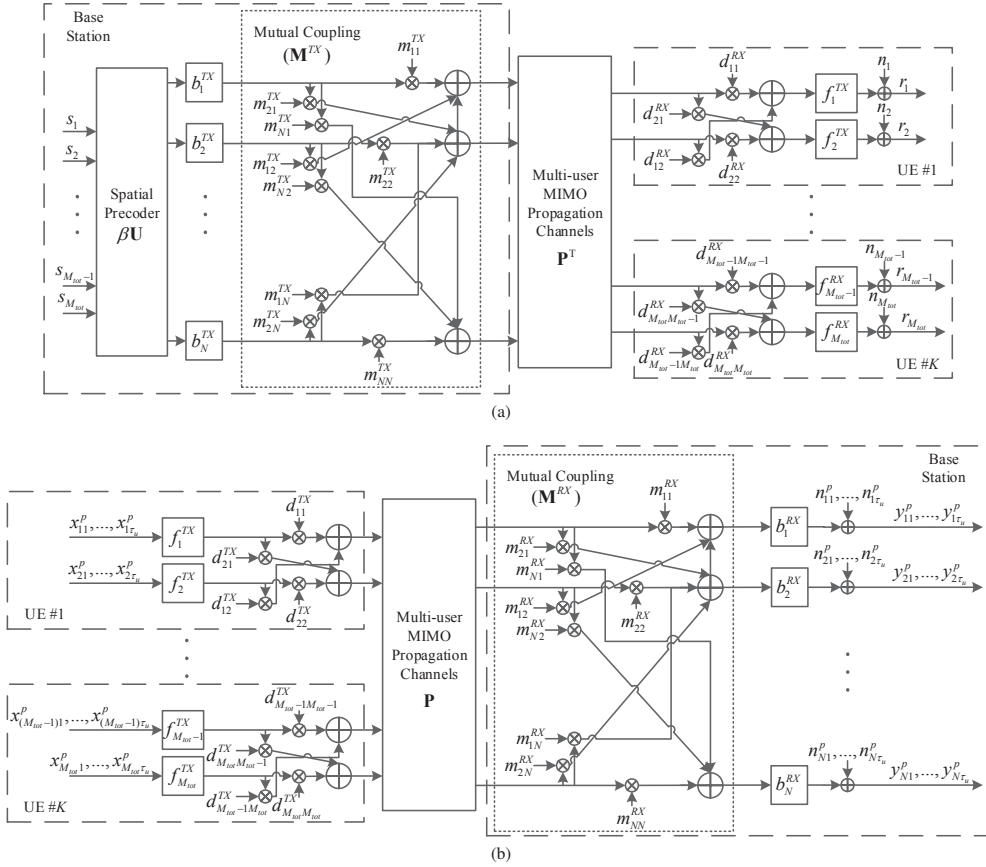


Fig. 1. Principal illustration of (a) DL and (b) UL transmissions and receptions including physical propagation channels, transceiver frequency responses and antenna mutual coupling in the devices in an example case of dual-antenna UEs.

but not, e.g., on the exact distributions of the NRC variables. In all the forth-coming analysis and derivations, we adopt the simplifying assumption or approximation that the elements of the effective UL channel \mathbf{G} are unit-variance i.i.d. Gaussians. While the exact distribution and correlation characteristics of real-world effective UL channel entries depend, among others, on the exact antenna array configuration and angular spread of the propagation environment, we adopt such simplifying approximation since the closed-form rate expressions that one can deduce by using such model have been shown to match very accurately with practical massive MIMO measurements [29]. This is a result of the channel hardening and favorable propagation phenomena, which makes the performance less dependent on the actual channel distribution. Hence, we use i.i.d. Rayleigh fading in this work to study the channel non-reciprocity aspects in a clean and rigorous manner.

C. Channel Estimation

To facilitate the channel estimation at the BS, the UEs simultaneously transmit mutually orthogonal UL pilot sequences of length τ_u such that $\mathbf{X}^p (\mathbf{X}^p)^H = \mathbf{I}_{M_{tot}}$ with $\tau_u \geq M_{tot}$.

To estimate the UL channels, the BS multiplies \mathbf{Y}^p in (1) by $(\mathbf{X}^p)^H$, which yields [7]

$$\mathbf{Y} = \mathbf{Y}^p (\mathbf{X}^p)^H = \sqrt{\tau_u \rho_u} \mathbf{G} + \mathbf{Q}, \quad (5)$$

where $\mathbf{Q} \in \mathbb{C}^{N \times M_{tot}}$ is the processed noise matrix with i.i.d. $\mathcal{CN}(0, 1)$ elements. Using minimum mean-square error (MMSE) channel estimator, the estimated effective UL channel $\hat{\mathbf{G}} \in \mathbb{C}^{N \times M_{tot}}$ can be shown to read [7], [28]

$$\hat{\mathbf{G}} = \frac{\sqrt{\tau_u \rho_u}}{\tau_u \rho_u + 1} \mathbf{Y} = \frac{\tau_u \rho_u}{\tau_u \rho_u + 1} \mathbf{G} + \frac{\sqrt{\tau_u \rho_u}}{\tau_u \rho_u + 1} \mathbf{Q}, \quad (6)$$

while the corresponding effective DL channel estimate, called $\hat{\mathbf{H}}$, that is utilized by the NRC-unaware BS for downlink precoding is obtained by $\hat{\mathbf{H}} = \hat{\mathbf{G}}^T$. Based on (6) and the orthogonality principle of MMSE estimators, the effective UL channel matrix \mathbf{G} can also be decomposed as [7], [28]

$$\mathbf{G} = \hat{\mathbf{G}} + \mathbf{E}^T = \hat{\mathbf{H}}^T + \mathbf{E}^T, \quad (7)$$

where $\mathbf{E} = [\mathbf{e}_1, \dots, \mathbf{e}_{M_{tot}}]^T \in \mathbb{C}^{M_{tot} \times N}$ accounts for the UL channel estimation errors and has i.i.d. $\mathcal{CN}(0, \frac{1}{\tau_u \rho_u + 1})$ elements. The estimated effective DL channel $\hat{\mathbf{H}}$ has i.i.d.

$\mathcal{CN}\left(0, \frac{\tau_u \rho_u}{\tau_u \rho_u + 1}\right)$ elements and is independent of \mathcal{E} . The considered pilot signaling and UL channel estimation method is the most common form of UL CSI acquisition for massive MIMO systems in the existing literature [3], [6], [7]. Alternative partial CSI acquisition based approaches, such as [30], are also important but are outside the scope of this paper.

Incorporating (7) into (3), we finally obtain the relation between the estimated and true effective DL channels as

$$\mathbf{H} = \mathbf{A} \mathbf{G}^T \mathbf{C} = \mathbf{A} \left(\hat{\mathbf{H}} + \mathcal{E} \right) \mathbf{C}, \quad (8)$$

which summarizes the joint effects of two co-existing non-ideality sources, namely, UL channel estimation error and the channel non-reciprocity, on the effective DL channel estimation.

III. PERFORMANCE ANALYSIS UNDER NRC AND IMPERFECT CSI

In this section, we characterize the impacts of coexisting NRC and imperfect CSI on the performance of linearly precoded multi-user massive MIMO DL transmission. In this respect, we will derive analytical expressions for the received SINR and achievable rates for both ZF and MRT precoding.

A. Downlink Received Signal Model and SINR

We first express the linearly precoded DL transmit vector $\mathbf{x} \in \mathbb{C}^{N \times 1}$ as

$$\mathbf{x} = \beta \mathbf{U} \mathbf{s}, \quad (9)$$

where $\mathbf{U} = [\mathbf{u}_1, \dots, \mathbf{u}_{M_{tot}}] \in \mathbb{C}^{N \times M_{tot}}$ is the precoder matrix. The normalized multi-user data vector including one stream per UE antenna is denoted by $\mathbf{s} = [s_1, \dots, s_{M_{tot}}]^T \in \mathbb{C}^{M_{tot} \times 1}$, where $\mathbb{E}[\mathbf{s} \mathbf{s}^H] = \mathbf{I}_{M_{tot}}$. The transmit sum-power normalization is achieved through β which constrains the total BS transmit sum-power to 1, i.e., $\mathbb{E}[\mathbf{x}^H \mathbf{x}] = 1$. In order to satisfy this condition, β is chosen as [28]

$$\beta = \left(\sqrt{\mathbb{E}[\text{Tr}(\mathbf{U}^H \mathbf{U})]} \right)^{-1}. \quad (10)$$

Substituting (9) in (1), the received DL multi-user signal vector corresponding to all M_{tot} antennas in the UE side reads

$$\mathbf{r} = \beta \sqrt{\rho_d} \mathbf{H} \mathbf{U} \mathbf{s} + \mathbf{n}. \quad (11)$$

We express the effective DL channel matrix as $\mathbf{H} = [\mathbf{h}_1, \dots, \mathbf{h}_{M_{tot}}]^T$, where \mathbf{h}_m^T is the effective DL channel from the BS to the m -th antenna at the UE side. Then, based on (8) and (11), the received DL signal at the m -th UE antenna, which is assumed to belong to UE k , can be expressed as

$$\begin{aligned} r_m &= \sqrt{\rho_d} \beta \mathbf{h}_m^T \mathbf{u}_m s_m + \sqrt{\rho_d} \beta \sum_{i=1, i \neq m}^{M_{tot}} \mathbf{h}_m^T \mathbf{u}_i s_i + n_m \\ &= \sqrt{\rho_d} \beta \sum_{l \in \text{UE}_k} a_{ml} \left(\hat{\mathbf{h}}_l^T + \boldsymbol{\varepsilon}_l^T \right) \mathbf{C} \mathbf{u}_m s_m \\ &\quad + \sqrt{\rho_d} \beta \sum_{i=1, i \neq m}^{M_{tot}} \sum_{l \in \text{UE}_k} a_{ml} \left(\hat{\mathbf{h}}_l^T + \boldsymbol{\varepsilon}_l^T \right) \mathbf{C} \mathbf{u}_i s_i + n_m, \end{aligned} \quad (12)$$

where UE_k refers to the set of logical antenna indices belonging to UE k .

Similar to [7], [22]–[24], we assume that the UEs rely only on the statistical properties of the beamformed channel to decode the received DL signal, i.e., the k -th UE uses only $\beta \mathbb{E}[\mathbf{h}_m^T \mathbf{u}_m]$ as the DL complex gain in detecting s_m . Therefore, the received signal in (12) can be decomposed as

$$r_m = \underbrace{\sqrt{\rho_d} \beta \mathbb{E}[\mathbf{h}_m^T \mathbf{u}_m]}_{\text{useful signal}} s_m + z_m^{\text{SI}} + z_m^{\text{ISI}} + n_m, \quad (13)$$

where z_m^{SI} and z_m^{ISI} are the self-interference (SI) and inter-stream interference (ISI), respectively, which can be explicitly expressed as

$$\begin{aligned} z_m^{\text{SI}} &= \sqrt{\rho_d} \beta \sum_{l \in \text{UE}_k} a_{ml} \left(\hat{\mathbf{h}}_l^T + \boldsymbol{\varepsilon}_l^T \right) \mathbf{C} \mathbf{u}_m s_m \\ &\quad - \sqrt{\rho_d} \beta \mathbb{E}[\mathbf{h}_m^T \mathbf{u}_m] s_m \\ z_m^{\text{ISI}} &= \sqrt{\rho_d} \beta \sum_{i=1, i \neq m}^{M_{tot}} \sum_{l \in \text{UE}_k} a_{ml} \left(\hat{\mathbf{h}}_l^T + \boldsymbol{\varepsilon}_l^T \right) \mathbf{C} \mathbf{u}_i s_i. \end{aligned} \quad (14)$$

Note that, in this definition, the ISI consists of both inter-stream interference from other streams targeted to the same UE and of inter-user interference (IUI) due to the streams of other UEs.

Based on (13), the effective SINR at the m -th antenna in the UE side can be written as

$$\text{SINR}_m = \frac{\text{Var}(\sqrt{\rho_d} \beta \mathbb{E}[\mathbf{h}_m^T \mathbf{u}_m] s_m)}{\text{Var}(z_m^{\text{SI}}) + \text{Var}(z_m^{\text{ISI}}) + 1}, \quad (15)$$

where in defining (15) we used the fact that z_m^{SI} and z_m^{ISI} are uncorrelated.

In deriving capacity lower bounds, we follow the same approach as in [7], [31]. The total noise/interference term is uncorrelated with the useful signal whose entropy is upper-bounded with the entropy of Gaussian noise with equal variance [32]. Hence, a lower-bound on the achievable sum-capacity can be expressed as

$$R = \sum_{m=1}^{M_{tot}} \log_2(1 + \text{SINR}_m). \quad (16)$$

Next, we derive analytical expressions for the SINR and achievable sum-capacity R , given in (15) and (16), respectively, for two different linear precoding techniques, namely, ZF and MRT.

B. Zero-Forcing

For the ZF precoding scheme, the precoder matrix is constructed using the pseudo-inverse of the estimated effective DL channel matrix as [7]

$$\mathbf{U}^{\text{ZF}} = \hat{\mathbf{H}}^H \left(\hat{\mathbf{H}} \hat{\mathbf{H}}^H \right)^{-1}. \quad (17)$$

Next, based on (10), the normalization scalar β^{ZF} reads [7]

$$\beta^{\text{ZF}} = \left(\sqrt{\mathbb{E}[\text{Tr}(\left(\hat{\mathbf{H}} \hat{\mathbf{H}}^H \right)^{-1})]} \right)^{-1} = \sqrt{\frac{(N - M_{tot}) \tau_u \rho_u}{M_{tot} (\tau_u \rho_u + 1)}}, \quad (18)$$

and based on (13), the useful signal term for the detection at the m -th antenna at the UE side is

$$\sqrt{\rho_d} \beta^{\text{ZF}} \mathbb{E}[\mathbf{h}_m^T \mathbf{u}_m^{\text{ZF}}] s_m = \sqrt{\rho_d} \beta^{\text{ZF}} s_m. \quad (19)$$

TABLE I
ESSENTIAL SECOND-ORDER STATISTICS OF NRC VARIABLES

Variable	Definition
$\sigma_{a'_{mm}}^2$	Variance of the m -th diagonal element of UE side NRC matrix \mathbf{A}'
$\sigma_{a'_{od}}^2$	Average of variances of off-diagonal elements of UE side NRC matrix \mathbf{A}'
$\sigma_{c'_d}^2$	Average of variances of diagonal elements of BS NRC matrix \mathbf{C}'
$\delta_{c'_d}^2$	Average of cross-correlations of diagonal elements of BS NRC matrix \mathbf{C}'
$\sigma_{c'_{od}}^2$	Average of variances of off-diagonal elements of BS NRC matrix \mathbf{C}'

By substituting (19) into (14) and (15), the effective SINR at the m -th antenna in the UE side for ZF precoding can be written as

$$\text{SINR}_m^{\text{ZF}} = \frac{N - M_{\text{tot}}}{M_{\text{tot}}} \times \frac{\tau_u \rho_u \rho_d}{I_{\text{RC}}^{\text{ZF}} + I_{\text{NRC},m}^{\text{ZF}}}, \quad (20)$$

where $I_{\text{RC}}^{\text{ZF}} = \rho_d + \tau_u \rho_u + 1$ is the interference plus noise power under ideal reciprocal channel (no NRC), whereas $I_{\text{NRC},m}^{\text{ZF}}$ denotes the additional interference power due to NRC, which can be explicitly written as

$$\begin{aligned} I_{\text{NRC},m}^{\text{ZF}} \approx & \rho_d \left[\left(1 + \frac{N - M_{\text{tot}}}{M_{\text{tot}}} \tau_u \rho_u \right) \text{Tr}(\mathbf{R}_{\mathbf{a}'_m}) \right. \\ & + \frac{\tau_u \rho_u}{M_{\text{tot}}} \left(\text{Tr}(\mathbf{R}_{\mathbf{a}'_m}) - \sigma_{a'_{mm}}^2 \right) \\ & + \frac{\tau_u \rho_u}{NM_{\text{tot}}} (1 + \text{Tr}(\mathbf{R}_{\mathbf{a}'_m})) \text{Sum}(\mathbf{R}_{\mathbf{c}'_d}) \\ & + \left[\frac{\tau_u \rho_u + 1}{N} (1 + \text{Tr}(\mathbf{R}_{\mathbf{a}'_m})) \right. \\ & \left. \left. - \frac{\tau_u \rho_u}{NM_{\text{tot}}} \left(\text{Tr}(\mathbf{R}_{\mathbf{a}'_m}) - \sigma_{a'_{mm}}^2 \right) \right] \right. \\ & \left. \times \left(\text{Tr}(\mathbf{R}_{\mathbf{c}'_d}) + \text{Tr}(\mathbf{R}_{\mathbf{c}'_{od}}) \right) \right]. \end{aligned} \quad (21)$$

Proof: See Appendix A.

Note that based on (21), the only NRC characteristics that eventually affect the power of interference are $\sigma_{a'_{mm}}^2$ (denoting the variance of the m -th diagonal element in \mathbf{A}'), $\text{Tr}(\mathbf{R}_{\mathbf{a}'_m})$ (denoting the sum of variances of all the elements in the corresponding row of \mathbf{A}'_k), $\text{Tr}(\mathbf{R}_{\mathbf{c}'_{od}})$ (denoting the sum of variances of off-diagonal elements in \mathbf{C}'), $\text{Tr}(\mathbf{R}_{\mathbf{c}'_d})$ (denoting the sum of variances of diagonal elements in \mathbf{C}'), and $\text{Sum}(\mathbf{R}_{\mathbf{c}'_d})$ (denoting the sum of variances and cross-correlations of diagonal elements in \mathbf{C}'). Whereas, other statistical quantities, namely, the cross-correlations of diagonal and off-diagonal elements in \mathbf{A}' as well as cross-correlations of off-diagonal elements in \mathbf{C}' , do not affect the interference power. In general, different entries of the involved NRC covariance matrices (the \mathbf{R} matrices) can have different values. However, since only the sum of the diagonal values or the sum of all the values in the covariance matrices have impact on the interference power, we parameterize these essential NRC characteristics by their average values for notational simplicity. Thus, the essential NRC characteristics which affect the interference power are listed in TABLE I. Note that when these NRC characteristics are set to 0, then $I_{\text{NRC},m}^{\text{ZF}} = 0$, and

if further interpreted in the special case of single-antenna UEs, (20) reduces to the SINR expression given in [7] for the ideal reciprocal case.

C. Maximum Ratio Transmission

For the MRT case, the precoder matrix is constructed as [28]

$$\mathbf{U}^{\text{MRT}} = \hat{\mathbf{H}}^{\text{H}}. \quad (22)$$

Therefore, based on (10), the normalization scalar β^{MRT} reads [28]

$$\beta^{\text{MRT}} = \left(\sqrt{\mathbb{E}[\text{Tr}(\hat{\mathbf{H}}\hat{\mathbf{H}}^{\text{H}})]} \right)^{-1} = \sqrt{\frac{\tau_u \rho_u + 1}{NM_{\text{tot}} \tau_u \rho_u}}. \quad (23)$$

Based on (13), the useful signal term for the detection at the m -th antenna in the UE side is

$$\sqrt{\rho_d} \beta^{\text{MRT}} \mathbb{E}[\mathbf{h}_m^{\text{T}} \mathbf{u}_m^{\text{MRT}}] s_m = \sqrt{\rho_d} \beta^{\text{MRT}} \frac{N \tau_u \rho_u}{\tau_u \rho_u + 1} s_m. \quad (24)$$

Stemming from this, the effective SINR at the m -th antenna in the UE side, defined in (15) can now be expressed as

$$\text{SINR}_m^{\text{MRT}} = \frac{N}{M_{\text{tot}}} \times \frac{\tau_u \rho_u \rho_d}{I_{\text{RC}}^{\text{MRT}} + I_{\text{NRC},m}^{\text{MRT}}}, \quad (25)$$

where $I_{\text{RC}}^{\text{MRT}} = (\rho_d + 1)(\tau_u \rho_u + 1)$ is the interference and noise power under reciprocal channel, whereas $I_{\text{NRC},m}^{\text{MRT}}$ denotes the additional interference power due to NRC, and can be explicitly written as

$$\begin{aligned} I_{\text{NRC},m}^{\text{MRT}} = & \rho_d \left[\left(1 + \frac{N + M_{\text{tot}}}{M_{\text{tot}}} \tau_u \rho_u \right) \text{Tr}(\mathbf{R}_{\mathbf{a}'_m}) \right. \\ & - \frac{\tau_u \rho_u}{M_{\text{tot}}} \left(\text{Tr}(\mathbf{R}_{\mathbf{a}'_m}) - \sigma_{a'_{mm}}^2 \right) \\ & + \frac{\tau_u \rho_u}{NM_{\text{tot}}} (1 + \text{Tr}(\mathbf{R}_{\mathbf{a}'_m})) \text{Sum}(\mathbf{R}_{\mathbf{c}'_d}) \\ & + \left[\frac{\tau_u \rho_u + 1}{N} (1 + \text{Tr}(\mathbf{R}_{\mathbf{a}'_m})) \right. \\ & \left. \left. - \frac{\tau_u \rho_u}{NM_{\text{tot}}} \left(\text{Tr}(\mathbf{R}_{\mathbf{a}'_m}) - \sigma_{a'_{mm}}^2 \right) \right] \right. \\ & \left. \times \left(\text{Tr}(\mathbf{R}_{\mathbf{c}'_d}) + \text{Tr}(\mathbf{R}_{\mathbf{c}'_{od}}) \right) \right]. \end{aligned} \quad (26)$$

Proof: See Appendix B.

With the very same reasoning as in the ZF precoding scenario, the only NRC characteristics which affect the power of interference are the ones listed in TABLE I. Thus, when these NRC parameters are set to 0, then $I_{\text{NRC},m}^{\text{MRT}} = 0$ and in the single-antenna UE scenario, (25) reduces again to the SINR expression given in [7] for the ideal reciprocal case.

IV. ASYMPTOTIC AND NON-ASYMPTOTIC COMPARISONS AND IMPLICATIONS

In this section, we will address several important implications stemming from the derived closed-form SINR and achievable rate expressions. To this end, both the asymptotic and non-asymptotic performance behavior of ZF and MRT precoding based systems are first derived and compared. Then, the SINR degradation due to NRC is quantified and analyzed for both precoding techniques.

A. Asymptotic Performance for Large N

For growing N , the previously-derived SINR expressions for ZF and MRT based systems, under NRC, can be shown to be asymptotically identical and have the saturation value

$$\lim_{N \rightarrow \infty} \text{SINR}_m^{\text{ZF}} = \lim_{N \rightarrow \infty} \text{SINR}_m^{\text{MRT}} = \frac{1}{\text{Tr}(\mathbf{R}_{\mathbf{a}'_m}) + t_{c'_d}^m \delta_{c'_d}^2 + t_{c'_{od}}^m \sigma_{c'_{od}}^2}, \quad (27)$$

where

$$t_{c'_d}^m = 1 + \text{Tr}(\mathbf{R}_{\mathbf{a}'_m}), \quad (28)$$

$$t_{c'_{od}}^m = M_{\text{tot}} \frac{\tau_u \rho_u + 1}{\tau_u \rho_u} (1 + \text{Tr}(\mathbf{R}_{\mathbf{a}'_m})) - \text{Tr}(\mathbf{R}_{\mathbf{a}'_m}) + \sigma_{a'_{mm}}^2.$$

Note that the number of mismatched transceiver chains and antenna units increases with the number of antennas which in turn increases the level of interference power due to NRC. Thus, the system is subject to additional interference which cannot be suppressed by NRC-unaware spatial precoders, even if the number of antennas tends towards infinity. Therefore, for massive MIMO systems with practical non-reciprocal transceivers and antenna systems, the advantage of ZF over MRT in terms of IUI suppression, and hence in SINR performance, reduces and eventually vanishes with increasing number of antennas and transceiver chains. This is one important finding and will be illustrated also through numerical examples in Section V.

We next quantify the relative achievable rate performance under ZF and MRT precoding schemes with the ratio $R^{\text{ZF}}/R^{\text{MRT}}$, where R^{ZF} and R^{MRT} are obtained by substituting (20) and (25) into (16), respectively. The asymptotic behavior of this relative achievable rate performance for large number of antennas can be shown to read

$$\lim_{N \rightarrow \infty} \frac{R^{\text{ZF}}}{R^{\text{MRT}}} = \lim_{N \rightarrow \infty} \frac{\sum_{m=1}^{M_{\text{tot}}} \log_2(1 + \text{SINR}_m^{\text{ZF}})}{\sum_{m=1}^{M_{\text{tot}}} \log_2(1 + \text{SINR}_m^{\text{MRT}})} = 1. \quad (29)$$

Based on above, the asymptotic behavior of relative achievable rate under NRC is similar to the reciprocal case presented in [7]. However, the implications of these two results are largely different. More specifically, the combination of (27) and (29) establishes that the achievable rates for both precoders have an identical and finite saturation level in the presence of NRC. This saturation level can be expressed in closed-form by substituting the expression in (27) to (16). Importantly, even if the UL pilot SNR (ρ_u) tends towards infinity, reflecting perfect uplink CSI, the rates saturate to an identical finite level. On the other hand, for an ideal reciprocal channel, by substituting zeros for all the NRC parameters in the denominator of (27), the asymptotic result implies that the SINRs, and therefore the rates, grow without bound for both precoding schemes even under finite UL pilot SNR [7], [29]. Hence, there is a fundamental difference in the impacts of NRC and UL channel estimation errors. These differences will be illustrated through numerical examples in Section V and are other important findings of this article.

B. Non-Asymptotic Comparison of SINR Performance

We next pursue a non-asymptotic comparison of the achievable SINRs at the m -th antenna in the UE side between ZF and MRT precoding schemes under NRC. Building on the SINR expressions in (20) and (25), the following relation can be deduced

$$\frac{\text{SINR}_m^{\text{ZF}}}{\text{SINR}_m^{\text{MRT}}} = 1 + \frac{M_{\text{tot}}}{N} (\text{SINR}_m^{\text{ZF}} - 1) + \left(1 - \frac{M_{\text{tot}}}{N}\right) \times \frac{2\rho_d \tau_u \rho_u (\text{Tr}(\mathbf{R}_{\mathbf{a}'_m}) - (\text{Tr}(\mathbf{R}_{\mathbf{a}'_m}) - \sigma_{a'_{mm}}^2)/M_{\text{tot}})}{\rho_d + \tau_u \rho_u + 1 + I_{\text{NRC},m}^{\text{ZF}}}. \quad (30)$$

Based on above, since $N > M_{\text{tot}}$, ZF outperforms MRT in the achievable SINR, and consequently in the capacity lower bound, if $\text{SINR}_m^{\text{ZF}} \geq 1$. In the special case of $N \rightarrow \infty$, the ratio in (30) tends towards one, conforming with the previous asymptotic results.

In practical scenarios where the channel non-reciprocity level is not overly high, and considering the high SNR region with reasonably good UL channel estimation accuracy, the SINR is always greater than one for ZF precoding scheme. Therefore, in the high SNR region, (30) shows that ZF has better non-asymptotic performance compared to MRT. On the other hand, in the low SNR region, the performance of both systems are limited by noise and the difference becomes negligible.

C. SINR Degradation at High SNR

In order to quantify the SINR degradation under non-reciprocal channels with respect to ideal reciprocal channel reference case, we define the metric

$$\alpha = \frac{\text{SINR}_{\text{RC}} - \text{SINR}_{\text{NRC}}}{\text{SINR}_{\text{RC}}}. \quad (31)$$

In (31), SINR_{NRC} stands for the SINR with non-reciprocal channels calculated based on (15) and for which closed-form analytic expressions are given in (20) and (25) under ZF and MRT precoding schemes, respectively. Furthermore, SINR_{RC} denotes the SINR with reciprocal channels for which closed-form expressions can be obtained under ZF and MRT precoding schemes from [7] for the single-antenna UE scenario, or by setting the NRC parameters to 0 in (20) and (25), respectively, in a more general case. To compare the relative SINR degradation of ZF and MRT precoding schemes, we also define the ratio $\alpha^{\text{ZF/MRT}} = \frac{\alpha^{\text{ZF}}}{\alpha^{\text{MRT}}}$, where α^{ZF} and α^{MRT} are calculated using (31) with their corresponding SINR_{NRC} and SINR_{RC} expressions for ZF and MRT precoding schemes, respectively.

In the high SNR region, when $\rho_d \gg 1$, this ratio for the m -th antenna in the UE side can be shown to read

$$\lim_{\rho_d \rightarrow \infty} \frac{\alpha_m^{\text{ZF}}}{\alpha_m^{\text{MRT}}} \triangleq \alpha_{\infty,m}^{\text{ZF/MRT}} = \frac{I_0 + \tau_u \rho_u I_{\text{NRC},m}^{\text{ZF}}/\rho_d}{I_0 + 2\tau_u \rho_u (\text{Tr}(\mathbf{R}_{\mathbf{a}'_m}) - (\text{Tr}(\mathbf{R}_{\mathbf{a}'_m}) - \sigma_{a'_{mm}}^2)/M_{\text{tot}})}, \quad (32)$$

where

$$I_0 = \left(2\tau_u \rho_u \left(\text{Tr}(\mathbf{R}_{\mathbf{a}'_m}) - \left(\text{Tr}(\mathbf{R}_{\mathbf{a}'_m}) - \sigma_{a'_{mm}}^2 \right) / M_{tot} \right) + I_{\text{NRC},m}^{\text{ZF}} / \rho_d + 1 \right) I_{\text{NRC},m}^{\text{ZF}} / \rho_d. \quad (33)$$

From (32), it can be seen that $\alpha_{\infty,m}^{\text{ZF/MRT}} > 1$ when $I_{\text{NRC},m}^{\text{ZF}} / \rho_d > 2 \left(\text{Tr}(\mathbf{R}_{\mathbf{a}'_m}) - \left(\text{Tr}(\mathbf{R}_{\mathbf{a}'_m}) - \sigma_{a'_{mm}}^2 \right) / M_{tot} \right)$, implying that ZF precoding is more sensitive to channel non-reciprocity than MRT, that is, the SINR degradation due to NRC is higher for ZF than for MRT, at large SNR. This is intuitive as the ZF based interference suppression requires accurate channel knowledge. Note that based on (21), for practical setting of $\tau_u \geq M_{tot}$, this holds when

$$\rho_u > \frac{1}{N - M_{tot}}. \quad (34)$$

This is because when $N \gg M_{tot}$, the inequality given in (34) boils down to $\rho_u > 1/N$, which will be satisfied, in general, for all practical values of ρ_u .

V. NUMERICAL RESULTS, IMPLICATIONS AND DISCUSSION

In this section, we provide extensive numerical evaluations of the derived analytical SINR and achievable rate expressions for precoded multi-user massive MIMO system under NRC and imperfect CSI. We also study the behavior of the DL system spectral efficiency, defined as [7]

$$\eta_s = \left(1 - \frac{\tau_u}{T} \right) R = \left(1 - \frac{\tau_u}{T} \right) \sum_{m=1}^{M_{tot}} \log_2(1 + \text{SINR}_m), \quad (35)$$

where T refers to the channel coherence interval measured in number of symbols. Finally, we will discuss and summarize the novel findings of this work based on the derived analytical expressions and obtained numerical results.

A. Obtained Numerical Results

The baseline evaluation scenario consists of a BS which is equipped with $N = 100$ antenna elements and either single-antenna, dual-antenna or 4-antenna UEs, with a total of $M_{tot} = 20$ antennas, that are served simultaneously through either ZF or MRT precoding. We assume that the channel coherence time is 1ms, which corresponds to one radio sub-frame in 3GPP LTE/LTE-Advanced radio network [33] and specifically each coherence interval contains $T = 196$ symbols, while the number of UE antenna-specific UL pilots is always equal to the total number of the UE side antennas, i.e., $\tau_u = M_{tot}$. The UL SNR is set to $\rho_u = 0$ dB, while DL SNR is chosen to be $\rho_d = 20$ dB. These are the baseline simulation settings, while some of the parameter values are also varied in the evaluations.

In the simulations, NRC matrices \mathbf{A} and \mathbf{C} are generated based on \mathbf{A}' and \mathbf{C}' since $\mathbf{A} = \mathbf{I}_{M_{tot}} + \mathbf{A}'$ and $\mathbf{C} = \mathbf{I}_N + \mathbf{C}'$. As shown in Section III and TABLE I, only the averages of certain variance and cross-correlation values affect the performance, while in principle the individual values could all be different. However, for simulation simplicity, we assume that all the individual entries of the involved second-order statistics, i.e. those listed in TABLE I, are the same as their average

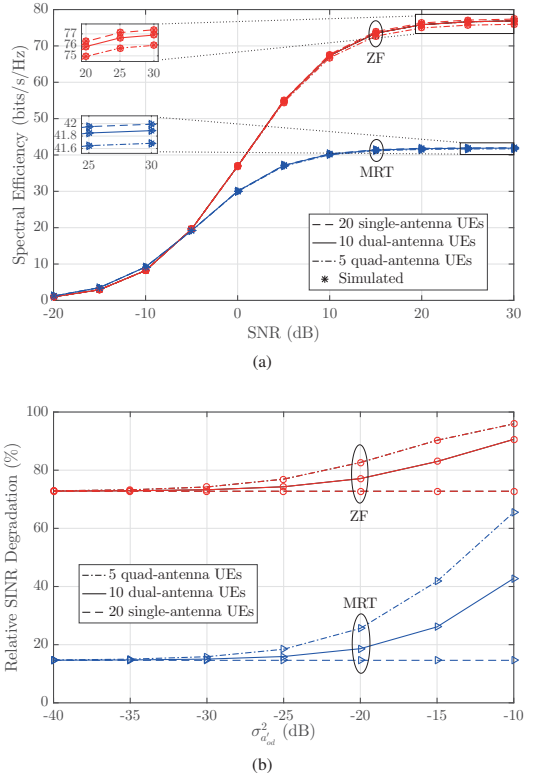


Fig. 2. (a) System spectral efficiency vs. DL SNR (ρ_d) with $\sigma_{a'_{od}}^2 = -30$ dB, and (b) relative SINR degradation (α) vs. $\sigma_{a'_{od}}^2$ with $\rho_d = 20$ dB, for $N = 100$, $M_{tot} = 20$, $\tau_u = M_{tot}$, $\rho_u = 0$ dB, $T = 196$, $\sigma_{a'_d}^2 = -20$ dB, $\sigma_{c'_d}^2 = -20$ dB, $\sigma_{c'_{od}}^2 = -30$ dB, and $\delta_{c'_d}^2 = -30$ dB.

values. We also assume that $\sigma_{a'_{mm}}^2$ is the same for all the values of m and is equal to $\sigma_{a'_d}^2$. Thus, for each realization, the block-diagonal matrix \mathbf{A}' is generated based on \mathbf{A}'_k in which the diagonal entries are generated as i.i.d. $\mathcal{CN}(0, \sigma_{a'_d}^2)$ whereas off-diagonal entries are i.i.d. $\mathcal{CN}(0, \sigma_{a'_{od}}^2)$. Similarly, the off-diagonal entries of \mathbf{C}' are generated as i.i.d. $\mathcal{CN}(0, \sigma_{c'_{od}}^2)$, while the diagonal entries have Gaussian distribution with zero mean and variance $\sigma_{c'_d}^2$ and cross-correlation $\delta_{c'_d}^2$. Kindly note that Gaussian distribution is chosen only as an example for the simulation and evaluation simplicity while the provided results apply to any distribution with the same variance and cross-correlation values. Also note that the independence assumption applies only to the entries whose cross-correlations do not have any impact on the system performance.

In Fig. 2(a), the system spectral efficiency is plotted against DL SNR for different number of antennas in each UE, while the total number of antennas in the UE side is fixed at $M_{tot} = 20$. In obtaining the curves, the derived analytical expressions in (20) and (25) are plugged into (35) for ZF and MRT precoding

schemes, respectively. In addition to that, simulated points are obtained via extensive empirical SINR and corresponding spectral efficiency evaluations, without any approximations, which are averaged over 1000 independent channel and NRC variable realizations. As can be seen, when the total number of antennas in the UE side is fixed, the spectral efficiency of the system is slightly higher in networks with lower number of antennas in each UE. This can be understood based on Fig. 2(b) where the relative SINR degradation is plotted against $\sigma_{a_{od}}^2$, which is an indicator of mutual coupling mismatch variance between the antenna elements of each individual UE (in dual- and quad-antenna UE cases). As illustrated, the number of antennas in each UE has essentially no impact on the performance when UE side mutual coupling mismatch level is small. Whereas, for higher values of $\sigma_{a_{od}}^2$, the relative SINR degradation is already clearly higher in the scenarios with higher number of antennas per UE and the difference gets larger as $\sigma_{a_{od}}^2$ increases. However, as shown in Fig. 2(a), even for relatively poorly NRC calibrated scenario (high practical NRC parameter values, e.g., $\sigma_{a_d}^2 = \sigma_{c_d}^2 = -20$ dB and $\sigma_{a_{od}}^2 = \sigma_{c_{od}}^2 = \delta_{c_d}^2 = -30$ dB), the difference between single-antenna and multi-antenna UE scenarios is very small. Therefore, in the continuation, we focus on single-antenna UE scenario which is commonly of highest interest in massive MIMO literature [3]–[8], [10], [18]–[22], [28], [31].

In Fig. 3 and Fig. 4, the spectral efficiency and relative SINR degradation curves are plotted against DL SNR for indicated NRC parameter settings. Simulated curves in Fig. 3 are similarly obtained via extensive empirical evaluations by averaging 1000 independent channel and NRC realizations. In general, as can be seen in Fig. 2 and Fig. 3, the analytical and simulated curves for both ZF and MRT have a perfect match evidencing the excellent accuracy of derived expressions despite the involved approximations. Thus, in the continuation we will use only the derived analytical expressions. As illustrated in Fig. 3 and Fig. 4, in low SNR region, the effect of channel non-reciprocity on both precoding schemes is negligible as the performance is limited by noise. On the other hand, in high SNR region, there is a substantial performance loss, especially for ZF precoding scheme. For instance, from Fig. 3 we can observe that for ZF at $\rho_d = 15$ dB, when the system is subject to relatively low-quality NRC calibration ($\sigma_{a_d}^2 = \sigma_{c_d}^2 = -20$ dB and $\sigma_{c_{od}}^2 = \delta_{c_d}^2 = -30$ dB), the system spectral efficiency has decreased by 27 bits/s/Hz compared to the fully reciprocal channel case. For the same settings, the degradation for MRT precoding scheme is only 3 bits/s/Hz showing that MRT is substantially less sensitive to channel non-reciprocity compared to ZF.

Based on the derived expressions in (21) and (26), the contributions of $\sigma_{c_{od}}^2$, $\sigma_{a_d}^2$, $\delta_{c_d}^2$, and $\sigma_{c_d}^2$ to the total received interference are proportional to $N \times \bar{M}_{tot}$, N , N , and M_{tot} , respectively. In typical settings with $N \gg \bar{M}_{tot}$ (which is also the case with $N = 100$ and $\bar{M}_{tot} = 20$), these cofactors satisfy the relation $N \times \bar{M}_{tot} > N > M_{tot}$, and hence the system has the highest sensitivity with respect to $\sigma_{c_{od}}^2$ and the lowest sensitivity with respect to $\sigma_{c_d}^2$. This is one of the important technical implications, relevant in practical large-array system

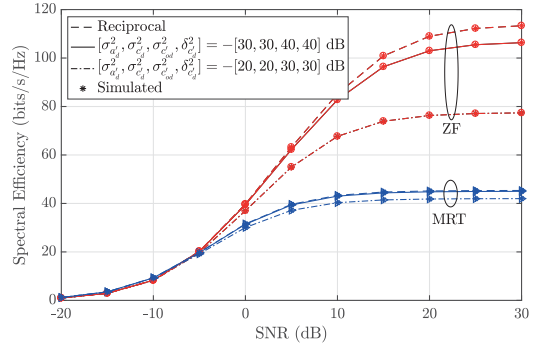


Fig. 3. System spectral efficiency vs. DL SNR (ρ_d) for $N = 100$, $M_{tot} = 20$, $K = 20$, $\tau_u = M_{tot}$, $\rho_u = 0$ dB, $T = 196$.

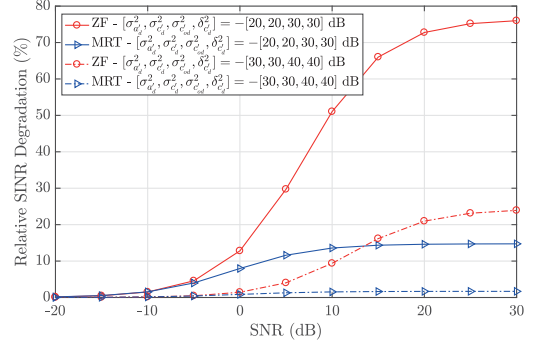


Fig. 4. Relative SINR degradation (α) vs. DL SNR (ρ_d) for $N = 100$, $M_{tot} = 20$, $K = 20$, $\tau_u = M_{tot}$, $\rho_u = 0$ dB, $T = 196$.

deployments and NRC calibration algorithm development, that are stemming from this work. In order to demonstrate this effect, in Fig. 5, the relative SINR degradation is plotted against different levels of each channel non-reciprocity parameter individually, i.e., when the level of one channel non-reciprocity parameter is varied, all other channel non-reciprocity parameter values are deliberately set to 0. Note that, in order to better demonstrate the impacts of $\delta_{c_d}^2$ on the SINR degradation, the effects of $\sigma_{c_d}^2$ and $\delta_{c_d}^2$ are grouped together, since the level of cross-correlation between elements in \mathbf{c}_d , $\delta_{c_d}^2$, is always upper-bounded by the corresponding variances of those elements, $\sigma_{c_d}^2$. The effects of both $\sigma_{c_d}^2$ and $\delta_{c_d}^2$ can be distinguished by the offset chosen between these two variables which ranges from $\delta_{c_d}^2 = \sigma_{c_d}^2$ to $\delta_{c_d}^2 = 0$. As expected, the obtained results show that both ZF and MRT precoding schemes are most sensitive to the variance of the off-diagonal elements of the BS non-reciprocity matrix. For instance, for the case with $\sigma_{c_{od}}^2 = -25$ dB, the SINR degradation is approximately 85% for ZF and 25% for MRT, which will be mapped to 42% and 13% of spectral efficiency degradation, respectively. The SINR degradation is, in turn, the least sensitive against the variance of the diagonal entries of BS side non-reciprocity matrix. It is seen that when $\delta_{c_d}^2 = 0$, ZF precoded system

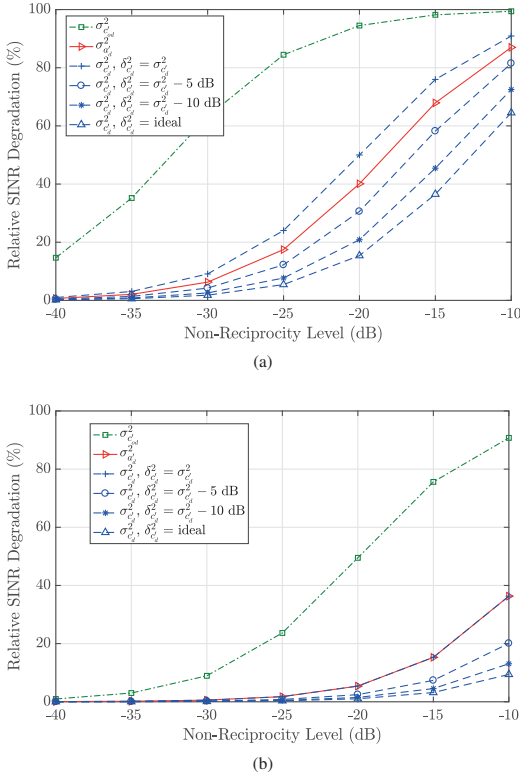


Fig. 5. Relative SINR degradation (α) in (a) ZF and (b) MRT precoded systems vs. the level of an individual non-reciprocity source (with others being zero, i.e., ideal) for $N = 100$, $M_{tot} = 20$, $K = 20$, $\rho_d = 20$, $\tau_u = M_{tot}$, $\rho_u = 0$ dB, $T = 196$.

starts to have observable performance loss, i.e., the SINR degradation is more than 10%, for values of $\sigma_{c_d}^2 > -23$ dB, whereas for MRT precoded system this threshold value is as high as $\sigma_{c_d}^2 > -10$ dB. The sensitivity with respect to the variance of diagonal elements in the UE side NRC matrix and the cross-correlations between diagonal elements in the BS side NRC matrix are also considerably high especially for ZF precoding. For instance, the SINR degradation increases from 17% to 40%, when $\sigma_{a_d}^2$ is increased from -25 dB to -20 dB, and from 24% to 50%, when $\delta_{c_d}^2$ and $\sigma_{c_d}^2$ are jointly increased from -25 dB to -20 dB.

The analytical expressions for the asymptotic achievable performance, derived in Section IV, indicated two new results and findings which differ from the ordinary reciprocal channel case; 1) there is a finite saturation level for both MRT and ZF precoding schemes, and 2) this saturation level is identical for both precoding techniques. In order to verify and demonstrate this behavior, the spectral efficiency is plotted against the number of BS antennas in Fig. 6. It can be clearly seen that both MRT and ZF spectral efficiency curves indeed saturate towards the levels predicted by the derived analytical expression in (27). As discussed earlier in Section IV-A, the system is

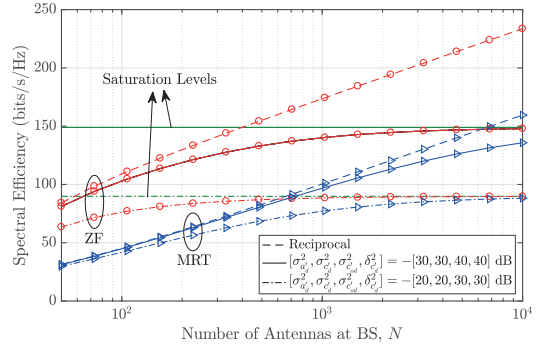


Fig. 6. System spectral efficiency vs. the number of antennas at BS (N) for $M_{tot} = 20$, $K = 20$, $\rho_d = 20$, $\tau_u = M_{tot}$, $\rho_u = 0$ dB, $T = 196$. Saturation levels based on (27) are plotted in green horizontal lines for the two indicated NRC parameter settings.

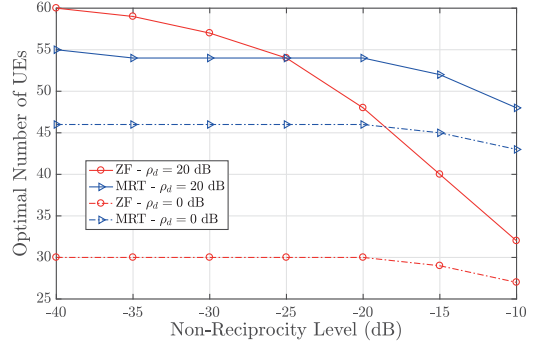


Fig. 7. Optimal number of single-antenna UEs to maximize system spectral efficiency vs. non-reciprocity level ($\sigma_{a_d}^2 = \sigma_{c_d}^2 = \text{NRC level}$, while $\delta_{c_d}^2 = \delta_{c_d}^2 = \text{NRC level} - 10$ dB) for $N = 100$, $M_{tot} = 20$, $K = 20$, $\tau_u = M_{tot}$, $\rho_u = 0$ dB, $T = 196$.

subject to increasing levels of SI and ISI with increasing number of antennas and corresponding mismatched transceiver chains. Since this interference cannot be suppressed by NRC-unaware spatial precoders, in contrast to the reciprocal case, the advantage of ZF over MRT in terms of inter-user interference suppression and higher achievable rates gradually vanishes. It is also important to note that these saturation levels are of large practical relevance since the NRC-induced saturation occurs already with antenna numbers in the order of 10^3 or even below, while the saturation levels caused, e.g., by pilot contamination often requires 10^5 antennas to be approached [34].

Fig. 7 shows the impact of channel non-reciprocity on the optimal number of simultaneously scheduled single-antenna UEs, K_{opt} , to achieve maximal spectral efficiency for two different values of DL SNR, namely, $\rho_d = 20$ dB, 0 dB. This optimum number is achieved by evaluating (16) for all the values of K in the range $N \geq K \geq 1$, and choosing the one which maximizes the spectral efficiency while the number of antennas in each UE is assumed to be one. The optimal number

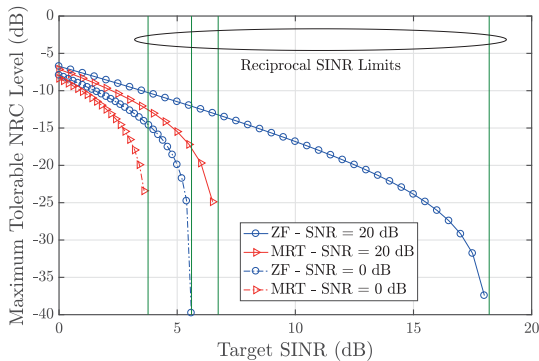


Fig. 8. Maximum tolerable non-reciprocity level vs. target SINR ($\sigma_{a_d}^2 = \sigma_{c_d}^2 = \text{NRC level}$, while $\sigma_{o_d}^2 = \delta_{c_d}^2 = \text{NRC level} - 10 \text{ dB}$) for $N = 100$, $M_{\text{tot}} = 20$, $K = 20$, $\tau_u = M_{\text{tot}}$, $\rho_u = 0 \text{ dB}$, $T = 196$.

of single-antenna UEs drops for both precoding techniques as the system is subject to increasing interference power with increasing non-reciprocity levels. In the low SNR regime (0 dB), this drop is not severe as the thermal noise has dominating impact on system performance. However, in the high SNR regime (20 dB), there is a significant drop in the optimal number of single-antenna UEs for ZF, even for moderate channel non-reciprocity levels, say $-30 \text{ dB} < \sigma_{a_d}^2 < -20 \text{ dB}$, whereas for MRT there is a drop only at fairly severe non-reciprocity levels, e.g., $\sigma_{a_d}^2 > -15 \text{ dB}$. An interesting and new observation is that, in contrast to high SNR regime behavior in the ordinary reciprocal case, the optimal number of UEs for MRT is higher than that of ZF under moderate channel non-reciprocity levels.

In Fig. 8, based on the derived closed-form expressions for SINR in (20) and (25), the maximum tolerable NRC level is evaluated as a function of target SINR in the UE side, for two example values of DL SNR, namely, $\rho_d = 20 \text{ dB}$, 0 dB. Based on the obtained results, in order to have SINR at UEs for example equal to 15 dB in ZF precoded system when $\rho_d = 20 \text{ dB}$, the maximum NRC level which can be tolerated is around -20 dB . This demonstrates the value and applicability of the provided analytical results in practical system design and deployments, in for example evaluating and extracting the required NRC calibration levels such that given DL transmission performance can be achieved.

B. Summary of New Findings and Future Work

In this subsection, we briefly summarize the novel scientific findings and concrete technical contributions of this work compared to the existing literature regarding the performance of massive MIMO systems with practical mismatched transceiver chains and antenna systems:

- 1) Based on (30), for the same channel non-reciprocity levels, ZF outperforms MRT in terms of the SINR and achievable rates. However, based on derived expressions in (32), the performance difference between the two precoding techniques starts to reduce as the level of channel non-reciprocity grows.

- 2) In previous literature, UE side non-reciprocity was assumed to have negligible effect on the total received interference [18]. However, this is only true when DL demodulation pilots are used to further enhance the detection at UEs. On the other hand, when UEs rely only on statistical channel properties, the UE side non-reciprocity has significant contribution to total received interference power. As can be inferred from derived expressions in (21) and (26), for both precoding techniques, this contribution scales with N which is a large number in the massive MIMO framework.
- 3) The received SINR and achievable rates of ZF and MRT precoded systems under NRC saturate at a finite and identical value asymptotically with increasing N . This is different from the reciprocal case where adding more antennas decreases the residual IUI and hence increases the spatial separation of UEs. This NRC-induced saturation phenomenon is due to the additional interference caused by adding more mismatched transceivers and antenna units with increasing N .
- 4) Optimal number of scheduled single-antenna UEs under MRT is higher than that with ZF when considering moderate channel non-reciprocity levels. This is in contrast to the ideal reciprocal case where the optimal number of scheduled users is always higher for ZF precoding scheme [7].

In general, in addition to the channel non-reciprocity problem, pilot contamination [10] and interference non-reciprocity [35] can easily be performance limiting factors, especially in multi-cell systems. Thus, joint consideration of these aspects together with NRC is an interesting research topic for our future work. Furthermore, extending the work to cover also more elaborate precoders in multi-antenna UE context, such as block-diagonalization, together with DL demodulation CSI acquisition, are interesting and important topics.

VI. CONCLUSION

Closed-form performance analysis of TDD-based linearly precoded massive MIMO DL system under channel non-reciprocity and imperfect CSI was carried out in this paper. The derived analytical SINR and achievable rate expressions show that in general ZF precoding scheme is more sensitive to NRC levels compared to MRT. The derived analytical expressions also show that with inaccurate NRC calibration, the performance gap between the two precoders decreases significantly. Moreover, in contrast to ideal reciprocal case, it was shown that the SINRs and achievable rates saturate to a finite and identical level with increasing antenna array size. Overall, the derived analytical expressions provide fundamentally useful and generic tools in dimensioning and designing practical massive MIMO systems with given performance targets, e.g., choosing the appropriate precoder based on performance-complexity trade-off, deciding the number of active antenna elements, and/or extracting the needed frequency and accuracy of adopted NRC calibration schemes.

APPENDIX

In order to calculate SINR in (15), we need to compute the powers of the different interference terms, namely, z_m^{SI} and z_m^{ISI} , under ZF and MRT precoding schemes. In the continuation, the following properties and approximations are used.

- *Property 1:*

$$\sum_{l=1}^N \sum_{p=1}^N \mathbb{E}[\epsilon_{ml} \epsilon_{mp}^*] = \sum_{l=1}^N \mathbb{E}[\epsilon_{ml} \epsilon_{ml}^*], \quad (36)$$

since $\mathbb{E}[\epsilon_{ml} \epsilon_{mp}^*] = 0$ for $l \neq p$.

- *Property 2:*

$$\sum_{l=1}^N \sum_{p=1}^N \mathbb{E}[u_{lm}^{\text{ZF}} u_{pm}^{\text{ZF}*}] = \sum_{l=1}^N \mathbb{E}[u_{lm}^{\text{ZF}} u_{lm}^{\text{ZF}*}], \quad (37)$$

since $\mathbb{E}[u_{lm}^{\text{ZF}} u_{pm}^{\text{ZF}*}] = 0$ for $l \neq p$.

- *Property 3:*

$$\sum_{l=1}^N \sum_{p=1}^N \mathbb{E}[\hat{h}_{ml} \hat{h}_{mp}^*] = \sum_{l=1}^N \mathbb{E}[\hat{h}_{ml} \hat{h}_{ml}^*], \quad (38)$$

since $\mathbb{E}[\hat{h}_{ml} \hat{h}_{mp}^*] = 0$ for $l \neq p$.

- *Approximation 1:* For mathematical tractability, we employ the following approximation [20]

$$u_{li}^{\text{ZF}} \approx \frac{\hat{h}_{li}}{v^{\text{ZF}}}, \quad (39)$$

where v^{ZF} is a constant that is chosen to satisfy $\mathbb{E}[|u_{li}^{\text{ZF}}|^2] = \frac{1}{N M_{\text{tot}}} \mathbb{E}[\text{Tr}(\mathbf{U}^{\text{ZFH}} \mathbf{U}^{\text{ZF}})]$, and hence can be expressed as

$$v^{\text{ZF}} = \sqrt{N(N - M_{\text{tot}})} \frac{\tau_u \rho_u}{\tau_u \rho_u + 1}. \quad (40)$$

While allowing us to derive the analytical closed-form expressions, the high accuracy of this approximation is demonstrated by the excellent match of the analytical and empirical results in Section V.

A. Interference Powers under ZF Precoding

Based on (14), (17), and (19), the power of the self interference can be expressed as

$$\begin{aligned} \text{Var}(z_m^{\text{SI,ZF}}) &= \mathbb{E} \left[\left| \sqrt{\rho_d} \beta^{\text{ZF}} \sum_{l \in \text{UE}_k} a_{ml} (\hat{\mathbf{h}}_l^{\text{T}} + \boldsymbol{\varepsilon}_l^{\text{T}}) \mathbf{C} \mathbf{u}_m^{\text{ZF}} s_m \right. \right. \\ &\quad \left. \left. - \sqrt{\rho_d} \beta^{\text{ZF}} s_m \right|^2 \right] \end{aligned} \quad (41)$$

$$\begin{aligned} &= \rho_d (\beta^{\text{ZF}})^2 \mathbb{E} \left[\underbrace{\left| a'_{mm} s_m + \sum_{\substack{l \in \text{UE}_k \\ l \neq m}} a_{ml} \hat{\mathbf{h}}_l^{\text{T}} \mathbf{u}_m^{\text{ZF}} s_m \right|^2}_{t_1^{\text{SI,ZF}}} \right] \\ &\quad + \rho_d (\beta^{\text{ZF}})^2 \mathbb{E} \left[\underbrace{\left| \sum_{l \in \text{UE}_k} a_{ml} \hat{\mathbf{h}}_l^{\text{T}} \mathbf{C}' \mathbf{u}_m^{\text{ZF}} s_m \right|^2}_{t_2^{\text{SI,ZF}}} \right] \\ &\quad + \rho_d (\beta^{\text{ZF}})^2 \mathbb{E} \left[\underbrace{\left| \sum_{l \in \text{UE}_k} a_{ml} \boldsymbol{\varepsilon}_l^{\text{T}} \mathbf{C} \mathbf{u}_m^{\text{ZF}} s_m \right|^2}_{t_3^{\text{SI,ZF}}} \right]. \end{aligned}$$

Next we will derive analytical expressions for the terms $t_1^{\text{SI,ZF}}$, $t_2^{\text{SI,ZF}}$, and $t_3^{\text{SI,ZF}}$. Starting with $t_1^{\text{SI,ZF}}$, we obtain

$$\begin{aligned} t_1^{\text{SI,ZF}} &= \mathbb{E} \left[\left(a'_{mm} s_m + \sum_{\substack{l \in \text{UE}_k \\ l \neq m}} a_{ml} \hat{h}_{lp} u_{pm}^{\text{ZF}} s_m \right) \right. \\ &\quad \times \left. \left(a'_{mm} s_m + \sum_{\substack{q \in \text{UE}_k \\ q \neq m}} \sum_{r=1}^N a_{mq} \hat{h}_{qr} u_{rm}^{\text{ZF}} s_m \right)^* \right] \\ &\approx \mathbb{E}[|a'_{mm}|^2] \\ &\quad + \frac{1}{(v^{\text{ZF}})^2} \sum_{\substack{l \in \text{UE}_k \\ l \neq m}} \sum_{p=1}^N \mathbb{E}[|a_{ml}|^2] \mathbb{E}[\hat{h}_{lp}^2] \mathbb{E}[\hat{h}_{mp}^2] \\ &= \sigma_{a'_{mm}}^2 + \frac{1}{N - M_{\text{tot}}} \left(\text{Tr}(\mathbf{R}_{\mathbf{a}'_m}) - \sigma_{a'_{mm}}^2 \right). \end{aligned} \quad (42)$$

In obtaining the expression on the third and the fourth lines, we used Approximation 1 and Property 3.

Following that, $t_2^{\text{SI,ZF}}$ can be expressed as

$$\begin{aligned} t_2^{\text{SI,ZF}} &\approx \frac{1}{(v^{\text{ZF}})^2} \sum_{l \in \text{UE}_k} \sum_{q \in \text{UE}_k} \sum_{p=1}^N \sum_{r=1}^N \sum_{i=1}^N \sum_{j=1}^N \mathbb{E}[a_{ml} a_{mq}^*] \\ &\quad \times \mathbb{E}[\hat{h}_{lp} \hat{h}_{mr}^* \hat{h}_{qi}^* \hat{h}_{mj}] \mathbb{E}[c'_{pr} c'_{ij}^*] \\ &= \frac{1}{(v^{\text{ZF}})^2} \underbrace{\sum_{p=1}^N \sum_{r=1}^N \sum_{i=1}^N \sum_{j=1}^N \mathbb{E}[|a_{mm}|^2]}_{t_{21}^{\text{SI,ZF}}} \\ &\quad \times \mathbb{E}[\hat{h}_{mp} \hat{h}_{mi}^* \hat{h}_{mr}^* \hat{h}_{mj}] \mathbb{E}[c'_{pr} c'_{ij}^*] \\ &\quad + \frac{1}{(v^{\text{ZF}})^2} \sum_{\substack{l \in \text{UE}_k \\ l \neq m}} \sum_{p=1}^N \sum_{r=1}^N \mathbb{E}[|a_{ml}|^2] \\ &\quad \times \mathbb{E}[\hat{h}_{lp}^2] \mathbb{E}[\hat{h}_{mr}^2] \mathbb{E}[c'_{pr}^2] \end{aligned} \quad (43)$$

$$= \frac{1}{(v^{ZF})^2} \left(t_{21}^{SI,ZF} + \left(\text{Tr}(\mathbf{R}_{\mathbf{a}'_m}) - \sigma_{a'_{mm}}^2 \right) \right. \\ \left. \times \left(\frac{\tau_u \rho_u}{\tau_u \rho_u + 1} \right)^2 \left(\text{Tr}(\mathbf{R}_{\mathbf{c}'_d}) + \text{Tr}(\mathbf{R}_{\mathbf{c}'_{od}}) \right) \right).$$

In above, we used Approximation 1 when obtaining the expression on the first two lines, whereas the expression on the third to the sixth lines are obtained using Property 3. In the next step, $t_{21}^{SI,ZF}$ is expressed as

$$t_{21}^{SI,ZF} = \mathbb{E} \left[|a_{mm}|^2 \sum_{p=1}^N \sum_{\substack{r=1 \\ r \neq p}}^N \mathbb{E} \left[|\hat{h}_{mp}|^2 \right] \mathbb{E} \left[|\hat{h}_{mr}|^2 \right] \mathbb{E} \left[|c'_{pr}|^2 \right] \right. \\ + \mathbb{E} \left[|a_{mm}|^2 \sum_{p=1}^N \sum_{\substack{j=1 \\ j \neq p}}^N \mathbb{E} \left[|\hat{h}_{mp}|^2 \right] \mathbb{E} \left[|\hat{h}_{mj}|^2 \right] \mathbb{E} \left[|c'_{pp} c'_{jj}^* \right] \right. \\ + \mathbb{E} \left[|a_{mm}|^2 \sum_{p=1}^N \mathbb{E} \left[|\hat{h}_{mp}|^4 \right] \mathbb{E} \left[|c'_{pp}|^2 \right] \right. \\ = \left(1 + \sigma_{a'_{mm}}^2 \right) \left(\frac{\tau_u \rho_u}{\tau_u \rho_u + 1} \right)^2 \\ \times \left(\text{Tr}(\mathbf{R}_{\mathbf{c}'_{od}}) + \text{Sum}(\mathbf{R}_{\mathbf{c}'_d}) + \text{Tr}(\mathbf{R}_{\mathbf{c}'_d}) \right), \quad (44)$$

where Property 3 is used in obtaining the expression in the first three lines.

Substituting (44) in (43), we have

$$t_2^{SI,ZF} \approx \frac{1}{N(N - M_{tot})} \left(\left(1 + \sigma_{a'_{mm}}^2 \right) \text{Sum}(\mathbf{R}_{\mathbf{c}'_d}) \right. \\ \left. + \left(1 + \text{Tr}(\mathbf{R}_{\mathbf{a}'_m}) \right) \left(\text{Tr}(\mathbf{R}_{\mathbf{c}'_d}) + \text{Tr}(\mathbf{R}_{\mathbf{c}'_{od}}) \right) \right). \quad (45)$$

Finally, the term $t_3^{SI,ZF}$ can be expressed as

$$t_3^{SI,ZF} = \sum_{l \in \text{UE}_k} \sum_{p=1}^N \sum_{r=1}^N \mathbb{E} \left[|a_{ml}|^2 \right] \\ \times \mathbb{E} \left[|\epsilon_{lp}|^2 \right] \mathbb{E} \left[|c_{pr}|^2 \right] \mathbb{E} \left[|u_{rm}^{ZF}|^2 \right] \\ = \frac{1 + \text{Tr}(\mathbf{R}_{\mathbf{a}'_m})}{N M_{tot} (\beta^{ZF})^2 (\tau_u \rho_u + 1)} \\ \times \left(N + \text{Tr}(\mathbf{R}_{\mathbf{c}'_d}) + \text{Tr}(\mathbf{R}_{\mathbf{c}'_{od}}) \right). \quad (46)$$

In obtaining the expression on the first two lines, we used Property 1 and Property 2.

Similarly, based on (14), the power of the ISI under ZF precoding scheme can be written as

$$\text{Var}(z_m^{ISI,ZF}) \\ = \mathbb{E} \left[\left| \sqrt{\rho_d} \beta^{ZF} \sum_{\substack{i=1 \\ i \neq m}}^{M_{tot}} \sum_{l \in \text{UE}_k} a_{ml} \left(\hat{\mathbf{h}}_l^T + \boldsymbol{\varepsilon}_l^T \right) \mathbf{C} \mathbf{u}_i^{ZF} s_i \right|^2 \right] \quad (47)$$

$$= \rho_d (\beta^{ZF})^2 \mathbb{E} \left[\left| \sum_{\substack{i \in \text{UE}_k \\ i \neq m}} a_{mi} s_i \right|^2 \right] \\ + \rho_d (\beta^{ZF})^2 \mathbb{E} \left[\left| \sum_{\substack{i=1 \\ i \neq m}}^{M_{tot}} \sum_{l \in \text{UE}_k} a_{ml} \hat{\mathbf{h}}_l^T \mathbf{C}' \mathbf{u}_i^{ZF} s_i \right|^2 \right] \\ + \rho_d (\beta^{ZF})^2 \mathbb{E} \left[\left| \sum_{\substack{i=1 \\ i \neq m}}^{M_{tot}} \sum_{l \in \text{UE}_k} a_{ml} \boldsymbol{\varepsilon}_l^T \mathbf{C} \mathbf{u}_i^{ZF} s_i \right|^2 \right].$$

Next, we will derive analytical expressions for the terms $t_1^{ISI,ZF}$, $t_2^{ISI,ZF}$ and $t_3^{ISI,ZF}$. Starting with $t_1^{ISI,ZF}$, we obtain

$$t_1^{ISI,ZF} = \sum_{\substack{i \in \text{UE}_k \\ i \neq m}} \mathbb{E} \left[|a_{mi}|^2 \right] \mathbb{E} \left[|s_i|^2 \right] = \text{Tr}(\mathbf{R}_{\mathbf{a}'_m}) - \sigma_{a'_{mm}}^2. \quad (48)$$

Following that, $t_2^{ISI,ZF}$ can be expressed as

$$t_2^{ISI,ZF} \approx \frac{1}{(v^{ZF})^2} \sum_{\substack{i=1 \\ i \neq m}}^{M_{tot}} \sum_{l \in \text{UE}_k} \sum_{p=1}^N \sum_{r=1}^N \sum_{o=1}^N \sum_{w=1}^N \mathbb{E} \left[|a_{ml}|^2 \right] \\ \times \mathbb{E} \left[\hat{h}_{lp} \hat{h}_{ir}^* \hat{h}_{lo}^* \hat{h}_{iw} \right] \mathbb{E} \left[|c'_{pr} c'_{ow}^*| \right] \\ = \frac{1}{(v^{ZF})^2} \sum_{\substack{i \in \text{UE}_k \\ i \neq m}} \mathbb{E} \left[|a_{mi}|^2 \right] \frac{t_{21}^{SI,ZF}}{\mathbb{E} \left[|a_{mm}|^2 \right]} \\ + \frac{1}{(v^{ZF})^2} \left(\sum_{\substack{i=1 \\ i \notin \text{UE}_k}}^{M_{tot}} \left(1 + \text{Tr}(\mathbf{R}_{\mathbf{a}'_m}) \right) \right. \\ \left. + \sum_{\substack{i \in \text{UE}_k \\ i \neq m}} \left(1 + \text{Tr}(\mathbf{R}_{\mathbf{a}'_m}) - \sigma_{a'_{mi}}^2 \right) \right) \\ \times \left(\frac{\tau_u \rho_u}{\tau_u \rho_u + 1} \right)^2 \left(\text{Tr}(\mathbf{R}_{\mathbf{c}'_d}) + \text{Tr}(\mathbf{R}_{\mathbf{c}'_{od}}) \right) \\ = \frac{1}{N(N - M_{tot})} \left(\left(\left(1 + \sigma_{a'_{mm}}^2 \right) + (M_{tot} - 2) \right) \right. \\ \times \left(1 + \text{Tr}(\mathbf{R}_{\mathbf{a}'_m}) \right) \left(\text{Tr}(\mathbf{R}_{\mathbf{c}'_d}) + \text{Tr}(\mathbf{R}_{\mathbf{c}'_{od}}) \right) \\ \left. + \left(\text{Tr}(\mathbf{R}_{\mathbf{a}'_m}) - \sigma_{a'_{mm}}^2 \right) \text{Sum}(\mathbf{R}_{\mathbf{c}'_d}) \right). \quad (49)$$

In above, we used the Approximation 1 in obtaining the expression on the first two lines and Property 3 in obtaining the expressions on the first six lines.

Then, $t_3^{ISI,ZF}$ can be expressed, similar to $t_3^{SI,ZF}$, as

$$t_3^{ISI,ZF} = (M_{tot} - 1) \frac{1 + \text{Tr}(\mathbf{R}_{\mathbf{a}'_m})}{N M_{tot} (\beta^{ZF})^2 (\tau_u \rho_u + 1)} \\ \times \left(N + \text{Tr}(\mathbf{R}_{\mathbf{c}'_d}) + \text{Tr}(\mathbf{R}_{\mathbf{c}'_{od}}) \right). \quad (50)$$

Here, we used Property 1 and Property 2.

The total interference power can be obtained by summing all the calculated interference terms. Then, it is straightforward to re-arrange the terms and express the total interference power as $I_{RC}^{ZF} + I_{NRC,m}^{ZF}$ after which we reach the SINR expression presented in (20).

B. Interference Powers under MRT Precoding

Based on (14), (22), and (24), the power of self interference under MRT precoding scheme can be expressed as

$$\begin{aligned} \text{Var}(z_m^{\text{SI,MRT}}) &= \mathbb{E} \left[\left| \sqrt{\rho_d} \beta^{\text{MRT}} \sum_{l \in \text{UE}_k} a_{ml} (\hat{\mathbf{h}}_l^T + \varepsilon_l^T) \mathbf{C} \mathbf{u}_m^{\text{MRT}} s_m \right|^2 \right] \\ &= \rho_d (\beta^{\text{MRT}})^2 \mathbb{E} \left[\left| a_{mm} \hat{\mathbf{h}}_m^T \hat{\mathbf{h}}_m^* s_m - \mathbb{E} [\hat{\mathbf{h}}_m^T \hat{\mathbf{h}}_m^*] s_m \right. \right. \\ &\quad \left. \left. + \sum_{\substack{l \in \text{UE}_k \\ l \neq m}} a_{ml} \hat{\mathbf{h}}_l^T \hat{\mathbf{h}}_m^* s_m \right|^2 \right] \\ &\quad \dots \underbrace{\dots}_{t_1^{\text{SI,MRT}}} \\ &\quad + \rho_d (\beta^{\text{MRT}})^2 \mathbb{E} \left[\left| \sum_{l \in \text{UE}_k} a_{ml} \hat{\mathbf{h}}_l^T \mathbf{C}' \hat{\mathbf{h}}_m^* s_m \right|^2 \right] \\ &\quad \underbrace{\dots}_{t_2^{\text{SI,MRT}}} \\ &\quad + \rho_d (\beta^{\text{MRT}})^2 \mathbb{E} \left[\left| \sum_{l \in \text{UE}_k} a_{ml} \varepsilon_l^T \mathbf{C} \hat{\mathbf{h}}_m^* s_m \right|^2 \right] \\ &\quad \underbrace{\dots}_{t_3^{\text{SI,MRT}}} \end{aligned} \quad (51)$$

Next we derive analytical expressions for the terms $t_1^{\text{SI,MRT}}$, $t_2^{\text{SI,MRT}}$ and $t_3^{\text{SI,MRT}}$. Starting with $t_1^{\text{SI,MRT}}$, we get

$$\begin{aligned} t_1^{\text{SI,MRT}} &= \mathbb{E} \left[\left| a_{mm} \hat{\mathbf{h}}_m^T \hat{\mathbf{h}}_m^* s_m - \mathbb{E} [\hat{\mathbf{h}}_m^T \hat{\mathbf{h}}_m^*] s_m \right|^2 \right] \\ &\quad \underbrace{\dots}_{t_{11}^{\text{SI,MRT}}} \\ &\quad + \mathbb{E} \left[\left| \sum_{\substack{l \in \text{UE}_k \\ l \neq m}} a_{ml} \hat{\mathbf{h}}_l^T \hat{\mathbf{h}}_m^* s_m \right|^2 \right] \\ &\quad \underbrace{\dots}_{t_{12}^{\text{SI,MRT}}} \end{aligned} \quad (52)$$

Following that, $t_{11}^{\text{SI,MRT}}$ can be expressed as

$$\begin{aligned} t_{11}^{\text{SI,MRT}} &= \mathbb{E} \left[\left| a_{mm} \hat{\mathbf{h}}_m^T \hat{\mathbf{h}}_m^* s_m \right|^2 \right] - \mathbb{E} \left[\left| \mathbb{E} [\hat{\mathbf{h}}_m^T \hat{\mathbf{h}}_m^*] s_m \right|^2 \right] \\ &= \mathbb{E} [a_{mm}^2] \left(\sum_{p=1}^N \sum_{\substack{r=1 \\ r \neq p}}^N \mathbb{E} [\hat{h}_{mp}^2] \mathbb{E} [\hat{h}_{mr}^2] \right) \\ &\quad + \sum_{p=1}^N \mathbb{E} [\hat{h}_{mp}^4] - N^2 \left(\frac{\tau_u \rho_u}{\tau_u \rho_u + 1} \right)^2 \end{aligned} \quad (53)$$

$$= N \left(1 + \sigma_{a'_{mm}}^2 (N+1) \right) \left(\frac{\tau_u \rho_u}{\tau_u \rho_u + 1} \right)^2.$$

Next we express $t_{12}^{\text{SI,MRT}}$ as

$$\begin{aligned} t_{12}^{\text{SI,MRT}} &= \sum_{\substack{l \in \text{UE}_k \\ l \neq m}} \sum_{p=1}^N \mathbb{E} [a_{ml}^2] \mathbb{E} [\hat{h}_{lp}^2] \mathbb{E} [\hat{h}_{mp}^2] \\ &= N \left(\text{Tr}(\mathbf{R}_{\mathbf{a}'_m}) - \sigma_{a'_{mm}}^2 \right) \left(\frac{\tau_u \rho_u}{\tau_u \rho_u + 1} \right)^2, \end{aligned} \quad (54)$$

where Property 3 is used in obtaining the expression on the first line.

Substituting (53) and (54) in (52), we have

$$t_1^{\text{SI,MRT}} = N \left(1 + N \sigma_{a'_{mm}}^2 + \text{Tr}(\mathbf{R}_{\mathbf{a}'_m}) \right) \left(\frac{\tau_u \rho_u}{\tau_u \rho_u + 1} \right)^2. \quad (55)$$

Then, we can express $t_2^{\text{SI,MRT}}$, similar to $t_2^{\text{SI,ZF}}$, as

$$\begin{aligned} t_2^{\text{SI,MRT}} &= \left(\frac{\tau_u \rho_u}{\tau_u \rho_u + 1} \right)^2 \left((1 + \sigma_{a'_{mm}}^2) \text{Sum}(\mathbf{R}_{\mathbf{c}'_d}) \right. \\ &\quad \left. + (1 + \text{Tr}(\mathbf{R}_{\mathbf{a}'_m})) (\text{Tr}(\mathbf{R}_{\mathbf{c}'_d}) + \text{Tr}(\mathbf{R}_{\mathbf{c}'_{od}})) \right). \end{aligned} \quad (56)$$

In obtaining the final expression, we used Property 3.

Following that, $t_3^{\text{SI,MRT}}$ can be expressed, similar to $t_3^{\text{SI,ZF}}$, as

$$\begin{aligned} t_3^{\text{SI,MRT}} &= \frac{\tau_u \rho_u}{(\tau_u \rho_u + 1)^2} (1 + \text{Tr}(\mathbf{R}_{\mathbf{a}'_m})) \\ &\quad \times (N + \text{Tr}(\mathbf{R}_{\mathbf{c}'_d}) + \text{Tr}(\mathbf{R}_{\mathbf{c}'_{od}})). \end{aligned} \quad (57)$$

In obtaining the final expression, we used Property 1 and Property 3.

Then, based on (14), the power of ISI under MRT precoding scheme can be written as

$$\begin{aligned} \text{Var}(z_m^{\text{ISI,MRT}}) &= \mathbb{E} \left[\left| \sqrt{\rho_d} \beta^{\text{MRT}} \sum_{\substack{i=1 \\ i \neq m}}^{M_{\text{tot}}} \sum_{l \in \text{UE}_k} a_{ml} (\hat{\mathbf{h}}_l^T + \varepsilon_l^T) \mathbf{C} \mathbf{u}_i^{\text{MRT}} s_i \right|^2 \right] \\ &= \rho_d (\beta^{\text{MRT}})^2 \left(\mathbb{E} \left[\left| \sum_{\substack{i=1 \\ i \neq m}}^{M_{\text{tot}}} \sum_{l \in \text{UE}_k} a_{ml} \hat{\mathbf{h}}_l^T \mathbf{C} \hat{\mathbf{h}}_i^* s_i \right|^2 \right] \right. \\ &\quad \underbrace{\dots}_{t_1^{\text{ISI,MRT}}} \\ &\quad \left. + \mathbb{E} \left[\left| \sum_{\substack{i=1 \\ i \neq m}}^{M_{\text{tot}}} \sum_{l \in \text{UE}_k} a_{ml} \varepsilon_l^T \mathbf{C} \hat{\mathbf{h}}_i^* s_i \right|^2 \right] \right. \\ &\quad \underbrace{\dots}_{t_2^{\text{ISI,MRT}}} \left. \right). \end{aligned} \quad (58)$$

Next, we will derive analytical expressions for the terms $t_1^{\text{ISI,MRT}}$ and $t_2^{\text{ISI,MRT}}$. Starting with $t_1^{\text{ISI,MRT}}$, similar to

$t_2^{\text{ISI,ZF}}$, we get

$$t_1^{\text{ISI,MRT}} = \left(\frac{\tau_u \rho_u}{\tau_u \rho_u + 1} \right)^2 \left((M_{\text{tot}} - 2) (1 + \text{Tr}(\mathbf{R}_{\mathbf{a}'_m})) + (1 + \sigma_{a'_{mm}}^2) \left(N + \text{Tr}(\mathbf{R}_{\mathbf{c}'_d}) + \text{Tr}(\mathbf{R}_{\mathbf{c}'_{od}}) \right) + \left(\text{Tr}(\mathbf{R}_{\mathbf{a}'_m}) - \sigma_{a'_{mm}}^2 \right) \left(N^2 + \text{Sum}(\mathbf{R}_{\mathbf{c}'_d}) \right) \right). \quad (59)$$

In obtaining the final expression, we used Property 3.

Following that, $t_2^{\text{ISI,MRT}}$ can be expressed, similar to $t_3^{\text{ISI,ZF}}$, as

$$t_2^{\text{ISI,MRT}} = (M_{\text{tot}} - 1) \frac{\tau_u \rho_u}{(\tau_u \rho_u + 1)^2} (1 + \text{Tr}(\mathbf{R}_{\mathbf{a}'_m})) \times \left(N + \text{Tr}(\mathbf{R}_{\mathbf{c}'_d}) + \text{Tr}(\mathbf{R}_{\mathbf{c}'_{od}}) \right). \quad (60)$$

In obtaining the final expression, we used Property 1 and Property 3.

Finally, the total interference power is obtained by summing all the calculated interference terms. Then, it is straightforward to re-arrange the terms and express the total interference power as $I_{\text{RC}}^{\text{MRT}} + I_{\text{NRC},m}^{\text{MRT}}$ after which we reach the SINR expression presented in (25).

REFERENCES

- [1] J. G. Andrews, S. Buzzi, W. Choi, S. V. Hanly, A. Lozano, A. C. K. Soong, and J. C. Zhang, "What will 5G be?" *IEEE Journal on Selected Areas in Communications*, vol. 32, no. 6, pp. 1065–1082, June 2014.
- [2] F. Boccardi, R. Heath, A. Lozano, T. L. Marzetta, and P. Popovski, "Five disruptive technology directions for 5G," *IEEE Communications Magazine*, vol. 52, no. 2, pp. 74–80, February 2014.
- [3] J. Hoydis, S. ten Brink, and M. Debbah, "Massive MIMO in the UL/DL of cellular networks: how many antennas do we need?" *IEEE Journal on Selected Areas in Communications*, vol. 31, no. 2, pp. 160–171, February 2013.
- [4] L. Lu, G. Y. Li, A. L. Swindlehurst, A. Ashikhmin, and R. Zhang, "An overview of massive MIMO: benefits and challenges," *IEEE Journal of Selected Topics in Signal Processing*, vol. 8, no. 5, pp. 742–758, Oct 2014.
- [5] T. L. Marzetta, "Noncooperative cellular wireless with unlimited numbers of base station antennas," *IEEE Transactions on Wireless Communications*, vol. 9, no. 11, pp. 3590–3600, November 2010.
- [6] H. Q. Ngo, E. G. Larsson, and T. L. Marzetta, "Energy and spectral efficiency of very large multiuser MIMO systems," *IEEE Transactions on Communications*, vol. 61, no. 4, pp. 1436–1449, April 2013.
- [7] H. Yang and T. L. Marzetta, "Performance of conjugate and zero-forcing beamforming in large-scale antenna systems," *IEEE Journal on Selected Areas in Communications*, vol. 31, no. 2, pp. 172–179, February 2013.
- [8] X. Gao, O. Edfors, F. Rusek, and F. Tufvesson, "Linear pre-coding performance in measured very-large MIMO channels," in *Vehicular Technology Conference (VTC Fall), 2011 IEEE*, Sept 2011, pp. 1–5.
- [9] M. Kobayashi, N. Jindal, and G. Caire, "Training and feedback optimization for multiuser MIMO downlink," *IEEE Transactions on Communications*, vol. 59, no. 8, pp. 2228–2240, August 2011.
- [10] E. G. Larsson, O. Edfors, F. Tufvesson, and T. L. Marzetta, "Massive MIMO for next generation wireless systems," *IEEE Communications Magazine*, vol. 52, no. 2, pp. 186–195, February 2014.
- [11] J. Haartsen, "Impact of non-reciprocal channel conditions in broadband TDD systems," in *IEEE 19th International Symposium on Personal, Indoor and Mobile Radio Communications (PIMRC)*, Sept 2008, pp. 1–5.
- [12] A. Bourdoux, B. Come, and N. Khaled, "Non-reciprocal transceivers in OFDM/SDMA systems: impact and mitigation," in *Radio and Wireless Conference, 2003. RAWCON '03. Proceedings*, Aug 2003, pp. 183–186.
- [13] J. Liu, A. Bourdoux, J. Craninckx, P. Wambacq, B. Come, S. Donnay, and A. Barel, "OFDM-MIMO WLAN AP front-end gain and phase mismatch calibration," in *Radio and Wireless Conference, 2004 IEEE*, Sept 2004, pp. 151–154.
- [14] B. Kouassi, I. Ghauri, and L. Deneire, "Estimation of time-domain calibration parameters to restore MIMO-TDD channel reciprocity," in *7th International ICST Conference on Cognitive Radio Oriented Wireless Networks and Communications (CROWNCOM)*, June 2012, pp. 254–258.
- [15] M. Petermann, M. Stefer, F. Ludwig, D. Wubben, M. Schneider, S. Paul, and K.-D. Kammeyer, "Multi-user pre-processing in multi-antenna OFDM TDD systems with non-reciprocal transceivers," *IEEE Transactions on Communications*, vol. 61, no. 9, pp. 3781–3793, September 2013.
- [16] Y. Zou, O. Raeesi, R. Wichman, A. Tolli, and M. Valkama, "Analysis of channel non-reciprocity due to transceiver and antenna coupling mismatches in TDD precoded multi-user MIMO-OFDM downlink," in *IEEE 80th Vehicular Technology Conference (VTC Fall)*, Sept 2014, pp. 1–7.
- [17] S. Durrani and M. E. Bialkowski, "Effect of mutual coupling on the interference rejection capabilities of linear and circular arrays in CDMA systems," *IEEE Transactions on Antennas and Propagation*, vol. 52, no. 4, pp. 1130–1134, April 2004.
- [18] O. Raeesi, Y. Zou, A. Tolli, and M. Valkama, "Closed-form analysis of channel non-reciprocity due to transceiver and antenna coupling mismatches in multi-user massive MIMO network," in *IEEE Global Communications Conference Workshops (GLOBECOM)*, Dec 2014, pp. 333–339.
- [19] H. Wei, D. Wang, and X. You, "Reciprocity of mutual coupling for TDD massive MIMO systems," in *Wireless Communications Signal Processing (WCSP), 2015 International Conference on*, Oct 2015, pp. 1–5.
- [20] F. Athley, G. Durisi, and U. Gustavsson, "Analysis of massive MIMO with hardware impairments and different channel models," in *2015 9th European Conference on Antennas and Propagation (EuCAP)*, May 2015, pp. 1–5.
- [21] H. Wei, D. Wang, J. Wang, and X. You, "Impact of RF mismatches on the performance of massive MIMO systems with ZF precoding," *Science China Information Sciences*, vol. 59, no. 2, pp. 1–14, 2016. [Online]. Available: <http://dx.doi.org/10.1007/s11432-015-5509-1>.
- [22] W. Zhang, H. Ren, C. Pan, M. Chen, R. de Lamare, B. Du, and J. Dai, "Large-scale antenna systems with UL/DL hardware mismatch: achievable rates analysis and calibration," *IEEE Transactions on Communications*, vol. 63, no. 4, pp. 1216–1229, April 2015.
- [23] J. Jose, A. Ashikhmin, P. Whiting, and S. Vishwanath, "Channel estimation and linear precoding in multiuser multiple-antenna TDD systems," *IEEE Transactions on Vehicular Technology*, vol. 60, no. 5, pp. 2102–2116, Jun 2011.
- [24] J. Jose, A. Ashikhmin, T. L. Marzetta, and S. Vishwanath, "Pilot contamination and precoding in multi-cell TDD systems," *IEEE Transactions on Wireless Communications*, vol. 10, no. 8, pp. 2640–2651, August 2011.
- [25] C. Shepard, H. Yu, N. Anand, E. Li, T. Marzetta, R. Yang, and L. Zhong, "Argos: Practical many-antenna base stations," in *Proceedings of the 18th*

Annual International Conference on Mobile Computing and Networking, ser. Mobicom '12. New York, NY, USA: ACM, 2012, pp. 53–64.

- [26] M. Guillaud, D. Slock, and R. Knopp, "A practical method for wireless channel reciprocity exploitation through relative calibration," in *Proceedings of the Eighth International Symposium on Signal Processing and Its Applications*, vol. 1, August 2005, pp. 403–406.
- [27] R. Rogalin, O. Y. Bursalioglu, H. Papadopoulos, G. Caire, A. F. Molisch, A. Michaloliakos, V. Balan, and K. Psounis, "Scalable synchronization and reciprocity calibration for distributed multiuser MIMO," *IEEE Transactions on Wireless Communications*, vol. 13, no. 4, pp. 1815–1831, April 2014.
- [28] H. Q. Ngo, E. G. Larsson, and T. L. Marzetta, "Massive MU-MIMO downlink TDD systems with linear precoding and downlink pilots," in *51st Annual Allerton Conference on Communication, Control, and Computing (Allerton)*, Oct 2013, pp. 293–298.
- [29] F. Rusek, D. Persson, B. K. Lau, E. Larsson, T. L. Marzetta, O. Edfors, and F. Tufvesson, "Scaling up MIMO: opportunities and challenges with very large arrays," *IEEE Signal Processing Magazine*, vol. 30, no. 1, pp. 40–60, Jan 2013.
- [30] D. Zhu, B. Li, and P. Liang, "A novel hybrid beamforming algorithm with unified analog beamforming by subspace construction based on partial CSI for massive MIMO-OFDM systems," *IEEE Transactions on Communications*, vol. 65, no. 2, pp. 594–607, Feb 2017.
- [31] H. Q. Ngo, E. G. Larsson, and T. L. Marzetta, "The multicell multiuser MIMO uplink with very large antenna arrays and a finite-dimensional channel," *IEEE Transactions on Communications*, vol. 61, no. 6, pp. 2350–2361, June 2013.
- [32] Q. H. Spencer, A. L. Swindlehurst, and M. Haardt, "Zero-forcing methods for downlink spatial multiplexing in multiuser MIMO channels," *IEEE Transactions on Signal Processing*, vol. 52, no. 2, pp. 461–471, Feb 2004.
- [33] Evolved Universal Terrestrial Radio Access (E-UTRA); Physical channels and modulation, The 3rd Generation Partnership Project (3GPP) Tech. Spec., V13.1.0, Release 13, TS 36.211, March 2016.
- [34] E. Björnson, E. G. Larsson, and M. Debbah, "Massive MIMO for maximal spectral efficiency: How many users and pilots should be allocated?" *IEEE Transactions on Wireless Communications*, vol. 15, no. 2, pp. 1293–1308, Feb 2016.
- [35] A. Tölli and M. Codreanu, "Compensation of interference non-reciprocity in adaptive TDD MIMO-OFDM systems," in *2004 IEEE 15th International Symposium on Personal, Indoor and Mobile Radio Communications (IEEE Cat. No.04TH8754)*, vol. 2, Sept 2004, pp. 859–863 Vol.2.



Orod Raeesi received his M.Sc. degree (with distinction) from Tampere University of Technology (TUT), Tampere, Finland, in 2011, and is currently pursuing the Ph.D. degree at TUT. Currently, he is working as a communications system specialist with Nokia Mobile Networks, Espoo, Finland. His research interests include IEEE 802.11 MAC and PHY layer challenges, massive MIMO systems, TDD channel non-reciprocity, ultra-reliable low latency communications, system-level simulations, and 5G mobile radio networks.



as an algorithm specialist with Huawei, Stockholm, Sweden.

Ahmet Gokceoglu received M.Sc. (2010) and Ph.D. Degrees (2014) from the Department of Electronics and Communications Engineering, Tampere University of Technology, Finland, where he also held a postdoctoral researcher position (2014–2016) together with a visiting researcher position at Linköping university (2015). His research interests are information theory, modeling and performance analysis of MIMO-OFDM systems, advanced transmitter and receiver signal processing techniques and algorithm design for MAC and physical layer. He is currently working



works as a research manager. She has published over 30 articles in international peer-reviewed journals and conferences, as well as one book chapter. Her general research interests are in physical layer design and RF implementation challenges of 5G and beyond communication system as well as related ICT Policies.

Yaning Zou received her Bachelor Degree in communications engineering from University Electronic Science and Technology of China (UESTC), Chengdu, China, in 2002, and the M.Sc. and Ph.D. Degrees in electrical engineering from Tampere University of Technology (TUT), Tampere, Finland, in 2005 and 2009, respectively. Then she worked as an Academy postdoctoral researcher at TUT, Finland, until August 2015. In September 2015, she joined the Vodafone Chair Mobile Communication Systems Technical University of Dresden, Germany, where she currently



communications, Massive MIMO, radio resource allocation, energy-efficient communications, and network design. He is on the editorial board of the IEEE TRANSACTIONS ON COMMUNICATIONS and the IEEE TRANSACTIONS ON GREEN COMMUNICATIONS AND NETWORKING. He is the first author of the textbooks *Massive MIMO Networks: Spectral, Energy, and Hardware Efficiency* (2017) and *Optimal Resource Allocation in Coordinated Multi-Cell Systems* (2013). He is dedicated to reproducible research and has made a large amount of simulation code publicly available. Dr. Björnson has performed MIMO research for more than ten years and has filed more than ten related patent applications. He received the 2016 Best PhD Award from EURASIP, the 2015 Ingvar Carlsson Award, and the 2014 Outstanding Young Researcher Award from IEEE ComSoc EMEA. He has co-authored papers that received best paper awards at WCSP 2015, IEEE ICC 2015, IEEE WCNC 2014, IEEE SAM 2014, IEEE CAMSAP 2011, and WCSP 2009.

Emil Björnson (S'07–M'12–SM'17) received the M.S. degree in Engineering Mathematics from Lund University, Sweden, in 2007. He received the Ph.D. degree in Telecommunications from KTH Royal Institute of Technology, Sweden, in 2011. From 2012 to mid 2014, he was a joint postdoc at the Alcatel-Lucent Chair on Flexible Radio, SUPELEC, France, and at KTH. He joined Linköping University, Sweden, in 2014 and is currently Associate Professor and Docent at the Division of Communication Systems. He performs research on multi-antenna



Communications Systems and Signal Processing Institute at SDSU, San Diego, CA. Currently, he is a Full Professor and Laboratory Head at the Laboratory of Electronics and Communications Engineering at TUT, Finland. His general research interests include radio communications, communications signal processing, estimation and detection techniques, signal processing algorithms for flexible radios, cognitive radio, full-duplex radio, radio localization, and 5G mobile radio networks.

Mikko Valkama (S'00–M'01–SM'15) was born in Pirkkala, Finland, on November 27, 1975. He received the M.Sc. and Ph.D. Degrees (both with honors) in electrical engineering (EE) from Tampere University of Technology (TUT), Finland, in 2000 and 2001, respectively. In 2002, he received the Best Ph.D. Thesis -award by the Finnish Academy of Science and Letters for his dissertation entitled "Advanced I/Q signal processing for wideband receivers: Models and algorithms". In 2003, he was working as a visiting post-doc research fellow with the

PUBLICATION III

O. Raeesi, Y. Zou, A. Tölli, and M. Valkama, “Closed-form analysis of channel non-reciprocity due to transceiver and antenna coupling mismatches in multi-user massive MIMO network,” in *2014 IEEE Globecom Workshops (GC Wkshps)*, Dec 2014, pp. 333–339.

© 2014 IEEE. Reprinted, with permission, from O. Raeesi, Y. Zou, A. Tölli, and M. Valkama, “Closed-form analysis of channel non-reciprocity due to transceiver and antenna coupling mismatches in multi-user massive MIMO network,” in *2014 IEEE Globecom Workshops (GC Wkshps)*, December 2014.

In reference to IEEE copyrighted material which is used with permission in this thesis, the IEEE does not endorse any of Tampere University’s products or services. Internal or personal use of this material is permitted. If interested in reprinting/republishing IEEE copyrighted material for advertising or promotional purposes or for creating new collective works for resale or redistribution, please go to http://www.ieee.org/publications_standards/publications/rights/rights_link.html to learn how to obtain a License from RightsLink.

Closed-form Analysis of Channel Non-Reciprocity Due to Transceiver and Antenna Coupling Mismatches in Multi-user Massive MIMO Network

Orod Raeesi¹, Yaning Zou¹, Antti Tölli² and Mikko Valkama¹

¹Department of Electronics and Communications Engineering, Tampere University of Technology, Tampere, Finland

²Department of Communications Engineering, University of Oulu, Oulu, Finland

Emails: orod.raeesi@tut.fi, yaning.zou@tut.fi, antti.tolli@ee.oulu.fi, mikko.e.valkama@tut.fi

Abstract — In this paper, we analyze the impact of channel non-reciprocity due to two implementation imperfections, namely, transceiver frequency-response and antenna mutual coupling mismatches at the base-station side in multi-user massive MIMO system context. Signal models are first developed to characterize the joint effects of these two imperfections in precoded multi-user downlink transmission, covering both zero-forcing (ZF) and maximum ratio transmission (MRT) based transmitter processing. Then closed-form expressions for evaluating the resulting performance degradation are derived in terms of effective SINR at terminal receiver input as well as lower bound of maximum achievable sum-rate in the system. Based on the derived results, it is also possible to directly evaluate non-reciprocity calibration requirements at the BS with given performance targets, e.g., desired effective SINR for each user or the overall system throughput, at given SNR level. The analysis also shows that the ZF precoding can be sensitive to the channel non-reciprocity problem even in the case that large amounts of antennas are deployed while the impact of implementation imperfections on MRT precoded system is less severe.

Keywords—channel reciprocity, massive MIMO, multi-user MIMO, mutual coupling, non-reciprocity, precoding, time-division duplexing, transceiver frequency response mismatch.

I. INTRODUCTION

As one important disruptive technology for the design of the fifth generation (5G) wireless networks [1], the so-called massive multiple-input multiple-output (MIMO) and large scale antenna systems have started to attract great interest in both academia and industry in recent years [2], [3]. One key element is to enable highly spectrally-efficient multi-user wireless access system by deploying very large antenna arrays at the base-station (BS) side, e.g., 100 and above, which is also much larger than the number of simultaneously served user equipment (UEs) in the BS coverage area. From practical system design point of view, in order to establish efficient downlink (DL) transmission from the BS to multiple UEs at the same time and at the same frequencies, the BS needs to acquire channel state information at the transmitter (CSIT). In FDD based systems, this is done by estimating DL CSI at the UEs and sending feedback signaling from the UEs back to the BS, which generally requires allocation

of system resources proportional to the number of antennas at the BS. As the number of antennas grows significantly in massive MIMO context, such feedback type channel estimation approach will consume extensive system resources and the processing time may even exceed channel coherence time.

As a result, system design of practical massive MIMO networks are likely to rely on channel reciprocity property of time division duplexing (TDD) based systems [3]. Under ideal channel reciprocity assumption, DL CSI can be directly obtained by measuring uplink (UL) channels at the BS, which consumes system resources proportional to the number of UEs in the coverage area instead of the number of antennas at the BS. But as discussed in [5]–[10] and reference therein, *effective UL and DL channels* are, in practice, not reciprocal due to the so-called *transceiver non-reciprocity problem*. Generally speaking, transceiver non-reciprocity problem is stemming from frequency-response (FR) mismatches between the transmitter (TX, containing, e.g., mixers, power amplifier and RF filtering) and receiver (RX, e.g., RF filtering, LNA, mixers, and lowpass filtering) chains implemented in the same transceiver. As described in [1]–[3], transceivers implemented in the massive MIMO BS may operate at much lower TX/RX power levels than those in more traditional BSs. This property can help transceivers to achieve better performance in terms of, e.g., enhanced linearity. Yet, it does not directly help in resolving the component differences between TX and RX stemming from unavoidable physical limitations of the used electronics [4], especially if rather low-cost transceivers are expected to be deployed and implemented at the BS [1]–[3] to keep the total costs feasible. The problem can become even worse when the channel non-reciprocity can also be influenced by the differences in antenna mutual coupling characteristics between the DL and UL antennas/RF chains [6], [10]. Thus, in general, the impact of channel non-reciprocity due to implementation imperfections in massive MIMO devices should be carefully studied and understood. As discussed in [6], the non-reciprocity at the BS side is the major problem and thus BS side calibration should be sufficient for addressing this problem. However, no systematic study has been reported yet in the existing literature, regarding the impact of increased number of antennas and reciprocity calibration requirements in massive MIMO system context.

This work was supported by the Finnish Funding Agency for Technology and Innovation (Tekes), Broadcom Communications Finland and Huawei Finland under the project “Energy-Efficient Wireless Networks and Connectivity of Devices – Densification (EWINE-D)”, the Academy of Finland under the projects 251138 “Digitally-Enhanced RF for Cognitive Radio Devices” and 138424 “Joint Analysis and DSP-Based Mitigation of Multiple RF Impairments in Future Radio Devices”, and TUT Graduate School.

In this paper, we analyze the impact of channel non-reciprocity due to transceiver FR and antenna mutual coupling mismatches on multi-user MIMO DL downlink transmission with large number of antennas at the BS. Both zero-forcing (ZF) and maximum ratio transmission (MRT) based precoding schemes are considered and detailed signal and system models are derived. Based on this modeling, closed-form expressions are then derived for evaluating the resulting performance degradation due to RF implementation imperfections, in terms of effective signal-to-interference-and-noise ratios (SINRs) and lower bounds on system sum-rate capacity. In general, ZF precoding based transmission is shown to be much more sensitive to the channel non-reciprocity problems than MRT precoding based system. Based on the obtained expressions and analysis, it is possible to directly calculate non-reciprocity calibration requirements at the BS with given performance targets, e.g., desired effective SINR for each user or overall system throughput, at given SNR level. Those findings establish a solid analytical foundation for fully understanding and appreciating the non-reciprocity problem on the performance of emerging massive MIMO systems.

The rest of the paper is organized as follows: Section II outlines the fundamental multi-user massive MIMO downlink system models and corresponding performance metrics. Essential transceiver non-reciprocity and antenna mutual coupling models are then formulated in Section III. In Section IV, these are combined to analyze the impact of channel non-reciprocity due to transceiver FR and antenna coupling mismatches on massive MIMO downlink transmission. Section V provides numerical evaluations and illustrations while conclusions are drawn in Section VI.

II. PRECODED MULTI-USER MASSIVE MIMO DOWNLINK TRANSMISSION

A. Principal downlink system model

We consider a general multi-user MIMO DL transmission system with one BS and K users, at arbitrary OFDM(A) subcarrier. The BS is equipped with a large number of antennas, denoted here by N_B , while each UE is assumed to have only one antenna for notational simplicity, hence indicating single-stream transmission per UE. At the BS side, a $K \times 1$ data vector $\mathbf{x} = [x_1, \dots, x_K]^T$ is precoded using an $N_B \times K$ matrix \mathbf{U} as

$$\mathbf{p} = \beta \mathbf{U} \mathbf{x} \quad (1)$$

where each element of \mathbf{x} has normalized power of the form $E[x_k^2] = \delta_x^2$ while the sum transmitted power of data vector \mathbf{x} is thus $\delta_{\mathbf{x}}^2 = \sum_{k=1}^K E[x_k^2] = K\delta_x^2$. Furthermore, β refers to a power normalization scalar that keeps the total aggregate signal power $\delta_{\mathbf{x}}^2$ unchanged after precoding and can be obtained by

$$\beta = \sqrt{K / \text{tr}(\mathbf{U}^H \mathbf{U})} \quad (2)$$

In general, the precoding matrix \mathbf{U} is constructed by combining different precoder column vectors as $\mathbf{U} = [\mathbf{u}_1, \dots, \mathbf{u}_K]$, each of which is responsible for precoding a specific data symbol for a specific user. For example, the precoded data for the k -th user in (1) can be written as

$$\mathbf{p}_k = \beta \mathbf{u}_k x_k \quad (3)$$

Next we assume the propagation channels from the BS to the k -th user, written as $1 \times N_B$ vector $\mathbf{h}_k^T = [h_{1,k}, \dots, h_{N_B,k}]$ with normal distribution of $CN(0, \mathbf{I}_{N_B})$ distributed entries. Then the received signal at the k -th user antenna input can be expressed as

$$y_k = \beta \mathbf{h}_k^T \mathbf{u}_k x_k + \beta \sum_{i=1, i \neq k}^K \mathbf{h}_k^T \mathbf{u}_i x_i + n_k \quad (4)$$

where we consider $\beta \mathbf{h}_k^T \mathbf{u}_k x_k$ as the desired signal and $\beta \sum_{i=1, i \neq k}^K \mathbf{h}_k^T \mathbf{u}_i x_i$ as inter-user-interference (IUI), while n_k refers to additive zero-mean complex Gaussian channel noise at the k -th user receiver input with variance $E[n_k^2] = \delta_k^2$.

By stacking next the receptions for all K users into a column vector, we build a system level MIMO transmission model as

$$\mathbf{y} = \mathbf{H} \mathbf{p} + \mathbf{n} = \beta \mathbf{H} \mathbf{U} \mathbf{x} + \mathbf{n} \quad (5)$$

where the overall DL channel matrix and noise vector are denoted by $\mathbf{H} = [\mathbf{h}_1, \dots, \mathbf{h}_K]^T$ and $\mathbf{n} = [n_1, \dots, n_K]^T$, respectively.

Based on (2) and (4), from individual user point of view, e.g., at the k -th UE reception, the instantaneous received SINR at each terminal reads

$$\begin{aligned} \text{SINR}_k &= \frac{|\beta^2 \mathbf{h}_k^T \mathbf{u}_k|^2 \delta_x^2}{\sum_{i=1, i \neq k}^K |\beta^2 \mathbf{h}_k^T \mathbf{u}_i|^2 \delta_x^2 + \delta_k^2} \\ &= \frac{|\mathbf{h}_k^T \mathbf{u}_k|^2 \rho}{\sum_{i=1, i \neq k}^K |\mathbf{h}_k^T \mathbf{u}_i|^2 \rho + \text{tr}(\mathbf{U}^H \mathbf{U})} \end{aligned} \quad (6)$$

where $\rho = \delta_x^2 / \delta_k^2 = \delta_x^2 K / \delta_k^2$ denotes the total transmitted signal-to-noise ratio (SNR) [2], [3]. The effective SINR, defined here, similar to, e.g., [11], as the ratio of the average desired signal power to the average interference plus noise power is then given by

$$\gamma_k = \frac{E[|\mathbf{h}_k^T \mathbf{u}_k|^2] \rho}{\sum_{i=1, i \neq k}^K E[|\mathbf{h}_k^T \mathbf{u}_i|^2] \rho + E[\text{tr}(\mathbf{U}^H \mathbf{U})]} \quad (7)$$

where γ_k approaches to the value of SINR_k when $N_B \rightarrow \infty$.

B. Sum-rate capacity of massive MIMO DL transmission

Based on the formulated instantaneous SINR at the k -th user input given in (6), it is possible to evaluate the maximum achievable sum-rate based on the classical capacity expressions over different channel realizations as

$$R = \sum_{k=1}^K E[\log_2(1 + \text{SINR}_k)] \quad (8)$$

As discussed, e.g., in [2], [3], [11], the interference term in (4) is non-Gaussian distributed and its entropy is upper-bounded by the entropy of Gaussian noise having the same variance. Therefore, the sum-rate R is also lower bounded by the rate evaluated using effective SINR or SNR in the presence of non-Gaussian distributed interference as

$$R \geq \sum_{k=1}^K \log_2(1 + \gamma_k) \quad (9)$$

The actual values of instantaneous and effective SINRs vary with different precoding techniques. In this paper, we considered two most prominent precoding candidates for multi-user massive MIMO DL transmission, namely, ZF and MRT [1]-[3].

C. System performance with ZF precoding

With ZF precoding, the precoder and power normalization parameter are constructed using the pseudo-inverse of the total channel matrix as

$$\mathbf{U}_{ZF} = \mathbf{H}^H (\mathbf{H}\mathbf{H}^H)^{-1}, \quad \beta_{ZF} = \sqrt{K / \text{tr}((\mathbf{H}\mathbf{H}^H)^{-1})} \quad (10)$$

Incorporating (10) into the link model in (5), the reception at the k -th user input can be written as

$$y_k^{ZF} = \beta_{ZF} \mathbf{h}_k^T \mathbf{U}_{ZF} \mathbf{x} + n_k = \beta_{ZF} x_k + n_k \quad (11)$$

which is, by design, totally IUI free. The resulting instantaneous and effective S(I)NRs at the k -th user reception then read

$$\begin{aligned} \text{SNR}_k^{ZF} &= \frac{|\beta_{ZF}^2| \delta_x^2}{\delta_k^2} = \frac{|\beta_{ZF}^2|}{K} \rho \\ \gamma_k^{ZF} &= \frac{\rho}{\text{E}[\text{tr}((\mathbf{H}\mathbf{H}^H)^{-1})]} \end{aligned} \quad (12)$$

respectively, where δ_x^2 and δ_k^2 refer to the powers of each transmitted symbol and channel noise at the k -th user receiver input respectively. As shown in [2], [3] and references therein, with large K and N_B , we have

$$\text{E}[\text{tr}((\mathbf{H}\mathbf{H}^H)^{-1})] = 1 / (\alpha - 1) \quad (13)$$

where $\alpha = N_B / K$ refers to the ratio between the number of antennas at the BS and the number of single-antenna UEs in the coverage area. Inherently, effective S(I)NR per terminal can be directly written as a function of α and transmitted SNR ρ as

$$\gamma_k^{ZF} = (\alpha - 1) \rho \quad (14)$$

D. System performance with MRT precoding

As described in [2], [3], MRT is a fairly simple technique where the precoding parameters are defined as

$$\mathbf{U}_{MRT} = \mathbf{H}^H, \quad \beta_{MRT} = \sqrt{K / \text{tr}(\mathbf{H}\mathbf{H}^H)} \quad (15)$$

Again, incorporating (15) into the link model in (4), the reception at the k -th user input can be written as

$$y_k^{MRT} = \beta_{MRT} \mathbf{h}_k^T \mathbf{h}_k^* x_k + \beta_{MRT} \sum_{i=1, i \neq k}^K \mathbf{h}_k^T \mathbf{h}_i^* x_i + n_k \quad (16)$$

which is now, in general, contaminated by both IUI and additive noise. The resulting instantaneous and effective SINRs then read

$$\begin{aligned} \text{SINR}_k^{MRT} &= \frac{|\mathbf{h}_k^T \mathbf{h}_k^*|^2 \rho}{\sum_{i=1, i \neq k}^K |\mathbf{h}_k^T \mathbf{h}_i^*|^2 \rho + \text{tr}(\mathbf{H}\mathbf{H}^H)} \\ \gamma_k^{MRT} &= \frac{\text{E}[|\mathbf{h}_k^T \mathbf{h}_k^*|^2] \rho}{\sum_{i=1, i \neq k}^K \text{E}[|\mathbf{h}_k^T \mathbf{h}_i^*|^2] \rho + \text{E}[\text{tr}(\mathbf{H}\mathbf{H}^H)]} \end{aligned} \quad (17)$$

respectively. As shown in [11], with large number of antennas at the BS, the transmission channels have the following properties

$$\begin{aligned} \text{E}[|\mathbf{h}_k^T \mathbf{h}_k^*|^2] &= N_B^2 + N_B \\ \text{E}[|\mathbf{h}_k^T \mathbf{h}_i^*|^2] &= N_B, \quad \text{if } i \neq k \\ \text{E}[\text{tr}(\mathbf{H}\mathbf{H}^H)] &= KN_B \end{aligned} \quad (18)$$

Based on (18), the effective SINR defined in (17) can then be further simplified as

$$\gamma_k^{MRT} = \frac{(N_B + 1) \rho}{\rho + 1} \approx \frac{\alpha \rho}{\rho + 1} \quad (19)$$

which is now a function of α and transmitted SNR ρ [2], [3].

III. TRANSCIEVER FR AND ANTENNA MUTUAL COUPLING MISMATCHES AND THEIR IMPACT ON TDD CHANNEL RECIPROCITY

In general, as outlined above, the design of both ZF and MRT precoders at the BS requires DL channel knowledge. In TDD systems, DL CSIT can be obtained by measuring UL channels, denoted here by \mathbf{H}_{UL} and $\mathbf{h}_{k,UL}^T$, as DL and UL operate at the same center-frequency, and thus ideally $\mathbf{H} = \mathbf{H}_{UL}^T$ and $\mathbf{h}_k = \mathbf{h}_{k,UL}^T$ [3]. However, as depicted in Figure 1 and Figure 2, the *effective DL and UL channels* are generally cascades of transceiver responses and antenna mutual coupling at the TX side, physical propagation channels, and antenna mutual coupling and transceiver responses at the RX side. Then, the effective DL and UL channel matrices between the BS and the k -th user device, and between the BS and all the users $k = 1, 2, \dots, K$, are given by

$$\begin{aligned} \bar{\mathbf{h}}_k^T &= a_{k,R} \mathbf{h}_k^T \mathbf{M}_{B,T} \mathbf{A}_{B,T} \\ \bar{\mathbf{h}}_{k,UL}^T &= \mathbf{A}_{B,R} \mathbf{M}_{B,R}^T \mathbf{h}_{k,UL}^T a_{k,T} \end{aligned} \quad (20)$$

where $\mathbf{A}_{B,T} = \text{diag}(a_{B,T,1}, \dots, a_{B,T,N_B})$ and $\mathbf{A}_{B,R} = \text{diag}(a_{B,R,1}, \dots, a_{B,R,N_B})$. In above, a_{B,T,n_B} , a_{B,R,n_B} , $a_{k,T}$ and $a_{k,R}$ refer to the frequency-responses of TX and RX chains, at considered subcarrier, in the n_B -th transceiver at the BS side and in the k -th UE while $\mathbf{M}_{B,R}$ and $\mathbf{M}_{B,T}$ are RX and TX mutual coupling matrices at the BS, respectively. In general, $[\mathbf{M}_{B,R(T)}]_{i,j}$ ($i \neq j$) represents the leakage coefficient from the j -th antenna to the i -th antenna at the RX and TX sides of the BS, respectively.

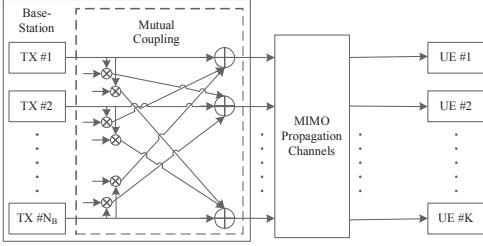


Figure 1: Principal illustration of physical DL transmission and reception including propagation channels, transceivers and antenna mutual coupling.

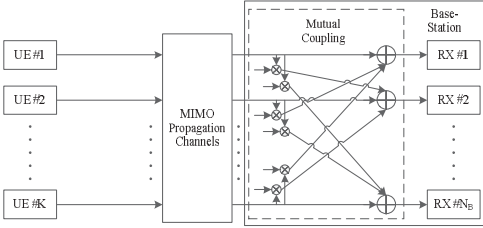


Figure 2: Principal illustration of physical UL transmission and reception including propagation channels, transceivers and antenna mutual coupling.

Based on (20), the *effective DL channels* can now be written, in terms of the *effective UL channels*, as

$$\begin{aligned}\bar{\mathbf{h}}_k^T &= a_k \left(\bar{\mathbf{h}}_{k,UL}^T \right)^T (\mathbf{A}_{B,R} \mathbf{M}_{B,R}^T)^{-T} \mathbf{M}_{B,T} \mathbf{A}_{B,T} \\ &\approx a_k \left(\bar{\mathbf{h}}_{k,UL}^T \right)^T \mathbf{M}_B \mathbf{A}_B \\ &= a_k \left(\bar{\mathbf{h}}_{k,UL}^T \right) \mathbf{C}_B\end{aligned}\quad (21)$$

where $a_k = a_{k,R} a_{k,T}^{-1}$ and $\mathbf{A}_B = \mathbf{A}_{B,T} \mathbf{A}_{B,R}^{-1}$ depict transceiver FR mismatches at the k -th user and at the BS, respectively [10]. $\mathbf{M}_B = \mathbf{M}_{B,R}^{-1} \mathbf{M}_{B,T}$ refers to the mutual coupling mismatch matrix at the BS while $\mathbf{C}_B = \mathbf{M}_B \mathbf{A}_B$ denotes the joint effects of transceiver FR and antenna mutual coupling mismatches.

In general, the transceiver frequency mismatch matrix \mathbf{A}_B is diagonal and antenna mutual coupling mismatch matrix \mathbf{M}_B is non-diagonal [6], [10]. Here, we define $\mathbf{C}'_B = \mathbf{C}_B - \mathbf{I}_{N_B}$. For analysis purposes, we assume that all entries of \mathbf{C}'_B are zero-mean complex Gaussian distributed random variables and each column of \mathbf{C}'_B , denoted by $[\mathbf{C}'_B]_{:,i}$, has equal sum-power of the form $\delta_C^2 = E[[\mathbf{C}'_B]_{:,i}^H [\mathbf{C}'_B]_{:,i}]$. For each column $[\mathbf{C}'_B]_{:,i}$, the power of diagonal entry $[\mathbf{C}'_B]_{i,i}$ and sum power of non-diagonal entries are denoted as δ_D^2 and δ_O^2 , respectively, and

$$\delta_C^2 = \delta_D^2 + \delta_O^2 \quad (22)$$

When the mutual coupling coefficients for TX and RX antennas are identical, implying $\mathbf{M}_B = \mathbf{I}$, and thus there is only transceiver FR mismatch at the BS, we have $\delta_O^2 = 0$ and $\delta_C^2 = \delta_D^2$.

IV. CLOSED-FORM ANALYSIS OF CHANNEL NON-RECIPROcity EFFECTS ON PRECODED MASSIVE MIMO DL TRANSMISSION

In this section, the performance degradation due to transceiver FR and antenna mutual coupling mismatches at the BS is analyzed in terms of effective SINR at each UE input and lower bound of achievable system downlink sum-rate in the multi-user massive MIMO context.

A. General signal model under channel non-reciprocity

We assume that the deployed precoder $\hat{\mathbf{U}} = [\hat{\mathbf{u}}_1, \dots, \hat{\mathbf{u}}_K]$ and normalization scalar $\hat{\beta}$ are constructed based on perfectly estimated *UL effective channel* matrix $\hat{\mathbf{H}} = \hat{\mathbf{H}}_{UL}^T = [\hat{\mathbf{h}}_{1,UL}^T, \dots, \hat{\mathbf{h}}_{K,UL}^T]^T$ where $\hat{\mathbf{h}}_k^T = \bar{\mathbf{h}}_{k,UL}^T$. Thus, incorporating (21) into the signal model in (4), the reception at the k -th user input becomes

$$\begin{aligned}y_k &= \hat{\beta} \bar{\mathbf{h}}_k^T \hat{\mathbf{u}}_k x_k + \sum_{i=1, i \neq k}^K \hat{\beta} \bar{\mathbf{h}}_k^T \hat{\mathbf{u}}_i x_i + n_k \\ &= \hat{\beta} a_k \bar{\mathbf{h}}_k^T \mathbf{C}_B \hat{\mathbf{u}}_k x_k + \sum_{i=1, i \neq k}^K \hat{\beta} a_k \bar{\mathbf{h}}_k^T \mathbf{C}_B \hat{\mathbf{u}}_i x_i + n_k\end{aligned}\quad (23)$$

and the instantaneous SINR at the k -th user input reads

$$\text{SINR}'_k = \frac{|\hat{\beta} a_k \bar{\mathbf{h}}_k^T \mathbf{C}_B \hat{\mathbf{u}}_k|^2 \delta_x^2}{\sum_{i=1, i \neq k}^K |\hat{\beta} a_k \bar{\mathbf{h}}_k^T \mathbf{C}_B \hat{\mathbf{u}}_i|^2 \delta_x^2 + \delta_x^2 / |\hat{\beta}|^2} \quad (24)$$

In the following, based on (24), we carry out closed-form analysis for evaluating the effective SINR over different channel and non-reciprocity coefficient realizations using ZF and MRT precoders, respectively. The lower bound of system sum-rate capacity can then be obtained through (9) in closed-form by applying the obtained effective SINR expressions.

B. Effective SINR using ZF precoding

By replacing \mathbf{H} with $\hat{\mathbf{H}}$ in (10), we construct the estimated ZF precoder $\hat{\mathbf{U}}_{ZF}$ and power normalization constant $\hat{\beta}_{ZF}$. Then, after passing through the effective DL channel, the receiver input signal at the k -th user reads

$$\begin{aligned}y_k'^{ZF} &= \hat{\beta}_{ZF} a_k \bar{\mathbf{h}}_k^T (\mathbf{I} + \mathbf{C}'_B) \hat{\mathbf{u}}_k^{ZF} x_k + \hat{\beta}_{ZF} \sum_{i=1, i \neq k}^K a_k \bar{\mathbf{h}}_k^T \mathbf{C}_B \hat{\mathbf{u}}_i^{ZF} x_i + n_k \\ &= \hat{\beta}_{ZF} a_k x_k + \hat{\beta}_{ZF} a_k \bar{\mathbf{h}}_k^T \mathbf{C}'_B \hat{\mathbf{H}}^H (\hat{\mathbf{H}} \hat{\mathbf{H}}^H)^{-1} \mathbf{x} + n_k\end{aligned}\quad (25)$$

The instantaneous SINR at k -th user input can then be expressed as

$$\text{SINR}'_{k,ZF} = \frac{|\hat{\beta}_{ZF} a_k \bar{\mathbf{h}}_k^T (\mathbf{I} + \mathbf{C}'_B) \hat{\mathbf{u}}_k^{ZF}|^2 \delta_x^2}{\sum_{i=1, i \neq k}^K |\hat{\beta}_{ZF} a_k \bar{\mathbf{h}}_k^T \mathbf{C}_B \hat{\mathbf{u}}_i^{ZF}|^2 \delta_x^2 + \delta_x^2} \quad (26)$$

As the entries of \mathbf{C}'_B are much smaller than 1 and $|\hat{\mathbf{h}}_k^T \mathbf{C}'_B \hat{\mathbf{u}}_k^{ZF}| \ll 1$ and $|\hat{\mathbf{h}}_k^T \mathbf{C}'_B \hat{\mathbf{u}}_i^{ZF}| \ll \sum_{i=1, i \neq k}^K |\hat{\mathbf{h}}_k^T \mathbf{C}'_B \hat{\mathbf{u}}_i^{ZF}|^2$ with large K , the effective SINR over different channel and non-reciprocity realizations can be approximated as

$$\gamma_k'^{ZF} \approx \frac{\mathbb{E} \left[|a_k|^2 \right] \delta_x^2}{\mathbb{E} \left[|a_k \hat{\mathbf{h}}_k^T \mathbf{C}'_B \hat{\mathbf{H}}^H (\hat{\mathbf{H}} \hat{\mathbf{H}}^H)^{-1} \mathbf{x}|^2 \right] + \delta_C^2 \mathbb{E} \left[\text{tr} \left((\hat{\mathbf{H}} \hat{\mathbf{H}}^H)^{-1} \right) \right] / K} \quad (27)$$

In general, the implementation impairment elements in \mathbf{C}'_B are independent of transmission channels $\hat{\mathbf{h}}_k^T$ and $\hat{\mathbf{H}}$. All the entries in \mathbf{C}'_B and $\hat{\mathbf{h}}_k^T$ ($\hat{\mathbf{H}}$) are thus independent random variables, and therefore the first term in the denominator of (27) can be simplified as

$$\begin{aligned} & \mathbb{E} \left[|\hat{\mathbf{h}}_k^T \mathbf{C}'_B \hat{\mathbf{H}}^H (\hat{\mathbf{H}} \hat{\mathbf{H}}^H)^{-1} \mathbf{x}|^2 \right] \\ &= \mathbb{E} \left[\mathbf{x}^H (\hat{\mathbf{H}} \hat{\mathbf{H}}^H)^{-H} \hat{\mathbf{H}}^H \left(\mathbb{E} \left[\mathbf{C}'_B \left(\mathbb{E} \left[\hat{\mathbf{h}}_k^* \hat{\mathbf{h}}_k^T \right] \right) \mathbf{C}'_B \right] \right) \hat{\mathbf{H}}^H (\hat{\mathbf{H}} \hat{\mathbf{H}}^H)^{-1} \mathbf{x} \right] \\ &= \delta_C^2 \delta_x^2 K / (\alpha - 1) \end{aligned} \quad (28)$$

Then, the closed-form expression for effective SINR at the k -th user input reads

$$\gamma_k'^{ZF} = \frac{|a_k|^2 \delta_x^2}{|a_k|^2 \delta_C^2 \delta_x^2 K / (\alpha - 1) + \frac{1}{(\alpha - 1)K} \delta_C^2 \rho + 1} \approx \frac{\rho(\alpha - 1)}{\delta_C^2 \rho + 1} \quad (29)$$

where the gain of UE non-reciprocity scalar is assumed to be close to one, i.e., $|a_k|^2 \approx 1$, which is most likely the case in practical UE implementation. Then the SINR performance loss due to the non-reciprocity at the BS can be quantified as

$$D_{ZF} = 10 \log_{10}(\gamma_k'^{ZF}) - 10 \log_{10}(\gamma_k^{ZF}) = 10 \log_{10}(\delta_C^2 \rho + 1) \quad (30)$$

and the relative SINR performance loss compared to the ideal effective SINR is defined as

$$\begin{aligned} D_R &= D_{ZF} / \log_{10}(\gamma_k^{ZF}) \\ &= \log_{10}(\delta_C^2 \rho + 1) / \log_{10}[(\alpha - 1)\rho] \end{aligned} \quad (31)$$

Based on (30), for given performance loss specification D_{ZF} , we can now derive calibration requirement for maximum tolerable mismatch noise power δ_C^2 , defined in (22), as

$$\delta_C^2 = (10^{D_{ZF}/10} - 1) / \rho \quad (32)$$

If there is no antenna mutual coupling mismatch at the BS and $\delta_O^2 = 0$, the corresponding calibration requirement for the maximum tolerable transceiver FR mismatch noise level δ_D^2 reads

$$\delta_D^2 = (10^{D_{ZF}/10} - 1) / \rho \quad (33)$$

We will discuss the implications of the obtained analysis results in (31)-(33) in more details in Section IV. D.

C. Effective SINR using MRT precoding

Again, by replacing \mathbf{H} with $\hat{\mathbf{H}}$ in (15), we construct estimated MRT precoder $\hat{\mathbf{U}}_{MRT}$ and power normalization constant $\hat{\beta}_{MRT}$. Then, after sending data using MRT precoding and experiencing effective DL channel, the reception at the k -th user input reads

$$y_k'^{MRT} = \hat{\beta}_{MRT} a_k \hat{\mathbf{h}}_k^T \mathbf{C}_B \hat{\mathbf{h}}_k^* x_k + \hat{\beta}_{MRT} \sum_{i=1, i \neq k}^K a_k \hat{\mathbf{h}}_k^T \mathbf{C}_B \hat{\mathbf{h}}_i^* x_i + n_k \quad (34)$$

The instantaneous SINR at the k -th receiver input can then be written as

$$\text{SINR}_k'^{MRT} = \frac{|\hat{\beta}_{MRT}|^2 |a_k \hat{\mathbf{h}}_k^T \mathbf{C}_B \hat{\mathbf{h}}_k^*|^2 \rho}{|\hat{\beta}_{MRT}|^2 \sum_{i=1, i \neq k}^K |a_k \hat{\mathbf{h}}_k^T \mathbf{C}_B \hat{\mathbf{h}}_i^*|^2 \rho + K} \quad (35)$$

Following similar procedures as when deriving (19) and (29), the effective SINR over different channel and non-reciprocity realizations can then be shown to read

$$\begin{aligned} \gamma_k'^{MRT} &= \frac{\mathbb{E} \left[|a_k \hat{\mathbf{h}}_k^T \mathbf{C}_B \hat{\mathbf{h}}_k^*|^2 \right] \rho}{\sum_{i=1, i \neq k}^K \mathbb{E} \left[|a_k \hat{\mathbf{h}}_k^T \mathbf{C}_B \hat{\mathbf{h}}_i^*|^2 \right] \rho + \mathbb{E} \left[1 / |\hat{\beta}_{MRT}|^2 \right] K} \\ &\approx \frac{\alpha \rho}{\rho(1 + \delta_C^2) + 1} \end{aligned} \quad (36)$$

where again, $|a_k|^2$ is assumed to be approximately equal to 1. Then, the SINR performance loss due to frequency-response mismatch inside transceiver and mutual coupling mismatch between antenna TX and RX modes can be written as

$$\begin{aligned} D_{MRT} &= 10 \log_{10}(\gamma_k'^{MRT}) - 10 \log_{10}(\gamma_k'^{MRT}) \\ &= 10 \log_{10} \left(\frac{\rho(1 + \delta_C^2) + 1}{\rho + 1} \right) \end{aligned} \quad (37)$$

Notice that with reasonable design and implementation resources, it should be reasonable to achieve mismatch level $\delta_C^2 \ll 1$ at the BS. Thus, based on the above expression, the performance degradation due to the considered implementation imperfections is fairly modest in MRT precoded massive MIMO system, i.e., D_{MRT} is close to 0dB.

D. Discussion

Considering ZF precoded massive MIMO DL with large K , analyzed in Section IV.B, the absolute SINR performance loss in (30) is only related to the mismatch noise level δ_C^2 at the BS side and transmitted SNR ρ while the relative SINR performance loss in (31) is related to δ_C^2 , ρ and also α . In general, the value of δ_C^2 is heavily dependent on detailed transceiver and antenna array implementation at the BS. In order to provide further insight on the obtained formulas (30) and (31), we consider the following two cases:

1) δ_C^2 and ρ are fixed for any large N_B

a) The absolute SINR performance loss at each UE input is independent of the number of UEs K served in the coverage area and the number of antennas N_B . It does not decrease by increasing N_B or $\alpha = N_B / K$.

b) Based on (9), the absolute performance loss in terms of sum-rate is proportional to the number of UEs K in the coverage area and is independent of N_B .

c) The relative SINR performance loss at each UE input is dependent on $\alpha = N_B / K$. With increasing α , D_R approaches to zero.

2) δ_C^2 varies as a function of N_B as $\delta_C^2 = \delta_{C_0}^2 F(N_B)$ and ρ is fixed for any N_B .

a) The absolute SINR performance loss D_{ZF} at each UE input is independent of the number of UEs K but dependent on the number of antennas N_B . If $F(N_B)$ increases or decreases with growing number of N_B , D_{ZF} increases or decreases as well.

b) The absolute performance loss in the system overall sum-rate is proportional to the number of UEs K in the coverage area and but also dependent on N_B , based on (9).

c) The relative SINR performance loss D_R at each UE input is dependent on $\alpha = N_B / K$. Depending on the exact function $F(N_B)$, D_R may even increase with growing α .

V. SIMULATIONS AND NUMERICAL RESULTS

In this Section, the derived analytical results are evaluated using extensive computer simulations. As a practical example, multi-user massive MIMO DL transmission using BS with 20-1000 antennas is assumed, serving 10-100 single-antenna UEs simultaneously over the same spectrum. The deployed carrier frequency is assumed to be 2 GHz.

First, the accuracy of the proposed closed-form analysis is examined. As shown in Figure 3-Figure 5, system sum-rates with zero impairments (for reference), with transceiver FR mismatch only ($\delta_D^2 = -20$ dB) and with joint effects of transceiver FR ($\delta_C^2 = -20$ dB) and antenna mutual coupling mismatches ($\delta_O^2 = -15$ dB) are compared with different system setups. The system setups for obtaining each figure are described in details below each figure. Here the empirical sum-rates are obtained by averaging instantaneous rates over different channel and impairment realizations as indicated in (8). Based on the simulation results, it is very interesting to observe that the analytical lower bounds of system sum-rates are very close to the actual system sum-rates even if the interference is not Gaussian distributed. The derived analytical results are, in general, seen to provide very good match to the empirical system sum-rates when transceiver FR and/or antenna mutual coupling mismatches are present, thus verifying and demonstrating the usefulness and validity of the analysis. In general, the impact of channel non-reciprocity on MRT precoded transmission is also seen to be very modest. In case of ZF precoded transmission, there is almost constant performance gap between ideal sum-rate and degraded sum-rate if δ_C^2 , ρ and K are fixed as in Figure 4.

Next, we consider ZF precoding only, and analyzing calibration requirements for the BS. Based on (32), we examine non-reciprocity calibration requirement at the BS with different performance loss margins and transmitted SNRs. As shown in Figure 6, targeting for near zero performance loss, the BS has to achieve non-reciprocity calibration accuracies in the order of $\delta_C^2 = -30, -35, -40$ dB for $\rho = 15, 20, 25$ dB, respectively. Targeting for 1dB performance loss, on the other hand, calibration accuracy δ_C^2 of around -25dB is already sufficient.

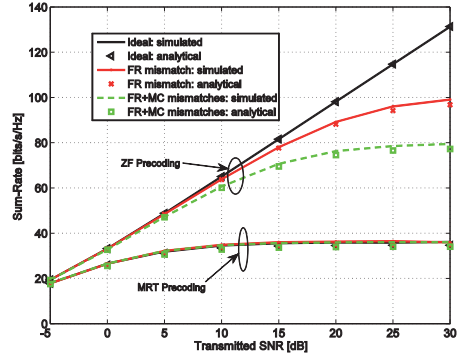


Figure 3: Comparison of simulated and analytical system sum-rate capacity of massive MIMO DL transmission with 10 users and 100 antennas at the BS. Both ZF and MRT precoders are considered with zero impairments (for reference), with transceiver FR mismatch only and with both transceiver FR and mutual coupling mismatches.

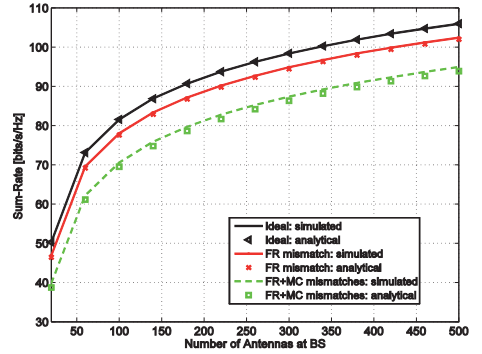


Figure 4: Comparison of simulated and analytical system sum-rate capacity of massive MIMO DL transmission with 10 users and 20 to 500 antennas at the BS. ZF precoding is considered with zero impairments (for reference), with only transceiver FR mismatch and with both transceiver FR and mutual coupling mismatches. $\rho = 15$ dB.

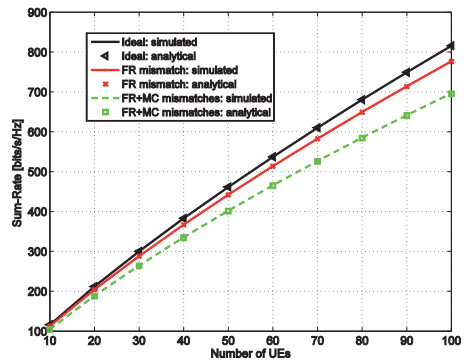


Figure 5: Comparison of simulated and analytical system sum-rate capacity of massive MIMO DL transmission with 10 to 100 users and 1000 antennas at the BS. ZF precoding is considered with zero impairments (for reference), with only transceiver FR mismatch and with both transceiver FR and mutual coupling mismatches. $\rho = 15$ dB.

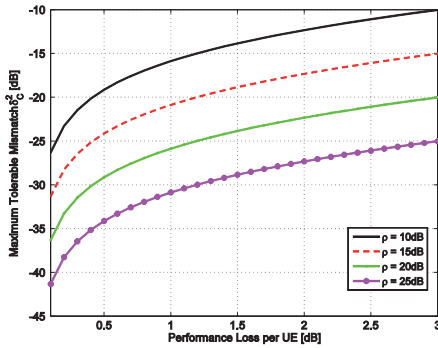


Figure 6: Calibration requirements for maximum tolerable mismatch level δ_C^2 against absolute SINR performance loss based on (32). ρ refers to transmitted SNR.

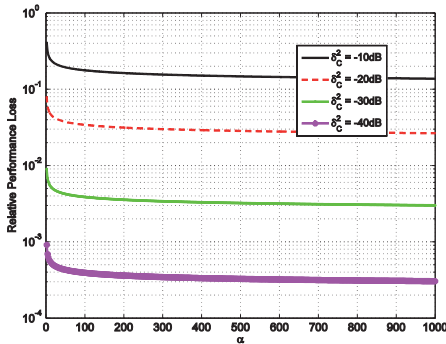


Figure 7: Relative SINR performance loss defined in (31) with fixed mismatch level δ_C^2 and varied value of α from 2 to 1000. $\rho = 15\text{dB}$.

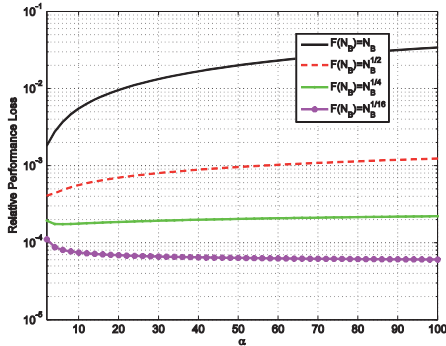


Figure 8: Relative SINR performance loss defined in (31) with varied mismatch level $\delta_C^2 = \delta_{C_0}^2 F(N_B)$ ($\delta_{C_0}^2 = -50\text{dB}$) and varied value of α from 2 to 1000. $\rho = 15\text{dB}$.

Finally, we evaluate the relative SINR performance loss defined in (31) with different numbers of $\alpha = N_B / K$. As shown in Figure 7, with fixed δ_C^2 , the relative performance loss is fairly constant except for the smallest values of α , and already with calibration accuracy of -20dB the relative loss is only around 3%. However, if $\delta_{C_0}^2$ grows when the number of antennas is increas-

ing at the BS, denoted by $\delta_C^2 = \delta_{C_0}^2 F(N_B)$, the relative SINR performance loss can grow as shown in Figure 8. For example, the benefits of using larger amounts of antennas at the BS is seriously reduced if the non-reciprocity mismatch noise $\delta_{C_0}^2$ grows linearly with increased N_B . On the other hand, the relative performance loss keeps almost unchanged with different antenna numbers if $F(N_B) = N_B^{1/4}$. Thus, in general, the derived analysis results provide efficient tools for system and circuit designers to fully understand and deal with the non-reciprocity problems in the massive MIMO systems.

VI. CONCLUSIONS

This paper studied the impact of channel non-reciprocity due to transceiver FR and antenna mutual coupling mismatches on the performance of multi-user massive MIMO DL transmission systems using both ZF and MRT precoded transmission schemes. Closed-form expressions for evaluating the performance degradation in terms of effective SINR at the UE input and lower bound of system sum-rate were derived. In general, ZF precoded system is found to be more sensitive to channel non-reciprocity problems than MRT precoded system. The analysis generally shows that the performance loss caused by the considered mismatch problems does not disappear with increased number of antennas implemented at the BS. However the negative impact imposed on the overall system performance becomes less severe with increased number of antennas at the BS unless the mismatch level grows substantially at the same time.

REFERENCES

- [1] F. Boccardi, R. Heath, A. Lozano, T. Marzetta, P. Popovski, "Five disruptive technology directions for 5G," *IEEE Communications Magazine*, vol.52, no.2, pp.74-80, Feb. 2014.
- [2] E. Larsson, F. Tufvesson, O. Edfors, and T. Marzetta, "Massive MIMO for Next Generation Wireless Systems", *IEEE Commun. Mag.*, vol. 52, no. 2, pp. 186-195, Feb. 2014.
- [3] F. Rusek, D. Persson, B. K. Lau, E. G. Larsson, T. L. Marzetta, O. Edfors, and F. Tufvesson, "Scaling up MIMO: Opportunities and Challenges with Very Large Arrays", *IEEE Signal Processing Mag.*, vol. 30, no. 1, pp. 40-46, Jan. 2013.
- [4] B. Razavi, *RF Microelectronics*. Englewood Cliffs, NJ: Prentice-Hall, 1998.
- [5] J. C. Haartsen, "Impact of non-reciprocal channel conditions in broadband TDD systems," in *Proc. IEEE PIMRC 2008*, pp.1-5, Sept. 2008.
- [6] Y. Zou, O. Raeesi, R. Wichman, A. Tolli, and M. Valkama, "Analysis of channel non-reciprocity due to transceiver and antenna coupling mismatches in TDD precoded multi-user MIMO-OFDM downlink", in *Proc. IEEE VTC2014-Fall*, pp. 1-5, Sept. 2014.
- [7] S. Durrani, and M. Bialkowski, "Effect of mutual coupling on the interference rejection capabilities of linear and circular arrays in CDMA systems," *IEEE Transactions on Antennas and Propagation*, vol.52, no.4, pp.1130-1134, April 2004.
- [8] J. Liu, A. Bourdoux, J. Craninckx, P. Wambacq, B. Come, S. Donnay, and A. Barel, "OFDM-MIMO WLAN AP Front-end Gain and Phase Mismatch Calibration," in *Proc. IEEE RAWCON*, Atlanta, Sept. 2004.
- [9] B. Kouassi, I. Ghauri, and L. Deneire, "Estimation of time-domain calibration parameters to restore MIMO-TDD channel reciprocity," in *Proc. CROWNCOM 2012*, pp.254-258, Jun. 2012.
- [10] M. Petermann, M. Stefer, F. Ludwig, D. Wubben, M. Schneider, S. Paul, and K. Kammeyer, "Multi-User Pre-Processing in Multi-Antenna OFDM TDD Systems with Non-Reciprocal Transceivers," *IEEE Trans. Commun.*, vol.61, no.9, pp.3781-3793, Sep. 2013.
- [11] H. Yang and T.L. Marzetta, "Performance of conjugate and zero-forcing beamforming in large-scale antenna systems," *IEEE J. Sel. Areas Commun.*, vol. 31, no. 2, pp.172-179, Feb. 2013.

PUBLICATION IV

O. Raeesi, A. Gokceoglu, Y. Zou, Q. Cui, and M. Valkama, “Estimation of BS transceiver non-reciprocity in multi-user massive MIMO systems,” in *European Wireless 2016; 22th European Wireless Conference*, May 2016, pp. 1–8.

© 2016 IEEE. Reprinted, with permission, from O. Raeesi, A. Gokceoglu, Y. Zou, Q. Cui, and M. Valkama, “Estimation of BS transceiver non-reciprocity in multi-user massive MIMO systems,” in *European Wireless 2016; 22th European Wireless Conference*, May 2016.

In reference to IEEE copyrighted material which is used with permission in this thesis, the IEEE does not endorse any of Tampere University’s products or services. Internal or personal use of this material is permitted. If interested in reprinting/republishing IEEE copyrighted material for advertising or promotional purposes or for creating new collective works for resale or redistribution, please go to http://www.ieee.org/publications_standards/publications/rights/rights_link.html to learn how to obtain a License from RightsLink.

Estimation of BS Transceiver Non-Reciprocity in Multi-User Massive MIMO Systems

Orod Raeesi*, Ahmet Gokceoglu*, Yaning Zou†, Qimei Cui‡, and Mikko Valkama*

*Department of Electronics and Communications Engineering, Tampere University of Technology, Tampere, Finland

†Technische Universität Dresden, Vodafone Chair Mobile Communications Systems, Dresden, Germany

‡Wireless Technology Innovation Institute, Beijing University of Posts and Telecommunications, 100876 Beijing, China

E-mail: orod.raeesi@tut.fi

Abstract—This paper proposes efficient algorithms for estimating the base-station transceiver non-reciprocity characteristics in precoded TDD multi-user MIMO-OFDM networks, such that the estimation processing is carried out on the user equipment (UE) side. First, detailed signal models are derived to characterize the effects of transceiver non-reciprocity on both base-station and UE sides, in case of zero-forcing precoded multi-user MIMO-OFDM downlink transmission. The developed signal models show that transceiver non-reciprocity on the base-station side is the main cause of downlink performance degradation, resulting in general to inter-user interference. Then, based on closed-form analysis of the overall interference or distortion level on the receiver side, two efficient UE-based algorithms are proposed, depending on the availability of downlink pilot symbols, to estimate the level of base-station transceiver non-reciprocity without any specific calibration procedure. The performance of the proposed estimation methods are evaluated using extensive computer simulations. The obtained results show that even without any downlink pilot symbols, the estimation of the base-station non-reciprocity characteristics is still feasible, while further improved estimation accuracy can be obtained if downlink pilots are available in the system. In general, by being able to estimate the level of base-station transceiver non-reciprocity on the UE side, dedicated calibration procedures and the associated system overhead can be avoided, thus enabling the base-stations to carry out calibration only when truly needed.

Keywords—Channel reciprocity, massive MIMO, multi-user MIMO, non-reciprocity, time-division duplexing, transceiver frequency response mismatch, non-reciprocity level estimation.

I. INTRODUCTION

Massive MIMO or large-scale antenna systems are commonly regarded as one of the most promising candidate technologies for the fifth generation (5G) wireless networks [1]. By employing very large numbers of antenna elements on the base-station (BS) side, highly-efficient multi-user (MU) MIMO where several user equipments (UEs) are served simultaneously can be realized with simple and computing-feasible linear processing in the devices [2]. This can enable significantly increased spectral- and radiated energy-efficiency in the networks [2].

In general, a majority of the associated spatial precoding techniques, such as maximum ratio transmission (MRT) and

zero-forcing (ZF), build on the availability of accurate channel state information (CSI) on the transmitter side [2]. In conventional frequency-division duplex (FDD) based MIMO systems, where the number of BS antennas is reasonably low, UEs estimate the downlink (DL) channels based on DL reference signals transmitted by the BS. Then, these estimated channel responses are communicated from UEs to the BS by means of feedback signaling. However, such CSI acquisition approach is not considered feasible in massive MIMO networks since it requires reference signal and feedback signaling resources proportional to the number of adopted antennas in the base station. Therefore, massive MIMO systems are commonly assumed to build on the time division duplexing (TDD) principle, resulting to the reciprocity between the uplink (UL) and downlink channels within the channel coherence time interval [3]. Hence, the BS can estimate the downlink channels based on the uplink reference signals, and calculate the precoders directly based on such estimates.

However, in practice, the hardware chains in the BS and UE transceivers are not fully reciprocal between the downlink and uplink. As discussed, e.g., in [4]–[7], even with the assumption of having reasonably good antenna isolation in each device, there are always unavoidable mismatches between the frequency responses (FRs) of transmitter and receiver chains in each individual device. Therefore, the resulting *effective DL and UL channels are not reciprocal* anymore which is commonly called channel non-reciprocity problem in TDD networks. As shown in [6]–[8], while the FR mismatches in the UE transceivers can be easily mitigated as part of the precoded effective DL channels, transceiver non-reciprocity on the BS side can cause severe performance degradation. As a result, specific calibration methods are proposed, e.g., in [9], in order to recover the reciprocal nature of the effective channels. However, such channel reciprocity calibration methods require both DL training signals from BS to UEs and feedback signaling from UEs to BS where the overhead in each phase is proportional to the number of antenna elements on the BS side. Thus, although calibrating the BS transceiver is certainly required in TDD systems, it should be done only if necessary, in order to minimize the associated system overhead. Furthermore, the rate at which the non-reciprocity characteristics deviate or change over time depends on the hardware configuration as well as the operating conditions, in particular operating temperature [10]. For these reasons, being able to estimate the level of BS transceiver non-reciprocity on UE side, during the normal downlink transmission, is intriguing and would be very beneficial in order to let the

This work was supported by the Finnish Funding Agency for Technology and Innovation (Tekes) and Huawei Finland under the project “Energy-Efficient Wireless Networks and Connectivity of Devices - densification (EWINE-D)”, the Academy of Finland under the projects 284694 and 288670, the Tuula and Yrjö Neuvo fund, and TUT Graduate School. The work was also supported by the National Natural Science Foundation of China (NSFC).

BS perform the non-reciprocity calibration only when truly needed. This is the leading theme of this paper.

In this paper, we develop efficient processing algorithms for estimating the BS transceiver non-reciprocity level in TDD multi-user massive MIMO-OFDM networks, with special focus on ZF precoded downlink transmission. First, detailed signal and system models are derived, incorporating the essential precoding, MIMO channel and non-reciprocity models. Based on the developed models, a closed-form expression is obtained for calculating the power of the overall distortion or interference on the UE side, stemming from the BS transceiver non-reciprocity. Building on this analysis, two alternative BS transceiver non-reciprocity level estimation methods are then proposed in which UEs are able to estimate the level of non-reciprocity during the normal DL transmission. Using such estimates, the UEs are then able to inform the BS whether or not to execute an actual reciprocity calibration round. The more detailed rationale of the estimation and associated signaling can be summarized as:

- 1) UEs estimate the level of BS transceiver non-reciprocity based on one of the proposed methods in Section IV.
- 2) The estimated values are then compared to a given threshold level, say Y . This threshold is chosen as the lowest BS transceiver non-reciprocity level causing considerable performance degradation [7], [8]. In each BS non-reciprocity level estimation round, the estimated values in UEs can be used either with or without averaging as
 - *with averaging*: UEs report the estimated values to the BS and the BS takes the average of received estimated values and compares it to Y .
 - *without averaging*: UEs directly compare their estimated values to Y and only send one bit flag whether or not the estimated value is higher than Y .
- 3) If the average or majority of the reported values are higher than Y , the BS initiates its transceiver non-reciprocity calibration round, e.g. the one described in [9]. Otherwise, no calibration is needed.

The rest of the paper is organized as follows. Section II outlines the fundamental ZF precoded multi-user MIMO OFDM downlink system models. Transceiver non-reciprocity and its impact on ZF precoded DL transmission are then formulated in Section III. In Section IV, two different BS transceiver non-reciprocity estimation methods are proposed by analyzing the power of the signal distortion on the UE side. Section V evaluates the performance of the proposed methods by means of comprehensive computer simulations. Finally, conclusions are drawn in Section VI.

Notations: We use upper (lower) bold letters to denote matrices (vectors). The superscripts T , $*$, and H stand for the transpose, conjugate, and conjugate-transpose, respectively. $\text{Tr}(\mathbf{A})$ denotes the trace of a matrix \mathbf{A} , while \mathbf{I}_n is the $n \times n$ identity matrix. The expectation operator is shown by $\mathbb{E}[\cdot]$, and finally, we use $\mathcal{CN}(0, 1)$ to denote a zero-mean unit-variance complex Gaussian distribution.

II. MULTI-USER MIMO SYSTEM MODEL

We consider ZF precoded multi-user MIMO DL transmission system with one BS and K UEs, at an arbitrary OFDM(A) subcarrier. For notational simplicity, the subcarrier index is dropped and thus not explicitly shown. The BS is equipped with large number of antenna elements denoted by $N \gg K$, while all UEs are assumed to be simple single-antenna devices. One data stream is allocated to each UE which results into having an overall of K streams transmitted simultaneously in the network. The data symbol vector in the BS is denoted by $\mathbf{s} = [s_1, \dots, s_K]^T \in \mathbb{C}^K$, where the average power of each element is $\mathbb{E}[|s_k|^2] = \delta_s^2$. The data vector \mathbf{s} is precoded using a zero-forcing precoder matrix $\mathbf{U} = [\mathbf{u}_1, \dots, \mathbf{u}_K] \in \mathbb{C}^{N \times K}$ constructed as [11]

$$\mathbf{U} = \mathbf{H}^H (\mathbf{H}\mathbf{H}^H)^{-1}, \quad (1)$$

where $\mathbf{H} \in \mathbb{C}^{K \times N}$ denotes the total DL channel matrix between the BS and all the UEs. The total channel matrix can be written as $\mathbf{H} = [\mathbf{h}_1, \dots, \mathbf{h}_K]^T$, where $\mathbf{h}_k^T = [h_{k1}, \dots, h_{kN}] \in \mathbb{C}^N$ is the spatial channel vector between the BS and the k -th UE with i.i.d. $\mathcal{CN}(0, 1)$ elements.

Using precoder matrix \mathbf{U} , the precoded transmit data vector can be written as

$$\mathbf{x} = \beta \mathbf{U} \mathbf{s}, \quad (2)$$

where β denotes a transmit power normalization scalar and is assumed to be constructed as follows [11]

$$\beta = \sqrt{K / \text{Tr}((\mathbf{U}^H \mathbf{U}))} = \sqrt{K / \text{Tr}((\mathbf{H}\mathbf{H}^H)^{-1})}. \quad (3)$$

The precoded data towards a particular UE k is thus of the form

$$\mathbf{x}_k = \beta \mathbf{u}_k s_k. \quad (4)$$

Therefore, the downlink signal received by k -th UE can be expressed as

$$r_k = \mathbf{h}_k^T \mathbf{x}_k + \sum_{i=1, i \neq k}^K \mathbf{h}_k^T \mathbf{x}_i + n_k, \quad (5)$$

where n_k denotes additive zero-mean complex Gaussian noise at the k -th UE with power $\mathbb{E}[|n_k|^2] = \delta_k^2$.

Incorporating (4) in (5), the received signal at the k -th UE can be re-written as

$$r_k = \beta \mathbf{h}_k^T \mathbf{u}_k s_k + \beta \sum_{i=1, i \neq k}^K \mathbf{h}_k^T \mathbf{u}_i s_i + n_k. \quad (6)$$

Stemming from the structure of ZF precoders in (1), it can be easily shown that $\mathbf{h}_k^T \mathbf{u}_k = 1$ and $\mathbf{h}_k^T \mathbf{u}_i = 0 \forall i \neq k$. Thus, the received signal at the k -th UE reads

$$r_k = \beta \mathbf{h}_k^T \mathbf{u}_k s_k + n_k = \beta s_k + n_k, \quad (7)$$

which is, by design, totally free from inter-user interference (IUI). While all developments above assume perfect CSI on the BS side, we next address how the transceiver and effective channel non-reciprocity impacts the transmission.

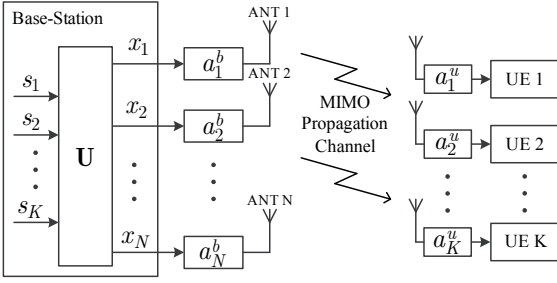


Fig. 1. Principal illustration of physical DL transmission and reception including propagation channels, transceivers and FR mismatches

III. IMPACTS OF TRANSCEIVER NON-RECIPROCITY ON ZF PRECODED TDD MU-MIMO DL TRANSMISSION

A. Effects of Transceiver Non-Reciprocity on TDD Channel Reciprocity

In order to construct ZF precoders as in (1), channel state information is obviously needed at the BS. In TDD systems, such information can be obtained via UL channel estimation, since DL and UL channels are in principle reciprocal within the channel coherence interval, written here as $\mathbf{H} = \mathbf{H}^{\text{DL}} = (\mathbf{H}^{\text{UL}})^T$.

However, as depicted in Fig. 1, in practice the *actual effective channels* also include the frequency responses of transmitter and receiver circuits. Due to the unavoidable non-idealities and tolerances in the analog circuits, there are always FR mismatches between the deployed transmitter and receiver chains in each transceiver. As a result, even with perfect channel estimation at the BS side, the effective DL and UL channels are not reciprocal. As discussed, e.g., in [6], [12] and references therein, the channel non-reciprocity model can be formulated as

$$\mathbf{H}^{\text{NR}} = \mathbf{A}_u (\mathbf{H}^{\text{UL}})^T \mathbf{A}_b = \mathbf{A}_u \hat{\mathbf{H}} \mathbf{A}_b, \quad (8)$$

where \mathbf{H}^{NR} , $\hat{\mathbf{H}}^{\text{UL}}$ and $\hat{\mathbf{H}}$ refer to the effective DL channel, effective UL channel, and estimated DL channel between the BS and UEs, respectively. Transceiver FR mismatches at UE and BS sides are denoted by \mathbf{A}_u and \mathbf{A}_b , respectively. Furthermore, \mathbf{A}_u can be expressed as $\mathbf{A}_u = \mathbf{I}_K + \mathbf{A}'_u$ while $\mathbf{A}_b = \mathbf{I}_N + \mathbf{A}'_b$. Both \mathbf{A}'_u and \mathbf{A}'_b are diagonal matrices, and it is assumed for analysis purposes that all the diagonal entries of both \mathbf{A}'_u and \mathbf{A}'_b are i.i.d. zero-mean circularly symmetric complex Gaussian random variables with variance δ_u^2 and δ_b^2 , respectively.

Based on above, the effective channel between the BS and UE k can be now expressed as

$$\mathbf{h}_k^{\text{NR}} = a_k^u \hat{\mathbf{h}}_k \mathbf{A}_b, \quad (9)$$

where $a_k^u = 1 + a_k^{u'}$ is the k -th diagonal element of \mathbf{A}_u and \mathbf{A}_b has diagonal elements $1 + a_1^{b'}, \dots, 1 + a_N^{b'}$, which are representing the transceiver FR mismatches at k -th UE and the BS, respectively. In general, the channel non-reciprocity values vary very slowly and thus the realization values of \mathbf{A}_u and \mathbf{A}_b can be assumed to remain constant over many channel coherence intervals.

B. Effects of Channel Non-Reciprocity on ZF Precoded TDD MU-MIMO DL Transmission

Under the channel non-reciprocity described in (8), the BS generates ZF precoders based on the estimated DL channel $\hat{\mathbf{H}}$, obtained using the UL pilots, as

$$\hat{\mathbf{U}} = \hat{\mathbf{H}}^H (\hat{\mathbf{H}} \hat{\mathbf{H}}^H)^{-1}, \quad (10)$$

while the normalization factor reads now

$$\hat{\beta} = \sqrt{K / \text{Tr}(\hat{\mathbf{U}}^H \hat{\mathbf{U}})} = \sqrt{K / \text{Tr}((\hat{\mathbf{H}} \hat{\mathbf{H}}^H)^{-1})}. \quad (11)$$

Thus, under non-reciprocal channels, the received DL transmission at the k -th UE receiver reads

$$\begin{aligned} r_k &= \hat{\beta} (\mathbf{h}_k^{\text{NR}})^T \hat{\mathbf{u}}_k s_k + \sum_{i=1, i \neq k}^K \hat{\beta} (\mathbf{h}_k^{\text{NR}})^T \hat{\mathbf{u}}_i s_i + n_k \\ &= \hat{\beta} a_k^u \hat{\mathbf{h}}_k^T \mathbf{A}_b \hat{\mathbf{u}}_k s_k + \sum_{i=1, i \neq k}^K \hat{\beta} a_k^u \hat{\mathbf{h}}_k^T (\mathbf{I}_N + \mathbf{A}'_b) \hat{\mathbf{u}}_i s_i + n_k \\ &= \hat{\beta} a_k^u \hat{\mathbf{h}}_k^T \mathbf{A}_b \hat{\mathbf{u}}_k s_k + \sum_{i=1, i \neq k}^K \hat{\beta} a_k^u \hat{\mathbf{h}}_k^T \mathbf{A}'_b \hat{\mathbf{u}}_i s_i + n_k. \end{aligned} \quad (12)$$

By defining

$$c_{ij} \triangleq \hat{\beta} a_i^u \hat{\mathbf{h}}_i^T \mathbf{A}_b \hat{\mathbf{u}}_j, \quad (13)$$

and

$$I_k = \sum_{i=1, i \neq k}^K c_{ki} s_i, \quad (14)$$

the expression (12) can also be re-written as

$$r_k = c_{kk} s_k + \sum_{i=1, i \neq k}^K c_{ki} s_i + n_k = c_{kk} s_k + I_k + n_k, \quad (15)$$

where I_k is IUI at the k -th UE caused by the effective channel non-reciprocity.

Based on (15), it can be observed that although the level of IUI at UE k depends on transceiver non-reciprocity at both BS and the UE itself, assuming the only imperfection in CSI is the channel non-reciprocity, IUI free reception can be achieved by having reciprocal transceiver at BS side. This follows directly from substituting $\mathbf{A}_b = \mathbf{I}_N$ in (12) and (13). This relation is next used to estimate the level of BS transceiver non-reciprocity δ_b^2 at UE side.

IV. ANALYSIS AND ESTIMATION OF THE LEVEL OF BS TRANSCEIVER NON-RECIPROCITY

In this section, we derive analytical expressions for the level of BS transceiver non-reciprocity, measurable at UE side, assuming either pilot based or statistical DL channel estimation in UEs. Building on that, we then propose an estimator to estimate the level of BS transceiver non-reciprocity on the UE side.

A. Measurable BS Transceiver Non-Reciprocity Level at UE

In order to estimate the BS transceiver non-reciprocity level δ_b^2 using the received signal in (15), UE k needs to estimate the effective precoded DL channel, c_{kk} . In general, conventional OFDM systems typically adopt DL pilots to acquire CSI for detection purposes. However, such approach is not necessarily efficient or feasible in massive MIMO systems, since the amount of overhead is proportional to the number of BS antennas N . Therefore, alternative techniques to acquire DL CSI are proposed in massive MIMO system context, e.g., in [11], [13], [14].

Assuming now that the k -th UE has estimated the effective precoded DL channel c_{kk} , denoted with \hat{c}_{kk} , the unwanted distortion or interference term can be extracted as

$$\begin{aligned} z_k &= r_k - \hat{c}_{kk}s_k = (c_{kk} - \hat{c}_{kk})s_k + I_k + n_k \\ &= \underbrace{\epsilon_k + I_k}_{d_k} + n_k, \end{aligned} \quad (16)$$

where d_k refers to interference plus the residual term of transmitted data s_k which reads

$$\epsilon_k = (c_{kk} - \hat{c}_{kk})s_k, \quad (17)$$

and is due to the estimation error of precoded DL channel at the k -th UE. Here, we assume that this processing is done after data decoding such that also s_k is available.

The power of the unwanted distortion or interference term z_k at the k -th UE, defined in (16), can then be written as

$$\begin{aligned} \delta_{z,k}^2 &= \mathbb{E}[|z_k|^2] = \mathbb{E}[(\epsilon_k + I_k + n_k)^* (\epsilon_k + I_k + n_k)] \\ &= \mathbb{E}[|\epsilon_k|^2] + \mathbb{E}[|I_k|^2] + \delta_k^2 \\ &= \mathbb{E}[|c_{kk} - \hat{c}_{kk}|^2] \delta_s^2 + \mathbb{E}[|I_k|^2] + \delta_k^2, \end{aligned} \quad (18)$$

where the expectation is over different data symbols and channel coherence intervals. We emphasize already here that due to the slowly-varying nature of the non-reciprocity characteristics, the underlying non-reciprocity parameters, namely the realized values of a_k^u and \mathbf{A}_b , can be assumed unknown but constants, within the processing interval, when evaluating (18) further in the forth-coming subsections.

Following from (18), the power of the term d_k denoted as $\delta_{d,k}^2 = \mathbb{E}[|d_k|^2]$ reads then

$$\delta_{d,k}^2 = \delta_{z,k}^2 - \delta_k^2 = \mathbb{E}[|c_{kk} - \hat{c}_{kk}|^2] \delta_s^2 + \mathbb{E}[|I_k|^2], \quad (19)$$

where the average IUI power can be written as

$$\mathbb{E}[|I_k|^2] = \mathbb{E}\left[\left|\sum_{i=1, i \neq k}^K \sum_{l=1}^N \hat{\beta} a_k^u \hat{h}_{kl} a_l^{b'} \hat{u}_{li}\right|^2\right] \delta_s^2, \quad (20)$$

in which \hat{u}_{li} represents the element at the l -th row and i -th column in precoder matrix $\hat{\mathbf{U}}$.

Assuming next that for large N , the element w_{ij} at the i -th row and j -th column of the matrix $\mathbf{W} = \hat{\mathbf{H}}\hat{\mathbf{H}}^H$, reads

$$w_{ij} = \hat{\mathbf{h}}_i^T \hat{\mathbf{h}}_j^* \approx \begin{cases} N & i = j \\ 0 & i \neq j \end{cases}, \quad (21)$$

and thus overall $\mathbf{W} \approx N\mathbf{I}_K$. Therefore, \hat{u}_{li} in (10) can be approximated by \hat{h}_{il}^*/N and $\hat{\beta} = \sqrt{K/\text{Tr}(\mathbf{W}^{-1})} \approx \sqrt{N}$ which result in

$$\begin{aligned} \mathbb{E}[|I_k|^2] &\approx \mathbb{E}\left[\left|\sum_{i=1, i \neq k}^K \sum_{l=1}^N \frac{1}{\sqrt{N}} a_k^u \hat{h}_{kl} a_l^{b'} \hat{h}_{il}^*\right|^2\right] \delta_s^2 \\ &= \left(\sum_{\substack{i=1 \\ i \neq k}}^K \sum_{\substack{j=1 \\ j \neq k}}^K \sum_{l=1}^N \sum_{m=1}^N \mathbb{E}[\hat{h}_{kl} \hat{h}_{km}^*] a_l^{b'} a_m^{b'*} \mathbb{E}[\hat{h}_{il}^* \hat{h}_{jm}]\right) \\ &\quad \times \frac{1}{N} |a_k^u|^2 \delta_s^2 \\ &= \frac{1}{N} |a_k^u|^2 \delta_s^2 \sum_{i=1, i \neq k}^K \sum_{l=1}^N \mathbb{E}[|\hat{h}_{kl}|^2] |a_l^{b'}|^2 \mathbb{E}[|\hat{h}_{il}|^2] \\ &\approx (K-1) |a_k^u|^2 \delta_b^2 \delta_s^2 \\ &\approx (K-1) \delta_b^2 \delta_s^2. \end{aligned} \quad (22)$$

The second approximation is due to the law of large numbers

$$\sum_{l=1}^N |a_l^{b'}|^2 \approx N \delta_b^2, \quad (23)$$

where the left hand side converges asymptotically to the right hand side with increasing N . Finally, the approximation on the last line of (22) is due to the fact that $|a_k^u|^2 \approx 1$.

Next, we derive expressions for $\delta_{d,k}^2$ under both pilot based as well as statistical DL channel estimation.

1) Pilot Based DL Channel Estimation: In order to acquire DL CSI at UE side, authors in [13] proposed beamforming-based DL training scheme. In this scheme, where the overhead is proportional to the number of UEs K , an appropriate pilot matrix is transmitted from BS to UEs while UEs then employ MMSE estimation to acquire DL CSI. It can be shown that by using this scheme, the estimated precoded DL channel at UE k can be expressed as

$$\hat{c}_{kk}^{\text{PILOT}} = c_{kk} + e_k, \quad (24)$$

where e_k is the estimation error with power $\mathbb{E}[|e_k|^2] = \delta_e^2$ where δ_e^2 is known to UEs [13].

Substituting next (24) in (19), the resulting power of the IUI and the residual part of transmitted data signal at the k -th UE reads

$$\delta_{d,k}^2 = \mathbb{E}[|e_k|^2] \delta_s^2 + \mathbb{E}[|I_k|^2]. \quad (25)$$

Incorporating finally (22) in (25), $\delta_{d,k}^2$ can be expressed as

$$\delta_{d,k}^2 \approx \delta_e^2 \delta_s^2 + (K-1) \delta_b^2 \delta_s^2. \quad (26)$$

2) Statistical DL Channel Estimation: In [11], [14], the authors deploy selected statistics of the channel, namely $\mathbb{E}[c_{kk}]$, to acquire DL CSI for detection purposes which gets more and more accurate as the number of antenna elements on the BS side N increases [13]. This is because with large N , c_{kk} becomes practically deterministic. The accuracy of such DL channel estimation is assumed sufficient for the UEs to decode their corresponding transmitted data, but is

not necessarily accurate enough to estimate the level of BS transceiver non-reciprocity. Therefore, another round of DL CSI acquisition is adopted, building on the already detected data. With the assumption that the received SNR is reasonably high and thus that the k -th UE is able to successfully decode its corresponding transmitted data s_k , the precoded DL channel in each coherence interval can be estimated, with higher accuracy, as

$$\begin{aligned}\hat{c}_{kk}^{\text{STAT}} &= \frac{1}{M} \sum_{m=1}^M \frac{r_k[m]}{s_k[m]} \\ &= \frac{1}{M} \sum_{m=1}^M \left(\hat{\beta} a_k^u \hat{\mathbf{h}}_k^T \mathbf{A}_b \hat{\mathbf{u}}_k + \frac{I_k[m] + n_k[m]}{s_k[m]} \right) \\ &\approx \hat{\beta} a_k^u \hat{\mathbf{h}}_k^T \mathbf{A}_b \hat{\mathbf{u}}_k,\end{aligned}\quad (27)$$

where M is the total number of data symbols within each coherence interval. The approximation on the last line is due to the fact that for practical scenarios $I_k[m] + n_k[m] \ll s_k[m]$ and $\mathbb{E}[I_k + n_k] = 0$ which get more and more accurate when the received SNR and the length of the observation period increase.

Using $\hat{c}_{kk}^{\text{STAT}}$ to estimate the precoded DL channel, the power of the residual part of transmitted data signal in (19) reads

$$\mathbb{E}[|\epsilon_k|^2] = \mathbb{E}\left[\left|\hat{\beta} a_k^u \hat{\mathbf{h}}_k^T \mathbf{A}_b \hat{\mathbf{u}}_k - \hat{c}_{kk}^{\text{STAT}}\right|^2\right] \delta_s^2 \approx 0, \quad (28)$$

which, based on (22), results then in

$$\delta_{d,k}^2 \approx \mathbb{E}[|I_k|^2] \approx (K-1) \delta_b^2 \delta_s^2. \quad (29)$$

B. Estimation of BS Transceiver Non-Reciprocity Level

In this subsection, based on the derived expressions in (26) and (29), practical sample estimators are proposed to estimate the level of BS transceiver non-reciprocity. Note that these estimates are then utilized in the mitigation and calibration of BS transceiver non-reciprocity as discussed in Section I.

First, the unwanted distortion or interference component is estimated based on the signal model in (16). In doing so, \hat{c}_{kk} is obtained either by (24) or (27) depending on the method to acquire DL CSI. Following that, and assuming that the mean is zero, the unwanted distortion or interference power at k -th UE is estimated via standard sample variance estimator as

$$\hat{\delta}_{z,k}^2 = \frac{1}{N_{coh}M} \sum_{i=1}^{N_{coh}M} |z_k[i]|^2, \quad (30)$$

where M is the number of processed symbols in one coherence interval and N_{coh} is the number of coherence intervals used in the BS non-reciprocity level estimation. We assume a slowly-varying fading channel such that M can be typically in the order of few hundreds, while all the modeling and estimator developments are applicable also in faster fading scenarios. Then, using (30), and assuming that the UE k knows the receiver thermal noise power δ_k^2 , the power of d_k can be estimated as

$$\hat{\delta}_{d,k}^2 = \hat{\delta}_{z,k}^2 - \delta_k^2. \quad (31)$$

Next, based on (26) and assuming that δ_s^2 and δ_e^2 are known to UEs [13], the level of BS transceiver non-reciprocity under pilot-based DL CSI can be estimated at k -th UE as

$$\hat{\delta}_{b,\text{PILOT}}^2 = \frac{\hat{\delta}_{d,k}^2 / \delta_s^2 - \delta_e^2}{K-1}. \quad (32)$$

Similarly, based on (29), the level of BS transceiver non-reciprocity under statistical DL CSI can be estimated at UE k as

$$\hat{\delta}_{b,\text{STAT}}^2 = \frac{\hat{\delta}_{d,k}^2}{(K-1) \delta_s^2}. \quad (33)$$

In the next section, we evaluate and discuss the quality of the above estimators given by (32) and (33) as functions of the essential system parameters, namely, received SNR, number of antennas at the BS, as well as levels of BS and UE transceiver non-reciprocity. For a particular set of non-reciprocity parameters, i.e., fixed \mathbf{A}_u and \mathbf{A}_b , the quality of the estimator is measured by the relative estimation error defined as

$$\psi = \frac{|\delta_b^2 - \hat{\delta}_b^2|}{\delta_b^2}. \quad (34)$$

This is then naturally averaged over multiple random realizations of the non-reciprocity parameters, to get reliable understanding of the estimation performance.

V. NUMERICAL EVALUATIONS AND ANALYSIS

In this section, we evaluate the performance of the algorithms proposed in Section IV for estimating the level of BS transceiver non-reciprocity at the UE side using extensive computer simulations. A single-cell multi-user massive MIMO network is deployed where the BS is equipped with large number of antennas and UEs are assumed to be single-antenna devices. The propagation environment between the BS and any individual UE, at an arbitrary OFDM subcarrier, is modeled as a frequency flat Rayleigh fading channel. The performance of each algorithm is evaluated in terms of relative estimation error, defined in (31). The number of data samples in each coherence interval is $M = 500$, number of coherence intervals in each BS non-reciprocity level estimation round is $N_{coh} = 50$, and all the results are averaged over 1000 non-reciprocity parameter realizations. In each simulation scenario, the accuracy of both proposed algorithms are shown by means of relative estimation error. In the case of pilot based DL channel estimation, the pilot scheme of [13] is adopted. The result are shown for both cases, where UEs either report the estimated non-reciprocity values to the BS and the BS takes the average of them, or there is no averaging on the BS side while the error between estimated value and the real value is calculated at the UE side.

The typical simulation scenario consists of a BS which is equipped with 100 antenna elements and 10 single-antenna UEs that are served simultaneously through ZF precoding, with each UE having transceiver non-reciprocity with relative variance $\delta_{u,\text{dB}}^2 = -20$ dB. The level of non-reciprocity in the BS transceivers is assumed to be as low as $\delta_{b,\text{dB}}^2 = -20$ dB which is shown in [8] to have only a fairly small impact on the system sum-rate. We specifically choose such relatively

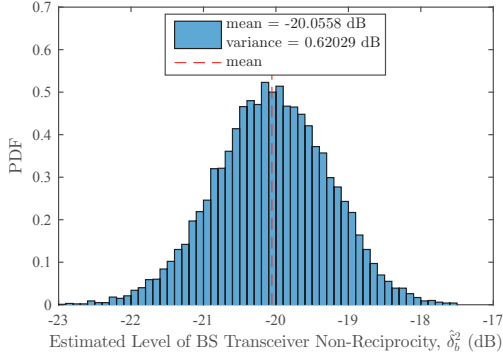


Fig. 2. Sample probability density function of estimated BS transceiver non-reciprocity level across all the UEs using pilot based DL channel estimation. The true value of non-reciprocity level is -20 dB.

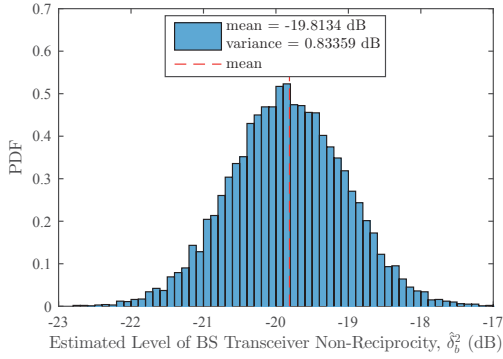


Fig. 3. Sample probability density function of estimated BS transceiver non-reciprocity level across all the UEs using statistical DL channel estimation. The true value of non-reciprocity level is -20 dB.

low non-reciprocity level, as the baseline case, to demonstrate that also low reciprocity levels can be reliably estimated. UE receiver SNR is set to 20 dB while e_k is assumed to be i.i.d zero-mean circularly symmetric complex Gaussian random sequence with relative variance $\delta_{e,\text{dB}}^2 = -20$ dB. These are the baseline values in all the simulations, but are also varied in the experiments as indicated in the result figures.

Figs. 2–5 show the sample probability density functions of estimated BS transceiver non-reciprocity level over different non-reciprocity parameter realizations, in a single UE or across all the UEs, for both DL channel estimation methods. The obtained results clearly show that the estimates have very well concentrated distribution around the true value which demonstrates the good reliability of the estimation process. More specifically, the variances are in the order of 1 dB in all cases, even when interpreted from a single UE perspective. Therefore, results from this process can indeed be used by BS after only a few coherence intervals N_{coh} .

Fig. 6 illustrates the accuracy of the estimators for different numbers of antenna elements N at the BS side. As can be seen, the accuracy improves as the number of antennas in the BS

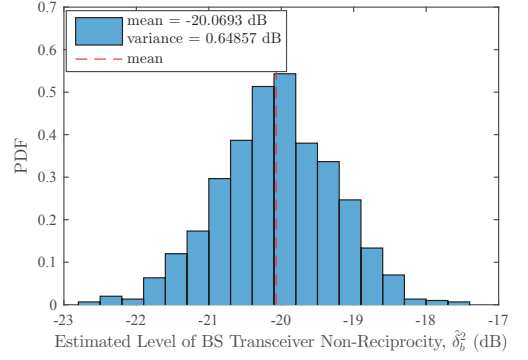


Fig. 4. Sample probability density function of estimated BS transceiver non-reciprocity level for one UE using pilot based DL channel estimation. The true value of non-reciprocity level is -20 dB.

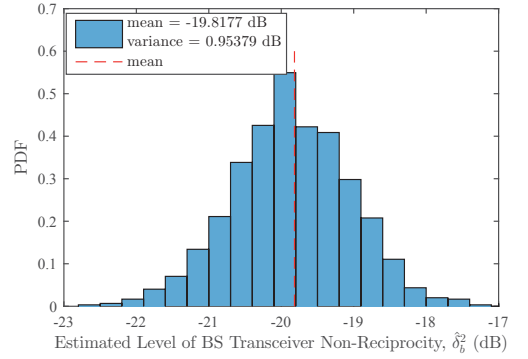


Fig. 5. Sample probability density function of estimated BS transceiver non-reciprocity level for one UE using statistical DL channel estimation. The true value of non-reciprocity level is -20 dB.

side increases. The reason is that the approximation used in (23) gets more accurate with higher values of N . Obtained results also clearly show that the accuracy of BS transceiver non-reciprocity level estimates is higher if the DL channel is estimated using DL pilots. In all cases, the estimation errors are always less than 20% which corresponds to at most 1 dB.

The effect of UE receiver SNR on the performance of both estimation methods is examined next in Fig. 7. As can be seen, the SNR does not practically have any effect on the estimation accuracy if DL pilots are used. In the case that the DL channel is estimated statistically, stemming from the estimation method in (27), the impact of the SNR on the estimation performance is, in turn, considerable, although the UEs are still able to estimate the level of BS transceiver non-reciprocity fairly reliably. Even for low SNR values, the estimation error is less than 3 dB.

In Fig. 8, the relative estimation error is measured for different levels of transceiver non-reciprocity at BS. As can be seen, using DL pilots, the estimation accuracy is excellent even for the lowest levels of BS transceiver non-reciprocity. On the other hand, if DL pilots are not available, the estimation error

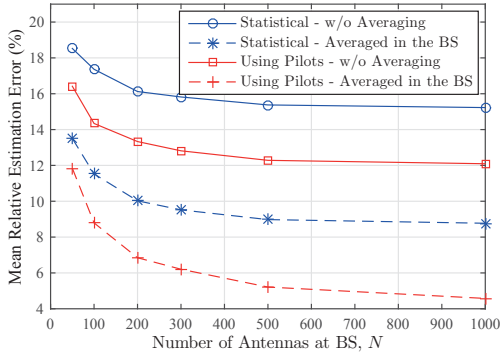


Fig. 6. Relative estimation error in identifying the level of BS transceiver non-reciprocity at the UE side with respect to the number of BS antennas.

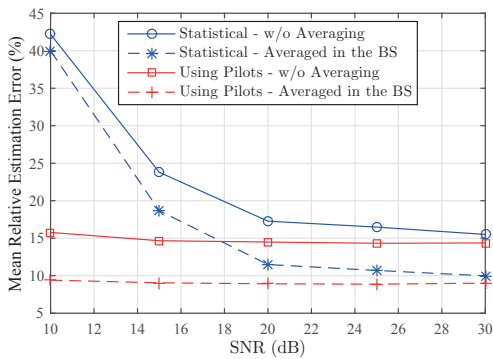


Fig. 7. Relative estimation error in identifying the level of BS transceiver non-reciprocity at the UE side with respect to the UE receiver SNR.

increases as BS transceiver non-reciprocity level decreases. However, it should be noted that UEs are still able to estimate BS transceiver non-reciprocity levels as low as $\delta_{b,\text{dB}}^2 = -30$ dB with error values lower than 3 dB.

The impact of transceiver non-reciprocity level at the UE side on the accuracy of estimation methods is shown in Fig. 9. Since the only approximation related to UE transceiver non-reciprocity ($|a_k^u|^2 \approx 1$) made in analyzing the level of IUI is common to both estimation methods, both methods are affected relatively similarly by the increase in δ_u^2 . It is important to observe that reliable estimates of BS transceiver non-reciprocity can be obtained, despite high levels of non-reciprocity at the UE side.

In general, as can be observed via the different simulated scenarios, the difference in mean relative estimation error between the cases with and without averaging in the BS is around 5% for low to moderate values of δ_u^2 . Therefore, there is basically no need to report the estimated BS transceiver non-reciprocity levels from the UE side to the BS for averaging purposes. Thus, based on the obtained results, it is sufficient that the UEs directly inform the BS, via one-bit feedback, whether or not to execute an actual BS transceiver calibration

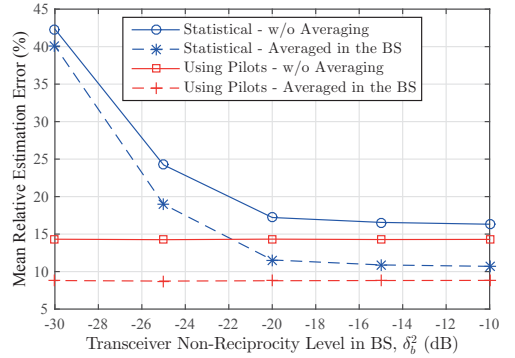


Fig. 8. Relative estimation error in identifying the level of BS transceiver non-reciprocity at the UE side with respect to the level of transceiver non-reciprocity in the BS transceivers on dB scale.

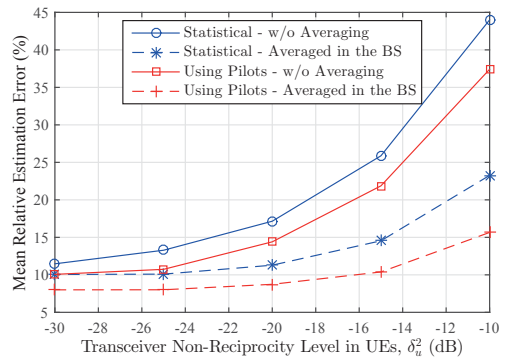


Fig. 9. Relative estimation error in identifying the level of BS transceiver non-reciprocity at the UE side with respect to the level of transceiver non-reciprocity in the UE transceivers on dB scale.

procedure. This is a substantial benefit, in terms of the reporting overhead, and overall enables executing the BS transceiver calibration only when truly needed. The one (or few) -bit flags can then be easily processed in the BS, through, e.g., a simple majority fusion rule.

VI. CONCLUSION

This paper proposed efficient methods to estimate the level of BS transceiver non-reciprocity at the UE side, in ZF precoded TDD multi-user MIMO-OFDM networks with large number of antenna units at BS. Stemming from the developed signal and system models, it was first shown that the BS transceiver non-reciprocity is the main cause of having unwanted inter-user interference in the received signal. Based on this observation, analytical expressions were derived to quantify the level of unwanted distortion or interference term at the UE receiver, depending on the availability of DL pilots to acquire DL CSI. Then, stemming from these expressions, two actual BS transceiver non-reciprocity level estimation algorithms were developed. The proposed estimation methods do not require any additional system overhead, and can operate

in both cases of with or without DL pilots in the system. Using extensive computer simulations, it was shown that both estimation methods have high accuracy in different practical scenarios, the performance being somewhat higher especially at low SNRs and low levels of BS non-reciprocity if DL pilots can be adopted to estimate the precoded DL channels. It was also shown, through numerical experiments, that the estimation accuracy of the BS transceiver non-reciprocity level does not benefit substantially from additional averaging of raw UE-based estimates in the BS. This leads to the conclusion that very simple one-bit feedback, whether or not to execute an actual BS transceiver calibration procedure, is sufficient where UE compares the estimated level to a given threshold. This is a substantial benefit, in terms of the reporting overhead, and can facilitate TDD network operation where the BS transceiver calibration is executed only when truly needed.

REFERENCES

- [1] F. Boccardi, R. Heath, A. Lozano, T. Marzetta, and P. Popovski, "Five disruptive technology directions for 5g," *IEEE Communications Magazine*, vol. 52, no. 2, pp. 74–80, February 2014.
- [2] F. Rusek, D. Persson, B. K. Lau, E. Larsson, T. Marzetta, O. Edfors, and F. Tufvesson, "Scaling up mimo: Opportunities and challenges with very large arrays," *IEEE Signal Processing Magazine*, vol. 30, no. 1, pp. 40–60, Jan 2013.
- [3] E. Larsson, O. Edfors, F. Tufvesson, and T. Marzetta, "Massive mimo for next generation wireless systems," *IEEE Communications Magazine*, vol. 52, no. 2, pp. 186–195, February 2014.
- [4] M. Petermann, M. Stefer, F. Ludwig, D. Wubben, M. Schneider, S. Paul, and K.-D. Kammeyer, "Multi-User Pre-Processing in Multi-Antenna OFDM TDD Systems with Non-Reciprocal Transceivers," *IEEE Transactions on Communications*, vol. 61, no. 9, pp. 3781–3793, September 2013.
- [5] B. Kouassi, I. Ghauri, and L. Deneire, "Estimation of time-domain calibration parameters to restore MIMO-TDD channel reciprocity," in *7th International ICST Conference on Cognitive Radio Oriented Wireless Networks and Communications (CROWNCOM)*, June 2012, pp. 254–258.
- [6] Y. Zou, O. Raeesi, R. Wichman, A. Tolli, and M. Valkama, "Analysis of Channel Non-Reciprocity Due to Transceiver and Antenna Coupling Mismatches in TDD Precoded Multi-User MIMO-OFDM Downlink," in *IEEE 80th Vehicular Technology Conference (VTC Fall)*, Sept 2014, pp. 1–7.
- [7] W. Zhang, H. Ren, C. Pan, M. Chen, R. de Lamare, B. Du, and J. Dai, "Large-scale antenna systems with ul/dl hardware mismatch: Achievable rates analysis and calibration," *IEEE Transactions on Communications*, vol. 63, no. 4, pp. 1216–1229, April 2015.
- [8] O. Raeesi, Y. Zou, A. Tolli, and M. Valkama, "Closed-form analysis of channel non-reciprocity due to transceiver and antenna coupling mismatches in multi-user massive mimo network," in *IEEE Global Communications Conference Workshops (GLOBECOM)*, Dec 2014, pp. 333–339.
- [9] Y. Zou, O. Raeesi, and M. Valkama, "Efficient Estimation and Compensation of Transceiver Non-Reciprocity in Precoded TDD Multi-User MIMO-OFDM Systems," in *IEEE 80th Vehicular Technology Conference (VTC Fall)*, Sept 2014, pp. 1–7.
- [10] M. Guillaud, D. Slock, and R. Knopp, "A practical method for wireless channel reciprocity exploitation through relative calibration," in *Proceedings of the Eighth International Symposium on Signal Processing and Its Applications*, vol. 1, August 2005, pp. 403–406.
- [11] J. Jose, A. Ashikhmin, P. Whiting, and S. Vishwanath, "Channel estimation and linear precoding in multiuser multiple-antenna tdd systems," *IEEE Transactions on Vehicular Technology*, vol. 60, no. 5, pp. 2102–2116, Jun 2011.
- [12] J. Haartsen, "Impact of non-reciprocal channel conditions in broadband TDD systems," in *IEEE 19th International Symposium on Personal, Indoor and Mobile Radio Communications (PIMRC)*, Sept 2008, pp. 1–5.
- [13] H. Q. Ngo, E. Larsson, and T. Marzetta, "Massive mu-mimo downlink tdd systems with linear precoding and downlink pilots," in *51st Annual Allerton Conference on Communication, Control, and Computing (Allerton)*, Oct 2013, pp. 293–298.
- [14] H. Yang and T. Marzetta, "Performance of conjugate and zero-forcing beamforming in large-scale antenna systems," *IEEE Journal on Selected Areas in Communications*, vol. 31, no. 2, pp. 172–179, February 2013.

PUBLICATION V

O. Raeesi, A. Gokceoglu, P. C. Sofotasios, M. Renfors, and M. Valkama, “Modeling and estimation of massive MIMO channel non-reciprocity: Sparsity-aided approach,” in *2017 25th European Signal Processing Conference (EUSIPCO)*, Aug 2017, pp. 2596–2600.

© 2017 IEEE. Reprinted, with permission, from O. Raeesi, A. Gokceoglu, P. C. Sofotasios, M. Renfors, and M. Valkama, “Modeling and estimation of massive MIMO channel non-reciprocity: Sparsity-aided approach,” in 2017 25th European Signal Processing Conference (EUSIPCO), August 2017.

In reference to IEEE copyrighted material which is used with permission in this thesis, the IEEE does not endorse any of Tampere University’s products or services. Internal or personal use of this material is permitted. If interested in reprinting/republishing IEEE copyrighted material for advertising or promotional purposes or for creating new collective works for resale or redistribution, please go to http://www.ieee.org/publications_standards/publications/rights/rights_link.html to learn how to obtain a License from RightsLink.

Modeling and Estimation of Massive MIMO Channel Non-Reciprocity: Sparsity-aided Approach

Orod Raeesi, Ahmet Gokceoglu, Paschalis Sofotasios, Markku Renfors, and Mikko Valkama
Tampere University of Technology, Laboratory of Electronics and Communications Engineering, Finland
E-mail: mikko.e.valkama@tut.fi

Abstract—In this paper, we study the estimation of channel non-reciprocity in precoded time division duplexing (TDD) based massive MIMO systems. The considered channel non-reciprocity model covers both the frequency-response and the mutual coupling mismatches between the transmitter and the receiver chains of a massive MIMO base-station. Based on the assumed non-reciprocity model, it is shown that the effective downlink channel can be decomposed as a product of the uplink channel and another sparse matrix, referred to as the BS transceiver non-reciprocity matrix. Stemming from such modeling, we then propose an efficient estimator of the BS transceiver non-reciprocity matrix exploiting its sparse nature, combined with an appropriate formulation of the associated over-the-air pilot-signaling. The mean-squared error (MSE) performance of the overall proposed estimation method is finally evaluated using extensive computer simulations which indicate that the non-reciprocity characteristics can be estimated very efficiently and accurately, thus potentially facilitating large system-level performance gains in multi-user massive MIMO systems.

Index Terms—Channel non-reciprocity, frequency-response mismatch, massive MIMO, mutual coupling, sparsity, time division duplexing (TDD).

I. INTRODUCTION

One of the key potential technologies for 5G systems is the so called large array or massive MIMO transmission which can facilitate very high cell-level and network-level spectral efficiencies [1]. The key element in such technology is to have high number of antenna units in the base stations (BSs) compared to the number of spatially multiplexed users (user equipment, UE) in the system. Massive MIMO systems typically rely on the reciprocity of the physical downlink (DL) and uplink (UL) channels in time-division duplex (TDD) based radio access to acquire DL channel state information (CSI) for precoding purposes using UL pilots, where the overhead is proportional to the number of UEs in the system [2]. The reason is that collecting DL CSI as in the conventional MIMO systems, where BSs send DL pilots to UEs and UEs report DL CSI back towards BSs using UL control channel or feedback signaling, requires system resources proportional to the number of antennas in the BS side which, in turn, is unfeasible in massive MIMO systems [3].

Although within a coherence interval the physical propagation channels can be assumed reciprocal [2], [3], the responses of transmitters and receivers hardware chains are commonly not identical. Therefore, the resulting effective DL and UL channels

are not reciprocal, which is known as channel non-reciprocity problem in TDD systems [4], [5]. As shown in [6], [7], channel non-reciprocity has two main sources, one is the frequency-response (FR) mismatches between transmitter and receiver chains of any individual transceiver, and the other one is the difference in the mutual coupling effects between the antenna elements in antenna array based devices in transmitting and receiving modes.

In literature, there are various works that study the achievable system performance under non-reciprocal channels. In this respect, [5] provides downlink sum-rate analysis for a general multi-user MIMO system with zero-forcing (ZF) or eigenbeamforming based DL precoding under channel non-reciprocity due to FR mismatch. Then, [8], [9] study achievable downlink sum-rates for maximum-ratio transmission (MRT) and ZF precoding schemes in massive MIMO systems, demonstrating significant performance degradation under practical values of channel non-reciprocity parameters. The results of such studies clearly show the need to estimate the channel non-reciprocity parameters in order to mitigate the non-reciprocity problem.

The estimation of channel non-reciprocity in TDD based MIMO systems has also been addressed in various works [3], [4], [6], [10]–[12]. These studies can be divided into three main categories. The first two refer to such methods which are performed in BS using a reference antenna and are called “self-calibration” methods [3], [4], [6], [10], [11]. These two categories can be further differentiated based on the availability of additional circuitry. The third category refers to over-the-air (OTA) methods in which BS transmits pilot signals to UEs and receives back properly precoded signals from UEs [6], [12] to facilitate non-reciprocity estimation.

In general, as shown in [10], [11], the channel non-reciprocity at the UE side does not have major impact on the system performance. Thus, in this work, we propose an OTA-based method to estimate the channel non-reciprocity due to BS side imperfections in multi-user massive MIMO systems. As novel contributions, we consider a massive MIMO system model which incorporates both FR mismatch and mutual coupling mismatches unlike many of the works that consider only FR mismatch such as [3], [4], [6], [10]–[12] or works that focus on more classical small scale MIMO systems [6], e.g., 2-4 BS antennas.

The paper is organized as follows. Fundamental effective channel non-reciprocity model is presented in Section II. In Section III, first a novel pilot signaling method between the BS and UEs is introduced. Then, we propose a novel BS side non-reciprocity matrix estimation method, building on the pilot-signaling and the

This work was supported by the Finnish Funding Agency for Technology and Innovation (Tekes) under the project “5th Evolution Take of Wireless Communication Networks (TAKE-5)”, by the Academy of Finland under the projects 284694 and 288670 and TUT Graduate School.

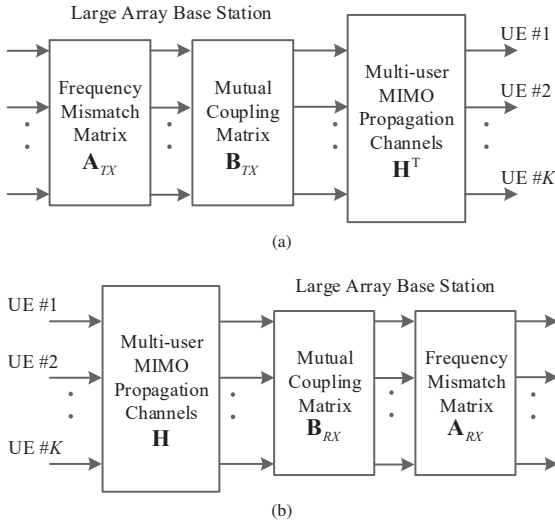


Fig. 1. Principal illustration of physical (a) DL and (b) UL transmissions and receptions including propagation channels, transceivers frequency responses and antenna mutual coupling in the BS.

associated system model sparsity characteristics. In Section IV, using the results of empirical performance evaluations, we evaluate and demonstrate the performance of our proposed channel non-reciprocity estimator in terms of normalized mean squared error (MSE) and compare it to the existing methods. Finally, conclusions are drawn in Section V.

Notations: We use upper-case (lower-case) bold letters to denote matrices (vectors), e.g., matrix \mathbf{X} and vector \mathbf{y} . The superscripts $(\cdot)^T$, $(\cdot)^*$, $(\cdot)^H$, and $(\cdot)^\dagger$ indicate transposition, complex-conjugation, Hermitian-transpose, and Moore-Penrose pseudo inverse operations, respectively. \mathbf{I}_n denotes the $n \times n$ identity matrix. Finally, we use $\mathcal{CN}(0, 1)$ to denote a circular-symmetric zero-mean unit-variance complex Gaussian distribution.

II. EFFECT OF TRANSCEIVER AND MUTUAL COUPLING MISMATCHES ON THE CHANNEL NON-RECIPROCITY

We consider a TDD based system and focus on a single cell with one BS and K single-antenna UEs, and carry out the basic modeling at an arbitrary OFDM(A) subcarrier. For notational simplicity, the subcarrier index is dropped and thus not explicitly shown. It is assumed that the BS is equipped with large number of antenna units, N , where $N \gg K$.

Owing to the assumed reciprocity of the physical channel in DL and UL transmissions in a TDD network, the BS forms DL precoders based on the estimated UL channel. This will lead to high beamforming gains and efficient spatial multiplexing capabilities in an ideal case where the effective DL and UL channels are assumed to be totally reciprocal. However, in practice, in addition to the reciprocal physical channel, the effective DL and UL channels also contain the hardware impacts of BS and UE sides. As mentioned earlier, in this work we focus only on the effects of BS transceivers and antenna array on the reciprocity of the effective channels as UE side transceiver non-reciprocity has

been shown to have negligible impact on the system performance [10], [11]. Thus, as shown in Fig. 1, the effective DL and UL channels at an arbitrary OFDM(A) subcarrier can be expressed as

$$\begin{aligned} \mathbf{H}_{DL} &= \mathbf{H}^T \mathbf{B}_{TX} \mathbf{A}_{TX} \\ \mathbf{H}_{UL} &= \mathbf{A}_{RX} \mathbf{B}_{RX} \mathbf{H}, \end{aligned} \quad (1)$$

where \mathbf{H} is the reciprocal physical multiuser MIMO channel, of size $N \times K$, and \mathbf{H}_{DL} and \mathbf{H}_{UL} are the corresponding effective DL and UL channels, respectively. In above, \mathbf{A} is a diagonal matrix and incorporates the BS frequency-response characteristics, \mathbf{B} is the antenna mutual coupling matrix of the BS, while the subscripts TX and RX denote the transmit and receive modes, respectively.

Based on (1), the relation between the effective DL and UL channels can be easily expressed as

$$\mathbf{H}_{DL} = \mathbf{H}_{UL}^T \mathbf{C}, \quad (2)$$

where the matrix \mathbf{C} is incorporating the overall transceiver non-reciprocity at the BS, and reads

$$\mathbf{C} = \mathbf{A}_{RX}^{-1} (\mathbf{B}_{RX}^T)^{-1} \mathbf{B}_{TX} \mathbf{A}_{TX}. \quad (3)$$

As can be seen in (2) and (3), due to the mismatches in BS hardware responses and mutual coupling between the transmitting and receiving modes, the effective DL and UL channels are not reciprocal. This phenomenon is referred to as channel non-reciprocity in literature [5], [6]. The fully reciprocal effective DL and UL channels is obtained as a special case in which $\mathbf{A}_{RX} = \mathbf{A}_{TX}$ and $\mathbf{B}_{RX} = \mathbf{B}_{TX}$, and thus $\mathbf{C} = \mathbf{I}_N$.

III. ESTIMATION OF BS TRANSCEIVER NON-RECIPROCITY

In order to retrieve the reciprocity of the effective DL and UL channels, the BS needs the knowledge of its overall non-reciprocity matrix \mathbf{C} . In practice, this information is not directly available to the BSs and thus needs to be estimated. In this respect, in this section, we present a novel method to estimate the BS transceiver non-reciprocity matrix building on simple pilot-signaling and the resulting sparsity of the corresponding signal model.

In general, the values of \mathbf{C} can be assumed to remain constant over many channel coherence intervals, since the channel non-reciprocity values vary very slowly compared to the variations in the propagation channel [12]. Therefore, as mentioned in [3], [10], there is no need to perform the BS transceiver non-reciprocity estimation frequently and it can be done, e.g. once in every 10 minutes or even once a day. This makes the system-level overhead of channel non-reciprocity estimation negligible, while offering the possibility for substantially improved system performance.

A. Pilot Signaling and Proposed Estimation Method

In order to estimate the BS transceiver non-reciprocity, we are proposing an OTA-based estimation approach which will allow us to have the information about the effective DL channel in BS. In this approach, the BS first transmits an $N \times N$ orthonormal pilot matrix called \mathbf{P} which yields

$$\mathbf{Y}_{UE} = \sqrt{\rho_d} \mathbf{H}_{DL} \mathbf{P} + \mathbf{N}_{UE} = \sqrt{\rho_d} \mathbf{H}_{UL}^T \mathbf{C} \mathbf{P} + \mathbf{N}_{UE}, \quad (4)$$

where \mathbf{Y}_{UE} collects the received pilot signals at UE side, $\sqrt{\rho_d}$ is the DL transmission signal to noise ratio (SNR), and \mathbf{N}_{UE} is a matrix of noise samples at UE receivers with $\mathcal{CN}(0, 1)$ i.i.d. elements.

Then, UEs conjugate their received signal samples and send them back in the UL phase to BS, which results into a received signal model of the form

$$\begin{aligned}\mathbf{Y}_{BS} &= \sqrt{\rho_u} \mathbf{H}_{UL} \mathbf{Y}_{UE}^* + \mathbf{N}_{BS} \\ &= \sqrt{\rho_u} \sqrt{\rho_d} \mathbf{H}_{UL} \mathbf{H}_{UL}^H \mathbf{C}^* \mathbf{P}^* + \mathbf{Q},\end{aligned}\quad (5)$$

where \mathbf{Y}_{BS} is the received signal matrix at BS, $\sqrt{\rho_u}$ is the UL transmission SNR, and \mathbf{N}_{BS} is the receiver noise matrix at BS with $\mathcal{CN}(0, 1)$ i.i.d. elements, while $\mathbf{Q} = \mathbf{H}_{UL} \mathbf{N}_{UE}^* + \mathbf{N}_{BS}$ incorporates the effects of noise sources in both DL and UL directions.

In the next step, the BS processes the received pilot signal samples as

$$\begin{aligned}\mathbf{R} &= \mathbf{Y}_{BS}^* \mathbf{P}^H \\ &= \sqrt{\rho_u} \sqrt{\rho_d} \mathbf{H}_{UL}^* \mathbf{H}_{UL}^T \mathbf{C} + \mathbf{Z},\end{aligned}\quad (6)$$

where \mathbf{R} is the processed overall signal and $\mathbf{Z} = \mathbf{Q}^* \mathbf{P}^H$ denotes the processed noise.

Assuming then that the BS has perfect UL CSI available, it can estimate its own transceiver non-reciprocity matrix as

$$\begin{aligned}\hat{\mathbf{C}} &= \underset{\mathbf{C}}{\operatorname{argmin}} \left\| \mathbf{R} - \sqrt{\rho_u} \sqrt{\rho_d} \mathbf{H}_{UL}^* \mathbf{H}_{UL}^T \mathbf{C} \right\|_F^2 \\ &= \underset{\mathbf{C}}{\operatorname{argmin}} \left\| \mathbf{R} - \mathbf{U} \mathbf{C} \right\|_F^2 = \underset{\mathbf{C}}{\operatorname{argmin}} \sum_{i=1}^K \left\| \mathbf{r}_i - \mathbf{U} \mathbf{c}_i \right\|^2,\end{aligned}\quad (7)$$

where $\mathbf{U} = \sqrt{\rho_u} \sqrt{\rho_d} \mathbf{H}_{UL}^* \mathbf{H}_{UL}^T$, \mathbf{r}_i and \mathbf{c}_i denote the i -th columns of \mathbf{R} and \mathbf{C} , respectively, while the subscript F shows the Frobenius norm. Since the i -th term in the summation is only depending on the i -th column of \mathbf{C} , the problem can be reformulated as

$$\hat{\mathbf{c}}_i = \underset{\mathbf{c}_i}{\operatorname{argmin}} \left\| \mathbf{r}_i - \mathbf{U} \mathbf{c}_i \right\|^2 \quad \forall i, \quad (8)$$

which means that estimating BS transceiver non-reciprocity matrix, as shown in (7), can be simplified to estimating each of its column independently.

As shown in (3), \mathbf{C} incorporates all the transceiver and antenna array mismatches, including both FR and antenna mutual coupling. Since the level of mutual coupling and its corresponding mismatch depends on the distance between the antennas, the power of off-diagonal entries decreases as the distance between two corresponding antenna elements grows. Therefore, if two antenna elements are far apart, the power of the corresponding element in \mathbf{C} is very low and its effect on the system performance is negligible. For that reason, we define a threshold for the distance between two antennas, called T , and try only to estimate the off-diagonal elements in \mathbf{C} which are corresponding to the antennas with distance T or less, assuming all the other elements are zero. This leads to having a sparse structure for \mathbf{C} and $\hat{\mathbf{C}}$ which clearly reduces the complexity of the BS non-reciprocity estimation process.

The index of the non-zero entries of \mathbf{C} can be determined by the BS antenna array geometry and architecture which are known to BS. Having the information regarding the sparse structure of BS transceiver non-reciprocity matrix, we define \mathbf{c}_i^{sp} which contains only the non-zero elements of \mathbf{c}_i . Similarly, we define \mathbf{U}_i^{sp} which contains only the columns with the same index as non-zero entries of \mathbf{c}_i , i.e., the j -th column of \mathbf{U} is kept only if j -th row of \mathbf{c}_i is kept while constructing \mathbf{c}_i^{sp} . Therefore, with the involved sparsity assumption, the estimation problem in (8) can be further simplified to

$$\hat{\mathbf{c}}_i^{sp} = \underset{\mathbf{c}_i^{sp}}{\operatorname{argmin}} \left\| \mathbf{r}_i - \mathbf{U}_i^{sp} \mathbf{c}_i^{sp} \right\|^2 \quad \forall i, \quad (9)$$

where the solution for $\hat{\mathbf{c}}_i^{sp}$ can be obtained as

$$\hat{\mathbf{c}}_i^{sp} = (\mathbf{U}_i^{sp})^\dagger \mathbf{r}_i. \quad (10)$$

Once the value of $\hat{\mathbf{c}}_i^{sp}$ is calculated, BS appends zeros to appropriate rows and obtains $\hat{\mathbf{c}}_i$.

B. Practical Considerations

In the proposed BS transceiver non-reciprocity estimation method, we assumed that the channel is fixed for the duration of pilot signaling which is $2N$ samples. The coherence time of the physical channel is mostly defined by the mobility of the UEs and is typically in the order of several milliseconds. Therefore, we essentially assume relatively low-mobility scenarios in which the channel coherence time is at least $2N$.

As mentioned earlier, all the derivations are for an arbitrary subcarrier of the underlying OFDM(A) radio access waveform. The transceiver responses and thus their mismatches can be modeled by very mildly frequency-selective transfer functions [6], and can be assumed to remain unchanged over a set of subcarriers M where typically $M \leq 10$, while depending on the frequency selectivity of the propagation channel, \mathbf{H}_{UL} can change from a subcarrier to another. Owing to that, in order to improve the estimation accuracy of the BS transceiver non-reciprocity characteristics, we take the average of calculated $\hat{\mathbf{C}}$ matrices over M subcarriers as

$$\hat{\mathbf{C}} = \frac{1}{M} \sum_{l=1}^M \hat{\mathbf{C}}_l, \quad (11)$$

where l denotes the subcarrier index inside one block of subcarriers over which the averaging is performed.

IV. NUMERICAL EVALUATIONS AND ANALYSIS

In this section, we evaluate the performance of the BS transceiver non-reciprocity estimation method proposed in Section III, using extensive computer simulations. The considered performance metric is the normalized MSE which is defined as

$$\Delta = \frac{\left\| \mathbf{C} - \hat{\mathbf{C}} \right\|_F^2}{\left\| \mathbf{C} \right\|_F^2}. \quad (12)$$

We also compare the performance of the proposed method to two other BS transceiver non-reciprocity estimation methods available in the existing literature, namely ‘‘Argos’’ [3] and ‘‘generalized neighbor least squares’’ [11], where the latter has already

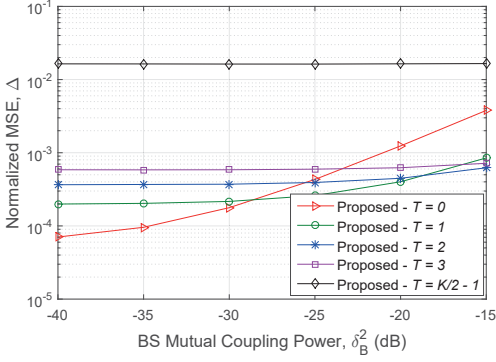


Fig. 2. BS transceiver non-reciprocity estimator's normalized MSE vs. δ_B^2 for $N = 100$, $K = 20$.

been shown to outperform several other BS non-reciprocity estimation methods available also in the literature [11] and will be called “GNELS” in the rest of the paper for notational simplicity.

A. Basic Simulation Settings

We consider a BS with linear array of infinitely thin $\lambda/2$ dipole antennas where $N = 100$, serving $K = 20$ single-antenna UEs simultaneously through spatial multiplexing. The UL channel \mathbf{H}_{UL} is assumed to have i.i.d. $\mathcal{CN}(0, 1)$ elements, for which multiple random realizations are drawn. The estimated BS transceiver non-reciprocity matrices are averaged over $M = 10$ subcarriers in the proposed method, while the values of \mathbf{C} are assumed to remain unchanged over those subcarriers. In the proposed method, the DL and UL SNRs for pilot signaling are assumed to be $\rho_d = 20$ dB and $\rho_u = 0$ dB, while for the other two reference methods, the SNR of the channel between two neighboring antennas is assumed to be 80 dB [11]. The operating frequency is chosen to be $f_c = 3.5$ GHz, based on which the BS input and the mutual impedances are computed as given in [13]. The detailed modeling of BS transceiver frequency responses and mutual couplings between antennas are based on [6], in which δ_A^2 denotes the variance of diagonal elements in \mathbf{A}_{TX} and \mathbf{A}_{RX} and is fixed to $\delta_A^2 = -20$ dB, while the power of elements in \mathbf{B}_{TX} and \mathbf{B}_{RX} is controlled by the reflection coefficient denoted here as δ_B^2 and here set to be $\delta_B^2 = -20$ dB. Throughout the simulations, the matrices \mathbf{A}_{TX} and \mathbf{A}_{RX} are chosen independently as well as the matrices \mathbf{B}_{TX} and \mathbf{B}_{RX} . These are the baseline values in all the simulations, but are also varied in the experiments as indicated in the result figures.

B. Obtained Numerical Results

As mentioned in Section III, the number of non-zero entries in each column of the estimated BS transceiver non-reciprocity matrix is depending on the sparsity threshold T . We define T as the antenna distance threshold relative to $\lambda/2$, which means that the coupling mismatch due to any two antennas with the distance greater than $T \times \lambda/2$ is assumed to be zero in the proposed BS transceiver non-reciprocity estimation method. In

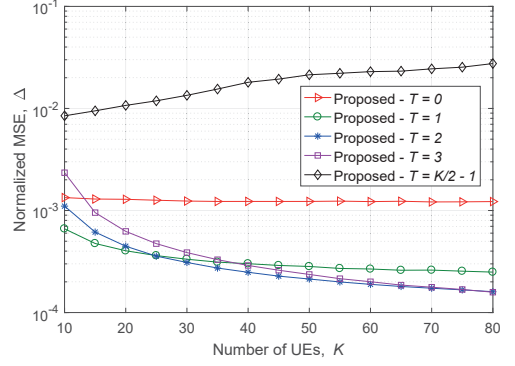


Fig. 3. BS transceiver non-reciprocity estimator's normalized MSE vs. number of UEs (K) for $N = 100$, $\delta_B^2 = -20$ dB.

order to find the optimum value of T for different scenarios, in Fig. 2, the effect of T on normalized MSE of BS transceiver non-reciprocity estimation is evaluated against various levels of δ_B^2 which controls the power of mutual coupling between the BS antennas. As can be seen, for low BS antenna mutual coupling power, say $\delta_B^2 \leq -30$ dB, $T = 0$ which corresponds to a purely diagonal estimation of BS transceiver non-reciprocity matrix produces the best result, whereas $T = 1$ has better performance in the cases where the power of antenna mutual coupling is moderate, say -20 dB $\geq \delta_B^2 > -30$ dB, and finally $T = 2$ is the best option if mutual coupling level is high, $\delta_B^2 > -20$ dB.

The effect of the number of scheduled UEs K on the performance of the proposed BS transceiver non-reciprocity estimation method is examined in Fig. 3. The results show that the normalized MSE of the proposed estimation method decreases as K grows. The reason is that the column space of \mathbf{U}_i^{sp} in (10) has higher dimensionality for larger values of K , since $\mathbf{H}_{UL}^* \mathbf{H}_{UL}^T$ in \mathbf{U} is positive semi-definite matrix and of rank K if \mathbf{H}_{UL} is of rank K . Fig. 3 also shows that when the number of scheduled UEs grows, say $K \geq 25$, the optimum value for sparsity distance increases, from $T = 1$ to $T = 2$.

Fig. 4 shows the comparison between the proposed estimation method and the two other methods with respect to the impact of the power of BS antenna mutual coupling on the normalized MSEs. As can be seen, Argos has the worst performance, while for low levels of BS antenna mutual coupling power GNELS method which only estimates the diagonal elements of \mathbf{C} is the best option. However, as the power of BS antenna mutual coupling grows the difference between the proposed method and GNELS method gets lower. From moderately low levels of BS antenna mutual coupling, say $\delta_B^2 > -27$ dB, the proposed method is outperforming all the other methods, since contrary to other two methods, it has the ability to estimate the off-diagonal elements of BS transceiver non-reciprocity matrix.

Fig. 5 compares the effect of the number of scheduled UEs on the normalized MSEs for all the considered BS transceiver non-reciprocity estimation methods. As can be seen, even for the lowest number of scheduled UEs $K = 10$, the proposed estima-

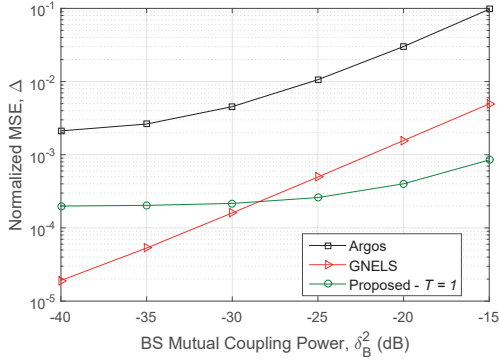


Fig. 4. BS transceiver non-reciprocity estimator's normalized MSE vs. δ_B^2 for $N = 100$, $K = 20$.

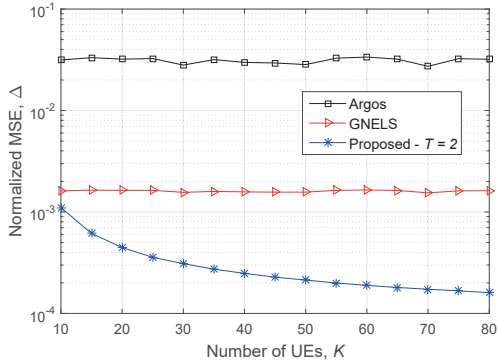


Fig. 5. BS transceiver non-reciprocity estimator's normalized MSE vs. number of UEs (K) for $N = 100$, $\delta_B^2 = -20$ dB.

tion method outperforms Argos and GNELS reference methods. The difference between the performance of the proposed method and the other two methods increases as K grows, up to the case of $K = 70$ where the accuracy of the proposed method is already around 10 times better than that of the GNELS method. The reason is that while increasing K does not have any effect on the performance of the other two estimation methods, as mentioned earlier it improves the accuracy of the proposed method as the rank of $\mathbf{H}_{UL}^* \mathbf{H}_{UL}^T$ in \mathbf{U} grows.

The estimation accuracy of the proposed method depicted in Fig. 4 and Fig. 5 can be improved when compared to two other methods, by adaptively selecting the optimum value of T according to the results shown in Fig. 2 and Fig. 3, respectively.

Overall, owing to the sparse nature of the BS transceiver non-reciprocity matrix \mathbf{C} , the proposed BS non-reciprocity estimation method outperforms other methods for moderate to high levels of BS mutual coupling power and/or higher numbers of scheduled UEs K as it can estimate off-diagonal entries of \mathbf{C} with high accuracy.

V. CONCLUSION

This paper proposed an efficient channel non-reciprocity estimation framework for fully capitalizing the channel reciprocity benefits in TDD massive MIMO networks with non-reciprocal transceiver and antenna array hardware. Based on the provided channel non-reciprocity model, it was first shown that the effective DL channel is the product of the effective UL channel and a sparse matrix which incorporates the effects of both transceiver FR and antenna array mutual coupling mismatches at BS. Then, exploiting the sparse nature of the BS transceiver non-reciprocity matrix, a novel OTA-based BS non-reciprocity estimation method with reasonable pilot overhead was proposed. The comprehensive computer simulations show the superiority of the proposed estimation method compared to two other well-known existing methods for practical levels of BS antenna mutual coupling power. It was also shown that the accuracy of the proposed channel non-reciprocity estimation method improves as the number of scheduled UEs in the system grows.

REFERENCES

- [1] F. Boccardi, R. W. Heath, A. Lozano, T. L. Marzetta, and P. Popovski, "Five disruptive technology directions for 5G," *IEEE Communications Magazine*, vol. 52, no. 2, pp. 74–80, February 2014.
- [2] E. G. Larsson, O. Edfors, F. Tufvesson, and T. L. Marzetta, "Massive MIMO for next generation wireless systems," *IEEE Communications Magazine*, vol. 52, no. 2, pp. 186–195, February 2014.
- [3] C. Shepard, H. Yu, N. Anand, E. Li, T. Marzetta, R. Yang, and L. Zhong, "Argos: Practical many-antenna base stations," in *Proceedings of the 18th Annual International Conference on Mobile Computing and Networking*, ser. Mobicom '12. New York, NY, USA: ACM, 2012, pp. 53–64.
- [4] A. Bourdoux, B. Come, and N. Khaled, "Non-reciprocal transceivers in OFDM/SDMA systems: Impact and mitigation," in *Radio and Wireless Conference, 2003. RAWCON '03. Proceedings*, Aug 2003, pp. 183–186.
- [5] Y. Zou, O. Raeesi, R. Wichman, A. Tolli, and M. Valkama, "Analysis of channel non-reciprocity due to transceiver and antenna coupling mismatches in TDD precoded multi-user MIMO-OFDM downlink," in *2014 IEEE 80th Vehicular Technology Conference (VTC2014-Fall)*, Sept 2014, pp. 1–7.
- [6] M. Petermann, M. Stefer, F. Ludwig, D. Wubben, M. Schneider, S. Paul, and K. D. Kammeyer, "Multi-user pre-processing in multi-antenna OFDM TDD systems with non-reciprocal transceivers," *IEEE Transactions on Communications*, vol. 61, no. 9, pp. 3781–3793, September 2013.
- [7] H. Wei, D. Wang, and X. You, "Reciprocity of mutual coupling for TDD massive MIMO systems," in *Wireless Communications Signal Processing (WCSP), 2015 International Conference on*, Oct 2015, pp. 1–5.
- [8] W. Zhang, H. Ren, C. Pan, M. Chen, R. C. de Lamare, B. Du, and J. Dai, "Large-scale antenna systems with UL/DL hardware mismatch: Achievable rates analysis and calibration," *IEEE Transactions on Communications*, vol. 63, no. 4, pp. 1216–1229, April 2015.
- [9] F. Athley, G. Durisi, and U. Gustavsson, "Analysis of massive MIMO with hardware impairments and different channel models," in *2015 9th European Conference on Antennas and Propagation (EuCAP)*, May 2015, pp. 1–5.
- [10] R. Rogalin, O. Y. Bursalioglu, H. Papadopoulos, G. Caire, A. F. Molisch, A. Michaloliakos, V. Balan, and K. Psounis, "Scalable synchronization and reciprocity calibration for distributed multiuser MIMO," *IEEE Transactions on Wireless Communications*, vol. 13, no. 4, pp. 1815–1831, April 2014.
- [11] J. Vieira, F. Rusek, and F. Tufvesson, "Reciprocity calibration methods for massive MIMO based on antenna coupling," in *2014 IEEE Global Communications Conference*, Dec 2014, pp. 3708–3712.
- [12] M. Guillaud, D. T. M. Slock, and R. Knopp, "A practical method for wireless channel reciprocity exploitation through relative calibration," in *Proceedings of the Eighth International Symposium on Signal Processing and Its Applications*, 2005., vol. 1, August 2005, pp. 403–406.
- [13] S. A. Schelkunoff and H. T. Friis, *Antennas Theory and Practice*. New York: John Wiley & Sons, 1952.

PUBLICATION VI

O. Raeesi, Y. Zou, A. Tölli, and M. Valkama, “On the effects of UE transceiver non-reciprocity in coordinated TDD multi-cell MIMO network,” in *2015 IEEE Global Communications Conference (GLOBECOM)*, Dec 2015, pp. 1–7.

© 2015 IEEE. Reprinted, with permission, from O. Raeesi, Y. Zou, A. Tölli, and M. Valkama, “On the effects of UE transceiver non-reciprocity in coordinated TDD multi-cell MIMO network,” in *2015 IEEE Global Communications Conference (GLOBECOM)*, December 2015.

In reference to IEEE copyrighted material which is used with permission in this thesis, the IEEE does not endorse any of Tampere University’s products or services. Internal or personal use of this material is permitted. If interested in reprinting/republishing IEEE copyrighted material for advertising or promotional purposes or for creating new collective works for resale or redistribution, please go to http://www.ieee.org/publications_standards/publications/rights/rights_link.html to learn how to obtain a License from RightsLink.

On the Effects of UE Transceiver Non-Reciprocity in Coordinated TDD Multi-Cell MIMO Network

Orod Raeesi¹, Yaning Zou¹, Antti Tölli² and Mikko Valkama¹

¹Department of Electronics and Communications Engineering, Tampere University of Technology, Tampere, FINLAND

²Department of Communications Engineering, University of Oulu, Oulu, FINLAND

Emails: orod.raeesi@tut.fi, yaning.zou@tut.fi, mikko.e.valkama@tut.fi, antti.tolli@ee.oulu.fi

Abstract— In this paper, we study the effects of effective channel non-reciprocity in coordinated TDD multi-cell MIMO network based on weighted sum rate (WSR) maximization. More specifically, we focus on UE transceiver non-reciprocity while the base stations (BS) are assumed to be perfectly calibrated, and both centralized and decentralized beamforming schemes are considered. In the centralized scheme, the cost function is constructed in a central controller using antenna specific UL pilots for channel estimation from all the connected BSs in the network. Then, even though the transceiver frequency response (FR) mismatches at the UE side corrupt the effective channel reciprocity, it is shown to have only a trivial impact on the WSR objective in such centralized case. However, when *decentralized beamforming* is deployed, the optimization is carried out in each BS and the corresponding cost function and optimization process depend on information acquired by over-the-air signaling between the BSs and all the users using precoded UL pilots. In this case, it is then shown that the *transceiver FR mismatches at the UE side can cause severe performance degradation* and even influence the convergence properties of the sum-rate optimization process. Further insight is provided for improving the performance by modifying the weight calculations in the optimization process and connecting users with good cell separations. Then a convergence-aware processing algorithm is also proposed to improve the performance of the decentralized scheme under UE transceiver non-reciprocity. Numerical experiments demonstrate that efficient processing algorithms for calibrating UE transceiver mismatches to be less than -30dB to -35dB are, in general, required in the decentralized system in order to achieve performance close to the ideal case without any RF imperfections.

Keywords—centralized beamforming, channel reciprocity, decentralized beamforming, multi-cell MIMO, precoding, time-division duplexing, transceiver frequency response mismatch.

I. INTRODUCTION

As one promising approach to improve network spectral efficiency, the coordinated multi-cell MIMO transmission concept has attracted lots of research interests in both academy and industry [1], [2]. By coordinating multiple BSs for achieving optimal overall network performance, it provides good frequency usage among neighboring cells and/or base-stations (BSs) and is especially suitable for the development of advanced small cell systems. In theory, a central controller can be deployed to collect downlink (DL) channel state information (CSI) from all the connected BSs via low-latency backhaul, compute optimal precoder

for each transmitted stream based on, e.g., weighted sum-rate (WSR) maximization, and then distribute precoder information to the BSs that transmit the corresponding streams [3]–[6]. However, in many scenarios, the central controller and the large amount of needed low-latency backhaul resources may not be available or feasible. Decentralized beamforming is then proposed, as an alternative, to enable multi-cell transmission where the optimization task is shifted from the central controller to each BS [7].

In both centralized and decentralized beamforming schemes, *acquisition of precise DL channel state information at the transmitter side (CSIT) is a very critical task* for the precoder optimization process. In time-division duplex (TDD) based networks, assuming TDD channel reciprocity within coherence time, the CSIT at the BS can be conveniently acquired via uplink (UL) channel estimation using antenna specific pilots. In practice, however, as discussed in [8]–[10], and reference therein, the TDD channel reciprocity is destroyed by the so-called *transceiver non-reciprocity problem* at both the BS and the UE sides. In general, the transceiver non-reciprocity stems from frequency-response (FR) mismatches between the transmitter and receiver chains implemented in the same transceiver. In the literature, the impacts of transceiver FR mismatches on basic multi-user (MU) MIMO transmission systems have been extensively studied with zero-forcing precoding [9], [10]. It has been shown that the transceiver non-reciprocity at the BS side is the major problem while the FR mismatches in the UE transceivers can be easily mitigated as a part of precoded channel matrix. This is a useful observation as reciprocity calibration is then only needed at the BS side which has more implementation resources than UEs. It thus imposes no additional cost at the UE side even when its own transceiver implementation is not perfectly reciprocal.

In the coordinated TDD multi-cell MIMO network, however, the construction of precoders requires more sophisticated processing than, e.g., simple zero-forcing precoding or eigen-beamforming. More specifically, dedicated signaling exchange between the BSs and connected UEs in the decentralized beamforming is needed as described in [7]. UE transceiver non-reciprocity will then potentially influence the over-the-air signaling process. To the best of our knowledge, there is no previous work addressing such UE transceiver non-reciprocity problem in the multi-cell MIMO network context. This is the leading theme of this paper.

In this paper, we investigate the impact of transceiver FR mismatches at the UE side on the performance of both centralized and decentralized beamforming in coordinated TDD multi-cell MIMO network. To this end, we analyze the effects of UE transceiver non-

This work was supported by the Finnish Funding Agency for Technology and Innovation (Tekes), Broadcom Communications Finland and Huawei Finland under the project “Energy-Efficient Wireless Networks and Connectivity of Devices – Densification (EWINE-D)”, the Academy of Finland under the projects 251138, 138424, 284694 and 288670, the Foundation of Nokia Corporation and TUT Graduate School.

reciprocity on the constructed cost function for optimization process in the coordinated beamforming. We assume that the CSI acquisition is carried out using antenna specific and precoded UL pilots for centralized and decentralized schemes, respectively [7]. The analysis shows that the UE transceiver non-reciprocity has only minimal impact on the performance of centralized beamforming while it results in severe performance degradation in the decentralized beamforming case. Based on the developed analysis and extensive computer simulations, further insight is provided for improving the performance of decentralized beamforming. A simple convergence aware processing algorithm is proposed to cope with convergence problem under non-reciprocity and thus improve the network performance. In general, the obtained results also motivate towards developing efficient non-reciprocity calibration algorithms at the UE side for achieving ideal network performance with imperfect UE transceivers.

The rest of the paper is organized as follows. Section II outlines the fundamental coordinated multi-cell MIMO downlink transmission system model as well as basic ideas of centralized and decentralized beamforming. The DL-UL channel relation under UE transceiver non-reciprocity is then formulated in Section III. In Section IV, the impact of transceiver FR mismatch at the UE side on coordinated multi-cell MIMO downlink transmission is studied. Section V provides numerical evaluations and illustrations while conclusions are drawn in Section VI.

II. COORDINATED MULTI-CELL MIMO DL TRANSMISSION BASED ON WEIGHTED SUM-RATE MAXIMIZATION

A. Multi-cell MIMO DL Transmission

In this paper, we consider a TDD multi-cell MIMO network with N_b BSs. Each BS is equipped with N_T antennas and K users are served at the same time-frequency resource. Each user device has N_R antennas and the k -th user is associated to only one BS in the network, i.e., BS b_k , $k = 1, \dots, K$. At the BS side, M_k streams are allocated to the k -th user where the m_k -th transmitted stream is denoted as s_{k,m_k} and the average power of each data streams is normalized to unity. In total, $M_{\text{tot}} = \sum_{k=1}^K M_k$ data streams are transmitted in the network. The DL MIMO channel matrix between BS b_j and k -th user is denoted by $\mathbf{H}_{j,k} \in \mathbb{C}^{N_R \times N_T}$ and $j = 1, \dots, N_b$.

In the DL transmission, the m_k -th stream of user k is first precoded with precoder \mathbf{u}_{k,m_k} at the BS b_k for all $m_k = 1, \dots, M_k$ and $k = 1, \dots, K$, and then transmitted simultaneously to all the users in the network. At the k -th user reception, after applying a minimum mean-square error (MMSE) receiver \mathbf{w}_{k,m_k}^H on the received signal for extracting the m_k -th stream, we have

$$y_{k,m_k} = \mathbf{w}_{k,m_k}^H \mathbf{H}_{b_k,k} \mathbf{u}_{k,m_k} s_{k,m_k} + \sum_{i=1}^K \sum_{\substack{m_i=1 \\ (i \neq k, m_i \neq m_k)}}^{M_i} \mathbf{w}_{k,m_k}^H \mathbf{H}_{b_i,k} \mathbf{u}_{i,m_i} s_{i,m_i} + \mathbf{w}_{k,m_k}^H \mathbf{n}_k \quad (1)$$

and the MMSE receiver reads

$$\mathbf{w}_{k,m_k} = \mathbf{R}_k^{-1} \mathbf{H}_{b_k,k} \mathbf{u}_{k,m_k} \quad (2)$$

where \mathbf{R}_k denotes covariance matrix at the k -th user reception and is given by

$$\mathbf{R}_k = \left(\sum_{i=1}^K \sum_{m_i=1}^{M_i} \mathbf{H}_{b_i,k} \mathbf{u}_{i,m_i} \mathbf{u}_{i,m_i}^H \mathbf{H}_{b_i,k}^H + \sigma_n^2 \mathbf{I} \right) \quad (3)$$

while σ_n^2 refers to the noise power.

If we consider $\mathbf{w}_{k,m_k}^H \mathbf{H}_{b_k,k} \mathbf{u}_{k,m_k} s_{k,m_k}$ as the desired signal and the second term in (1) as interference, the resulting signal-to-interference-plus-noise ratio (SINR) can be expressed as

$$\text{SINR}_{k,m_k} = \frac{|\mathbf{w}_{k,m_k}^H \mathbf{H}_{b_k,k} \mathbf{u}_{k,m_k}|^2}{\sum_{i=1}^K \sum_{\substack{m_i=1 \\ (i \neq k, j \neq m_k)}}^{M_i} |\mathbf{w}_{k,m_k}^H \mathbf{H}_{b_i,k} \mathbf{u}_{i,m_i}|^2 + \|\mathbf{w}_{k,m_k}^H\|^2 \sigma_n^2} \quad (4)$$

Meanwhile, using the optimum MMSE receiver, we can also calculate the minimum mean-square error (MSE) for receiving the m_k -th stream of the k -th user as

$$\begin{aligned} \varepsilon_{k,m_k} &= 1 - 2 \text{Re} \left(\mathbf{w}_{k,m_k}^H \mathbf{H}_{b_k,k} \mathbf{u}_{k,m_k} \right) \\ &+ \sum_{i=1}^K \sum_{m_i=1}^{M_i} |\mathbf{w}_{k,m_k}^H \mathbf{H}_{b_i,k} \mathbf{u}_{i,m_i}|^2 + \|\mathbf{w}_{k,m_k}^H\|^2 \sigma_n^2 \\ &= 1 - \mathbf{w}_{k,m_k}^H \mathbf{H}_{b_k,k} \mathbf{u}_{k,m_k} \\ &= \frac{1}{1 + \text{SINR}_{k,m_k}} \end{aligned} \quad (5)$$

B. Centralized Beamforming

In order to achieve optimal network performance in the considered multi-cell network, a central controller is adopted to collect CSI between all the connected BSs and all the serving UEs, denoted by $\mathbf{H}_{j,k}$ for $j = 1, \dots, N_b$ and $k = 1, \dots, K$, and obtained via UL channel estimation using antenna specific pilots. Network-level weighted sum-rate maximization is then carried out at the central controller to find the optimal precoder and decoder set $\{\mathbf{u}_{k,m_k}\}$ and $\{\mathbf{w}_{k,m_k}\}$, for $m_k = 1, \dots, M_k$ and $k = 1, \dots, K$. Using the relation between the rate and MSE per stream, $R_{k,m_k} = \log_2(1 + \text{SINR}_{k,m_k}) = -\log_2(\varepsilon_{k,m_k})$, WSR maximization can be formulated as the equivalent log-MSE minimization problem under per-BS power constraint as

$$\begin{aligned} \min_{\mathbf{u}_{k,m_k}, \mathbf{w}_{k,m_k}} \quad & \sum_{k=1}^K \sum_{m_k=1}^{M_k} \mu_k \log_2(\varepsilon_{k,m_k}) \\ \text{s. t.} \quad & \sum_{k=1, b_k=b}^{K} \sum_{m_k=1}^{M_i} \|\mathbf{u}_{k,m_k}\|^2 \leq \mathcal{P} \quad \forall b \end{aligned} \quad (6)$$

where μ_k is the weight indicating the scheduling priority of the k -th user. As described in [4]-[7], finding optimal precoder and decoder set based on (6) is generally a non-convex problem that is hard to be solved in a reasonable time. For practical network implementation, several algorithms have been proposed to find suboptimal precoder set via iterative processing [4]-[7].

C. Decentralized Beamforming

In many scenarios, a central controller is not available and/or there are very limited low-latency backhaul resources in the network. Decentralized beamforming can then be deployed to maximize network sum-rate via optimization carried out at each BS as shown in [7]. This is achieved by decomposing network-level cost function in (6) into different parts that are contributed by individual BSs. Together with using different UE-BS signaling

strategies, the cost function for local optimization can be constructed at each BS. In addition, as described in [7] and reference therein, for achieving optimal linear receiver processing, it is sufficient to obtain optimal precoders from the set that diagonalizes all the MMSE matrices without any loss in WSR or breach of power constraints. Thus, with given receiver filter, precoder optimization process can then be carried out in each BS independently as

$$\min_{\mathbf{u}_{k,m_k}} \varepsilon_b \quad \text{s.t.} \sum_{k=1, b_k=b}^K \sum_{m_k=1}^{M_k} \|\mathbf{u}_{k,m_k}\|^2 \leq \mathcal{P} \quad \forall b, \quad (7)$$

where ε_b is the cost function at BS b .

As shown in [7], the decentralized beamforming can achieve similar performance as the centralized beamforming. Here, for understanding the effects of UE transceiver non-reciprocity, we briefly describe following two strategies proposed in [7].

1) *Strategy A : Network-wide iterations with busy bursts*

As shown in [7], it is possible to decouple contribution of BS b to the network-level cost function in (6) as

$$\begin{aligned} \varepsilon_b^A = & -2 \sum_{k=1, b_k=b}^K \sum_{m_k=1}^{M_k} \text{Re} \left\{ \left(p_{k,m_k} \mathbf{w}_{k,m_k}^H \mathbf{H}_{b_k,k} \mathbf{u}_{k,m_k} \right) \right\} \\ & + \sum_{k=1}^K \sum_{m_k=1}^{M_k} \sum_{k'=1}^K \sum_{m'_k=1}^{M'_k} p_{k',m'_k} \left| \mathbf{w}_{k,m_k}^H \mathbf{H}_{b_k,k} \mathbf{u}_{k',m'_k} \right|^2 \end{aligned} \quad (8)$$

where b_k refers to the BS which serves k -th UE. The second term in (8) contains all the signal and interference power generated by the BS b .

In order to evaluate (8), the BS b needs to know MMSE receivers of all the UEs as well as the DL channels $\mathbf{H}_{b,k}$ to all the UEs in the network. One efficient way to acquire this information is proposed in [7]. To this end, with given precoders, each UE calculates its own MMSE receiver as in (2) and then precodes the pilots with this MMSE receiver. The precoded pilots are denoted as busy bursts. At the BS b , the equivalent channels $\mathbf{w}_{k,m_k}^H \mathbf{H}_{b_k,k}$, for $k = 1, \dots, K$ and $m_k = 1, \dots, M_k$, are then estimated from the precoded pilots. For each stream, a weight value p_{k,m_k} is also¹ calculated as $p_{k,m_k} = \varepsilon_{k,m_k}^{-1} = \left(1 - \mathbf{w}_{k,m_k}^H \mathbf{H}_{b_k,k} \mathbf{u}_{k,m_k} \right)^{-1}$ at BS b_k based on (5). If $b_k \neq b$, the information on p_{k,m_k} is sent from BS b_k to BS b via backhaul [7]. After repeating the above-mentioned procedures until convergence for BS $b = 1, \dots, N_b$, suboptimal precoder sets can be found with little coordination between BSs.

However, the above strategy A may require a large number of over-the-air adaptation steps and hence slow convergence. This is due to the fact that the MMSE receiver update is only sent for one precoder update step in one BS at a time. In the following, another strategy is introduced which allows each BS locally iterate over the transmitters and receivers of its own cell and thus improve the overall convergence speed.

2) *Strategy B: Cell-specific iterations with separate busy bursts and channel sounding*

As described in [7], instead of sending MMSE receiver at each UE, this strategy precodes channel sounding pilot transmission from k -th UE with whitening filter \mathbf{Q}_k that intends to whiten inter-cell interference and noise at the k -th user reception as

$$\mathbf{Q}_k^H \mathbf{Q}_k = \bar{\mathbf{R}}_k^{-1} \quad (9)$$

where $\bar{\mathbf{R}}_k$ refers to the covariance matrix of inter-cell interference and noise observed at the k -th user and is defined as

$$\bar{\mathbf{R}}_k = \sum_{i=1, b_i \neq b_k}^K \sum_{m_i=1}^{M_i} \mathbf{H}_{b_k,i} \mathbf{u}_{i,m_i} \mathbf{u}_{i,m_i}^H \mathbf{H}_{b_k,i}^H + \sigma_n^2 \mathbf{I} \quad (10)$$

with given precoders. After passing through UL channels from the k -th user to BS b_k the following knowledge can be obtained at the BS b_k given by

$$\mathbf{G}_{b_k,k} = \mathbf{Q}_k \mathbf{H}_{b_k,k} \quad (11)$$

With given precoders, the MMSE receiver for receiving the m_k -th stream of the k -th user can be also evaluated at the BS b_k as

$$\bar{\mathbf{w}}_{k,m_k} = \left(\sum_{i=1, b_i=b_k}^K \sum_{m_i=1}^{M_i} \mathbf{G}_{b_k,i} \mathbf{u}_{i,m_i} \mathbf{u}_{i,m_i}^H \mathbf{G}_{b_k,i}^H + \mathbf{I} \right)^{-1} \mathbf{G}_{b_k,k} \mathbf{u}_{k,m_k} \quad (12)$$

and based on (9)-(12), we can obtain the MMSE precoded equivalent channels again as

$$\bar{\mathbf{w}}_{k,m_k}^H \mathbf{G}_{b_k,k} = \mathbf{w}_{k,m_k}^H \mathbf{H}_{b_k,k} \quad (13)$$

Next, as shown in [7], the cost function for WSR maximization at the BS b reads

$$\begin{aligned} \varepsilon_b^B = & \sum_{k=1, b_k=b}^K \left\{ \bar{p}_k - 2 \sum_{m_k=1}^{M_k} \text{Re} \left(p_{k,m_k} \bar{\mathbf{w}}_{k,m_k}^H \mathbf{G}_{b_k,k} \mathbf{u}_{k,m_k} \right) \right. \\ & + p_{k,m_k} \sum_{m_k=1}^{M_k} \bar{\mathbf{w}}_{k,m_k}^H \left[\mathbf{G}_{b_k,k} \mathbf{u}_{k,m_k} \left(\mathbf{G}_{b_k,k} \mathbf{u}_{k,m_k} \right)^H + \mathbf{I} \right] \bar{\mathbf{w}}_{k,m_k} \left. \right\} \\ & + \sum_{k'=1, b_{k'} \neq b}^K \sum_{m'_k=1}^{M'_k} \sum_{k=1, b_k=b}^K \sum_{m_k=1}^{M_k} p_{k',m'_k} \left| \mathbf{w}_{k',m'_k}^H \mathbf{H}_{b,k} \mathbf{u}_{k,m_k} \right|^2 \\ = & \sum_{k=1, b_k=b}^K \left(\bar{p}_k - \sum_{m_k=1}^{M_k} p_{k,m_k} \mathbf{u}_{k,m_k}^H \mathbf{H}_{b_k,k}^H \bar{\mathbf{R}}_k^{-1} \mathbf{H}_{b_k,k} \mathbf{u}_{k,m_k} \right) + \text{INT}_b \end{aligned} \quad (14)$$

where

$$\begin{aligned} \bar{\mathbf{R}}_k = & \left(\sum_{i=1, b_i=b_k}^K \sum_{m_i=1}^{M_i} \mathbf{H}_{b_k,i} \mathbf{u}_{i,m_i} \mathbf{u}_{i,m_i}^H \mathbf{H}_{b_k,i}^H + \bar{\mathbf{R}}_k \right) \\ \text{INT}_b = & \sum_{k'=1, b_{k'} \neq b}^K \sum_{m'_k=1}^{M'_k} \sum_{k=1, b_k=b}^K \sum_{m_k=1}^{M_k} p_{k',m'_k} \left| \mathbf{w}_{k',m'_k}^H \mathbf{H}_{b,k} \mathbf{u}_{k,m_k} \right|^2 \end{aligned}$$

$\bar{p}_k = \text{Tr}(\mathbf{P}_k - \log \det \mathbf{P}_k)$ and $\mathbf{P}_k = \text{diag}\{p_{k,1}, \dots, p_{k,M_k}\}$. The term INT_b in (14) represents inter-cell interference seen by the BS b . In order to evaluate INT_b , we need information from other cells as well. For this purpose, each UE calculates also MMSE receivers \mathbf{w}_{k,m_k} and their weights $p_{k,m_k} = \varepsilon_{k,m_k}^{-1}$ and broadcasts $\varepsilon_{k,m_k}^{-1/2} \mathbf{w}_{k,m_k}$ to be used by the interfering BSs. For streams served at BS b , the corresponding weights are calculated at BS b as $p_{k,m_k} = \varepsilon_{k,m_k}^{-1} = \left(1 - \bar{\mathbf{w}}_{k,m_k}^H \mathbf{G}_{b_k,k} \mathbf{u}_{k,m_k} \right)^{-1}$ stemming from (5). Then the suboptimal precoders can be calculated based on the constructed cost function (14) for BS b via in-cell and over-the-air iteration process using (7) as described in more details in [7].

III. IMPACTS OF TRANSCIVER NON-RECIPROCITY ON TDD CHANNEL RECIPROCITY

As elaborated in Section II, UL channel estimation and/or UL signaling are needed to construct the cost functions defined in (6) and (7) at the BS. This is based on the TDD channel reciprocity assumption implying that the UL channel matrix is the transposed version of DL channel matrix within coherence time. However, due to the FR mismatches between transmitter and receiver implemented in the same transceiver, even with perfect channel estimation and without any additive noise, the effective DL and UL channels are not reciprocal. As discussed in [9], [10], and reference therein, the channel non-reciprocity model between BS b_j and k -th user can be formulated as

$$\hat{\mathbf{H}}_{b_j,k}^{\text{DL}} = \left(\hat{\mathbf{H}}_{b_j,k}^{\text{UL}} \right)^T = \mathbf{A}_k \mathbf{H}_{b_j,k}^{\text{DL}} \mathbf{A}_{b_j} \quad (15)$$

where $\hat{\mathbf{H}}_{b_j,k}^{\text{DL}}$, $\hat{\mathbf{H}}_{b_j,k}^{\text{UL}}$ and $\mathbf{H}_{b_j,k}^{\text{DL}}$ refer to the estimated DL channel, effective UL channel and effective DL channel between BS b_j and k -th user, respectively. \mathbf{A}_k and \mathbf{A}_{b_j} are diagonal matrices which represent the FR mismatches at the UE and BS sides, respectively. Here we focus only on FR mismatches at the UE side. Thus assuming perfect reciprocity calibration at the BS, the non-reciprocity model in (15) reads

$$\hat{\mathbf{H}}_{b_j,k}^{\text{DL}} = \mathbf{A}_k \mathbf{H}_{b_j,k}^{\text{DL}} \quad (16)$$

The FR mismatch matrix \mathbf{A}_k can also be rewritten as $\mathbf{A}_k = \mathbf{I} + \mathbf{A}'_k$, where all the diagonal entries of \mathbf{A}'_k are assumed to be zero-mean complex Gaussian random variables with variance equal to $\delta_{\mathbf{A}_k}^2$. The effective DL and UL channels are fully reciprocal when we have $\delta_{\mathbf{A}_k}^2 = 0$.

IV. EFFECTS OF UE TRANSCIVER NON-RECIPROCITY IN COORDINATED MULTI-CELL MIMO NETWORK

In this section, we analyze the effects of UE transceiver non-reciprocity in the considered coordinated multi-cell MIMO network described in Section II, deploying the non-reciprocity models reported in Section III.

A. Effects in Centralized Beamforming

In centralized beamforming, the acquired DL channel matrices between all the connected BSs and all the serving UEs are contaminated by the UE transceiver non-reciprocity as $\hat{\mathbf{H}}_{j,k}^{\text{DL}} = \mathbf{A}_k \mathbf{H}_{j,k}^{\text{DL}}$ for $j = 1, \dots, N_b$ and $k = 1, \dots, K$. Incorporating such contaminated channel knowledge in (2) and (5), with given precoders, the MMSE receiver and cost function read

$$\begin{aligned} \hat{\mathbf{w}}_{k,m_k} &= \left(\sum_{i=1}^K \sum_{m_j=1}^{M_i} \hat{\mathbf{H}}_{b_i,k} \mathbf{u}_{i,m_i} \mathbf{u}_{i,m_i}^H \hat{\mathbf{H}}_{b_i,k}^H + \sigma_n^2 \mathbf{I} \right)^{-1} \hat{\mathbf{H}}_{b_k,k} \mathbf{u}_{k,m_k} \\ &= \mathbf{A}_k^{-H} \mathbf{R}_k'^{-1} \mathbf{H}_{b_k,k} \mathbf{u}_{k,m_k} \\ \hat{\varepsilon}_{k,m_k} &= 1 - 2 \operatorname{Re} \left(\hat{\mathbf{w}}_{k,m_k}^H \hat{\mathbf{H}}_{b_k,k} \mathbf{u}_{k,m_k} \right) \\ &\quad + \left(\sum_{i=1}^K \sum_{m_i=1}^{M_i} \left| \hat{\mathbf{w}}_{k,m_k}^H \hat{\mathbf{H}}_{b_i,k} \mathbf{u}_{i,m_i} \right|^2 + \sigma_n^2 \left\| \hat{\mathbf{w}}_{k,m_k}^H \right\|^2 \right) \\ &= 1 - \mathbf{u}_{k,m_k}^H \mathbf{H}_{b_k,k}^H \mathbf{R}_k'^{-1} \mathbf{H}_{b_k,k} \mathbf{u}_{k,m_k} \end{aligned} \quad (17)$$

where

$$\begin{aligned} \mathbf{R}_k' &= \sum_{i=1}^K \sum_{m_j=1}^{M_i} \mathbf{H}_{b_i,k} \mathbf{u}_{i,m_i} \mathbf{u}_{i,m_i}^H \mathbf{H}_{b_i,k}^H + \sigma_n^2 \mathbf{A}_k^{-1} \mathbf{A}_k^{-H} \\ &= \mathbf{R}_k + \Omega(\mathbf{A}_k'') \end{aligned}$$

$$\Omega(\mathbf{A}_k'') = \sigma_n^2 \mathbf{A}_k'' \mathbf{A}_k''^H - 2\sigma_n^2 \operatorname{Re}(\mathbf{A}_k'')$$

$$\text{and } \mathbf{A}_k'' = \mathbf{A}_k^{-1} - \mathbf{I}.$$

With fixed precoder \mathbf{u}_{k,m_k} and the same weights, the difference between the cost functions in (5) and (17) is given by

$$\hat{\varepsilon}_{k,m_k} - \varepsilon_{k,m_k} = \mathbf{u}_{k,m_k}^H \mathbf{H}_{b_k,k} (\mathbf{R}_k^{-H} - \mathbf{R}_k'^{-H}) \mathbf{H}_{b_k,k}^H \mathbf{u}_{k,m_k} \quad (18)$$

and after some straightforward manipulations, we have

$$\mathbf{R}_k^{-1} - \mathbf{R}_k'^{-1} = \mathbf{R}_k^{-1} \Omega(\mathbf{A}_k'') \{ \Omega(\mathbf{A}_k'') + \mathbf{R}_k \}^{-1} \quad (19)$$

In the special case of perfect RF implementation, i.e., $\mathbf{A}_k'' = \mathbf{A}'_k = 0$, we have $\mathbf{R}_k'^{-1} - \mathbf{R}_k^{-1} = 0$ and $\varepsilon_{k,m_k} - \hat{\varepsilon}_{k,m_k} = 0$. With practical non-reciprocity level at the UE and reasonable high SNR, we also have $\Omega(\mathbf{A}_k'') \ll \mathbf{R}_k$ and $\mathbf{R}_k'^{-1} - \mathbf{R}_k^{-1} \approx \mathbf{R}_k^{-1} \Omega(\mathbf{A}_k'') \mathbf{R}_k^{-1} \approx 0$. Thus, with the fixed precoder, the cost function under UE non-reciprocity $\hat{\varepsilon}_{k,m_k}$ is practically the same as the cost function constructed with ideal channel knowledge ε_{k,m_k} . Unless both the non-reciprocity and additive noise levels are very high (e.g., $\delta_{\mathbf{A}_k}^2 = -10$ dB and 0dB SNR), the UE transceiver non-reciprocity is expected to impose no essential impact on the performance.

B. Effects in Decentralized Beamforming

Here, we consider the two decentralized schemes described in Section II.C operating under the effects of UE transceiver non-reciprocity. Notice that under UE transceiver non-reciprocity, it can be shown that the last two steps of (5) for calculating MSE of each stream reception at the BS side do not exactly hold any more. However, without taking into account the above-mentioned problem in the WSR optimization design, similar to [7], if we apply the same formulas to calculate the MSE of each stream given by $\hat{\varepsilon}_{k,m_k} = 1 - \hat{\mathbf{w}}_{k,m_k}^H \hat{\mathbf{H}}_{b_k,k} \mathbf{u}_{k,m_k}$ and $\hat{\varepsilon}_{k,m_k} = 1 - \hat{\mathbf{w}}_{k,m_k}^H \hat{\mathbf{G}}_{b_k,k} \mathbf{u}_{k,m_k}$ for strategy A and strategy B, respectively, the obtained MSE information is certainly not correct. The resulting weight calculation using the obtained MSE information as $\hat{p}_{k,m_k} = \hat{\varepsilon}_{k,m_k}^{-1}$ is deviated from the ideal weight calculation using correct MSE information. Next assuming fixed \hat{p}_{k,m_k} , we study further the impact of UE non-reciprocity problem and particularly its impact on the cost functions.

1) Strategy A

Again, in order to construct the cost function in each BS as defined in (8), k -th user calculates the MMSE receiver for m_k -th stream reception and sends it back via busy burst to all the BSs. Under UE transceiver non-reciprocity, the received information at the BS b is not $\mathbf{w}_{k,m_k}^H \mathbf{H}_{b,k}$ but actually reads $\mathbf{w}_{k,m_k}^H \mathbf{A}_k \mathbf{H}_{b,k}$. Then by applying this impaired information, the cost function becomes

$$\begin{aligned} \hat{\varepsilon}_b^A &= -2 \sum_{k=1}^K \sum_{m_k=1}^{M_k} \operatorname{Re} \left\{ \left(\hat{p}_{k,m_k} \mathbf{w}_{k,m_k}^H \mathbf{A}_k \mathbf{H}_{b,k} \mathbf{u}_{k,m_k} \right) \right\} \\ &\quad + \sum_{k=1}^K \sum_{m_k=1}^{M_k} \sum_{k'=1}^K \sum_{m_{k'}=1}^{M_{k'}} \hat{p}_{k,m_k} \left| \mathbf{w}_{k,m_k}^H \mathbf{A}_k \mathbf{H}_{b,k} \mathbf{u}_{k',m_{k'}} \right|^2 \end{aligned} \quad (20)$$

With fixed precoders and weights at the BS b , the difference between the cost functions in (8) and (20) can be evaluated as

$$\begin{aligned} \hat{\varepsilon}_b^A - \varepsilon_b^A = & \sum_{k=1}^K \sum_{m_k=1}^{M_k} \sum_{k'=1}^K \sum_{m_{k'}=1}^{M_{k'}} \hat{p}_{k,m_k} \left| \mathbf{w}_{k,m_k}^H \mathbf{A}_k' \mathbf{H}_{b,k} \mathbf{u}_{k',m_{k'}} \right|^2 \\ & + 2 \operatorname{Re} \left\{ \sum_{k=1}^K \sum_{m_k=1}^{M_k} \sum_{k'=1}^K \sum_{m_{k'}=1}^{M_{k'}} \hat{p}_{k,m_k} \mathbf{w}_{k,m_k}^H \mathbf{A}_k' \mathbf{H}_{b,k} \mathbf{u}_{k',m_{k'}} \right. \\ & \left. \times (\mathbf{w}_{k,m_k}^H \mathbf{H}_{b,k} \mathbf{u}_{k',m_{k'}})^H - \sum_{k=1}^K \sum_{m_k=1}^{M_k} \hat{p}_{k,m_k} \mathbf{w}_{k,m_k}^H \mathbf{A}_k' \mathbf{H}_{b,k} \mathbf{u}_{k,m_k} \right\} \end{aligned} \quad (21)$$

Based on (21), the difference between the two cost functions is dependent the transceiver non-reciprocity characteristics \mathbf{A}_k' of all the connected UEs in the network, $k = 1, \dots, K$. Together with deviation of weight calculation for \hat{p}_{k,m_k} , severe performance degradation is thus expected. More detailed discussion will be given in Subsection IV.B.3).

2) Strategy B

In this strategy, in order to construct the cost function at each BS, the k -th user first calculates whitening filter based on (9) and sends it back via channel sounding to the connected BS. It then calculates MMSE receiver for the m_k -th stream based on (2) and broadcasts it via busy bursts to BSs other than the connected BS [7]. Under UE transceiver non-reciprocity, the received information at the BS b reads $\hat{\mathbf{G}}_{b_k,k} = \mathbf{Q}_k \mathbf{A}_k \mathbf{H}_{b,k}$ for $b_k = b$ and $\mathbf{w}_{k',m_{k'}}^H \mathbf{A}_{k'}' \mathbf{H}_{b,k'}$ for $b_{k'} \neq b$. Then with fixed precoder, the equivalent MMSE receiver and cost function at the BS b are obtained as

$$\begin{aligned} \hat{\mathbf{w}}_{k,m_k} = & \left(\sum_{i=1, b_i=b_k}^K \sum_{m_i=1}^{M_i} \hat{\mathbf{G}}_{b_k,i} \mathbf{u}_{i,m_i} \mathbf{u}_{i,m_i}^H \hat{\mathbf{G}}_{b_k,i}^H + \mathbf{I} \right)^{-1} \hat{\mathbf{G}}_{b_k,m_k} \mathbf{u}_{k,m_k} \quad (22) \\ = & \mathbf{Q}_k^{-H} \mathbf{A}_k^{-H} \bar{\mathbf{R}}_k^{-1} \mathbf{H}_{b_k,k} \mathbf{u}_{k,m_k} \\ \hat{\varepsilon}_b^B = & \sum_{k=1}^K \left\{ \hat{p}_k - 2 \sum_{m_k=1}^{M_k} \operatorname{Re} \left(p_{k,m_k} \hat{\mathbf{w}}_{k,m_k}^H \hat{\mathbf{G}}_{b_k,k} \mathbf{u}_{k,m_k} \right) \right. \\ & \left. + p_{k,m_k} \sum_{m_k=1}^{M_k} \hat{\mathbf{w}}_{k,m_k}^H \left[\hat{\mathbf{G}}_{b_k,k} \mathbf{u}_{k,m_k} \left(\hat{\mathbf{G}}_{b_k,k} \mathbf{u}_{k,m_k} \right)^H + \mathbf{I} \right] \hat{\mathbf{w}}_{k,m_k} \right\} \quad (23) \\ & + \sum_{k'=1}^K \sum_{m_{k'}=1}^{M_{k'}} \sum_{k=1}^K \sum_{m_k=1}^{M_k} p_{k',m_{k'}} \left| \hat{\mathbf{w}}_{k',m_{k'}}^H \hat{\mathbf{H}}_{b,k'} \mathbf{u}_{k,m_k} \right|^2 \\ = & \sum_{k=1}^K \left(\hat{p}_k - \sum_{m_k=1}^{M_k} \hat{p}_{k,m_k} \mathbf{u}_{k,m_k}^H \mathbf{H}_{b,k}^H \bar{\mathbf{R}}_k^{-H} \mathbf{H}_{b,k} \mathbf{u}_{k,m_k} \right) + \operatorname{INT}_b' \end{aligned}$$

where

$$\begin{aligned} \hat{p}_k = & \operatorname{Tr}(\hat{\mathbf{P}}_k - \log \det \hat{\mathbf{P}}_k) \\ \bar{\mathbf{R}}_k = & \left(\sum_{i=1, b_i=b_k}^K \sum_{m_i=1}^{M_i} \mathbf{H}_{b_k,i} \mathbf{u}_{i,m_i} \mathbf{u}_{i,m_i}^H \mathbf{H}_{b_k,i}^H + \mathbf{A}_k^{-1} \bar{\mathbf{R}}_k \mathbf{A}_k^{-H} \right) \\ = & \bar{\mathbf{R}}_k + \Omega'(\mathbf{A}_k'') \\ \operatorname{INT}_b' = & \sum_{k'=1}^K \sum_{m_{k'}=1}^{M_{k'}} \sum_{k=1}^K \sum_{m_k=1}^{M_k} p_{k',m_{k'}} \left| \mathbf{w}_{k',m_{k'}}^H \mathbf{A}_{k'}' \mathbf{H}_{b,k'} \mathbf{u}_{k,m_k} \right|^2 \end{aligned}$$

$\Omega'(\mathbf{A}_k'') = \mathbf{A}_k'' \bar{\mathbf{R}}_k \mathbf{A}_k''^H + 2 \operatorname{Re}(\mathbf{A}_k'' \bar{\mathbf{R}}_k)$ and $\hat{\mathbf{P}}_k = \operatorname{diag}\{\hat{p}_{k,1}, \dots, \hat{p}_{k,M_k}\}$. Notice that the weighting value used for calculating INT_b' in (23) is the ideal weighting value $p_{k',m_{k'}}$ as it is calculated at the UE side and sent back via busy burst signaling.

With fixed precoder at the BS b as well as fixed weights \hat{p}_{k,m_k} and $p_{k',m_{k'}}$, the difference between cost functions in (14) and (23) reads now

$$\begin{aligned} \hat{\varepsilon}_b^B - \varepsilon_b^B = & \sum_{k=1}^K \sum_{m_k=1}^{M_k} \hat{p}_{k,m_k} \mathbf{u}_{k,m_k} \mathbf{H}_{b,k} (\bar{\mathbf{R}}_k^{-H} - \bar{\mathbf{R}}_k'^{-H}) \mathbf{H}_{b,k}^H \mathbf{u}_{k,m_k}^H \\ & + \sum_{k'=1}^K \sum_{m_{k'}=1}^{M_{k'}} \sum_{k=1}^K \sum_{m_k=1}^{M_k} p_{k',m_{k'}} \left(\left| \mathbf{w}_{k',m_{k'}}^H \mathbf{A}_{k'}' \mathbf{H}_{b,k'} \mathbf{u}_{k,m_k} \right|^2 \right. \\ & \left. + 2 \operatorname{Re} \left\{ \mathbf{w}_{k',m_{k'}}^H \mathbf{A}_{k'}' \mathbf{H}_{b,k'} \mathbf{u}_{k,m_k} \left(\mathbf{w}_{k',m_{k'}}^H \mathbf{H}_{b,k'} \mathbf{u}_{k,m_k} \right)^H \right\} \right) \end{aligned} \quad (24)$$

and $\bar{\mathbf{R}}_k^{-1} - \bar{\mathbf{R}}_k'^{-1} = \bar{\mathbf{R}}_k^{-1} \Omega'(\mathbf{A}_k'') \bar{\mathbf{R}}_k^{-1} + \bar{\mathbf{R}}_k'^{-1}$. Again, as shown in (24), the difference between two cost functions is dependent the transceiver non-reciprocity characteristics \mathbf{A}_k' of all the connected UEs in the network, $k = 1, \dots, K$. However, when inter-cell interference approaches to 0, the second term in (24) also approaches to 0. If the channel noise is also small, $\bar{\mathbf{R}}_k \rightarrow 0$ as well, and assuming practical non-reciprocity level at the UEs, we then have $\Omega'(\mathbf{A}_k'') \rightarrow 0$, $(\bar{\mathbf{R}}_k'^{-1} - \bar{\mathbf{R}}_k^{-1}) \approx \bar{\mathbf{R}}_k^{-1} \Omega'(\mathbf{A}_k'') \bar{\mathbf{R}}_k^{-1} \rightarrow 0$ and hence $(\hat{\varepsilon}_b^B - \varepsilon_b^B) \rightarrow 0$. This implies that, in high SNR range, if cell separation is good in the network and there is little inter-cell interference at the UE receivers, UE transceiver non-reciprocity will not play a big role in the decentralized beamforming using strategy B. This, however, applies only under such limiting assumptions. When inter-cell interference vanishes, the considered network is equivalent to a single-cell network and the impact of transceiver non-reciprocity in UEs on system performance becomes to be again marginal.

3) Discussion

Performance degradation: As shown in (21) and (24), when $\mathbf{A}_k' \neq 0$, there is clear deviation between the cost function constructed with ideal channel knowledge and with imperfect channel knowledge due to UE transceiver FR mismatches. In general, it is rather challenging to directly map these differences into the resulting performance degradation analytically, as the considered sum-rate optimization process is iterative and small deviations in cost function may lead to very different optimization results. As will be shown later through computer simulations, *performance degradation is severe even with realistic fairly small non-reciprocity levels*. Thus, the UE transceiver non-reciprocity problem clearly forms an adverse and performance-limiting factor in the decentralized beamforming design and deployment.

Convergence: Due to the mismatch between the constructed cost function at the BS under UE transceiver FR mismatches and ideal cost function with perfect DL channel and user information, when strategy B is deployed, the achievable network sum-rate deteriorates after certain number of iterations, as illustrated in Figure 1. This thus indicates that it is possible to improve the network performance by detecting the sum-rate deteriorating point and stopping the iterative optimization process. We assume that there is anyway certain amount of low-latency backhaul information available in the network, and the BSs can exchange sum-rate information in the optimization process. Then we pro-

pose a convergence-aware processing algorithm for the BS side, given in Table 1. It is based on the observation that the sum-rate calculated at the BS side can indicate the convergence property of the achievable sum-rate over iterations even if it is not the same as the actual rate realized in the network. Then the BS side can stop the WSR optimization process after the calculated sum-rate drops consecutively in two iterations. As will be shown in the computer simulations section, by applying the proposed procedures, we can effectively compensate for the performance degradation caused by convergence problem.

Weight calculation at the BS: In decentralized beamforming, the weights are calculated based on the MSE calculation at the BS using the simplified formula $\varepsilon_{k,m_k} = 1 - \mathbf{w}_{k,m_k}^H \mathbf{H}_{b_k,k} \mathbf{u}_{k,m_k}$ with known \mathbf{w}_{k,m_k}^H , $\mathbf{H}_{b_k,k}$ and \mathbf{u}_{k,m_k} in (5). However, under UE transceiver non-reciprocity, such equality is not valid any more. If the same formula is still used, severe performance degradation is certainly expected because the decentralized WSR objective in (7) is not equivalent to the centralized WSR objective in (6) any more. In addition to cope with the convergence problem at the BS side, system designers thus need to take non-reciprocity problem into account and modify the weight calculation algorithm accordingly for the decentralized scheme.

UE calibration: Even though the above-mentioned convergence and weight calculation problems can be tackled with proper system design, efficient UE reciprocity estimation-calibration algorithm is potentially still needed in order to achieving close to ideal network performance. This generally increases implementation complexity of the system and needs to be taken into account in the network design. This is a direct consequence of the findings reported in this paper, and forms an interesting topic for our future work.

V. SIMULATIONS AND NUMERICAL RESULTS

In this Section, we evaluate the impacts of UE non-reciprocity on the performance of different beamforming schemes using extensive computer simulations. An example multi-cell network with 2 BSs and 6 UEs is considered. Each BS is equipped with 4 antennas and each UE employs 2 antennas. The propagation environment between a BS and a UE is modeled as a frequency flat Rayleigh fading channel. The average path loss between a BS and its own associated UEs and non-associated users are set by default to be 0dB and 3dB respectively. This represents a scenario where all the users are close to cell edge. For strategy B, 15 iteration of in-cell optimization is deployed to accelerate convergence speed. The level of the FR mismatch in the UE side is defined as the variances of the diagonal element of the mismatch matrices **A** and is denoted by δ_A^2 in dB scale. The system performance is evaluated in terms of achievable network sum-rate, and all the results are averaged over 1000 random channel realizations.

First, we examine the convergence properties of the considered schemes in Figure 1. The results show that when the strategy B is deployed, under UE transceiver non-reciprocity, the sum-rate value starts to drop after certain number of iterations in the decentralized beamforming network. This convergence problem can be tackled with the proposed convergence-aware algorithm presented in Table 1.

Table 1: Description of the proposed convergence-aware processing algorithm

Algorithm 1 Convergence-Aware Processing	
1:	Initialize <i>Sum_flag</i> , <i>Rate</i> , and <i>Old_rate</i> to 0
2:	BS <i>b</i> $\forall b$: Initialize $\mathbf{u}_{k,m_k}^H \forall k, m_k$
3:	BS <i>b</i> $\forall b$: Receive over-the-air signaling from all UEs
4:	BS <i>b</i> $\forall b$: Compute cost function $\hat{\varepsilon}_b$ based on (20) or (23) using precoder $\mathbf{u}_{k,m_k}^H, \forall k, m_k$ and UE information. Then, send the acquired information to BS b_0 .
5:	BS b_0 calculate network sum-rate based on (6) and put in <i>Rate</i>
6:	If <i>Old_rate</i> > <i>Rate</i> , increment <i>Sum_flag</i>
7:	If <i>Sum_flag</i> = 2, stop the algorithm and choose \mathbf{u}_{k,m_k}^H corresponding to the highest sum-rate as the optimum sum-rate, $\forall k, m_k$. Jump to 11.
8:	If <i>Sum_flag</i> \neq 2, make <i>Old_rate</i> equal to <i>Rate</i> .
9:	BS <i>b</i> $\forall b$: Compute precoder $\mathbf{u}_{k,m_k}^H, \forall k, m_k$ based on received UE information and estimated $\hat{\varepsilon}_b$
10:	Repeat steps 3-9 (until total allowed number of iterations is reached)
11:	End.

Then average achievable sum-rate per BS for both the ideal reciprocal channel case and the case with transceiver FR mismatch at the UE side are examined with 30 iterations. As shown in Figure 2, the imperfections at the UEs have essentially no impact on the system performance of centralized beamforming. Decentralized beamforming, on the other hand, suffers from substantial performance degradation. In general, strategy A is found to be much more sensitive to the non-reciprocity problem than the strategy B. This can be partially explained by the fact that the impact of UE non-reciprocity on strategy B is highly related to the inter-cell interference level while the impact of UE non-reciprocity on strategy A depends on the joint effects of the useful signal and all the interference.

Next, the relative performance degradations compared to the ideal network sum-rate with different levels of UE FR mismatch are illustrated in Figure 3. As can be seen, at an example SNR = 20dB, in case of the centralized scenario, even with extreme values of UE non-reciprocity ($\delta_A^2 = 0$ dB), the system has close to ideal performance. At lower SNR's, like SNR = 0 dB, and assuming non-reciprocity as high as $\delta_A^2 > -10$ dB, certain performance degradation can be observed. On the other hand, *even small FR mismatches at the UEs clearly impact the performance of both decentralized methods*. In the considered transmission scenario, to achieve close-to-ideal performance, maximum tolerable level of transceiver FR mismatch at the UEs is around -40dB with strategy A, and around -30dB with strategy B. In general, these are very challenging levels to achieve, especially without specific calibration procedures.

As discussed in Subsection IV.B. 2), in strategy B, the impact of UE transceiver non-reciprocity on the network performance is related to the level of inter-cell interference power. As shown in Figure 4, the relative performance degradation decreases as the cell separation increases. When the cell separation is sufficiently large, e.g., around 15dB, there is almost no performance degradation as was already envisioned in Subsection IV.B. This property should be also taken into account in the network design of decentralized beamforming. However, in order to achieve close to ideal performance with any network parameters,

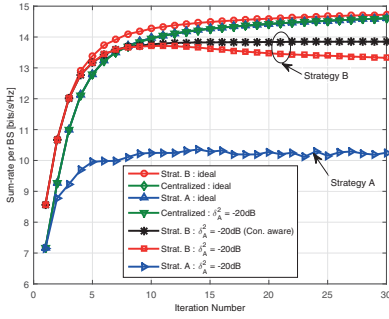


Figure 1: Performance comparison of different beamforming schemes in terms of average sum-rate per BS vs. iteration number, with 3dB cell separation and 20dB SNR.

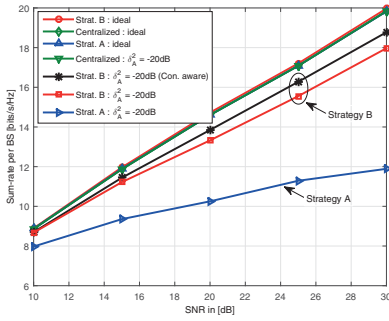


Figure 2: Performance comparison of different beamforming schemes in terms of average sum-rate per BS vs. SNR, with 3dB cell separation.

the results demonstrate that accurate non-reciprocity estimation-calibration algorithms are in any case required at the UE side. Such finding has not been reported earlier in the literature.

VI. CONCLUSIONS

This paper studied the effects of channel non-reciprocity due to UE transceiver FR mismatches in the coordinated TDD multi-cell MIMO DL transmission systems. Both centralized and decentralized beamforming schemes were considered in the analysis. Based on the developed signal models, centralized beamforming was shown to be resistant to UE transceiver non-reciprocity problem while decentralized beamforming using precoded UL pilot signaling suffers from severe performance degradation with non-reciprocal UE transceiver implementations. In this context, several insights were provided for alleviating the performance losses via proper system design. The analysis also shows, in addition to the widely recognized BS reciprocity calibration requirement, that efficient reciprocity calibration algorithms should be developed also at the UE side for achieving desired performance in the coordinated TDD multi-cell systems with decentralized beamforming scheme. This forms an important topic for future work.

REFERENCES

[1] D. Gesbert, S. Hanly, H. Huang, S. Shamai Shitz, O. Simeone, and W. Yu, "Multi-Cell MIMO Cooperative Networks: A New Look at

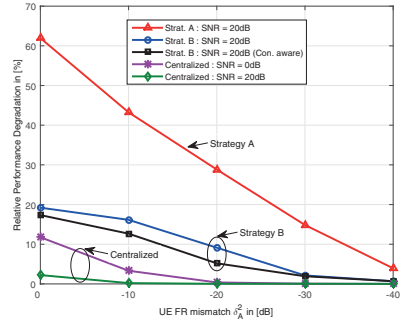


Figure 3: Comparison of different beamforming schemes in terms of percentage difference of their average sum-rate per BS between the ideal case and the case with UE FR mismatch vs. UE FR mismatch, with 3dB cell separation.

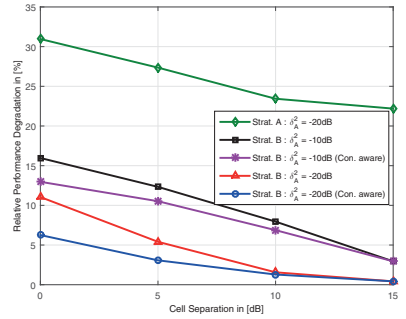


Figure 4: Comparison of two decentralized beamforming methods in terms of percentage difference of their average sum-rate per BS between the ideal case and the case with UE FR mismatch vs. cell separation.

Interference," *IEEE J. Selected Areas Commun.*, vol. 28, no. 9, pp. 1380–1408, December 2010.

[2] H. Dahrouj and W. Yu, "Coordinated beamforming for the multicell multi-antenna wireless system," *IEEE Trans. Wireless Communications*, vol. 9, no. 5, pp. 1748–1759, May 2010.

[3] K. Wang, X. Wang, W. Xu, and X. Zhang, "Coordinated Linear Precoding in Downlink Multicell MIMO-OFDMA Networks," *IEEE Trans. Signal Processing*, vol. 60, no. 8, pp. 4264–4277, Aug 2012.

[4] S. Kaviani and W. Krzymien, "Sum Rate Maximization of MIMO Broadcast Channels with Coordination of Base Stations," in *Proc. IEEE WCNC 2008*, March 2008, pp. 1079–1084.

[5] J. Kaleva, A. Tolli, and M. Juntti, "Weighted sum rate maximization for interfering broadcast channel via successive convex approximation," in *Proc. IEEE GLOBECOM 2012*, Dec 2012, pp. 3838–3843.

[6] Q. Shi, M. Razaviyayn, Z.-Q. Luo, and C. He, "An iteratively weighted mmse approach to distributed sum-utility maximization for a mimo interfering broadcast channel," *IEEE Trans. Signal Processing*, vol. 59, no. 9, pp. 4331–4340, Sept 2011.

[7] P. Komulainen, A. Tolli, and M. Juntti, "Effective CSI Signaling and Decentralized Beam Coordination in TDD Multi-Cell MIMO Systems," *IEEE Trans. Signal Processing*, vol. 61, no. 9, pp. 2204–2218, May 2013.

[8] J. Haartsen, "Impact of non-reciprocal channel conditions in broadband TDD systems," in *Proc. IEEE PIMRC*, Sept 2008, pp. 1–5.

[9] B. Kouassi, I. Ghauri, and L. Deneire, "Estimation of time-domain calibration parameters to restore MIMO-TDD channel reciprocity," in *Proc. CROWNCOM 2012*, June 2012, pp. 254–258.

[10] Y. Zou, O. Raeesi, R. Wichman, A. Tolli, and M. Valkama, "Analysis of Channel Non-Reciprocity Due to Transceiver and Antenna Coupling Mismatches in TDD Precoded Multi-User MIMO-OFDM Downlink," in *Proc. IEEE VTC 2014 Fall*, Sept 2014, pp. 1–7.

PUBLICATION VII

Y. Zou, O. Raeesi, R. Wichman, A. Tölli, and M. Valkama, “Analysis of channel non-reciprocity due to transceiver and antenna coupling mismatches in TDD precoded multi-user MIMO-OFDM downlink,” in *2014 IEEE 80th Vehicular Technology Conference (VTC2014-Fall)*, Sept 2014, pp. 1–7.

© 2014 IEEE. Reprinted, with permission, from Y. Zou, O. Raeesi, R. Wichman, A. Tölli, and M. Valkama, “Analysis of channel non-reciprocity due to transceiver and antenna coupling mismatches in TDD precoded multi-user MIMO-OFDM downlink,” in *2014 IEEE 80th Vehicular Technology Conference (VTC2014-Fall)*, September 2014.

In reference to IEEE copyrighted material which is used with permission in this thesis, the IEEE does not endorse any of Tampere University’s products or services. Internal or personal use of this material is permitted. If interested in reprinting/republishing IEEE copyrighted material for advertising or promotional purposes or for creating new collective works for resale or redistribution, please go to http://www.ieee.org/publications_standards/publications/rights/rights_link.html to learn how to obtain a License from RightsLink.

Analysis of Channel Non-reciprocity due to Transceiver and Antenna Coupling Mismatches in TDD Precoded Multi-user MIMO-OFDM Downlink

Yaning Zou¹, Orod Raeesi¹, Risto Wichman², Antti Tölli³ and Mikko Valkama¹

¹Department of Electronics and Communications Engineering, Tampere University of Technology, Tampere, Finland

²Department of Signal Processing and Acoustics, Aalto University, Espoo, Finland

³Department of Communications Engineering, University of Oulu, Oulu, Finland

Email: yaning.zou@tut.fi

Abstract — This paper studies the impact of two implementation imperfections, namely, transceiver frequency-response non-reciprocity and antenna mutual coupling mismatches at the base-station and user equipment on the channel reciprocity assumption in TDD systems. Comprehensive signal models are first developed to analyze the joint effects of these two imperfections in the TDD multi-user MIMO-OFDM downlink transmission system context, covering both zero-forcing (ZF) and eigenbeamforming based transmitter processing. The corresponding performance degradation is then evaluated in terms of SINRs and maximum achievable sum-rate. The analysis shows that during downlink transmission, the transceiver non-reciprocity and antenna mutual coupling mismatches at the base-station introduce inter-user interference (IUI) and are the major causes for the resulting performance degradation. Implementation imperfections at user equipment side, in turn, only introduce inter-stream interference (ISI) that can be fairly easily suppressed in detector processing as part of effective precoded channels. In order to achieve throughputs close to the ideal case, transceiver frequency-response mismatches and antenna mutual coupling at the base-station side need to be extremely well calibrated, generally below 35-40dB in terms of relative mismatch levels.

Index Terms — channel reciprocity, multi-user MIMO-OFDM, mutual coupling, non-reciprocity, precoding, time-division duplexing, transceiver frequency response mismatch.

I. INTRODUCTION

Time division duplexing (TDD) based wireless systems are drawing more and more interest, not only in wireless local area networks (WLAN/WiFi) but also in mobile cellular networks [1]. Based on the so-called channel reciprocity property, one important advantage of TDD systems, compared to frequency division duplexing (FDD), is the ability to acquire channel state information at transmitter (CSIT) by measuring reverse channels without using dedicated feedback signaling [1]. If multiple antennas are implemented at the base-station (BS), several multi-user (MU) MIMO-OFDM transmission schemes stemming, e.g., from zero-forcing (ZF) precoding [2] or eigenbeamforming [4], can then be developed based on the available downlink (DL)

CSIT to spatially multiplex users to share the same spectral resources. This, in turn, can substantially improve the system spectral efficiency and user equipment throughputs with reasonable complexity.

However, in practice, the *effective physical channels* linking the devices include also all the transceivers and antennas used in the transmitting and receiving devices. As discussed in [5] and [6], there are unavoidable mismatches already between the frequency responses (FRs) of transmitter (TX) and receiver (RX) chains of any individual transceiver, as well as further mutual coupling effects between the antenna elements in multiantenna devices. The resulting effective downlink (DL) and uplink (UL) channels are thus not reciprocal anymore and performance degradation is expected in any system that is building on the reciprocity assumption. In the existing literature, in [7]-[9] and reference therein, the effect of transceiver non-reciprocity is studied in the ZF precoded MU MIMO-OFDM context. In [8] and [9], antenna mutual coupling mismatches are also mentioned yet their impact on the signal and system characteristics is not analyzed. Also another important precoding technique, i.e., eigenbeamforming based transmitter processing [4], has not been analyzed in this context in the existing literature.

In this paper, we analyze and characterize the joint impacts of channel non-reciprocity due to transceiver FR and antenna mutual coupling mismatches on precoded TDD multiuser (MU) MIMO-OFDM downlink transmission. Both ZF and eigenbeamforming based precoding schemes are considered, and detailed signal and system models are derived. Based on this modeling, the resulting performance degradation in terms of maximum achievable signal-to-interference-and-noise ratios (SINRs) and the corresponding downlink sum-rate are analyzed. The analysis shows that the implementation imperfections *at the BS side* are the key limiting factor for the achievable system performance, while the corresponding UE imperfection effects can be more easily handled in downlink detector processing. In general, the system performance is also shown to be more sensitive to antenna mutual coupling mismatch than transceiver frequency response mismatches. Thus, the analysis outcomes developed in this paper strongly motivate and call for the development of ad-

This work was supported by the Finnish Funding Agency for Technology and Innovation (Tekes), Broadcom Communications Finland and Huawei Finland under the project “Energy-Efficient Wireless Networks and Connectivity of Devices – Densification (EWINE-D)”, the Academy of Finland under the projects 251138 “Digitally-Enhanced RF for Cognitive Radio Devices” and 138424 “Joint Analysis and DSP-Based Mitigation of Multiple RF Impairments in Future Radio Devices”, and TUT Graduate School.

vanced reciprocity calibration techniques at the BS side in the emerging TDD-based multi-user wireless systems.

The rest of the paper is organized as follows: Section II outlines the fundamental precoded multi-user MIMO-OFDM downlink system models. Essential transceiver non-reciprocity and antenna mutual coupling models are then formulated in Section III. In Section IV, these are combined to analyze the impact of imperfect CSIT due to non-reciprocity and antenna coupling mismatches on downlink transmission. Section V provides numerical evaluations and illustrations while conclusions are drawn in Section VI.

Notations: The statistical expectation is denoted with operator $E[\cdot]$, while $\text{diag}[\cdot]$ and $\text{bdiag}[\cdot]$ denote diagonal and block-diagonal matrices, respectively, formed from their input arguments. Physical propagation channel matrices are denoted with \mathbf{H} while the *corresponding effective channel matrices* are denoted with $\bar{\mathbf{H}}$ which incorporates transmit chains' frequency responses, transmitter and receiver antenna coupling effects, and receiver chains' frequency responses. The ij -th element of matrix \mathbf{H} is denoted with $[\mathbf{H}]_{i,j}$. The i -th row and j -th column of matrix \mathbf{H} are denoted with $[\mathbf{H}]_{i,:}$ and $[\mathbf{H}]_{:,j}$, respectively.

II. PRECODED MULTI-USER (MU) MIMO-OFDM DOWNLINK TRANSMISSION

A. Principal Downlink System Model

Here, we consider a generic precoded L -user multiantenna MIMO-OFDM DL transmission system. The number of antennas at the BS side is assumed to be N_B while the l -th user equipment has N_U^l antennas, $l = 1, 2, \dots, L$. Altogether there are thus $N_U = \sum_{l=1}^L N_U^l$ antennas at the users' side. During DL transmission, OFDM waveforms are constructed using N -point IFFT preceded by proper sub-carrier level precoding and stream multiplexing. At k -th subcarrier, a total of Q parallel data symbols (Q streams) $\mathbf{s}(k)$ are precoded into N_B transmission layers using $N_B \times Q$ precoding matrix $\mathbf{W}_T(k)$ and transmitted from N_B transmit antennas using OFDM modulation. The precoding is written here as

$$\mathbf{x}(k) = \beta_k \mathbf{W}_T(k) \mathbf{s}(k) \quad (1)$$

where $\mathbf{s}(k) = [\bar{\mathbf{s}}_1(k)^T, \bar{\mathbf{s}}_2(k)^T, \dots, \bar{\mathbf{s}}_L(k)^T]^T$, $\bar{\mathbf{s}}_l(k)$ denotes a $Q_l \times 1$ data vector of the l -th user given as $\bar{\mathbf{s}}_l(k) = [s_{l,1}(k), s_{l,2}(k), \dots, s_{l,Q_l}(k)]^T$, $\sum_{l=1}^L Q_l = Q$ and β_k is the normalization scalar that adjusts total sum power to be unchanged after precoding at the BS at k -th subcarrier, i.e., $\beta_k = \sqrt{Q / \text{tr}(\mathbf{W}_T^H(k) \mathbf{W}_T(k))}$.

After propagating through a noisy multi-path channel, the input at the l -th user receiver at k -th subcarrier is given by

$$\mathbf{r}_l(k) = \mathbf{H}_{DL,l}(k) \mathbf{x}(k) + \mathbf{n}_l(k) \quad (2)$$

where $\mathbf{H}_{DL,l}(k)$ denotes $N_U^l \times N_B$ DL propagation channel matrix and $\mathbf{n}_l(k)$ is $N_U^l \times 1$ noise vector at the receiver input. Then by applying $N_U^l \times Q_l$ spatial filter $\mathbf{W}_{R,l}(k)$, the receiver detector input is given by

$$\begin{aligned} \mathbf{y}_l(k) &= \mathbf{W}_{R,l}^H(k) \mathbf{r}_l(k) \\ &= \beta_k \mathbf{W}_{R,l}^H(k) \mathbf{H}_{DL,l}(k) \mathbf{W}_T(k) \mathbf{s}(k) + \mathbf{W}_{R,l}^H(k) \mathbf{n}_l(k) \end{aligned} \quad (3)$$

In the multi-user transmission context, the precoder $\mathbf{W}_T(k)$ and combiners $\mathbf{W}_{R,l}^H(k)$ are generally designed so that inter-user interference (IUI) and inter-stream interference (ISI) are controlled or minimized at detector input. In this paper, we consider two precoding schemes, namely zero-forcing (ZF) [2] and eigenbeamforming [4]. For both schemes, we first assume that full CSIT, i.e., $\mathbf{H}_{DL}(k) = [\mathbf{H}_{DL,1}^T(k), \mathbf{H}_{DL,2}^T(k), \dots, \mathbf{H}_{DL,L}^T(k)]^T$, is perfectly known at the BS. Then, in Sections III and IV, the impacts of non-reciprocity and antenna mutual coupling mismatches are explicitly modeled and taken into account.

B. Zero-Forcing (ZF) Precoding

Based on the ZF criterion [2], and assuming $Q_l = N_U^l$ for simplicity, the total $N_B \times Q$ precoding matrix at the k -th subcarrier is constructed through pseudo-inverse of the full CSIT as

$$\mathbf{W}_{T,ZF}(k) = \mathbf{H}_{DL}(k) (\mathbf{H}_{DL}(k) \mathbf{H}_{DL}^H(k))^{-1} \quad (4)$$

and $\beta_{k,ZF} = \sqrt{Q / \text{tr}(\mathbf{W}_{T,ZF}^H(k) \mathbf{W}_{T,ZF}(k))}$. Then, the reception at the l -th user device is given by

$$\begin{aligned} \mathbf{r}_{l,ZF}(k) &= \beta_{k,ZF} \mathbf{H}_{DL,l}(k) \mathbf{W}_{T,ZF}(k) \mathbf{s}(k) + \mathbf{n}_l(k) \\ &= \beta_{k,ZF} \bar{\mathbf{s}}_l(k) + \mathbf{n}_l(k) \end{aligned} \quad (5)$$

showing that all the IUI and ISI is suppressed. A variant of ZF is block diagonalisation [3], which is not covered in this paper. In practice, further LMMSE receiver processing against, e.g., interference from other co-channel transmissions can be deployed. We elaborate on this later in the paper.

C. Eigenbeamforming-based Precoding

As shown in [4], eigenbeamforming is based on singular value decomposition (SVD) of DL channel matrices $\mathbf{H}_{DL,l}(k)$ from the BS to the l -th user at the k -th subcarrier, written as

$$\mathbf{H}_{DL,l}(k) = \mathbf{U}_{l,h}(k) \Lambda_{l,h}(k) \mathbf{V}_{l,h}^H(k) \quad (6)$$

where $\mathbf{U}_{l,h}(k)$ and $\mathbf{V}_{l,h}(k)$ are complex unitary matrices, containing the left and the right singular vectors as columns, and $\Lambda_{l,h}(k)$ represents a (rectangular) diagonal matrix with positive singular values on its diagonal. Now, a reduced-size matrix $\mathbf{V}_l(k)$ is formed by collecting the first N_U^l right singular vectors (first N_U^l columns of $\mathbf{V}_{l,h}(k)$), while another matrix $\mathbf{W}(k)$ is calculated as $\mathbf{W}(k) = \mathbf{V}(k) (\mathbf{V}^H(k) \mathbf{V}(k))^{-1}$ where $\mathbf{V}(k) = [\mathbf{V}_1(k), \mathbf{V}_2(k), \dots, \mathbf{V}_L(k)]$. Finally, the total precoder can then be constructed as

$$\mathbf{W}_{T,EM}(k) = [\bar{\mathbf{W}}_1(k), \bar{\mathbf{W}}_2(k), \dots, \bar{\mathbf{W}}_L(k)] \quad (7)$$

where $\bar{\mathbf{W}}_l(k)$ contains the first Q_l columns of $\mathbf{W}_l(k)$ and $\mathbf{W}(k) = [\mathbf{W}_1(k), \mathbf{W}_2(k), \dots, \mathbf{W}_L(k)]$. The transmit power normalization scalar is then calculated as $\beta_{k,EM} = \sqrt{Q / \text{tr}(\mathbf{W}_{T,EM}^H(k) \mathbf{W}_{T,EM}(k))}$.

After experiencing DL propagation channel, the reception at the l -th user is given by

$$\begin{aligned}\mathbf{r}_{l,ZF}(k) &= \beta_{k,EM} \mathbf{H}_{DL,l}(k) \mathbf{W}_{T,EM}(k) \mathbf{s}(k) + \mathbf{n}_l(k) \\ &= \beta_{k,EM} \mathbf{U}_l(k) \Lambda_l(k) \bar{\mathbf{s}}_l(k) + \mathbf{n}_l(k)\end{aligned}\quad (8)$$

where $\mathbf{U}_l(k)$ contains Q_l left singular vectors (columns of $\mathbf{U}_{l,h}(k)$) and $\Lambda_l(k)$ is an ordinary diagonal matrix with the Q_l largest singular values of $\mathbf{H}_{DL,l}(k)$ as entries [4]. Then the desired parallel signals can be separated by applying a receiver $\mathbf{W}_{R,l}^H(k)$ that can be, e.g., $\mathbf{U}_l^H(k)$, stemming from orthogonality of singular vectors, or more generally an LMMSE-based spatial filter which can accommodate also external co-channel interference.

III. IMPACTS OF TRANSCEIVER NON-RECIPROcity AND ANTENNA COUPLING MISMATCH ON CHANNEL RECIPROcity

In TDD systems, DL and UL transmissions basically share the same spectrum. If channel coherence time is sufficiently long and thus the channels change fairly slowly over time, CSIT at the BS can be obtained from the UL received signals directly, and thus directly deployed in downlink transmission as $\bar{\mathbf{H}}_{DL}(k) = \bar{\mathbf{H}}_{UL}^T(k)$ where $\bar{\mathbf{H}}_{UL}(k)$ refers to estimated uplink channel responses.

However, as depicted in Fig. 1 and Fig. 2, the *effective DL and UL channels* are generally cascades of transceivers and antenna mutual coupling at TX side, physical propagation channels, and antenna mutual coupling and transceivers at RX side. Then, the effective DL and UL channel matrices between the BS and the l -th user device, and respectively between the BS and all the users $l = 1, 2, \dots, L$, are given by

$$\begin{aligned}\bar{\mathbf{H}}_{DL,l}(k) &= \mathbf{A}_{l,R}(k) \mathbf{C}_{l,R}(k) \mathbf{H}_{DL,l}(k) \mathbf{C}_{B,T}(k) \mathbf{A}_{B,T}(k) \\ \bar{\mathbf{H}}_{UL,l}(k) &= \mathbf{A}_{B,R}(k) \mathbf{C}_{B,R}(k) \mathbf{H}_{UL,l}(k) \mathbf{C}_{l,T}(k) \mathbf{A}_{l,T}(k) \\ \bar{\mathbf{H}}_{DL}(k) &= \mathbf{A}_{U,R}(k) \mathbf{C}_{U,R}(k) \mathbf{H}_{DL}(k) \mathbf{C}_{B,T}(k) \mathbf{A}_{B,T}(k) \\ \bar{\mathbf{H}}_{UL}(k) &= \mathbf{A}_{B,R}(k) \mathbf{C}_{B,R}(k) \mathbf{H}_{UL}(k) \mathbf{C}_{U,T}(k) \mathbf{A}_{U,T}(k)\end{aligned}\quad (9)$$

where

$$\begin{aligned}\mathbf{A}_{B,T}(k) &= \text{diag}(a_{B,T,1}(k), \dots, a_{B,T,N_B}(k)) \\ \mathbf{A}_{B,R}(k) &= \text{diag}(a_{B,R,1}(k), \dots, a_{B,R,N_B}(k)) \\ \mathbf{A}_{l,T}(k) &= \text{diag}(a_{l,T,1}(k), \dots, a_{l,T,N_l^t}(k)) \\ \mathbf{A}_{l,R}(k) &= \text{diag}(a_{l,R,1}(k), \dots, a_{l,R,N_l^r}(k)) \\ \mathbf{A}_{U,T}(k) &= \text{bdiag}(\mathbf{A}_{1,T}(k), \dots, \mathbf{A}_{L,T}(k)) \\ \mathbf{A}_{R,T}(k) &= \text{bdiag}(\mathbf{A}_{1,R}(k), \dots, \mathbf{A}_{L,R}(k))\end{aligned}\quad (10)$$

in which $a_{B,T,n_B}(k)$, $a_{B,R,n_B}(k)$, $a_{l,T,n_l^t}(k)$ and $a_{l,R,n_l^r}(k)$ refer to the frequency-responses of TX and RX chains in the n_B -th transceiver at the BS side and in the n_l^t -th transceiver at the l -th UE side. $\mathbf{C}_{l,R}(k)$, $\mathbf{C}_{l,T}(k)$, $\mathbf{C}_{B,R}(k)$ and $\mathbf{C}_{B,T}(k)$, in turn, are RX and TX mutual coupling matrices at the l -th UE and BS, respectively, while $\mathbf{C}_{U,R}(k) = \text{bdiag}(\mathbf{C}_{1,R}(k), \dots, \mathbf{C}_{L,R}(k))$ and $\mathbf{C}_{U,T}(k) = \text{bdiag}(\mathbf{C}_{1,T}(k), \dots, \mathbf{C}_{L,T}(k))$ are the overall RX and TX mutual coupling matrices at the UE side.

Based on (9), propagation channel reciprocity $\mathbf{H}_{DL}(k) = \mathbf{H}_{UL}^T(k)$, and simple manipulations, the *effective UL channels* can now be written, in terms of *effective DL channels*, as

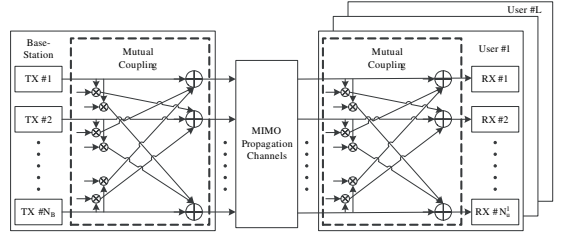


Fig. 1. Principal illustration of physical DL transmission and reception including propagation channels, transceivers and antenna mutual coupling in the devices.

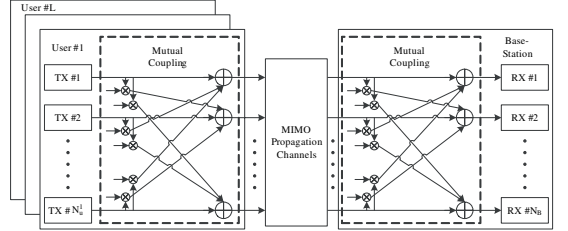


Fig. 2. Principal illustration of physical UL transmissions and reception including propagation channels, transceivers and antenna mutual coupling in the devices.

$$\begin{aligned}\bar{\mathbf{H}}_{UL}(k) &= \mathbf{A}_B(k) \mathbf{C}_B(k) (\bar{\mathbf{H}}_{DL}(k))^T \mathbf{C}_U(k) \mathbf{A}_U(k) \\ \bar{\mathbf{H}}_{UL,l}(k) &= \mathbf{A}_B(k) \mathbf{C}_B(k) (\bar{\mathbf{H}}_{DL,l}(k))^T \mathbf{C}_l(k) \mathbf{A}_l(k)\end{aligned}\quad (11)$$

where $\mathbf{A}_l(k) = \mathbf{A}_{l,T}(k) \mathbf{A}_{l,R}^{-1}(k)$, $\mathbf{A}_U(k) = \mathbf{A}_{U,T}(k) \mathbf{A}_{U,R}^{-1}(k)$, $\mathbf{A}_B(k) = \mathbf{A}_{B,T}^{-1}(k) \mathbf{A}_{B,R}(k)$, $\mathbf{C}_l(k) = \mathbf{C}_{l,T}(k) \mathbf{C}_{l,R}^{-1}(k)$, $\mathbf{C}_U(k) = \mathbf{C}_{U,T}(k) \mathbf{C}_{U,R}^{-1}(k)$ and $\mathbf{C}_B(k) = \mathbf{C}_{B,T}(k) \mathbf{C}_{B,R}^{-1}(k)$ are transceiver frequency response and mutual coupling mismatch matrices, respectively, at the l -th user, as well as in all the users $l = 1, 2, \dots, L$, and the BS side. Both type of mismatches (frequency responses and antenna coupling) are typically mildly frequency-selective over several MHz transmission bandwidths [5], [6], and hence depend on subcarrier index k .

Unlike diagonal frequency response mismatch matrices, mutual coupling mismatch matrices are generally non-diagonal and the exact values of $\mathbf{C}_B(k)$ and $\mathbf{C}_l(k)$ are dependent on the detailed implementation of antenna arrays. In [6], as a practical example, a fairly simple and widely-used coupling model is established where the circuit-level coupling matrix is of the form $\mathbf{C} = (\mathbf{Z}_A + \mathbf{Z}_T)(\mathbf{Z} + \mathbf{Z}_T \mathbf{I}_N)^{-1}$ where the parameters \mathbf{Z}_A and \mathbf{Z}_T and the elements of the matrix \mathbf{Z} depend on the impedances of the antenna elements and the associated transceiver circuits [6]. In this paper, to simplify the notations and the presentation, the diagonal elements of mutual coupling matrices are assumed to be normalized to 1, i.e., $[\mathbf{C}_{B(l),R(T)}(k)]_{i,i} = 1$ [6]. In general, $[\mathbf{C}_{B(l),R(T)}(k)]_{i,j}$ ($i \neq j$) represents the leakage coefficient from the j -th antenna to the i -th antenna at the RX and TX sides of the BS and the l -th UE, respectively.

Now, if CSIT at the BS is obtained by measuring effective UL channel matrices, biased estimation is unavoidable due to

mismatches (even without any additive noise or other interferences in the estimation process). This is established here, deploying (11), as

$$\begin{aligned}\hat{\mathbf{H}}_{DL}(k) &= \bar{\mathbf{H}}_{UL}^T(k) \\ &= \mathbf{A}_U^T(k) \mathbf{C}_U^T(k) \bar{\mathbf{H}}_{DL}(k) \mathbf{C}_B^T(k) \mathbf{A}_B^T(k) \\ &= \mathbf{G}_U^T(k) \bar{\mathbf{H}}_{DL}(k) \mathbf{G}_B(k) \\ &= (\mathbf{G}_U'(k) + \mathbf{I}_{N_U})^{-1} \bar{\mathbf{H}}_{DL}(k) (\mathbf{G}_B'(k) + \mathbf{I}_{N_B})^{-1}\end{aligned}\quad (12)$$

where $\mathbf{G}_U(k) = \mathbf{A}_U^T(k) \mathbf{C}_U^T(k)$, $\mathbf{G}_B(k) = \mathbf{C}_B^T(k) \mathbf{A}_B^T(k)$, $\mathbf{G}_U'(k) = \mathbf{G}_U^{-1}(k) - \mathbf{I}_{N_U}$ and $\mathbf{G}_B'(k) = \mathbf{G}_B^{-1}(k) - \mathbf{I}_{N_B}$. When the mismatch matrices $\mathbf{G}_U'(k) = \mathbf{G}_B'(k) = 0$, transceiver FR and mutual coupling are perfectly matched at the UE and BS sides.

IV. ANALYSIS OF CHANNEL NON-RECIPROCITY EFFECTS ON PRECODED MU MIMO-OFDM DL TRANSMISSION

In this section, the impacts of biased or imperfect channel estimates obtained through uplink reception, as given in (12), are analyzed in the precoded TDD MU MIMO-OFDM DL transmission context, in terms of instantaneous received SINR and achievable downlink sum-rate.

A. Effects of Channel Non-reciprocity in ZF Precoded MU MIMO-OFDM Systems

With imperfect CSIT given in (12), the ZF precoder in (4) reads now

$$\hat{\mathbf{W}}_{T,ZF}(k) = \hat{\mathbf{H}}_{DL}^H(k) (\hat{\mathbf{H}}_{DL}(k) \hat{\mathbf{H}}_{DL}^H(k))^{-1} \quad (13)$$

and $\hat{\beta}_{k,ZF} = \sqrt{Q / \text{tr}(\hat{\mathbf{W}}_{T,ZF}^H(k) \hat{\mathbf{W}}_{T,ZF}(k))}$. Then incorporating (13) in the downlink system model in (2) with the effective downlink channel matrix $\bar{\mathbf{H}}_{DL,l}(k)$ for the l -th user, the l -th user received signal reads

$$\begin{aligned}\mathbf{r}'_{l,ZF}(k) &= \hat{\beta}_{k,ZF} \bar{\mathbf{H}}_{DL,l}(k) \hat{\mathbf{W}}_{T,ZF}(k) \mathbf{s}(k) + \mathbf{n}_l(k) \\ &= \hat{\beta}_{k,ZF} \mathbf{G}_l^{-1}(k) \hat{\mathbf{H}}_{DL,l}(k) \mathbf{G}_B'(k) \hat{\mathbf{W}}_{T,ZF}(k) \mathbf{s}(k) + \mathbf{n}_l(k) \\ &= \hat{\beta}_{k,ZF} \mathbf{G}_l^{-1}(k) \bar{\mathbf{s}}_l(k) + \mathbf{C}_{ZF}(k) \mathbf{s}(k) + \mathbf{n}_l(k)\end{aligned}\quad (14)$$

where $\mathbf{C}_{ZF}(k) = \hat{\beta}_{k,ZF} \mathbf{G}_l^{-1}(k) \hat{\mathbf{H}}_{DL,l}(k) \mathbf{G}_B'(k) \hat{\mathbf{W}}_{T,ZF}(k)$ and $\mathbf{G}_l(k) = \mathbf{A}_l^T(k) \mathbf{C}_l^T(k)$. In above, the first term consists of the desired streams while the second term is mostly IUI.

Now, based on (14), it is interesting to observe that IUI free reception ($\mathbf{C}_{ZF}(k) = 0$) can be obtained, despite of transceiver frequency response and antenna mutual coupling mismatches at the UE device side, if the BS device has perfect matching. This follows directly from (14), and the expressions below it, by substituting $\mathbf{G}_B'(k) = 0$ (i.e. perfect match at BS side). This then reduces the observation to $\mathbf{r}'_{l,ZF}(k) = \hat{\beta}_{k,ZF} \mathbf{G}_l^{-1}(k) \bar{\mathbf{s}}_l(k) + \mathbf{n}_l(k)$. Hence, the first outcome of the analysis is that *BS device matching characteristics are clearly more critical than the UE side*.

In the general case, when either transceiver frequency response mismatch or antenna mutual coupling (or both) appear at the BS side, meaning that $\mathbf{G}_B'(k) \neq 0$, then $\mathbf{C}_{ZF}(k)$ becomes a non-zero matrix with entries depending on the values of DL effective channel matrix $\bar{\mathbf{H}}_{DL}(k)$ and the mismatch parameters. In this general case, both IUI and ISI occur at the l -th user reception

even if the implementation at the UE side is perfect. At the l -th user receiver, applying standard receiver spatial processing denoted by $\mathbf{W}_{R,l}^H(k)$ and operating on the received signal in (14), the processed signal is given by

$$\begin{aligned}\mathbf{y}'_{l,ZF}(k) &= \mathbf{W}_{R,l}^H(k) \mathbf{r}'_{l,ZF}(k) \\ &= \hat{\beta}_{k,ZF} \mathbf{W}_{R,l}^H(k) \bar{\mathbf{H}}_{DL,l}(k) \hat{\mathbf{W}}_{T,ZF}(k) \mathbf{s}(k) + \mathbf{W}_{R,l}^H(k) \mathbf{n}_l(k) \\ &= \mathbf{W}_{R,l}^H(k) \mathbf{F}_l^{(l)}(k) \bar{\mathbf{s}}_l(k) + \bar{\mathbf{n}}_l(k) \\ &= \mathbf{W}_{R,l}^H(k) \mathbf{F}_l^{(l)}(k) \bar{\mathbf{s}}_l(k) + \sum_{i=1, i \neq l}^L \mathbf{W}_{R,l}^H(k) \mathbf{F}_i^{(l)}(k) \bar{\mathbf{s}}_i(k) + \bar{\mathbf{n}}_l(k) \\ &= \bar{\mathbf{F}}_l^{(l)}(k) \bar{\mathbf{s}}_l(k) + \sum_{i=1, i \neq l}^L \bar{\mathbf{F}}_i^{(l)}(k) \bar{\mathbf{s}}_i(k) + \bar{\mathbf{n}}_l(k)\end{aligned}\quad (15)$$

where $\mathbf{F}_l^{(l)}(k) = \hat{\beta}_{k,ZF} \bar{\mathbf{H}}_{DL,l}(k) \hat{\mathbf{W}}_{T,ZF}(k) = [\mathbf{F}_1^{(l)}(k), \mathbf{F}_2^{(l)}(k), \dots, \mathbf{F}_L^{(l)}(k)]$, $\mathbf{F}_i^{(l)}(k)$ is an $N_U^l \times Q_l$ matrix, $\bar{\mathbf{F}}_i^{(l)}(k) = \mathbf{W}_{R,l}^H(k) \mathbf{F}_i^{(l)}(k)$ and $\bar{\mathbf{n}}_l(k) = \mathbf{W}_{R,l}^H(k) \mathbf{n}_l(k)$. Then the processed reception at the q_l -th spatial stream at the l -th user is given by

$$\begin{aligned}[\mathbf{y}'_{l,ZF}(k)]_{q_l} &= [\bar{\mathbf{F}}_l^{(l)}(k)]_{q_l, q_l} s_{l, q_l}(k) + \sum_{i=1, i \neq q_l}^{Q_l} [\bar{\mathbf{F}}_i^{(l)}(k)]_{q_l, i} s_{l, i}(k) \\ &\quad + \sum_{i=1, i \neq l}^L [\bar{\mathbf{F}}_i^{(l)}(k)]_{q_l, i} \bar{\mathbf{s}}_i(k) + \bar{\mathbf{n}}_l(k)\end{aligned}\quad (16)$$

where $\sum_{i=1, i \neq q_l}^{Q_l} [\bar{\mathbf{F}}_i^{(l)}(k)]_{q_l, i} s_{l, i}(k)$ is the residual ISI and $\sum_{i=1, i \neq l}^L [\bar{\mathbf{F}}_i^{(l)}(k)]_{q_l, i} \bar{\mathbf{s}}_i(k)$ depicts the IUI in the reception.

In general, $\mathbf{W}_{R,l}^H(k)$ can be designed to primarily suppress ISI while it is much more difficult to suppress IUI due to limited degrees of freedom, especially when the number of UE antennas is close to the number of own streams. Clear system performance degradation due to IUI is thus expected. Here, we seek to quantify this issue, especially from IUI perspective. Considering thus the first term, say $y_{l, q_l}(k) = [\bar{\mathbf{F}}_l^{(l)}(k)]_{q_l, q_l} s_{l, q_l}(k)$, in (16) as the desired useful signal and other terms as the overall interference and noise, respectively, the corresponding *instantaneous signal-to-interference-plus-noise ratio* (SINR) for the l -th user's q_l -th data stream is given by

$$\begin{aligned}\gamma_{l,ZF}^{q_l}(k) &= \frac{E \left[\left| y_{l, q_l}(k) \right|^2 \right]}{E \left[\left| [\mathbf{y}'_{l,ZF}(k)]_{q_l} - y_{l, q_l}(k) \right|^2 \right]} \\ &= \frac{\left| [\bar{\mathbf{F}}_l^{(l)}(k)]_{q_l, q_l} \right|^2}{P_{ZF,l}^{q_l}(k) + P_{ZF,l}'(k) + [\mathbf{W}_{R,l}^H(k) \mathbf{W}_{R,l}(k)]_{q_l, q_l} / \rho}\end{aligned}\quad (17)$$

where

$$\begin{aligned}P_{ZF,l}^{q_l}(k) &= \sum_{i=1, i \neq q_l}^{Q_l} \left| [\bar{\mathbf{F}}_i^{(l)}(k)]_{q_l, i} \right|^2 \\ P_{ZF,l}'(k) &= \sum_{i=1, i \neq l}^L \left| [\bar{\mathbf{F}}_i^{(l)}(k)]_{q_l, 0} \right| \left([\bar{\mathbf{F}}_i^{(l)}(k)]_{q_l, 0} \right)^H\end{aligned}\quad (18)$$

and $\rho = \sigma_s^2 / \sigma_n^2$ represents the so-called transmitted signal-to-noise ratio (SNR), per stream and subcarrier, and equal stream powers are assumed for simplicity. The concept of *instantaneous SINR* is here to be understood as being defined for given effective

tive channel matrix $\bar{\mathbf{H}}_{DL}(k)$ realization and given mismatch parameters. Then the system sum-rate over streams and users, and averaged over subcarriers and different channel and impairment realizations, can be evaluated as

$$r_{ZF} = \frac{1}{N} \sum_{k=1}^N \sum_{l=1}^L \sum_{q=1}^{Q_l} E \left[\log_2(1 + \gamma_{l,ZF}^q(k)) \right] \quad (19)$$

Notice that the above characterization is carried out for arbitrary receiver processing, hence any particular receiver $\mathbf{W}_{R,l}^H(k)$ can be deployed. Widely used receiver principle is LMMSE which can be written for user l as

$$\mathbf{W}_{R,l}^{LMMSE}(k) = \left(\sum_{i=1}^L \mathbf{F}_i^{(l)}(k) \left(\mathbf{F}_i^{(l)}(k) \right)^H + \mathbf{I}_{N_U'} / \rho \right)^{-1} \left(\mathbf{F}_l^{(l)}(k) \right) \quad (20)$$

where the associated precoded effective channel matrices \mathbf{F} are defined below (15). This is deployed in the forthcoming numerical evaluations in Section V.

B. Effects of Channel Non-reciprocity in Eigenbeamforming-based MU MIMO-OFDM DL Systems

Next similar analysis is carried out for eigenbeamforming based system. With imperfect CSIT in (12), the eigenbeamforming based precoder $\hat{\mathbf{W}}_{T,EM}(k)$ is constructed by decomposition of the UE level sub-matrices of $\hat{\mathbf{H}}_{DL}(k)$ in (12) into $\hat{\mathbf{V}}_l(k)$, $\hat{\mathbf{U}}_l^H(k)$ and $\hat{\Lambda}_l(k)$ following the procedures described in Section II.C. After precoding and experiencing the effective transmission channels, the signal arrives at the l -th user receiver as

$$\begin{aligned} \mathbf{r}'_{l,EM}(k) &= \hat{\beta}_{k,EM} \bar{\mathbf{H}}_{DL}(k) \hat{\mathbf{W}}_{T,EM}(k) \mathbf{s}(k) + \mathbf{n}_l(k) \\ &= \hat{\beta}_{k,EM} \mathbf{G}_l^{-1}(k) \hat{\mathbf{H}}_{DL,l}(k) \mathbf{G}_B^{-1}(k) \hat{\mathbf{W}}_{T,EM}(k) \mathbf{s}(k) + \mathbf{n}_l(k) \\ &= \hat{\beta}_{k,EM} \mathbf{G}_l^{-1}(k) \hat{\mathbf{U}}_l(k) \hat{\Lambda}_l(k) \bar{\mathbf{s}}_l(k) + \mathbf{G}_l^{-1}(k) \mathbf{C}_{EM}(k) \bar{\mathbf{s}}(k) + \mathbf{n}_l(k) \end{aligned} \quad (21)$$

where $\hat{\beta}_{k,EM} = \sqrt{Q / \text{tr}(\hat{\mathbf{W}}_{T,EM}^H(k) \hat{\mathbf{W}}_{T,EM}(k))}$ and $\mathbf{C}_{EM}(k) = \hat{\beta}_{k,EM} \mathbf{G}_l^{-1}(k) \hat{\mathbf{H}}_{DL,l}(k) \mathbf{G}_B^{-1}(k) \hat{\mathbf{W}}_{T,EM}(k)$.

In the case that $\mathbf{G}_B'(k) = 0$ which corresponds to perfect transceiver reciprocity and zero antenna mutual coupling at the BS side, there is no IUI at the l -th user reception as it directly follows that $\mathbf{C}_{EM}(k) = 0$. Only ISI cancellation is then needed at the UE side.

In the more general case of $\mathbf{G}_B'(k) \neq 0$, $\mathbf{C}_{EM}(k)$ appears to be a non-zero matrix with entries which are dependent on $\bar{\mathbf{H}}_{DL}(k)$ and the mismatch parameters. Again, both IUI and ISI are then present at the UE receptions. Applying now standard receiver spatial processing of the form $\mathbf{W}_{R,l}^H(k)$ on the reception in (21), the detector input at the l -th user receiver then reads

$$\begin{aligned} \mathbf{y}'_{l,EM}(k) &= \mathbf{W}_{R,l}^H(k) \mathbf{r}'_{l,EM}(k) \\ &= \hat{\beta}_{k,EM} \mathbf{W}_{R,l}^H(k) \bar{\mathbf{H}}_{DL,l}(k) \hat{\mathbf{W}}_{T,EM}(k) \mathbf{s}(k) + \mathbf{W}_{R,l}^H(k) \mathbf{n}_l(k) \\ &= \mathbf{W}_{R,l}^H(k) \mathbf{F}_l^{(l)}(k) \mathbf{s}(k) + \bar{\mathbf{n}}'_l(k) \\ &= \mathbf{W}_{R,l}^H(k) \mathbf{F}_l^{(l)}(k) \bar{\mathbf{s}}_l(k) \\ &+ \sum_{i=1, i \neq l}^L \mathbf{W}_{R,l}^H(k) \mathbf{F}_i^{(l)}(k) \bar{\mathbf{s}}_i(k) + \bar{\mathbf{n}}'_l(k) \\ &= \tilde{\mathbf{F}}_l^{(l)}(k) \bar{\mathbf{s}}_l(k) + \sum_{i=1, i \neq l}^L \tilde{\mathbf{F}}_i^{(l)}(k) \bar{\mathbf{s}}_i(k) + \bar{\mathbf{n}}'_l(k) \end{aligned} \quad (22)$$

where $\mathbf{F}^{(l)}(k) = \hat{\beta}_{k,EM} \bar{\mathbf{H}}_{DL,l}(k) \hat{\mathbf{W}}_{T,EM}(k) = [\mathbf{F}_1^{(l)}(k), \mathbf{F}_2^{(l)}(k), \dots, \mathbf{F}_L^{(l)}(k)]$, $\mathbf{F}_i^{(l)}(k)$ is an $N_U' \times Q_l$ matrix, $\tilde{\mathbf{F}}_i^{(l)}(k) = \mathbf{W}_{R,l}^H(k) \mathbf{F}_i^{(l)}(k)$ and $\bar{\mathbf{n}}'_l(k) = \mathbf{W}_{R,l}^H(k) \mathbf{n}_l(k)$. Then the reception for the q_l -th stream at the l -th user reads

$$\begin{aligned} [\mathbf{y}'_{l,EM}(k)]_{q_l} &= [\tilde{\mathbf{F}}_l^{(l)}(k)]_{q_l, q_l} s_{l, q_l}(k) + \sum_{i=1, i \neq q_l}^{Q_l} [\tilde{\mathbf{F}}_i^{(l)}(k)]_{q_l, i} s_{l, i}(k) \\ &+ \sum_{i=1, i \neq l}^L [\tilde{\mathbf{F}}_i^{(l)}(k)]_{q_l, 0} \bar{\mathbf{s}}_i(k) + \bar{\mathbf{n}}'_l(k) \end{aligned} \quad (23)$$

where $\sum_{i=1, i \neq q_l}^{Q_l} [\tilde{\mathbf{F}}_i^{(l)}(k)]_{q_l, i} s_{l, i}(k)$ and $\sum_{i=1, i \neq l}^L [\tilde{\mathbf{F}}_i^{(l)}(k)]_{q_l, i} \bar{\mathbf{s}}_i(k)$ denote the residual IUI and ISI in the reception, respectively. Again, we quantify the received signal quality, especially from IUI perspective below. Considering thus that the first component $y'_{l, q_l}(k) = [\tilde{\mathbf{F}}_l^{(l)}(k)]_{q_l, q_l} s_{l, q_l}(k)$ in (23) is the desired useful signal term while the others represent interference and noise, respectively, the corresponding *instantaneous SINR* for the l -th user's q_l -th data stream at k -th subcarrier is given by

$$\begin{aligned} \gamma_{l,EM}^{q_l}(k) &= \frac{E \left[|y'_{l, q_l}(k)|^2 \right]}{E \left[\left| [\mathbf{y}'_{l,EM}(k)]_{q_l} - y'_{l, q_l}(k) \right|^2 \right]} \\ &= \frac{\left| [\tilde{\mathbf{F}}_l^{(l)}(k)]_{q_l, q_l} \right|^2}{P_{EM,l}^{q_l}(k) + P_{EM,l}'^{q_l}(k) + [\mathbf{W}_{R,l}^H(k) \mathbf{W}_{R,l}(k)]_{q_l, q_l} / \rho} \end{aligned} \quad (24)$$

where

$$\begin{aligned} P_{EM,l}^{q_l}(k) &= \sum_{i=1, i \neq q_l}^{Q_l} \left| [\tilde{\mathbf{F}}_i^{(l)}(k)]_{q_l, i} \right|^2 \\ P_{EM,l}'^{q_l}(k) &= \sum_{i=1, i \neq l}^L \left| [\tilde{\mathbf{F}}_i^{(l)}(k)]_{q_l, i} \right|^2 \left([\tilde{\mathbf{F}}_i^{(l)}(k)]_{q_l, i} \right)^H \end{aligned} \quad (25)$$

and $\rho = \sigma_s^2 / \sigma_n^2$ is again the per-stream transmitted SNR at an arbitrary subcarrier. Then the system sum-rate over streams and users, which is averaged over subcarriers and different channel and impairment realizations, can be obtained as

$$r_{EM} = \frac{1}{N} \sum_{k=1}^N \sum_{l=1}^L \sum_{q=1}^{Q_l} E \left[\log_2(1 + \gamma_{l,EM}^q(k)) \right] \quad (26)$$

As in the previous section, one example of widely-deployed RX processing matrix $\mathbf{W}_{R,l}(k)$ can be constructed following the LMMSE receiver principle as

$$\mathbf{W}_{R,l}^{LMMSE}(k) = \left(\sum_{i=1}^L \mathbf{F}_i^{(l)}(k) \left(\mathbf{F}_i^{(l)}(k) \right)^H + \mathbf{I}_{N_U'} / \rho \right)^{-1} \mathbf{F}_l^{(l)}(k) \quad (27)$$

where the associated precoded effective channel matrices \mathbf{F}' are defined below (22).

In general, following from the above analysis, and illustrated numerically in the following section, transceiver non-reciprocity and antenna mutual coupling at the BS side can be substantial sources of IUI thus resulting to severe performance degradation. Implementation imperfections at the UE side, on the other hand,

cause only ISI at the reception which is fairly well processed by the receiver as part of precoded effective channel matrix. This observation provides important insight and motivation for the development of efficient reciprocity calibration techniques in the emerging TDD MU MIMO-OFDM systems.

V. SIMULATIONS AND NUMERICAL RESULTS

In this Section, the derived analysis results are evaluated and illustrated numerically. As a practical example, MU MIMO-OFDM DL transmission scenario with 4-antenna BS is considered, serving two UEs simultaneously over the same subcarriers. In more details, the BS is sending two parallel data streams to UE #1 and a single data stream to UE #2. In case of ZF precoding, UE #1 is assumed to contain two antennas while UE #2 is equipped with only a single antenna. In the eigenbeamforming-based precoding case, both UEs are assumed to be equipped with two antennas so that UE #2 can have enhanced reception through receiver diversity. We emphasize that these assumptions are made only to have a concrete and fairly practical evaluation scenario, and any other antenna and stream configurations could also be used. The deployed carrier frequency is assumed to be 2 GHz, and a total of 1024 subcarriers, out of which 600 are active, are deployed in the OFDM waveform processing with sub-carrier spacing of 15 kHz conforming to the basic 3GPP-LTE specifications [1].

The wireless propagation environment is modeled as a Rayleigh fading multipath channel with extended Vehicular A channel power delay profile [10]. Frequency response mismatches over the 10MHz waveform bandwidth at each transceiver at both the BS and UE sides are characterized as 9 tap FIR filters with randomly selected coefficients in time-domain. The level of these mismatches is controlled such that the variances of diagonal elements of the mismatch matrices $\mathbf{A}_B(k)$ and $\mathbf{A}_U(k)$, denoted with $\delta_{F,B}^2$ and $\delta_{F,U}^2$, respectively, are set to given values. The mutual antenna coupling matrices, in turn, are set such that only the neighboring antenna elements interfere with each other, i.e., $[\mathbf{C}_{B(U),R(T)}(k)]_{i,j} = 0$ if $|i - j| > 1$, and the mutual coupling mismatches between neighboring antenna elements, i.e., $[\mathbf{C}_{B(U),R}(k)\mathbf{C}_{B(U),T}^{-1}(k)]_{i,j}$ for $|i - j| = 1$, are modeled by zero mean complex normal distributed random variables with controllable variances $\delta_{C,B}^2$ and $\delta_{C,U}^2$. In the result figures, these variances are given in relative dB scale as $10 \log_{10}(\delta^2)$. First, the achievable average system sum-rates with transceiver frequency-response mismatches and/or mutual coupling mismatches at the BS and/or UEs are examined, individually as well as jointly. As shown in Fig. 3 (ZF precoded) and Fig. 4 (eigenbeamforming), the imperfections at the UEs have no noticeable impact on the system performance. Mismatches at the BS, on the other hand, result in substantial performance degradation especially when average SNRs are higher than 15dB. This confirms the initial insight established already in Section IV.

Next, the performance degradation with different levels of BS mismatches is compared at an example SNR of $\rho = 25$ dB.

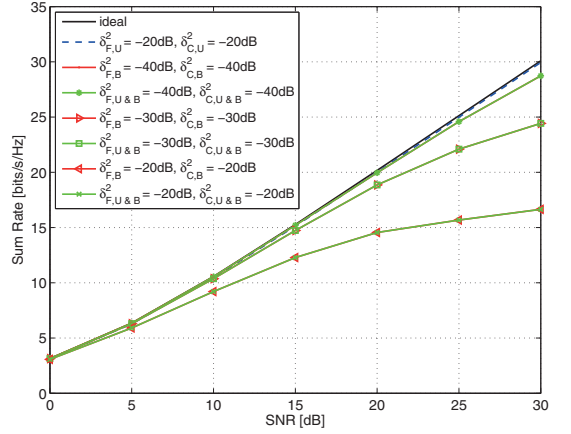


Fig. 3. Comparison of average sum-rates for two-user ZF pre-coded MIMO-OFDM DL system with different frequency response mismatch and antenna coupling mismatch levels at the base-station and/or UEs. δ^2 denotes the relative mismatch variances, expressed in dB's. X-axis refers to average transmitted per-stream, per-subcarrier SNR.

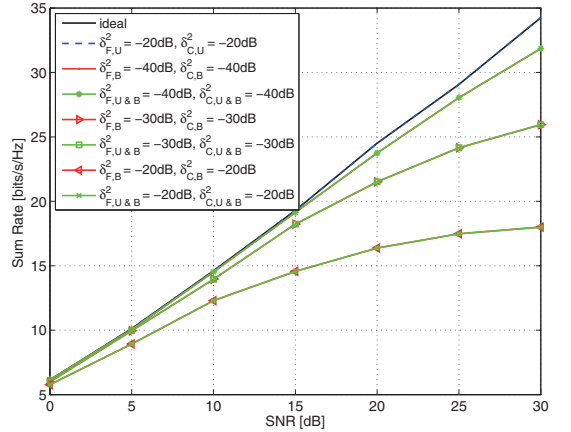


Fig. 4. Comparison of average sum-rates for two-user eigenbeamforming-based MIMO-OFDM DL system with different frequency response mismatch and antenna coupling mismatch levels at the base-station and/or UEs. δ^2 denotes the relative mismatch variances, expressed in dB's. X-axis refers to average transmitted per-stream, per-subcarrier SNR.

As illustrated in Fig. 5 and Fig. 6, with both precoding schemes, the system is more sensitive to antenna mutual coupling mismatches than transceiver frequency response mismatches. However, both BS imperfections clearly impact the performance. In the considered transmission scenario, to achieve close to ideal performance, maximum tolerable levels of transceiver frequency response mismatches and mutual coupling mismatches at the BS side are around -35dB and -40dB with ZF precoding, and around -40dB and -45dB with eigenbeamforming, respectively. Thus accurate BS calibration techniques are required in order to truly capitalize the channel reciprocity.

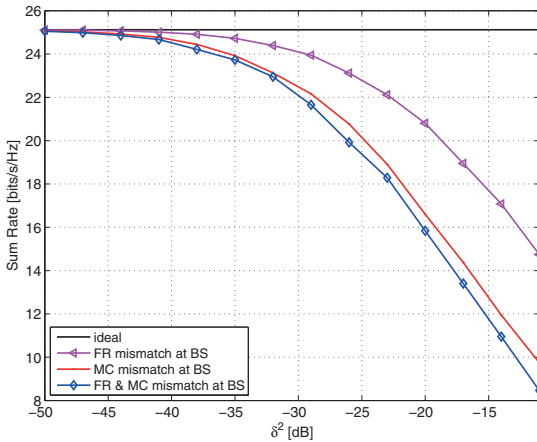


Fig. 5. Comparison of average sum-rates for two-user ZF precoded MIMO-OFDM DL system with frequency response mismatch or/and antenna mutual coupling mismatch at the BS. δ^2 denotes the relative mismatch variances, expressed in dB's. UE devices are ideal (zero mismatches). The average transmitted per-stream, per-subcarrier SNR is fixed to $\rho = 25\text{dB}$.

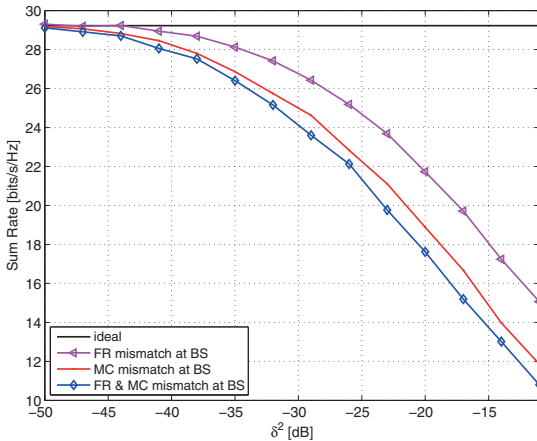


Fig. 6. Comparison of average sum-rates for two-user eigenbeamforming-based MIMO-OFDM DL system with frequency response mismatch or/and antenna mutual coupling mismatch at the BS. δ^2 denotes the relative mismatch variances, expressed in dB's. UE devices are ideal (zero mismatches). The average transmitted per-stream, per-subcarrier SNR is fixed to $\rho = 25\text{dB}$.

VI. CONCLUSIONS

This paper studied the impact of channel non-reciprocity due to transceiver frequency response and antenna mutual coupling mismatches on the performance of TDD-based precoded MU MIMO-OFDM DL transmission systems. Based on the developed signal and system models, performance degradation in terms of UE receiver instantaneous SINR and average system sum-rate were analyzed and evaluated. The analysis shows that the transceiver non-reciprocity and antenna mutual coupling mismatches at the BS side cause both IUI and ISI whereas the

implementation imperfections at the UE cause only ISI. In general, the system performance is more sensitive to antenna mutual coupling than transceiver frequency responses mismatches, but both clearly affect the performance. Thus, overall, the analysis results strongly motivate towards accurate (non)reciprocity estimation and calibration techniques and their development at the BS side in the emerging TDD-based multi-user wireless systems.

REFERENCES

- [1] H. Holma and A. Toskala, *LTE for UMTS: Evolution to LTE-Advanced*, 2nd ed., West Sussex, John Wiley & Sons, 2011.
- [2] Taesang and A. Goldsmith, "On the optimality of multiantenna broadcast scheduling using zero-forcing beamforming," *IEEE Journal on Selected Areas in Communications*, vol.24, no.3, pp.528-541, Mar. 2006.
- [3] A. Tölli, "Resource management in cooperative MIMO-OFDM cellular system", Ph.D. dissertation, University of Oulu, Oulu, Finland, Apr. 2008.
- [4] G. Lebrun, J. Gao and M. Faulkner, "MIMO transmission over a time-varying channel using SVD," *IEEE Transactions on Wireless Commun.*, vol. 4, no. 2, 2005.
- [5] J. C. Haartsen, "Impact of non-reciprocal channel conditions in broadband TDD systems," in *Proc. IEEE 19th Int. Sym. Personal, Indoor and Mobile Radio Commun., 2008 (PIMRC 2008)*, pp.1-5, 15-18 Sep. 2008.
- [6] S. Durrani, and M. Bialkowski, "Effect of mutual coupling on the interference rejection capabilities of linear and circular arrays in CDMA systems," *IEEE Transactions on Antennas and Propagation*, vol.52, no.4, pp.1130-1134, Apr. 2004.
- [7] J. Liu, A. Bourdoux, J. Craninckx, P. Wambacq, B. Come, S. Donnay, and A. Barel, "OFDM-MIMO WLAN AP Front-end Gain and Phase Mismatch Calibration," in *Proc. IEEE Radio and Wireless Conference (RAWCON)*, pp. 151-154, Atlanta, USA, Sep. 2004.
- [8] B. Kouassi, I. Ghauri, and L. Deneire, "Estimation of time-domain calibration parameters to restore MIMO-TDD channel reciprocity," in *Proc. 7th International ICST Conference on Cognitive Radio Oriented Wireless Networks and Communications (CROWNCOM)*, vol., no., pp.254-258, Jun. 2012.
- [9] M. Petermann, M. Stefer, F. Ludwig, D. Wubben, M. Schneider, S. Paul, and K. Kammeyer, "Multi-User Pre-Processing in Multi-Antenna OFDM TDD Systems with Non-Reciprocal Transceivers," *IEEE Transactions on Communications*, vol.61, no.9, pp.3781-3793, Sep. 2013.
- [10] T. B. Sorensen, P. E. Mogensen, and F. Frederiksen, "Extension of the ITU channel models for wideband (OFDM) systems," in *Proc. IEEE Veh. Technol. Conf.*, Dallas, TX, pp. 392-396, Sep. 2005.

PUBLICATION VIII

Y. Zou, O. Raeesi, and M. Valkama, “Efficient estimation and compensation of transceiver non-reciprocity in precoded TDD multi-user MIMO-OFDM systems,” in *2014 IEEE 80th Vehicular Technology Conference (VTC2014-Fall)*, Sept 2014, pp. 1–7.

© 2014 IEEE. Reprinted, with permission, from Y. Zou, O. Raeesi, and M. Valkama, “Efficient estimation and compensation of transceiver non-reciprocity in precoded TDD multi-user MIMO-OFDM systems,” in 2014 IEEE 80th Vehicular Technology Conference (VTC2014-Fall), September 2014.

In reference to IEEE copyrighted material which is used with permission in this thesis, the IEEE does not endorse any of Tampere University’s products or services. Internal or personal use of this material is permitted. If interested in reprinting/republishing IEEE copyrighted material for advertising or promotional purposes or for creating new collective works for resale or redistribution, please go to http://www.ieee.org/publications_standards/publications/rights/rights_link.html to learn how to obtain a License from RightsLink.

Efficient Estimation and Compensation of Transceiver Non-reciprocity in Precoded TDD Multi-User MIMO-OFDM Systems

Yaning Zou, Orod Raeesi, and Mikko Valkama

Department of Electronics and Communications Engineering
Tampere University of Technology
Tampere, Finland

yaning.zou@tut.fi, orod.raeesi@tut.fi, mikko.e.valkama@tut.fi

Abstract— In this paper, we propose an efficient transceiver non-reciprocity estimation-compensation framework for precoded TDD multi-user MIMO-OFDM downlink transmission systems. General signal models are first developed to analyze the effects of transceiver non-reciprocity at both the base-station and user equipment sides. The analysis shows that transceiver non-reciprocity at the base-station causes inter-user interference and thus substantial performance degradation, while the impact of transceiver non-reciprocity at the user equipment side can be fairly easily handled with downlink detector processing. Next, an over-the-air (OTA) type pilot-based estimation algorithm is devised for efficient identification of base-station non-reciprocity parameters, which are then used in pre-compensating or precoding the multiuser data properly in the base-station. Compared to the existing work in the literature, the proposed approach does not require the use of feedback signaling or complicated channel matrix decomposition techniques for extracting the non-reciprocity parameters. The resulting link and system performance of the proposed estimation-compensation framework is then evaluated using extensive computer simulations in linear precoded TDD multiuser MIMO-OFDM system context. Based on the obtained results, the proposed estimation-compensation approach can provide a simple, practical and flexible solution to efficiently restore the channel reciprocity with reasonable calibration overhead.

Keywords— channel reciprocity; transceiver non-reciprocity; reciprocity calibration; multiuser MIMO-OFDM.

I. INTRODUCTION

Channel reciprocity is considered as one of the most important elements in the development and efficient deployment of time-division duplexing (TDD) based multi-user (MU) MIMO-OFDM systems [1]-[3]. In TDD systems, downlink (DL) and uplink (UL) operate at the same center frequency and thus the DL channel state information at transmitter (CSIT) can be acquired by the base-station (BS) through simply measuring the UL signals, given that the UL-DL switching period is

sufficiently short relative to the channel coherence time. In practice, however, the *effective transmission channels* include also the radio hardware of the devices, namely transmit chains, receive chains and antennas [7]-[10]. Even if assuming reasonably good antenna isolation in each device, there are always unavoidable frequency response (FR) mismatches between the transmitter (TX, containing, e.g., mixers, power amplifier and RF filtering) and receiver (RX, e.g., RF filtering, LNA, mixers, and lowpass filtering) chains implemented in the same transceiver, which, in turn, distort the reciprocal nature of the effective DL and UL channels. As shown in [5]-[10], if the CSIT at the BS is obtained by measuring the UL signals under transceiver non-reciprocity, inter-user interference (IUI) occurs at user equipment (UE) reception and thus causes severe performance degradation in TDD MU MIMO-OFDM DL transmission.

In order to cope with transceiver non-reciprocity problem, two types of estimation-compensation approaches have been proposed in the literature. In [5]-[8], direct offline hardware estimation-calibration is proposed. It provides a standard independent solution yet adds substantial implementation complexity and cost for each device. In [8]-[10], as an alternative to hardware based approaches, over-the-air (OTA) type estimation-compensation algorithms are developed which require establishing a test calibration and feedback link with external test equipment (TE) for parameter estimation. This approach does not require implementation of extra hardware in the base-station devices but is based on dedicated calibration period in which communication takes place with the TE. In this type of OTA estimation, the current solutions in the literature [8]-[10] assume further that the DL channel matrix towards the TE is always known by the BS, e.g. via accurate high-rate feedback signaling. Then, the non-reciprocity parameters are extracted by measuring the UL channel matrix from the TE transmission, followed by comparison and decomposition of the measured TE DL and UL channel matrices. The performance of such approach is, however, always limited in practice by the finite rate of feedback signaling from TE towards the BS. Furthermore, the computational complexity of deployed matrix decompositions applied in [8]-[10] are far from trivial.

In this paper, we develop an efficient estimation-compensation framework and algorithms for the compensation

This work was supported by the Finnish Funding Agency for Technology and Innovation (Tekes), Broadcom Communications Finland and Huawei Finland under the project “Energy-Efficient Wireless Networks and Connectivity of Devices – Densification (EWINE-D)”, the Academy of Finland under the projects 251138 “Digitally-Enhanced RF for Cognitive Radio Devices” and 138424 “Joint Analysis and DSP-Based Mitigation of Multiple RF Impairments in Future Radio Devices”, and TUT Graduate School.

of BS transceiver non-reciprocity in TDD precoded MU MIMO-OFDM DL transmission systems. First, based on the developed signal and system models, the non-reciprocal transceivers at the BS side are shown to be a major cause of downlink performance degradation, stemming from IUI while non-reciprocal transceivers at UEs result only in inter-stream interference (ISI) which can be fairly easily handled in downlink detector processing. Then, an OTA type pilot-based estimation framework is proposed to estimate the essential non-reciprocity parameters at the BS. The proposed approach does not require the use of any feedback signaling nor computationally intensive channel matrix decomposition techniques as done in the existing reference methods in the literature. Incorporating the estimated non-reciprocity characteristics properly into the spatial precoding in the actual data transmission phase, close to ideal linear precoded MU-MIMO downlink performance can be achieved. This is explored and demonstrated through extensive computer simulations. Furthermore, in the estimation phase, only short training period is required incorporating low system overhead.

II. EFFECT OF TRANSCIVER NON-RECIPROCITY IN LINEAR PRECODED TDD MU MIMO-OFDM DL TRANSMISSION

A. Link Model of Linear Precoded MU MIMO-OFDM DL Transmission System

Here, we consider an L -user $N_U \times N_B$ linearly precoded MIMO-OFDM DL transmission system. As shown in Figure 1, N_B transmission antennas are deployed at the BS side while N_U^l antennas are deployed at the l -th user equipment, and thus altogether there are $N_U = \sum_{l=1}^L N_U^l$ antennas at the UE side. Furthermore, OFDM transmission is assumed with a total of N subcarriers. At the k -th subcarrier, $Q \times 1$ size overall data vector $\mathbf{s}(k)$ is precoded into N_B streams using $N_B \times Q$ precoding matrix $\mathbf{W}_T(k)$ and transmitted using the N_B transmit antennas deploying OFDM waveform. The total precoded subcarrier spatial vector reads thus

$$\mathbf{x}(k) = \mathbf{W}_T(k)\mathbf{s}(k) \quad (1)$$

where $\mathbf{s}(k) = [\bar{\mathbf{s}}_1(k)^T, \dots, \bar{\mathbf{s}}_l(k)^T, \dots, \bar{\mathbf{s}}_L(k)^T]^T$ and $\bar{\mathbf{s}}_l(k)$ denotes the $Q_l \times 1$ data vector of the l -th user at the considered k -th subcarrier and $Q = \sum_{l=1}^L Q_l$.

After experiencing multipath MIMO radio propagation from the BS to the l -th user, the receiver input vector at the l -th user at the k -th subcarrier is given by

$$\begin{aligned} \mathbf{r}_l(k) &= \mathbf{H}_{DL,l}(k)\mathbf{x}(k) + \mathbf{n}_l(k) \\ &= \mathbf{H}_{DL,l}(k)\mathbf{W}_T(k)\mathbf{s}(k) + \mathbf{n}_l(k) \end{aligned} \quad (2)$$

where $\mathbf{H}_{DL,l}(k)$ refers to $N_U^l \times N_B$ DL channel matrix from the BS to the l -th user and $\mathbf{n}_l(k)$ is $N_U^l \times 1$ noise vector at the l -th user receiver at the k -th subcarrier. Now, based on (1) and (2), in order to avoid inter-user interferences (IUI) at the l -th user reception, the linear precoder $\mathbf{W}_T(k)$ deployed at TX should be designed such that the overall equivalent $N_U^l \times Q$ transmission matrix $\mathbf{T}_l(k) = \mathbf{H}_{DL,l}(k)\mathbf{W}_T(k)$ can be structured as

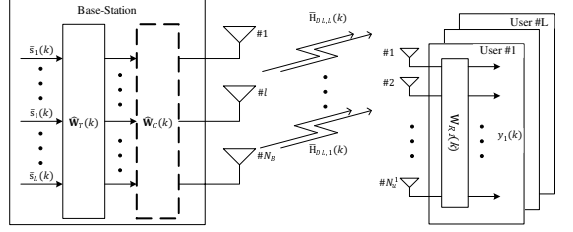


Figure 1: Principal illustration of the proposed base-station transceiver non-reciprocity mitigation scheme for linear precoded TDD MU MIMO-OFDM DL transmission with L users.

$$\mathbf{T}_l(k) = \begin{bmatrix} \mathbf{0} & \mathbf{C}_{Q_l}(k) \mathbf{0} \\ \mathbf{0} & \mathbf{0} \end{bmatrix} \quad (3)$$

This precoder design guarantees that the impact of streams of all other users are nulled at the target receiver and thus the reception in (2) becomes essentially

$$\mathbf{r}_l(k) = \mathbf{C}_{Q_l}(k)\bar{\mathbf{s}}_l(k) + \mathbf{n}_l(k) \quad (4)$$

where $\mathbf{C}_{Q_l}(k)$ denotes $N_U^l \times Q_l$ matrix with non-zero diagonal entries. Then by applying $Q_l \times N_U^l$ spatial filter $\mathbf{W}_{R,l}^H(k)$, the detector input $\mathbf{y}_l(k) = \mathbf{W}_{R,l}^H(k)\mathbf{r}_l(k)$ at the l -th user receiver is given by

$$\mathbf{y}_l(k) = \mathbf{W}_{R,l}^H(k)\mathbf{C}_{Q_l}(k)\bar{\mathbf{s}}_l(k) + \mathbf{W}_{R,l}^H(k)\mathbf{n}_l(k) \quad (5)$$

where the receiver $\mathbf{W}_{R,l}^H(k)$ can be designed, e.g., to minimize the interstream interference (ISI) and noise power at the filter output using the linear minimum mean square error (LMMSE) principle as $\mathbf{W}_{R,l}(k) = \left(\mathbf{C}_{Q_l}(k)(\mathbf{C}_{Q_l}(k))^H + \mathbf{I}_{N_U^l} / \rho \right)^{-1} \mathbf{C}_{Q_l}(k)$ where ρ denotes the ratio of subcarrier-level per-stream transmit power and the subcarrier-level received noise power. Furthermore, if the receiver has sufficient amount of antennas, the receiver spatial filter can also partially assist in IUI reduction (if precoder does not null it perfectly), which implies that the total spatial channel $\mathbf{W}_{R,l}^H(k)\mathbf{H}_{DL,l}(k)\mathbf{W}_T(k)$ suppresses the effect of other users' streams while also controlling the ISI between own streams and noise.

B. Modeling Transceiver Non-reciprocity and Its Impact on Channel Reciprocity in TDD Mode

In general, as outlined above, the design of optimal linear precoder $\mathbf{W}_T(k)$ at the BS requires DL channel knowledge. In TDD systems, DL CSIT can be obtained by measuring UL channels, denoted here by $\mathbf{H}_{UL,l}(k)$, as DL and UL operate at the same center-frequency, and thus ideally $\mathbf{H}_{DL,l}(k) = \mathbf{H}_{UL,l}^T(k)$ [1], [2]. However, in practice, the actual *effective DL and UL channels*, say $\bar{\mathbf{H}}_{DL,l}(k)$ and $\bar{\mathbf{H}}_{UL,l}(k)$, include also the responses of electronics components used in the transmitting and receiving devices. Due to circuit and process variations, there are thus always some unavoidable mismatches between the frequency responses (FRs) of transmitter and receiver chains of any individual transceiver. As modeled in more details in [5]-[10], under such transceiver non-reciprocity at both the BS and UE

sides, and even with perfect channel estimation, the estimated effective DL channel matrices $\hat{\mathbf{H}}_{DL,l}(k)$ obtained from the estimated UL channel matrices $\hat{\mathbf{H}}_{UL,l}(k)$ as $\hat{\mathbf{H}}_{DL,l}(k) = \hat{\mathbf{H}}_{UL,l}^T(k)$ are thus always biased. Using now the notation

$$\begin{aligned}\bar{\mathbf{H}}_{DL}(k) &= [\bar{\mathbf{H}}_{DL,1}^T(k), \dots, \bar{\mathbf{H}}_{DL,L}^T(k)]^T \\ \bar{\mathbf{H}}_{UL}(k) &= [\bar{\mathbf{H}}_{UL,1}^T(k), \dots, \bar{\mathbf{H}}_{UL,L}^T(k)]^T\end{aligned}$$

and similarly for the corresponding estimated effective channels, the *downlink channel non-reciprocity* can be described as

$$\begin{aligned}\hat{\mathbf{H}}_{DL,l}(k) &= \hat{\mathbf{H}}_{UL,l}^T(k) = \mathbf{A}_l(k) \bar{\mathbf{H}}_{DL,l}(k) \mathbf{A}_B(k) \\ \hat{\mathbf{H}}_{DL}(k) &= \hat{\mathbf{H}}_{UL}^T(k) = \mathbf{A}_U(k) \bar{\mathbf{H}}_{DL}(k) \mathbf{A}_B(k)\end{aligned}\quad (6)$$

where $\mathbf{A}_l(k)$, $\mathbf{A}_U(k)$ and $\mathbf{A}_B(k)$ are *diagonal matrices* depicting transceiver FR mismatches at the l -th user, at all the users and at the BS, respectively. Clearly, under *transceiver non-reciprocity*, $\mathbf{A}_l(k)$, $\mathbf{A}_U(k)$ and $\mathbf{A}_B(k)$ are not identity matrices and thus in general it follows that $\hat{\mathbf{H}}_{DL,l}(k) \neq \bar{\mathbf{H}}_{DL,l}(k)$ and $\hat{\mathbf{H}}_{DL}(k) \neq \bar{\mathbf{H}}_{DL}(k)$. As shown in [7], the FR mismatches in each transceiver is typically mildly frequency-selective within commonly deployed waveform bandwidths in the order of several or several tens of MHz.

C. Impact of Channel Non-reciprocity on Linear Precoded MU MIMO-OFDM Systems

Under channel non-reciprocity described in (6), the realizable precoder $\hat{\mathbf{W}}_T(k)$ is obtained through estimated CSIT $\hat{\mathbf{H}}_{DL}(k)$. Using similar precoder optimization principle as in (3), but under estimated CSIT, the *effective precoded channel* towards l -th user from precoder optimization perspective reads now

$$\begin{aligned}\mathbf{T}_l'(k) &= \hat{\mathbf{H}}_{DL,l}(k) \hat{\mathbf{W}}_T(k) \\ &= \begin{bmatrix} \mathbf{0} & \mathbf{C}'_{Q_l}(k) & \mathbf{0} \\ \mathbf{0}_{N_U' \times \sum_{q_1=1}^{l-1} Q_{q_1}} & & \mathbf{0}_{N_U' \times \sum_{q_1=l+1}^L Q_{q_1}} \end{bmatrix}\end{aligned}\quad (7)$$

where $\mathbf{C}'_{Q_l}(k)$ denotes $N_U' \times Q_l$ matrix with non-zero diagonal entries. However, the actual downlink transmission towards the l -th UE is subject to the true effective channel $\bar{\mathbf{H}}_{DL,l}(k)$, and thus the reception at the l -th user receiver reads

$$\begin{aligned}\mathbf{r}_l'(k) &= \bar{\mathbf{H}}_{DL,l}(k) \hat{\mathbf{W}}_T(k) \mathbf{s}(k) + \mathbf{n}_l(k) \\ &= \mathbf{A}_l^{-1}(k) \bar{\mathbf{H}}_{DL,l}(k) \mathbf{A}_B^{-1}(k) \hat{\mathbf{W}}_T(k) \mathbf{s}(k) + \mathbf{n}_l(k) \\ &= \mathbf{A}_l^{-1}(k) \mathbf{C}'_{Q_l}(k) \bar{\mathbf{s}}_l(k) + \mathbf{C}(k) \mathbf{s}(k) + \mathbf{n}_l(k)\end{aligned}\quad (8)$$

where $\mathbf{A}_B'(k) = \mathbf{A}_B(k) - \mathbf{I}_{N_B}$ and $\mathbf{C}(k) = \mathbf{A}_l^{-1}(k) \bar{\mathbf{H}}_{DL,l}(k) \times \mathbf{A}_B'(k) \hat{\mathbf{W}}_T(k)$. Now, if transceivers at the BS are reciprocal and thus $\mathbf{A}_B'(k) = \mathbf{0}$, it implies that $\mathbf{C}(k) = \mathbf{0}$ and there is no IUI in the reception. Inter-stream interference, in turn, appears at the reception if and when $\mathbf{C}'_{Q_l}(k)$ is a non-diagonal matrix but it can be easily suppressed in the receiver spatial processing. On the other hand, in the case that the transceivers at the BS are non-reciprocal and thus $\mathbf{A}_B'(k) \neq \mathbf{0}$, it directly implies that $\mathbf{C}(k) \neq \mathbf{0}$ which in turn means that both IUI and inter-stream interference take place in the receiver. In the general case, especially if the number of own streams is close to the number of

UE antennas, IUI cannot be efficiently suppressed by receiver processing, and hence significant performance degradation is expected. This, in turn, calls for the development of advanced reciprocity calibration or restoration techniques at the BS side to prevent such performance losses.

III. COMPENSATION OF TRANSCEIVER NON-RECIPROCITY IN PRECODED TDD MU MIMO-OFDM SYSTEMS

Ideally, if all the transceiver non-reciprocity parameters of the BS device ($\mathbf{A}_B(k)$) and the UEs ($\mathbf{A}_U(k)$) are perfectly known at the BS side, the transceiver non-reciprocity problem can be easily solved by calibrating the estimated UL channel matrix to correspond to the actual effective DL channel matrix before constructing the precoder as

$$\hat{\mathbf{H}}_{DL,l}(k) = \mathbf{A}_l^{-1}(k) \hat{\mathbf{H}}_{UL,l}(k) \mathbf{A}_B^{-1}(k) = \bar{\mathbf{H}}_{DL,l}(k) \quad (9)$$

However, in modern cellular systems, the UEs accessing the channel change dynamically, through dynamic scheduling. Furthermore, the exact frequency responses of the transceivers are actually time-dependent due to, e.g., temperature changes. Thus, it is very challenging to track the transceiver non-reciprocity parameters $\mathbf{A}_l(k)$ of all the connected UEs in the network in a timely manner, without causing a large amount of overhead. Therefore, direct channel non-reciprocity correction as described in (9) is not a realistic solution. On the other hand, as discussed in Section II.C, only the transceiver non-reciprocity at the BS is causing IUI in the UE receivers, while the transceiver non-reciprocity at the UE side can actually be suppressed by proper RX processing.

Based on the above reasoning, we propose a BS-UE transceiver non-reciprocity co-processing framework operating as follows. Firstly, as illustrated in Figure 1, a compensator filter $\mathbf{W}_C(k)$ is applied on the precoded signal in the BS so that after propagating through the MIMO channels, the reception at the l -th user receiver is given by

$$\begin{aligned}\mathbf{r}_{l,C}'(k) &= \bar{\mathbf{H}}_{DL,l}(k) \mathbf{W}_C(k) \hat{\mathbf{W}}_T(k) \mathbf{s}(k) + \mathbf{n}_l(k) \\ &= \mathbf{A}_l^{-1}(k) \mathbf{T}_l''(k) \mathbf{s}(k) + \mathbf{n}_l(k) \\ &= a_C(k) \mathbf{A}_l^{-1}(k) \mathbf{C}''_{Q_l}(k) \bar{\mathbf{s}}_l(k) + \mathbf{n}_l(k)\end{aligned}\quad (10)$$

where $a_C(k)$ is a free design parameter that can be used, e.g., to adjust and keep the overall transmission power unchanged after non-reciprocity compensation, $\mathbf{C}''_{Q_l}(k)$ denotes a $Q_l \times Q_l$ matrix with non-zero diagonal entries and

$$\begin{aligned}\mathbf{T}_l''(k) &= \bar{\mathbf{H}}_{DL,l}(k) \mathbf{A}_B^{-1}(k) \mathbf{W}_C(k) \hat{\mathbf{W}}_T(k) \\ &= a_C(k) \begin{bmatrix} \mathbf{0} & \mathbf{C}''_{Q_l}(k) & \mathbf{0} \\ \mathbf{0}_{Q_l \times \sum_{q_1=1}^{l-1} Q_{q_1}} & & \mathbf{0}_{Q_l \times \sum_{q_1=l+1}^L Q_{q_1}} \end{bmatrix}\end{aligned}\quad (11)$$

Due to the structure of $\mathbf{T}_l''(k)$, this compensation processing results to zero IUI, despite of transceiver non-reciprocity. At the UE receiver side, the desired signal vector $\bar{\mathbf{s}}_l(k)$ can then be efficiently recovered by applying RX processing $\mathbf{W}_{R,l}^H(k)$ on the reception $\mathbf{r}_{l,C}'(k)$. A widely used receiver principle is the LMMSE receiver which can now be written for the user l as

$$\mathbf{W}_{R,l}(k) = \left(\mathbf{F}^{(l)}(k) \left(\mathbf{F}^{(l)}(k) \right)^H + \mathbf{I}_{N_U} / \rho \right)^{-1} \left(\mathbf{F}^{(l)}(k) \right) \quad (12)$$

where $\mathbf{F}^{(l)}(k) = a_C(k) \mathbf{A}_U^{-1}(k) \mathbf{C}_{Q_d}^H(k)$.

To elaborate further on the processing solution, we proceed as follows. Based on (8), one simple solution is to set $\mathbf{A}_B^{-1}(k) \mathbf{W}_C(k) = a_C(k) \mathbf{I}_{N_B}$ so that $\mathbf{T}_l''(k) = a_C(k) \bar{\mathbf{H}}_{DL,l}(k) \bar{\mathbf{W}}_T(k) = a_C(k) \mathbf{T}_l'(k)$. The compensator itself can then be obtained as

$$\mathbf{W}_C(k) = a_C(k) \mathbf{A}_B(k) \quad (13)$$

As the above developments demonstrate, the derived pre-compensation solution calls for efficient estimation of the BS transceiver non-reciprocity matrix $\mathbf{A}_B(k)$. It is also interesting to notice that according to (11) and (13), the BS in fact does not need to estimate the exact value of $\mathbf{A}_B(k)$ but it is sufficient to estimate it up to scalar scaling, say $a_C(k) \mathbf{A}_B(k)$, as shown in (13). Such estimation procedure is next proposed and formulated in detail.

IV. ESTIMATION OF TRANSCIVER NON-RECIPROCY PARAMETERS AT THE BASE-STATION

In order to estimate the transceiver non-reciprocity parameters at the BS, a radio link between the BS and a test-equipment (TE) is assumed to be established as shown in Figure 2. This TE can in practice be one of the UE devices or a separate device, and is here assumed to operate with a single antenna. The frequency response mismatch coefficient at the k -th subcarrier in TE device is denoted by $a_e(k) = a_{e,RX}(k) / a_{e,TX}(k)$. The effective DL channel vector at the k -th subcarrier is denoted as $\bar{\mathbf{h}}_{e,DL}(k) = [h_{e,1}(k), h_{e,2}(k), \dots, h_{e,N_B}(k)]$ while the effective UL channel vector can now be written in terms of $\bar{\mathbf{h}}_{e,DL}(k)$ and non-reciprocity parameters as $\bar{\mathbf{h}}_{e,UL}(k) = \mathbf{A}_B(k) \bar{\mathbf{h}}_{e,DL}(k) a_e(k)$. Both DL and UL channels are assumed to stay constant during the estimation period. For notational convenience, we ignore the additive channel noise in the below estimator developments but is naturally included properly in all performance simulations.

A. Pilot-based Estimation of Transceiver Non-reciprocity at the BS

As the estimation period starts, a complex pilot sequence of length N_B OFDM symbols, written here at subcarrier k as $s_{p,1}^d(k), \dots, s_{p,N_B}^d(k)$, is first transmitted from the BS to the TE without precoding. As the TE is a single-antenna device, we assume that the BS transmits one OFDM symbol through one antenna at a time, hence overall there are N_B OFDM symbols transmitted towards TE. Using next a diagonal matrix representation $\mathbf{S}_P^{DL}(k) = \text{diag}([s_{p,1}^d(k), \dots, s_{p,N_B}^d(k)]^T)$ for the pilot sequence at subcarrier k , the received signal at the test-equipment over N_B consecutive OFDM symbols is then given by

$$\mathbf{r}_P^{DL}(k) = \bar{\mathbf{h}}_{e,DL}(k) \mathbf{S}_P^{DL}(k) \quad (14)$$

Then, a straight-forward approach is to deploy pure zero-forcing type inverse processing at TE side and estimate the effective downlink channel vector from N_B BS antennas to TE antenna as

$$\hat{\bar{\mathbf{h}}}_{e,DL}(k) = \mathbf{r}_P^{DL}(k) \mathbf{S}_P^{DL}(k)^{-1} \quad (15)$$

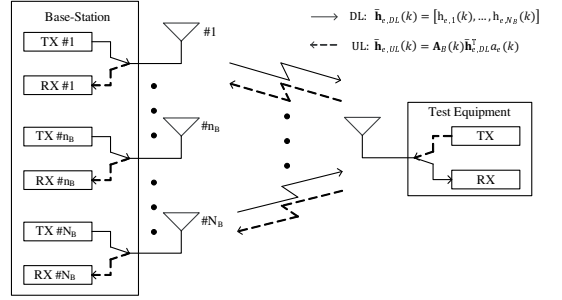


Figure 2: Principal illustration of the proposed estimation framework for BS non-reciprocity parameter identification deploying a test equipment (TE) and comprising of one round of DL and one round of UL transmissions, respectively.

Notice that due to diagonal structure, the above processing maps simply to subcarrier-wise processing. In [8]-[10], in order to extract the non-reciprocity parameters of the BS, this estimated DL channel matrix $\hat{\bar{\mathbf{h}}}_{e,DL}(k)$ is next assumed to be sent back to the BS via perfectly accurate (infinite) feedback signaling from TE. In practice, however, the accuracy of feedback signaling is obviously always limited to finite rate, thus directly compromising the accuracy of the effective channel estimates. Furthermore, extracting transceiver non-reciprocity parameters from DL and UL channel matrices can be computationally very complex as shown in [8]-[10].

To avoid the above problems of the existing solutions, we proceed as follows. An uplink pilot sequence of length N_B OFDM symbols, denoted here at subcarrier k by $\mathbf{s}_P^{UL}(k) = [s_{p,1}^u(k), \dots, s_{p,N_B}^u(k)]^T$, is ZF-precoded in time using the obtained TE DL channel responses as

$$\begin{aligned} \mathbf{x}_P^{UL}(k) &= \text{diag}(\hat{\bar{\mathbf{h}}}_{e,DL}(k))^{-1} \mathbf{s}_P^{UL}(k) \\ &= [s_{p,1}^u(k) / \hat{h}_{e,1}(k), \dots, s_{p,N_B}^u(k) / \hat{h}_{e,N_B}(k)]^T \end{aligned} \quad (16)$$

This is implemented at all deployed subcarriers and the precoded uplink pilot is transmitted using N_B OFDM symbols from the TE to the BS. Assume the DL channel estimates are perfect as $\hat{h}_{e,n_B}(k) = \bar{h}_{e,n_B}(k)$ for $n_B = 1, \dots, N_B$. The BS receives the pilot transmission in parallel with all the N_B antennas, and over the N_B consecutive OFDM symbols, yielding a total received signal matrix of the form

$$\begin{aligned} \mathbf{R}_P^{UL}(k) &= \bar{\mathbf{h}}_{e,UL}(k) \mathbf{x}_P^{UL}(k)^T \\ &= \mathbf{A}_B(k) a_e(k) \begin{bmatrix} s_{p,1}^u(k), & \dots, & \frac{s_{p,N_B}^u(k) h_{e,1}(k)}{h_{e,N_B}(k)} \\ & s_{p,2}^u(k) & \\ \vdots & \ddots & \vdots \\ \frac{s_{p,1}^u(k) h_{e,N_B}(k)}{h_{e,1}(k)}, & \dots, & s_{p,N_B}^u(k) \end{bmatrix} \end{aligned} \quad (17)$$

where the individual columns correspond to received spatial

vectors at individual OFDM symbol instants. Thus, as shown in (17), the combination of ZF precoding with downlink channel estimate and propagation through effective uplink channel results in an observation matrix $\mathbf{R}_p^{UL}(k)$ at BS receiver where the diagonal entries depend only on the non-reciprocity characteristics. Then, applying a zero-forcing type processing on those diagonal entries of the BS observation matrix with the known pilot sequence $\mathbf{s}_p^{UL}(k)$, an estimate of the non-reciprocity matrix $\hat{\mathbf{A}}_B(k)$ of the BS can be obtained up to constant scaling. This is written here as

$$\hat{\mathbf{A}}_B(k) = \text{diag}(\mathbf{s}_p^{UL}(k))^{-1} \times \text{diag}(\text{diag}(\mathbf{R}_p^{UL}(k))) \quad (18)$$

$$= a_e(k) \mathbf{A}_B(k)$$

In above, $\text{diag}(\cdot)$ operator, when operating on matrix, will yield a column vector of the argument matrix diagonal elements. Notice that the computational complexity of the above processing is almost trivial and can in practice be implemented as just a parallel collection of N_B complex multiplications. Furthermore, the deployed pilot sequences \mathbf{s}_{p,n_B}^d and \mathbf{s}_{p,n_B}^u for the DL and UL pilot transmissions, respectively, can in practice be freely optimized for efficient implementation purposes. As a practical example, the so-called Zadoff Chu sequences [1] can be deployed which are already in use, e.g., in 3GPP LTE/LTE-Advanced mobile cellular radio systems. Finally, after estimating the non-reciprocity parameters of the BS, the pre-compensator is constructed as explained in Section III, i.e.

$$\hat{\mathbf{W}}_C(k) = \bar{a}_C(k) \hat{\mathbf{A}}_B(k) \quad (19)$$

In above, $\bar{a}_C(k)$ is an additional design parameter which can be used to adjust, e.g., the transmission power at each subcarrier.

B. Practical Aspects

In practice, additive channel noise is naturally always present in the test link which has impact on the estimation accuracy. As shown in [8], in order to achieve system performance close to the ideal case, the BS requires very accurate knowledge on the channel non-reciprocity characteristics. Denoting the error first by $\mathbf{e}_B(k) = \hat{\mathbf{A}}_B(k) - a_C(k) \mathbf{A}_B(k)$, it follows that the maximum tolerable parameter estimation error variance, expressed here as $10 \log_{10}(\delta_{\hat{\mathbf{A}}_B}^2)$, should be in the range of -35 to -40dB [8]. In the context of the proposed OTA estimation algorithm, we propose the following enhancement strategies to improve the efficiency and accuracy of the proposed estimation algorithm.

1) *Averaging*: It is possible to obtain multiple estimates as in (18) by processing multiple consecutive pilot slots. This can be done with the single dedicated TE or with different TEs. Then, the final estimation quality of BS non-reciprocity characteristics can be directly improved by averaging over the obtained estimates. This naturally also increases the calibration time.

2) *Nulling*: In the basic formulation in the previous subsection, the estimation processing is basically carried out at all the subcarriers while the transceiver non-reciprocity parameters $\mathbf{A}_B(k) = \text{diag}(a_{B,1}(k), \dots, a_{B,N_B}(k))$ are in practice only *mildly frequency-selective* [7]. This then implies that if each diagonal entry of $\mathbf{A}_B(k)$ is modeled in *time-domain* as an L_e -tap FIR filter with impulse response $a_{B,n_B}^t(n)$, the

length of such non-reciprocity filter $a_{B,n_B}^t(n)$ is much shorter than the size of the used IFFT/FFT, i.e., $L_e \ll N$. Thus, the effect of estimation errors in the core estimation processing can be filtered down by transforming the diagonal entries of $\mathbf{A}_B(k)$, denoted here with $\hat{a}_{B,n_B}(k)$, to time-domain with N point IFFT yielding $\hat{a}_{B,n_B}^t(n)$ and then nulling the last N_{null} samples as

$$\vec{\hat{a}}_{B,n_B}^t(n) = \begin{cases} \hat{a}_{B,n_B}^t(n) & 1 \leq n < N_{null} \\ 0 & N_{null} \leq n \leq N \end{cases} \quad (20)$$

where $N - N_{null} > L_e$. Such additional processing is very effective in suppressing noise, especially if $N - L_e$ and $N - N_{null}$ are close to N . Similarly, if the propagation channel in the test link has a short delay spread, the same noise reduction technique described in (20) can also be applied for DL channel estimation step in (15) as well.

3) *Choice of TE*: If otherwise feasible, it is preferable to choose a device that has good channel connection with the BS (e.g., short delay spread and small path loss), implying reduced noise effects in the estimation.

4) *Periodic updates*: In general, frequency responses of the used transceivers can change over time, due to e.g. temperature changes. Hence, the non-reciprocity characteristics need to be also updated periodically. Further details are subject to BS operating conditions, mounting location, and other circuitry and environment-related aspects.

5) *Pilot sequence time-frequency mapping*: The basic estimator developments in Subsection A did not explicitly address the time-frequency mapping of the pilot sequences. One practical possibility is to follow the DL and UL reference signal features of 3GPP LTE [1], e.g. scattered demodulation reference symbol (DMRS) in downlink and sounding reference signal (SRS) type signal structure in the uplink.

V. SIMULATIONS AND NUMERICAL RESULTS

In this Section, we evaluate the performance of the proposed transceiver non-reciprocity estimation-compensation framework using extensive computer simulations. As a practical example, a four antenna BS is deployed and transmits OFDM waveforms using a total of 1024 subcarriers out of which 600 are active. Furthermore, the subcarrier spacing is 15 kHz conforming to the basic 3GPP-LTE specifications [1], and an operating carrier frequency of 2GHz is assumed. Frequency response mismatches over the 10MHz waveform bandwidth at each transceiver at both the BS and UE sides are characterized as 9 tap FIR filters with randomly selected coefficients (Gaussian distribution) in time-domain. The level of these mismatches is controlled such that the variances of the diagonal elements of the mismatch matrices $\mathbf{A}_B(k)$ and $\mathbf{A}_U(k)$, denoted with δ_B^2 and δ_U^2 , respectively, are set to be -20dB when given in dB scale (i.e., $10 \log_{10}(\delta_{B(U)}^2)$).

As depicted in Figure 2, one or more calibration links are first established between the BS and the TE(s). The propagation environment between the BS and each TE is modeled as a Rayleigh fading multipath channel with pedestrian A channel power delay profile with delay spread of 410ns [1]. For parameter estimation purposes, the reference signals specified in LTE standard are utilized here as the downlink and uplink

calibration pilot sequences with 3dB transmission power boost [1]. More specifically, cell-specific reference signal (RS) targeted for serving 4 antenna port transmission in one subframe is applied for constructing $\mathbf{S}_p^{DL}(k)$ at assigned subcarriers and symbol positions [1] while the sounding reference signals (SRS) from two subframes are deployed for constructing $\mathbf{s}_p^{UL}(k)$ at assigned subcarriers and symbol positions [1]. As both RS and SRS used by the DL and UL estimators are sparsely located along the subcarriers, a linear interpolator is implemented at both the BS and UE sides for obtaining the estimates $\hat{\mathbf{h}}_{e,DL}(k)$ and $\hat{\mathbf{A}}_B(k)$ at all the subcarriers. Then by conducting the proposed calibration flow, non-reciprocity parameter estimate $\hat{\mathbf{A}}_B(k)$ is obtained at the BS side. In these experiments, both one TE and two TE cases are explored, and also the effect of deploying the nulling technique as described in (20) is demonstrated. The nulling technique is applied in both DL channel estimation in (15) with $N_{null} = 30$ and non-reciprocity parameter estimation in (18) with $N_{null} = 20$.

First, we experiment the parameter estimation performance alone. As shown in Figure 3, adding one extra test link with another TE can improve the performance, through averaging, by around 3dB while the proposed nulling procedure in (20) can improve the parameter estimation accuracy even up to 10dB in this experimentation scenario. In general, at average transmitted SNR values of 20dB and 25dB, meaning the ratio of transmit power and received channel noise power, the proposed estimators can achieve close to -35dB and -40dB estimation accuracy, respectively.

Next, we apply the obtained non-reciprocity parameter estimates in the actual downlink transmission. The considered example scenario is that the 4-antenna BS is serving simultaneously 2 UEs, equipped for generality with two and one antennas, respectively. Thus overall, it can be seen as a 4×3 MU MIMO-OFDM DL system [3]. Furthermore, ZF precoding is deployed together with non-reciprocity pre-compensation in the BS transmitter. The non-reciprocity parameters are obtained using one or two TE(s) together with the nulling technique while the SNRs at DL and UL receiver inputs are set either to 20dB or 25dB in the calibration phase. In the actual downlink data transmission phase, the BS is transmitting two parallel data streams to UE #1 (with two UE antennas) and one data stream to UE #2 (single-antenna device). The wireless transmission environment in the data transmission is modeled as a Rayleigh fading multipath channel with extended Vehicular A channel power delay profile [11]. 64QAM is used as the subcarrier data modulation, and the downlink detection error rates are analyzed over multiple independent channel and impairment realizations. As described in (10)-(12), the developed pre-compensation and precoding calls for additional RX processing at the UE in order to remove the non-reciprocity of UE transceiver as well as the residual channel distortion due to pre-compensation scaling carried out at the BS as given in (19). In case of single-antenna UE, the receiver processing reduces to constant scaling while for dual-antenna UE this corresponds to spatial processing between the antennas. For the estimation of the effective precoded channel matrix $\mathbf{F}^{(i)}(k)$ at UE receiver, cell-specified RS specified for 4 antenna port transmission in 3GPP LTE standard [1] is again deployed with sparsely located pilot positions along frequency and a linear interpolator is, again, applied to obtain response estimates at the actual data subcarriers. Then, the

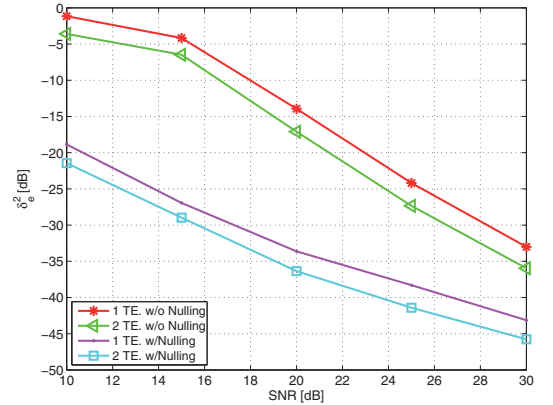


Figure 3: Estimation error variances (in dB scale) in identifying transceiver non-reciprocity parameters when different numbers of TEs are used, and with (w/) and without (w/o) the nulling technique. SNR refers to the ratio of average transmit power and received noise power.

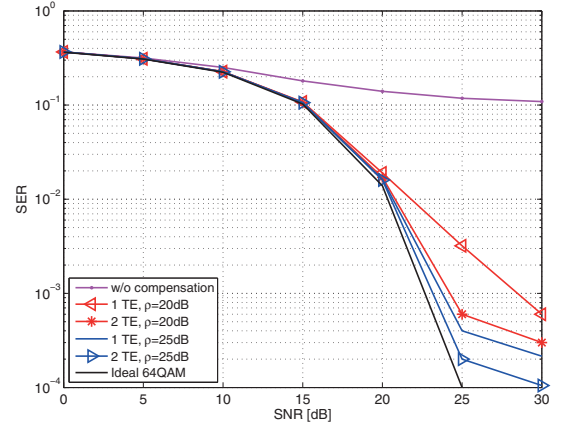


Figure 4: Performance comparison of the proposed estimation-compensation algorithm using 1 and 2 TE(s) and with 20dB or 25 dB SNR (ρ) in the test link, in terms of average SER in MU MIMO-OFDM downlink transmission with two UEs. X-axis refers to the average transmitted per-stream per-subcarrier SNR in the actual downlink MU MIMO transmission phase.

LMMSE receiver in (12) is calculated and applied before detecting the data.

As shown in Figure 4 and Figure 5, and without compensation, the resulting link and system performance degradation in terms of average symbol error rate (SER) and system data transmission sum-rate are substantial. The sum-rate is here calculated from realized received SINRs at each UE, which are mapped to rates through classical Shannon link capacity formula. These are then averaged over different channel and non-reciprocity parameter realizations to get reliable average sum-rates. As the BS only needs to update parameter estimates periodically for the calibration purpose

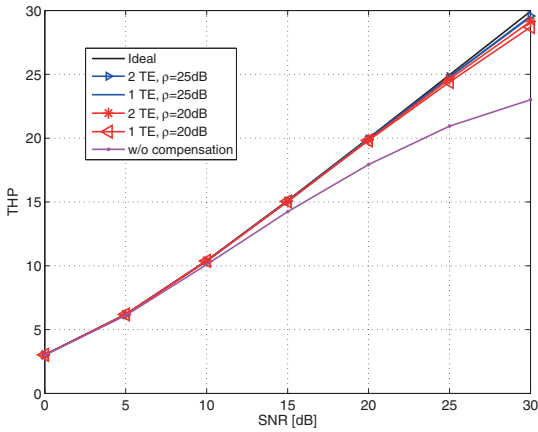


Figure 5: Performance comparison of the proposed estimation-compensation algorithm using 1 and 2 TE(s) and with 20dB or 25 dB SNR (ρ) in the test link, in terms of average data transmission sum-rate in MU MIMO-OFDM downlink system with two UEs. X-axis refers to the average transmitted per-stream per-subcarrier SNR in the actual downlink MU MIMO transmission phase.

and the proposed estimation algorithm actually requires very few signaling overhead for each update time, the rate loss during parameter estimation period is hereby not considered in the sum-rate calculation for simplicity. Then, the figures show the corresponding performance characteristics when the proposed estimation-compensation is deployed. As seen from the figures, by deploying two TEs for calibration and assuming calibration link SNR of 25dB, the proposed estimation-compensation scheme can achieve link and system performances very close to the ideal ZF pre-coded MU MIMO-OFDM system.

VI. CONCLUSIONS

This paper proposed an efficient transceiver non-reciprocity estimation-compensation framework for fully capitalizing the channel reciprocity in TDD linear precoded MU MIMO-OFDM DL transmission systems under non-reciprocal RF components and antennas. Based on the developed link models, it was first shown that reciprocity calibration at the BS is sufficient to remove all the inter-user interference and the effect of transceiver non-reciprocity at user equipment side can be compensated as part of the precoded channels applying proper RX processing. Then, an over-the-air (OTA) type pilot-based approach for the estimation of transceiver non-reciprocity parameters at the BS was proposed and developed which can provide accurate and flexible parameter identification with low system overhead and computational complexity. It was also demonstrated using comprehensive computer simulations that all the essential

interference due to transceiver non-reciprocity can be efficiently removed with reasonable amount of pilot symbols and system resources, in realistic MU-MIMO OFDM system context.

REFERENCES

- [1] H. Holma and A. Toskala, *LTE for UMTS: Evolution to LTE-Advanced*, 2nd ed., West Sussex, John Wiley & Sons, 2011.
- [2] D. Tse and P. Viswanath, *Fundamentals of Wireless Communication*, Cambridge University Press, 2005.
- [3] Y. Taesang and A. Goldsmith, "On the optimality of multiantenna broadcast scheduling using zero-forcing beamforming," *IEEE J. Selected Areas in Commun.*, vol.24, no.3, pp.528-541, Mar. 2006.
- [4] J. C. Haartsen, "Impact of non-reciprocal channel conditions in broadband TDD systems," in *Proc. IEEE 19th Int. Sym. Personal, Indoor and Mobile Radio Commun., 2008 (PIMRC 2008)*, pp.1-5, Sept. 2008.
- [5] L. Bruhl, C. Degen, W. Keusgen, B. Rembold, and C. M. Walke, "Investigation of front-end requirements for MIMO-systems using downlink pre-distortion," in *Proc. European Personal Mobile Communication Conference*, pp. 472-476, Apr. 2003.
- [6] J. Liu, G. Vandersteen, J. Craninckx, M. Libois, M. Wouters, F. Petre, A. Barel, "A novel and low-cost analog front-end mismatch calibration scheme for MIMO-OFDM WLANs," in *Proc. IEEE Radio and Wireless Symposium, 2006 (RWS 2006)*, pp. 219-222, Jan. 2006.
- [7] R. Rogalin, O. Y. Bursalioglu, H. Papadopoulos, G. Caire, A. Molisch, A. Michaloliakos, V. Balan, and K. Psounis, "Scalable Synchronization and Reciprocity Calibration for Distributed Multiuser MIMO", *IEEE Trans. Wireless Commun.*, Mar. 2014.
- [8] M. Petermann, M. Stefer, F. Ludwig, D. Wubben, M. Schneider, S. Paul, and K. Kammeyer, "Multi-User Pre-Processing in Multi-Antenna OFDM TDD Systems with Non-Reciprocal Transceivers," *IEEE Transactions on Communications*, vol.61, no.9, pp.3781-3793, Sep. 2013.
- [9] B. Kouassi, I. Ghauri, and L. Deneire, "Estimation of time-domain calibration parameters to restore MIMO-TDD channel reciprocity," in *Proc. Cognitive Radio Oriented Wireless Networks and Communications (CROWNCOM)*, vol., no., pp.254-258, Jun. 2012.
- [10] P. Zetterberg, "Experimental Investigation of TDD Reciprocity-Based Zero-Forcing Transmit Precoding," *EURASIP Journal on Advances in Signal Processing*, vol. 2011, 2011.
- [11] T. B. Sorensen, P. E. Mogensen, and F. Frederiksen, "Extension of the ITU channel models for wideband (OFDM) systems," in *Proc. IEEE Vehicular Technology Conference (VTC2005-Fall)*, pp. 392-396, Dallas, TX, Sep. 2005.

